AFRPL-TR-76-70

AFRPL GRAPHITE PERFORMANCE PREDICTION PROGRAM

FINAL REPORT

IMPROVED CAPABILITY FOR THE DESIGN AND ABLATION PERFORMANCE
PREDICTION OF ADVANCED AIR FORCE SOLID PROPELLANT ROCKET NOZZLES

Acurex Corporation/Aerotherm Division
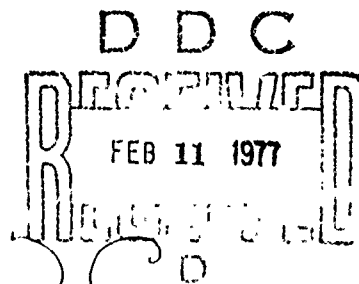485 Clyde Avenue
Mountain View, California 94042

Authors: H. Tong
          G. J. Hartman
          E. K. Chu
          A. J. Murphy

December 1976

D D C

FEB 11 1977

REPORT DOCUMENTATION PAGE

READ INSTRUCTIONS
BEFORE COMPLETING FORM

1. REPORT NUMBER	2. GOVT ACCESSION NO.	3. RECIPIENT'S CATALOG NUMBER
AFRPL-TR-76-70		

4. TITLE (and Subtitle)

AFRPL GRAPHITE PERFORMANCE PREDICTION PROGRAM.
Improved Capability for the Design Ablation
Performance Prediction of Advanced Air Force
Propellant Rocket Nozzles

5. TYPE OF REPORT & PERIOD COVERED

Final rept.
1 May 1974 —
31 July 1976

6. PERFORMING ORG. REPORT NUMBER

TR 76-16 (7113)

7. AUTHOR(s)

H. Tong, G. J. Hartman, E. K. Chu, A. J. Murphy

8. CONTRACT OR GRANT NUMBER(s)

F04611-74-C-0023

9. PERFORMING ORGANIZATION NAME AND ADDRESS

Acurex Corporation/Aerotherm Division
485 Clyde Avenue
Mountain View, California 94042

10. PROGRAM ELEMENT, PROJECT, TASK AREA & WORK UNIT NUMBERS

JON 305909HU   62302F

11. CONTROLLING OFFICE NAME AND ADDRESS

Air Force Rocket Propulsion Laboratory/AFSC
Edwards Air Force Base, California 93523

12. REPORT DATE

December 1976

13. NUMBER OF PAGES

257

14. MONITORING AGENCY NAME & ADDRESS(if different from Controlling Office)

Aerotherm-TR-76-16 (7113)

15. SECURITY CLASS. (of this report)

UNCLASSIFIED

15a. DECLASSIFICATION/DOWNGRADING SCHEDULE

16. DISTRIBUTION STATEMENT (of this Report)

Approved for Public Release; Distribution Unlimited

17. DISTRIBUTION STATEMENT (of the abstract entered in Block 20, if different from Report)

18. SUPPLEMENTARY NOTES

19. KEY WORDS (Continue on reverse side if necessary and identify by block number)

Rocket nozzle materials
Ablation
Graphite
Carbon-carbon

20. ABSTRACT (Continue on reverse side if necessary and identify by block number)

A combined experimental and analytic program was conducted to develop
improved procedures for predicting the ablation performance of graphite
materials in rocket nozzles. Particular emphasis was placed on conditions
representative of the throat region of an MX nozzle design which would use
graphite materials that are representative of the current state of materials
development. → over

DD FORM 1473   EDITION OF 1 NOV 65 IS OBSOLETE

UNCLASSIFIED

New kinetic response correlation functions were developed for G-90 and ATJ bulk graphites, 15% silicon carbide modified pyrolytic graphite, c plane pyrolytic graphite, and Pyrocarb 901 carbon-carbon. These functions were included into the Aerotherm GASKET code along with several modifications to improve on thermochemical modeling accuracy. This modified code, GASKET2, includes a number of new chemical species, improved generalized input requirements, and kinetically controlled carbon sublimation models. The GASKET2 code was used in a number of performance studies to predict the performance of a number of rocket nozzles to be tested in other Air Force programs.

The rocket nozzle ablation performance prediction procedures for several rocket motor fabricators were mutually compared to determine the probable ranges of predicted variables. These ranges were used in an ablation rate sensitivity study to define the most critical parameters. The mass transfer coefficient and the kinetic rate constants were shown to be the most critical parameters to be accurately known.

ACKNOWLEDGEMENT

White Section ☑
Buff Section ☐
☐

FACILITY CODES

X SPECIAL

A

D D C

FEB 11 1977

D

TABLE OF CONTENTS

LIST OF ILLUSTRATIONS

LIST OF ILLUSTRATIONS (Concluded)

LIST OF TABLES

LIST OF SYMBOLS

A_c	calorimeter area
A_i	pre-exponential factor
B'	normalized mass rate
C_M	mass transfer Stanton number
C_H	Stanton number
D	diameter (in.)
E	arc voltage
E_i	activation energy
h	enthalpy (Btu/lbm)
I	arc current
K_i	mass fraction of ith chemical species
K_p	equilibrium constant
Le	Lewis number
$\dot{m}$	mass flowrate (lbm/sec)
n	aluminum loading
n_i	temperature exponent
p	pressure (atm)
Pr	Prandtl number
q	heat flux (Btu/ft²sec)
R	mass ratio of plenum injected to arc heated gases, gas constant
s	surface recession (mils)
$\dot{s}$	surface recession rate (mils/sec)

T	temperature (°R, °K)
ϵ	emissivity
μ	velocity (ft/sec)
Ψ	inhibition coefficient
ρ	density (lbm/ft^3)
σ	statistical standard deviation, Stefan-Boltzman constant
θ	time (sec)

Subscripts

amb	ambient condition
ave	average condition
B	Bartz
c	coolant, carbon
diff	diffusion limited
e	boundary layer edge
hw	hot wall
o	chamber conditions
ref	reference enthalpy condition
s	stream
w	wall

T	temperature (°R, °K)
ε	emissivity
μ	velocity (ft/sec)
Ψ	inhibition coefficient
ρ	density (lbm/ft³)
σ	statistical standard deviation, Stefan-Boltzman constant
θ	time (sec)

Subscripts

amb	ambient condition
ave	average condition
B	Bartz
c	coolant, carbon
diff	diffusion limited
e	boundary layer edge
hw	hot wall
o	chamber conditions
ref	reference enthalpy condition
s	stream
w	wall

SECTION 1

SUMMARY

A combined experimental and analytic program was conducted to obtain required data and develop improved procedures for predicting the ablation performance of graphitic materials in rocket nozzles. Particular emphasis was placed on conditions representative of the throat region of an MX nozzle with graphitic materials which are representative of the current state of materials development. Significant results of this program are:

- The acquisition of a large body of full characterization ablation data using an arc plasma generator which simulates rocket nozzle environments

- The harmonizing of this data with available rocket motor data to obtain kinetic correlation functions which may be used to predicc ablation response. Correlation functions were obtained for

  - G-90 and ATJ bulk graphite

  - 15% silicon carbide modified pyrolytic graphite

  - c plane pyrolytic graphite

  - Pyrocarb 901 ($\rho \sim 1.83$ gm/cc)

- The development of the GASKET2 code. This code is a modification of the GASKET code to include the new correlation functions, new JANNAF species data, improved generalized input requirements, and kinetically-controlled carbon sublimation models.

- An evaluation of rocket nozzle thermal performance procedures currently used by rocket motor designers to predict the thermal performance of a solid propellant rocket nozzle. A significant conclusion of this evaluation is that errors in the mass transfer coefficient have a direct and significant influence on the predicted ablation rate. With the exception of the kinetic model, all other variables were shown to have a small effect on the mass loss rate in the throat region of a typical MX nozzle. Thus, future efforts should concentrate on accurate predictions of the mass transfer coefficient and accurate kinetic models.

● An analytic evaluation of the relative performance of different graphitic materials in the MX throat and nose cap environments

● Pretest predictions of the ablation performance of several AFRPL advanced technology rocket nozzles

● The acquisition of limited characterization ablation data for comparing the relative ablation performance of materials in given generic classes. These classes and the limited characterization materials were

- Bulk graphites   — P03

                                         — ATJS

- Pyrolytic graphites   — Hitco a-b plane

                                         — Pfizer c plane

                                         5% SiC/PG

                                         — 23% SiC/PG

                                         — 65% HfC/PG

- Carbon/carbons   — Pyrocarb 903 ($\rho \sim 1.83$ gm/cc)

                                         — Pyrocarb 903 HD ($\rho \sim 1.90$ gm/cc)

                                         — HRX 5125 ($\rho \sim 1.50$ gm/cc)

                                         — HRX 5875 ($\rho \sim 1.80$ gm/cc)

                                         — MDAC 3D($\rho \sim 2.00$ gm/cc)

SECTION 2

INTRODUCTION

The rate at which graphite nozzle components are consumed by hot propellant gases depends upon the composition of these gases. In addition, however, it is known that different generic classes (e.g., bulk graphites or pyrolytic graphites) respond differently to the same environments. Although higher density materials often have lower ablation rates, the contrasting ablation performance of a-b oriented pyrolytic graphite compared with c oriented pyrolytic graphite clearly demonstrates that density is not the only important factor. Past experience (References 1-5) has shown that surface reaction kinetics have an important, if not dominant, role in controlling carbon consumption rates.

With current technology it is not possible to write elementary chemical reactions which will define the carbon consumption process. Yet, some basic analytic expressions or procedures are required for design and performance analyses of rocket motors. The Air Force Rocket Propulsion Laboratory recognized this need and initiated a program (Reference 6) to develop a semiemperical procedure to predict ablation response. At that time a-b oriented pyrolytic graphite was considered to be a viable rocket nozzle material. Thus Reference 6 concentrated on the development of a general analytic model and its validation using a-b oriented pyrolytic graphite data.

The analytic model was, by necessity, based on an engineering approximation of the overall ablation reaction. The ablation data used for determining the correlation coefficients in this model were obtained by exposing a large number of models to simulated hot propellant environments. The resultant analytic model and the correlations for pyrolytic graphite were assembled into the GASKET code (Reference 7). The GASKET code was then integrated into an overall rocket nozzle ablation performance prediction procedure.

Since the completion of the above work, thermostructural problems associated with a-b oriented pyrolytic graphite have cast doubt on their use as rocket nozzle liner material. Other materials considered and applied to rocket nozzles include bulk graphites, carbon/carbons, c oriented pyrolytic graphites and carbide codeposited pyrolytic graphites. A need therefore existed to generate correlation coefficients for these other materials. Because of the many varieties of materials in each of these generic classes, it is not economically practical to kinetically characterize all possible graphitic materials.

3

To satisfy the requirement for predicting ablation response of other graphitic materials, the program described in this report was conducted. The program included full characterization of select materials from each generic class and limited characterization of a larger number of materials. The behavior of the limited characterization materials was deduced by comparing their ablation response to that of fully characterized materials in the same generic class. Appropriate data was obtained from controlled ablation tests using an arc plasma generator and analyses of available rocket motor data. The data analysis procedure was very similar to that described in Reference 8.

Data for full characterizations were obtained for:

- ATJ bulk graphite

- G-90 bulk graphite

- 15% SiC codeposited pyrolytic graphite

- Pyrocarb 901 carbon/carbon (ρ = 1.83 lbm/ft^3)

Data for limited characterizations were obtained for:

- Pyrocarb 903 carbon/carbon (ρ = 1.82)

- High Density Pyrocarb 903 carbon/carbon (ρ = 1.90)

- HRX 5125 carbon/carbon (ρ = 1.50)

- HRX 5875 carbon/carbon (ρ = 1.86)

- MDAC 3-D carbon/carbon (ρ = 2.02)

- ATJ-S bulk graphite

- 5% SiC codeposited pyrolytic graphite

- 23% SiC codepositied pyrolytic graphite

- 65% HfC codeposited pyrolytic graphite

- c oriented pyrolytic graphite (Pfizer)

- a-b oriented pyrolytic graphite (Hitco)

Full characterization data was analyzed to obtain appropriate correlation coefficients which were compatible with the GASKET code. The GASKET code was modified to include this new data base and designated as GASKET2 (Reference 9). The validity or accuracy of the GASKET2 code was then assessed by comparing predicted and post-test measured responses of rocket motors.

Each of the test materials were examined for pre- and post-test microstructural and chemical characteristics. Characterization data included photomicrographs, scanning electron microscopy, porosity, chemadsorption, thermal expansion coefficients, and lattice parameters. These data were examined and where possible, the ablation performance was related to the observed characteristics.

The GASKET2 code was also used in a series of performance calculations (References 10-14) to predict the response of various graphitic materials in propellant environments similar to those expected for an MX rocket motor. These analyses were

1. Third stage Hercules MX nozzle analysis (Reference 10)

2. Rocketdyne Condor test nozzle analysis (Reference 11)

3. Third stage Hercules MX nozzle analysis using Pyrocarb 901 kinetics (Reference 12)

4. Material/propellant sensitivity study for the throat location of the standard 7-inch test nozzle (Reference 13)

5. Material sensitivity study for the nose cap of the standard 7 inch test nozzle (Reference 14).

In addition to the above thermal ablation studies, a thermostructural analysis was performed on the BATES motor to identify probable causes for nozzle failures. The results of this study are presented in Reference 15.

5/6

SECTION 3

PROCEDURE FOR MATERIAL CHARACTERIZATION

The surface recession of carbon rocket nozzles due to chemical erosion by propellant gases is a complex phenomenon. It includes events such as: diffusion of the reactive species to the carbon surface, adsorption and desorption of the reactive species and reaction products at the surface, heterogeneous reactions, and diffusion of the reaction products into the bulk stream. With the present state of the art, an exact analytical model describing these events is not attainable. Hence, an engineering approximation representing the overall observed phenomenon is used as an alternative.

Under U.S. Air Force Contract F04611-69-C-0081 (Reference 6), a combined analytical and empirical procedure was developed to correlate the ablation rate of pyrolytic graphite. This procedure included ablation tests under simulated environments in the arc plasma generator, determination of the correlation function, and identification of the kinetically controlled reactions. This procedure was applied to the consumption rate of a-b plane oriented pyrolytic graphite. The resulting correlation has been applied extensively in designing rocket nozzles, and satisfactory predictions have been obtained.

Under the current U.S. Air Force Contract F04611-74-C-0023, carbon materials were characterized using two procedures. The first procedure used a full characterization procedure similar to Reference 6. Five commonly used carbon materials were selected from generic types of pyrolytic graphite, modified pyrolytic graphite, bulk graphite, and carbon/carbon. These underwent the full procedure to determine correlations of their ablation rates. The second procedure, which only determined the relative ablative performances, was called limited characterization. Considerably fewer APG data were taken for this type of characterization since the determination of the empirical correlation was not required. The carbon materials which were characterized are shown in Table 1.

This section will describe the experimental apparatus of the Aerotherm 1-megawatt arc plasma generator, its application to the material characterization procedure, the selection of the APG test gases and test conditions, and the correlation procedure. Additional details are available in Reference 16.

TABLE 1.   CARBON MATERIALS CHARACTERIZED

Manufacturer Source	Material	Test[a]		Number of Models
		F	S	
ARC	15% SiC/PG	X		33
HITCO	Pyrocarb 901	X		28
UC	ATJ	X		28
Carborandum	G-90	X		28
ARC	5% SiC/PG		X	3
ARC	23% SiC/PG		X	10
Raytheon	HfC/PG		X	10
Hitco	A-B PG		X	10
Super Temp	PG Plate		X	10
Pfizer	PG Plate		X	10
Hitco	Pyrocarb 903		X	10
Haveg	HRX-5125		X	10
Haveg	HRX-5875		X	5
McDac	3-D C/C		X	6
UC	ATJ-S		X	10
Pure Carbon	P03		X	10
Hitco	High Density Pyrocarb 903		X	5

[a]F — full characterization

S — limited characterization

8

3.1 EXPERIMENTAL APPARATUS

The experimental apparatus consisted of the arc plasma generator used to produce the high temperature reactive environments, the test nozzles which were exposed to these environments, the fume collection, cooling and scrubbing system used to remove the test gases from the facility, and the instrumentation used to characterize the test conditions and model response. The arc plasma generator and support equipment are discussed in Section 3.1.1. The test nozzles are described in Section 3.1.2. The fume collection system is described in Section 3.1.3 and the instrumentation is presented in Section 3.1.4.

3.1.1 Arc Plasma Generator

The Aerotherm 1-megawatt constricted arc plasma generator (APG) is shown schematically in Figure 1 and physically in Figure 2. The APG is a constant mass flowrate device with a flowrate controlled by throttling at the gas injection ports. The APG uses a segmented constrictor arc with a tungsten cathode and a water-cooled copper anode to transfer energy to the primary test gas. This test gas is injected tangentially between the cathode and the first constrictor segment to provide a stable, high voltage operation. Additional gases to simulate propellant gases are injected downstream of the anode and mixed with the primary arc-heated gas in a plenum chamber. Thermochemical equilibrium is achieved in this plenum and the resulting simulation gases are expanded through a choked converging-diverging nozzle. The test section is the throat region of this nozzle.

The arc unit is water-cooled with ambient temperature, high pressure deionized water. The APG input power is supplied by a 600 kW continuous rated, saturable core reactor, dc rectifier power supply. A maximum overload power level of 1.2 MW is achievable for 5 minutes. The power supply has 1000, 2000, or 4000 volts open circuit voltage modes to match APG operating characteristics for various test gases, flowrates, and pressures. Arc starting is accomplished by imposing power supply open circuit voltages across the APG electrodes while an argon flow is maintained. Then a momentary RF discharge in the APG column provides an initial ionization path for the arc. Once the arc is started, test gases are immediately introduced as necessary to provide the required test gas composition.

The arc unit exhibits very low contamination levels. Based on the results of Reference 17, total gas stream contamination should not exceed 200 parts per million (0.02 percent). The major sources of this contamination are the tungsten cathode and copper anode. A third potential source of contamination is the boron nitride insulators of the constrictor section; however, their contribution to the above figure is felt to be very small.
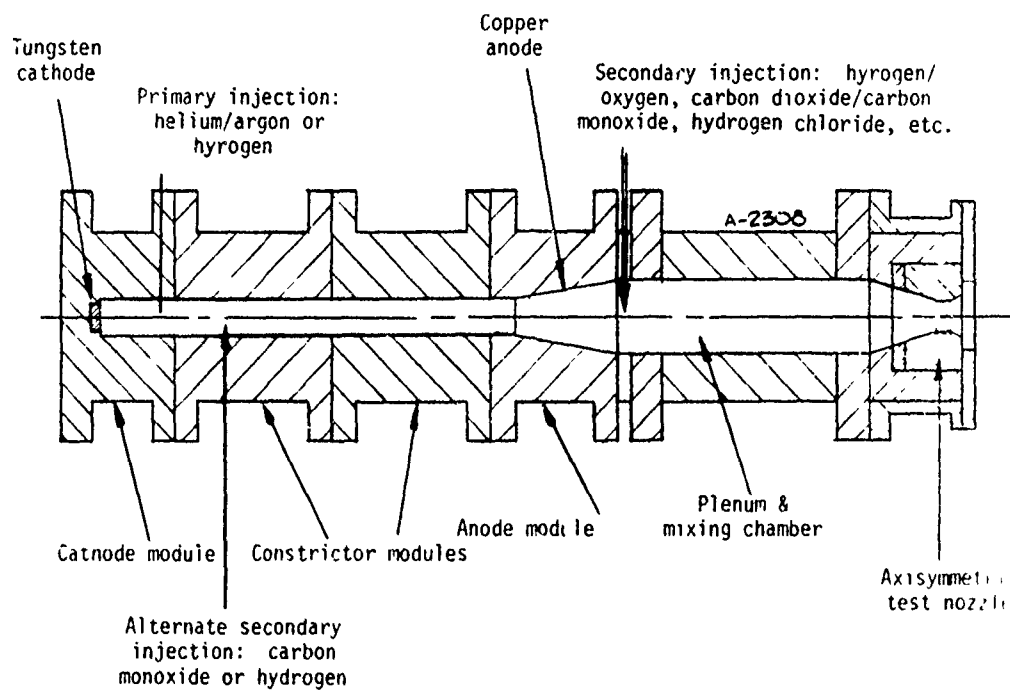
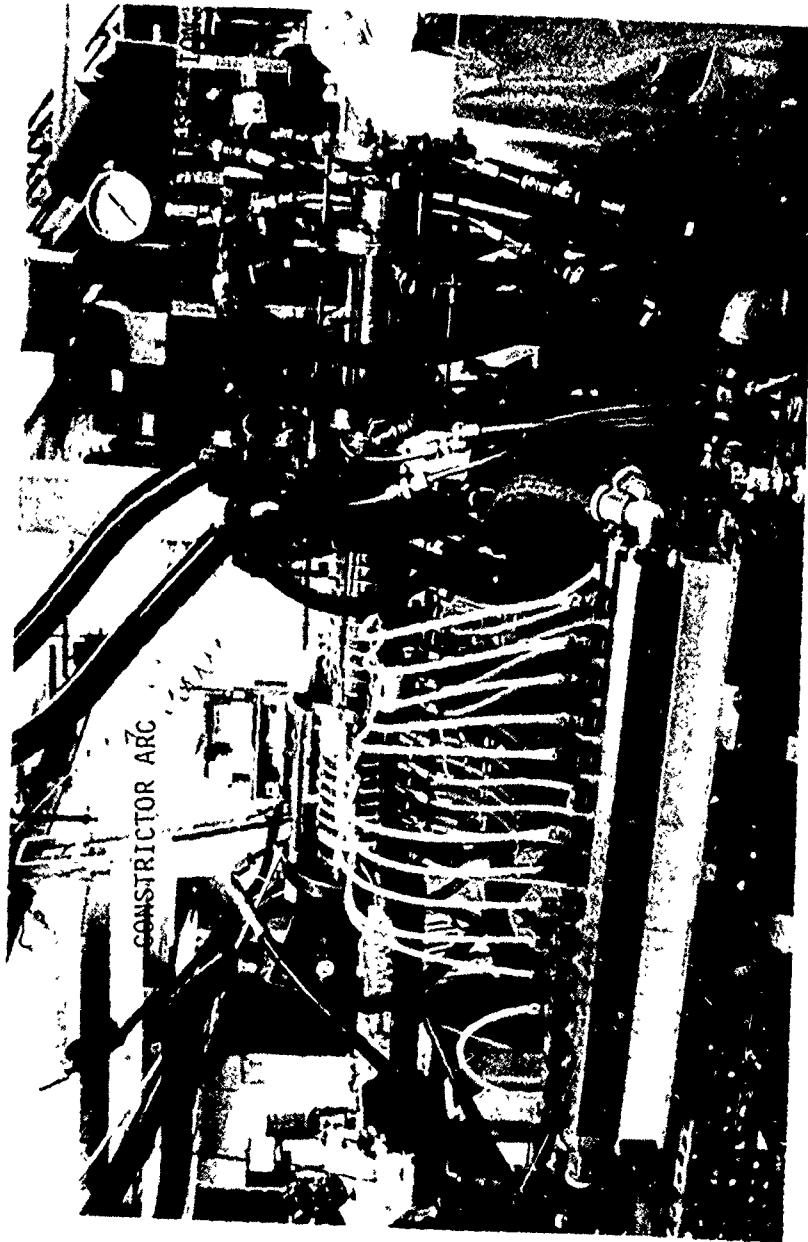Figure 1. Aerotherm 1-MW constrictor arc heater.

Figure 2. Aerotherm 1-MW constrictor arc heater.

3.1.2 Test Nozzle Configurations

The nominal test configuration was an axisymmetric nozzle as shown in Figure 3. The test section inserts formed the throat region of the nozzle. The PG washer immediately upstream of the test section insert insured a smooth transition into the insert and held the boundary layer trip. This trip, a thin Grafoil disk, was employed to promote turbulent flow, and therefore high transfer coefficients, in the throat. The test section insert was retained by a crushable high temperature insulator and could expand thermally without suffering excessive compressive stresses. The test section insert configuration is shown in Figure 4. This s the nominal-dimension configuration; the details of the actual test insert depend on the particular requirements of the test material, e.g., backwall insulation in the throat region.

An appropriate ablation sample or a water-cooled, steady state calorimeter was placed in the test section. The calorimeter and test sample both have the nominal interior dimensions shown in Figure 4, so that the test conditions during an ablation test could be inferred from a corresponding calorimeter test. The calorimeter installation is shown in Figure 5 and a view of the assembly is shown in Figure 6.

3.1.3 Fume Collection System

The APG for these tests was run on the atmospheric test stand with the test gases exiting directly into the test bay. A fume collection system was employed to collect, cool, clean, and exhaust the gases outside the test area. The system is shown schematically in Figure 7.

The first component of the system is the heat exchanger section. The high temperature of the test gases as they left the APG required a "cooldown" to less than 250°F before they entered the remainder of the system. This section is constructed of a high temperature alloy, Hastelloy Alloy C-276, and provided a set of spray nozzles which "quench" or cool the gases with a water spray. Also included in this section are two view ports to allow pyrometer viewing of the test section.

The gases were then ducted to the fume scrubber mounted outside the test bay. This scrubber is of the packed tower type and is designed to remove all toxic fumes ($HC\ell$, HF) from the gas stream before they are exhausted to the atmosphere. The scrubbing fluid was water used in the once-through mode.

The final component of the system is the exhaust fan, mounted on the roof of the test bay. This provides the positive draft required to draw the gases through the heat exchanger section and
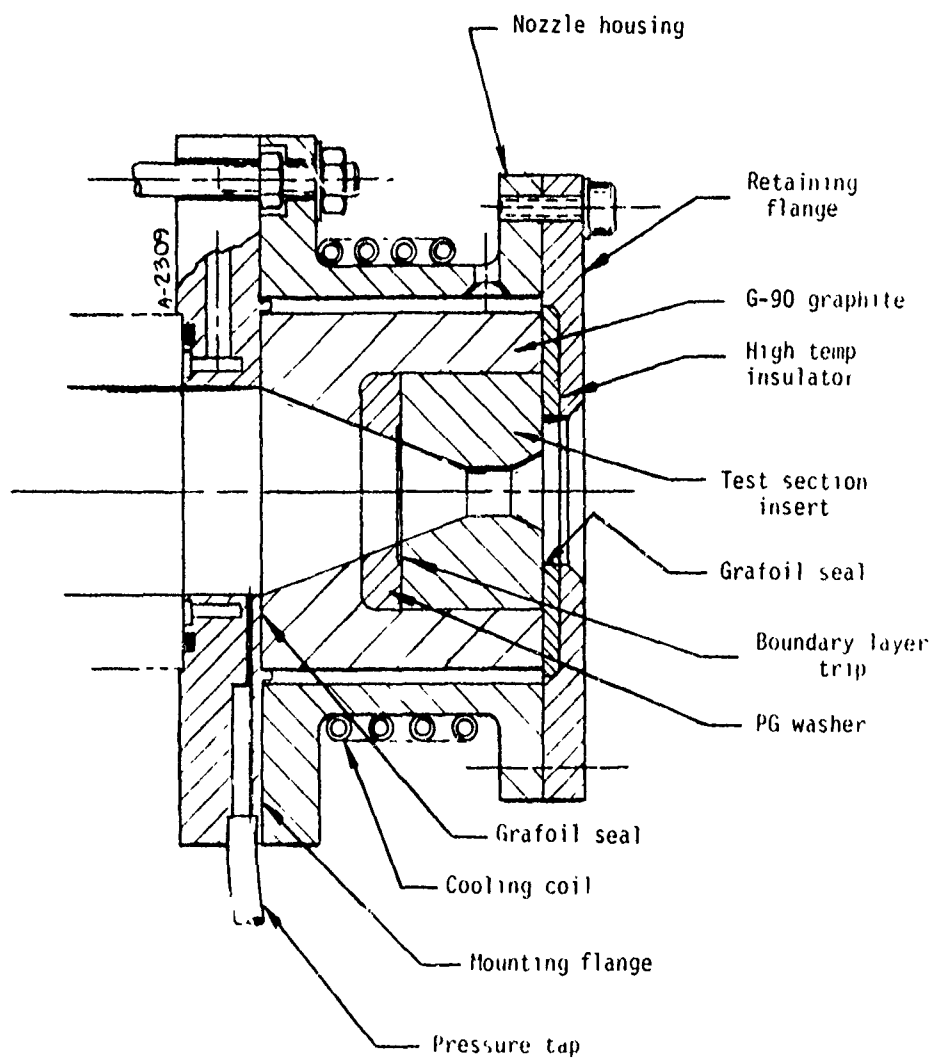
Figure 3. Axisymmetric nozzle assembly.
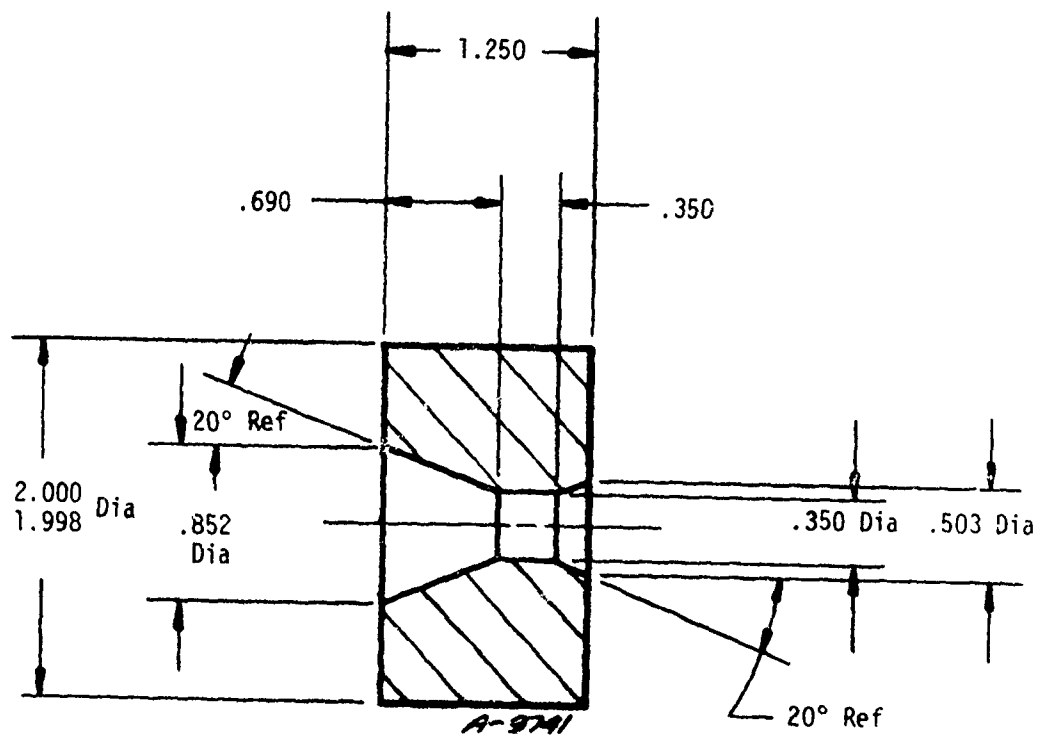
Figure 4. Nominal test section insert configuration.

15
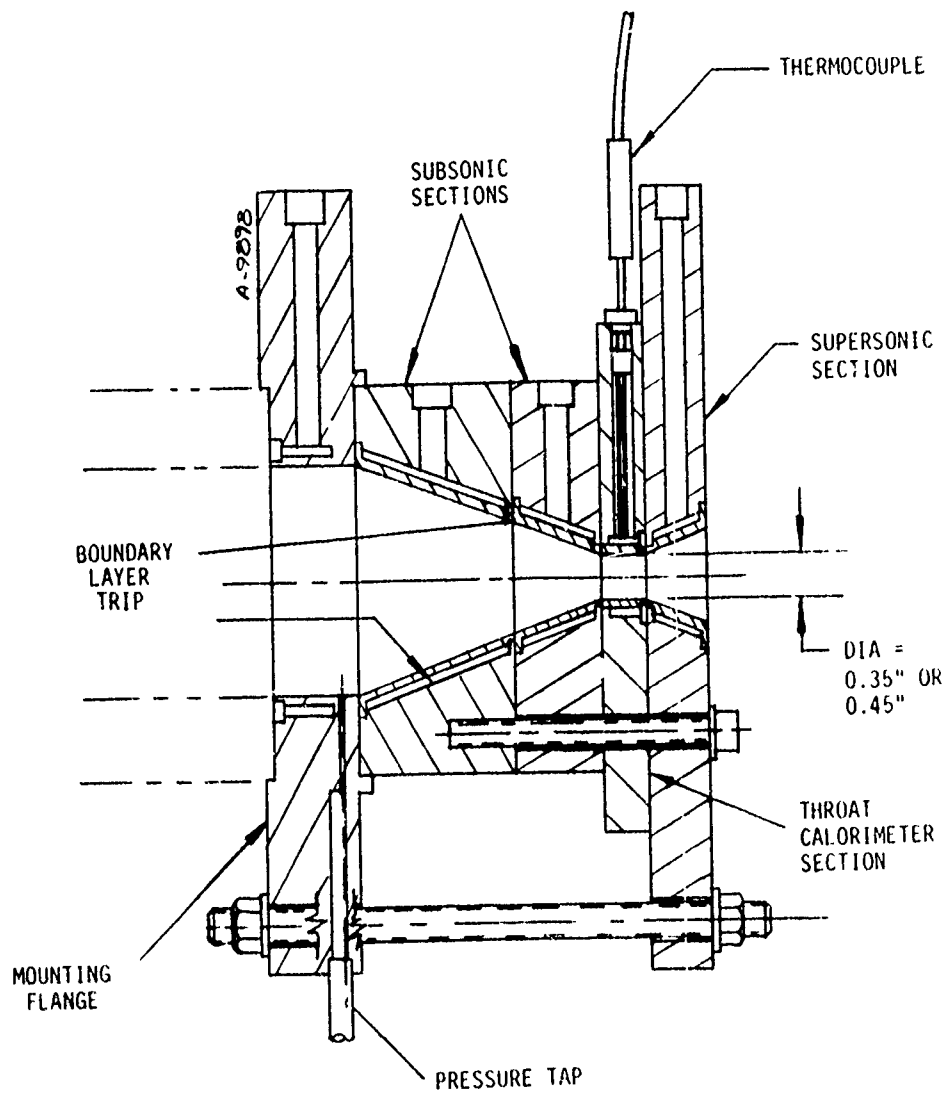
Figure 5. Calorimeter nozzle assembly.

THERMOCOUPLE

SUBSONIC
SECTIONS

A-9898

SUPERSONIC
SECTION

BOUNDARY
LAYER
TRIP

DIA =
0.35" OR
0.45"

THROAT
CALORIMETER
SECTION

MOUNTING
FLANGE
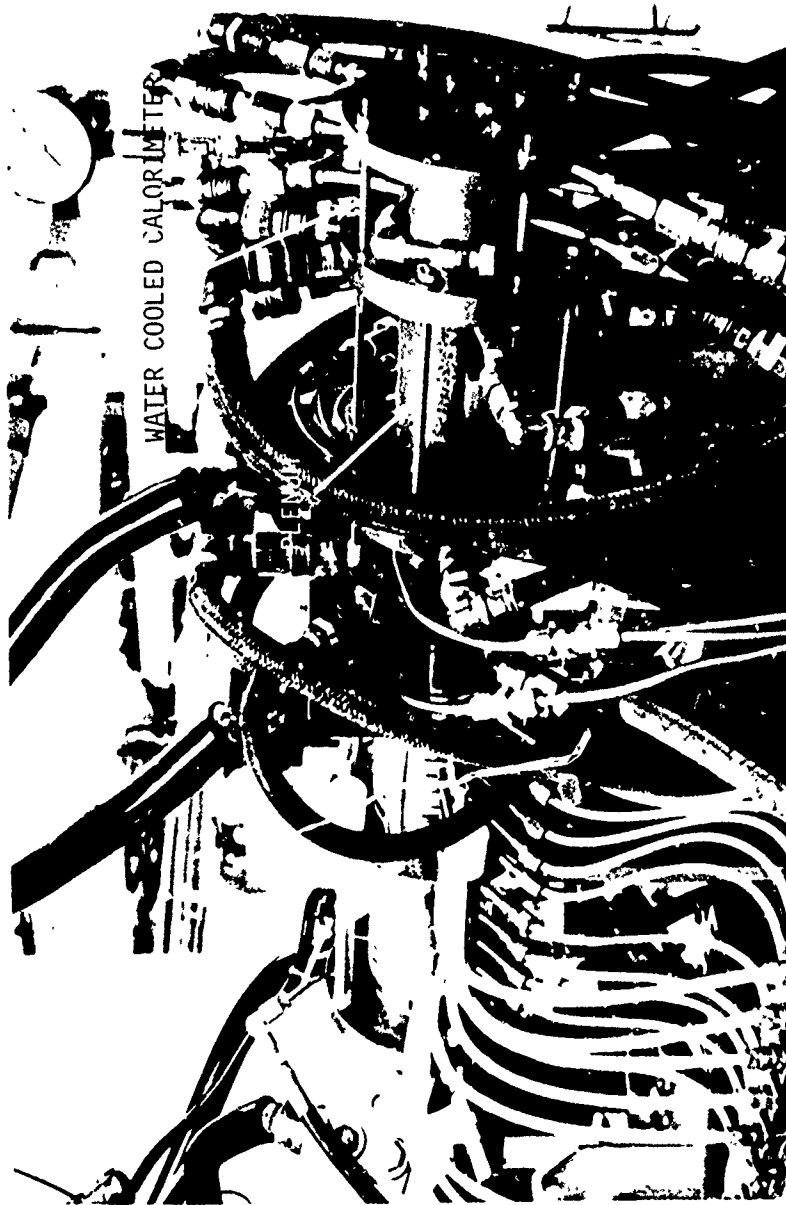
PRESSURE TAP

Figure 6. Axisymmetric test section, Calorimeter installed.

Exhaust
fan

Test bay

Fume
scrubber

APG

Duct

Pyrometer
viewing
port

Heat exchanger
section
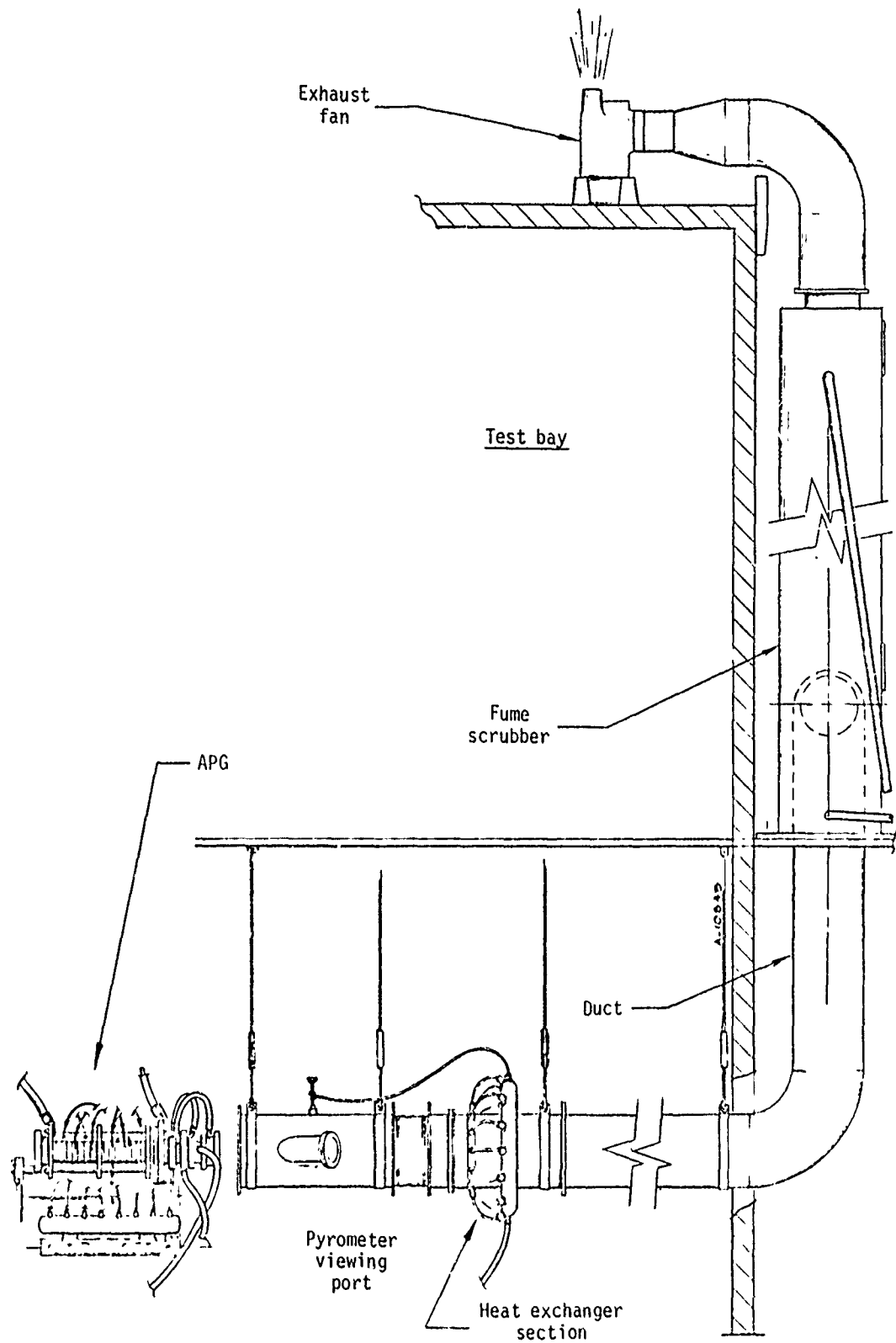
Figure 7. Fume collection system.

19

the scrubber. The fan has been sized to provide a slightly negative pressure in the system when it is used in the blanked-off mode. This is necessary when hazardous or toxic test gases are used as it prevents the release of such gases into the test bay and insures personal safety.

Due to the corrosive nature of certain of the test gases (HCℓ or HF), the fan, scrubber and all ducting exclusive of the heat exchanger section are constructed of Rigedon 4837-AT-HF. This is a fire-retardant, fiberglass-reinforced polyester plastic resistant to corrosive attack by both acids and alkali and, in addition, is provided with a special Dynel veil for protection against fluoride attack.

3.1.4 Instrumentation

The measurements to characterize the test conditions and material response were:

- Test Condition

    - Gas Total Enthalpy, h_o

    - Chamber Pressure, P_o

    - Cold Wall Heat Flux, $q_{c.w.}$

    - Reactive Gas Composition, K_i

- Material Response

    - Surface Temperature History, T_w and $\theta_{experimental}$

    - Surface Recession, S

    - Qualitative Surface Condition

Tne gas total enthalpy was defined by an energy balance on the arc heater including the plenum chamber, i.e.,

$$h_o - h_{amb} = \Delta h_{arc} = \frac{\text{Power In-Cooling Water Losses}}{\text{Total Gas Flowrate}} \tag{1}$$

$$= \frac{0.948 \times 10^{-3} \, EI - \dot{m}_c \Delta T_c \, C_p}{\dot{m}_{gas}}$$

where h_{amb} is the enthalpy of the test gases at room temperature. Voltage E and current I were recorded continuously on a digital data recording system; measurements from panel meters were also taken as a check. The cooling water flowrate, $\dot{m}_c$, was measured continuously during each test with

a sharp-edged orifice and differential pressure transducer and its temperature rise, ΔT_c, was measured continuously with a differential thermopile. The total gas flow rate, $\dot{m}_{gas}$, was the sum of all gas flowrates delivered to the APG. All gas flowrates were measured with ASME sharp-edged orifices and differential pressure gauges, except hydrogen-chloride which was measured with a rotameter with a magnetic float follower.

The chamber pressure was measured continuously with strain gauge pressure transducers. The pressure taps are located at the downstream end of the plenum-mixing chamber (Figure 3). The chamber temperature was determined from the calibrated net enthalpy addition due to arc heating, the measured chamber pressure, the test gas composition, and an ACE computer code computation of chamber conditions.

Cold wall heat flux was measured at the throat of the water-cooled copper calibration nozzle with a steady state, water-cooled calorimeter section. The coolant water temperature rise ΔT_c was measured with a single-pair, copper-constantan differential thermopile, the output of which was recorded continuously. The calorimeter water flow, $\dot{m}_c$, was measured with a standard glass tube rotameter and the heat flux then calculated from the equation:

$$q_{cw} = \frac{\dot{m}_c \, \Delta T_c}{A_c} \tag{2}$$

where A_c is the calorimeter heated area.

Surface temperature history was measured with a Thermodot TD-9CH optical pyrometer which is calibrated with a high temperature source. For each nozzle ablation test, this pyrometer, which has a sensing wavelength of 0.8 microns, viewed the nozzle throat at an angle of approximately 40° from the APG centerline. Output data was recorded both visually from the instrument meter and in digital form from the data acquisition system. In some tests, a second pyrometer was used as a check on the primary unit. This secondary unit was a Thermodot TD-9FH optical pyrometer similar to the primary instrument except calibrated in degrees Fahrenheit.

The test sample surface recession was obtained from pre- and post-test measurements of the throat diameter. Measurements were made at three axial stations in the throat region, namely, the entrance, center, and exit. In addition, at each station, the diameters were determined at two angular positions 90° apart. The measurement accuracy is approximately ±0.0005 inch.

3.2   TEST GASES AND TEST CONDITIONS

3.2.1 Test Gas Selection Criteria

The selection of gases for APG testing is very important since, ideally, one would like to minimize the extent to which experimental results must be extrapolated in order to predict actual conditions. Three questions must therefore be addressed in selecting appropriate gases.

1. What rocket motor environments are anticipated?

2. What are the important surface reactions?

3. What are the operating limitations of the APG?

Test gases must be defined for two different kinds of tests. First, a comprehensive set of gas mixtures must be defined to allow a full kinetic characterization of the test material. Second, a gas mixture or a set of gas mixtures must be defined for experimental screening or ranking of materials similar to those which have received the full characterization treatment. Although it is likely but not necessary, the screening gases and their test conditions will be a subset of the full characterization test matrix.

3.2.1.1 Rocket Motor Environments

Rocket motor environments were based on three advanced MX propellants, namely,

● XLDB

● HTPB

● PEG/FEFO

Representative elemental compositions and flame temperatures are given in Table 2. For the purpose of studying surface kinetics only, the elemental composition of the propellant gas needs to be considered. The solid Al_2O_3 does not enter into the surface kinetics problem although it probably contributes to surface erosion rates. Table 3 gives representative compositions of the propellant gases with all the Al and an appropriate amount of oxygen removed as Al_2O_3. The ACE/GASKET program was used to determine the concentration of gas species which would exist at the carbon surface for three conditions: (1) surface equilibrium, (2) very small surface ablation, and (3) a nonreacting surface at typical surface temperatures (2200°K to 3300°K). Those species with significant concentrations would then be candidates for reactants and/or poisons. A typical distribution of surface species as a function of temperature for an HTPB propellant is shown in Figure 8. This solution represents the kinetically controlled ablation of edge-oriented pyrolytic graphite at a throat

TABLE 2. REPRESENTATIVE COMPOSITION AND FLAME
TEMPERATURE OF ADVANCED MX PROPELLANTS

Propellant Flame Temperatures (°K) (°F)	XLDB 3880 6524	HTPB 3690 6182	PEG/FEFO 3787 6360
Mass Fraction			
H	2.5	4.0	2.6
C	13.5	8.4	12.5
N	24.0	9.0	23.0
O	39.5	40.0	37.9
F	—	—	1.5
Aℓ	18.5	17.6	18.5
Cℓ	2.0	21.0	4.0

TABLE 3. PROPELLANT GAS COMPOSITION
($Aℓ_2O_3$ REMOVED)

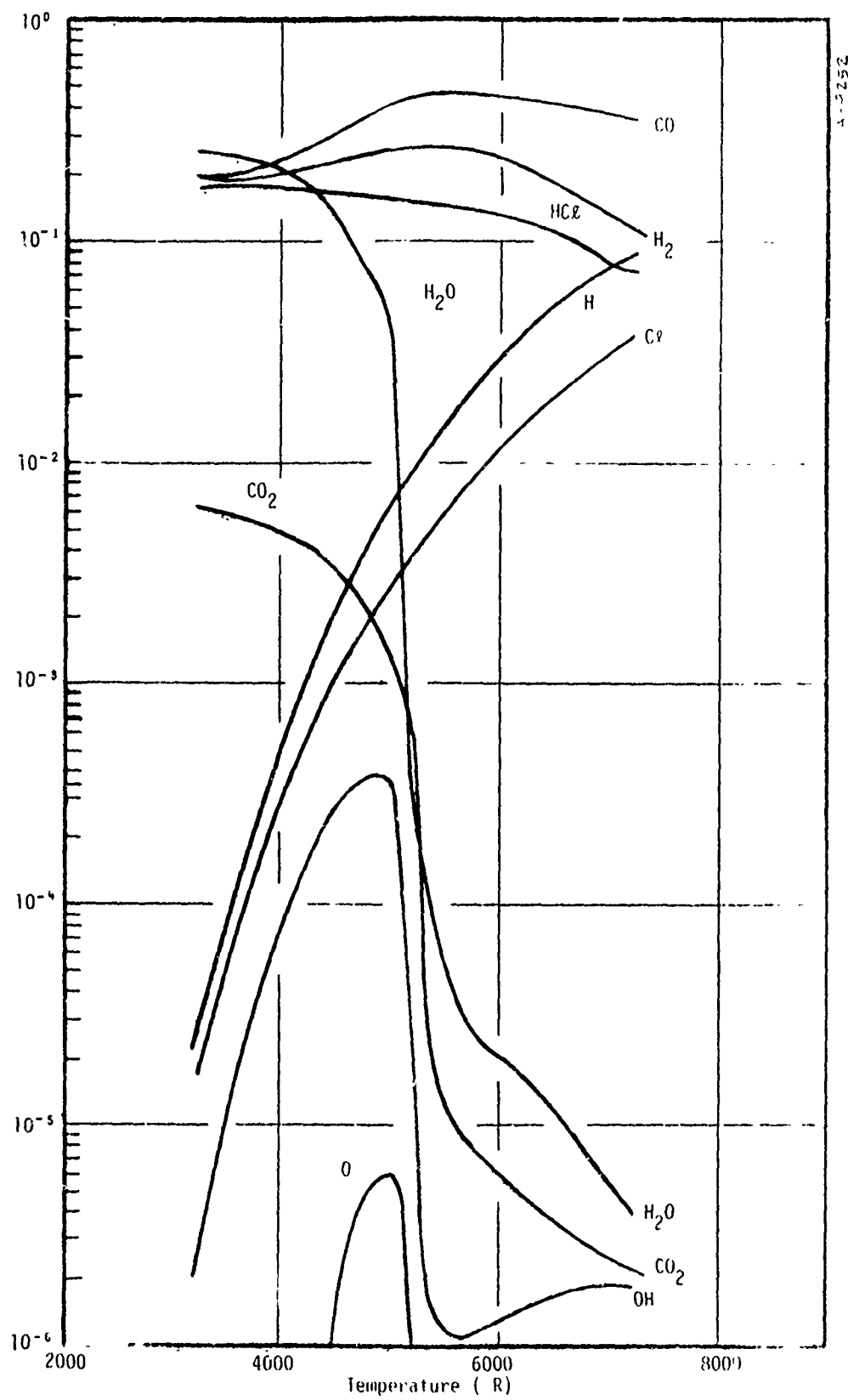| Propellant	XLDB	HTPB	PEG/FEFO
Mass Fraction			
H	3.8	6.1	4.0
C	20.8	12.7	19.2
N	36.9	13.6	35.4
O	35.5	35.2	32.9
F	—	—	2.3
Cℓ	3.0	32.4	6.2

23

Figure 8. Typical surface gas composition at throat for c plane PG.

pressure of 39.4 atm from the ACE/GASKET calculations. Those species considered as possibly significant reactants (molar concentrations greater than 0.1 percent) are:

- CO

- H_2O

- H_2

- N_2

- CO_2

- HCℓ

- HF (HF not a specie for the HTPB solution)

It should be noted that other species, such as Cℓ and H, appear in representative amount and may also be important. Still other species, such as O and OH, though present only in small quantities, may have very fast reaction rates. The concentrations of these latter species decrease rapidly as the surface temperature increases. In fact, at typical rocket motor temperatures, these concentrations are too low to cause any significant amount of carbon removal. Atomic hydrogen has been shown, at least in one case,* to react slower than H_2 and since the concentrations of H_2 are an order of magnitude greater than that of H, ablation due to the latter will probably be insignificant. Cℓ, a halogen, is a potential poison; however, there is no firm evidence for this behavior. Thus, the species of interest are those previously listed.

3.2.1.2 Important Surface Reactions

The most probable surface reactions can be identified by considering the available species, the possible reactions with carbon, and the equilibrium constant for each reaction. (The equilibrium rate serves as an upper limit to the surface kinetic rate.) Of the reactions considered, only the following have sufficiently large equilibrium constants in the temperature range of interest:

$$C* + H_2O \rightarrow CO + H_2$$

$$C* + CO_2 \rightarrow 2CO$$

$$2C* + H_2 \rightarrow C_2H_2{}^{\dagger}$$

---
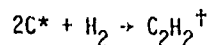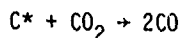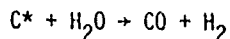
*Personal communication. Professor D. Rosner, Yale University.

†Although C_2H_2 does not appear in the list of gas species, the reactions should not be ruled out. Hydrogen is present in large concentrations (approximately 25 percent by mole) and the C_2H_2 coming off the surface may be eliminated by gas phase reactions.

The reactions of carbon with CO, N_2, HCℓ, and HF are not considered significant since the equilibrium formation rates are too small. However, they may have inhibitor properties.

The mechanism of poisoning, or inhibition of surface reactions, is basically one of active site competition. That is, a poison specie may occupy an active lattice site and thus prevent a reactant from occupying that site. Of the seven species listed as possible poisons, only N_2 will not be considered because it appears to be inert as far as surface kinetics are concerned.* Although H_2O and CO_2 readily react with the carbon surface they also occupy lattice sites and thus, in that sense, are poisons for each other.

3.2.1.3 Arc Plasma Generator Limitations

The design and operation of the arc plasma generator imposes restrictions on the choice and the use of certain test gases. There are two basic areas of concern; first, the effect of a particular gas on the vital components of the APG (cathode, anode, constrictor segments, etc.) and second, the stability of the arc when operating with a particular gas or combination of gases. The situation is further complicated by the desire to produce a test gas at the highest possible temperature. This generally requires arc heating of the largest possible portion of the total test gas flow to the maximum temperature achievable, i.e., maximum energy input, while minimizing the energy losses to the cooled walls of the APG.

With the design of the APG currently being used, it is necessary to avoid injecting any oxidizing species into the arc heater as the primary gas. This is due to the tungsten material used in the cathode, which when rapidly removed through oxidation processes can both limit APG run times to the order to seconds and cause catastrophic failure of the arc heater. The normal solution employed is the injection of such gases several constrictor duct diameters downstream of the cathode. This has been highly successful when the required test gas is simulated air, using individually injected nitrogen and oxygen. However, in the case of propellant simulation, there is an additional problem. The reactive nature of the base species, hydrogen, which for reasons of arc efficiency and maximum power input is the arc heated gas, requires the injection of oxidizing species downstream of the arc heater portion of the APG, in the plenum section (see figure 1). This is primarily due to the combustion induced turbulence which adversely affects the stability of the arc, resulting in failure of the constrictor segments. Therefore, the primary or arc-heated gases must be either inert or nonoxidizing; the remainder of the test gases required to make up the

---

*Kinetic rate data in Reference 6 substantiates the inert behavior of N_2.

propellant simulation are injected in the plenum section. This results in lower overall APG effi-
ciencies due to the portion of the test gas which is not directly arc heated and the losses to the
plenum section from both the arc heated primary gases and the exothermic reactions which take place
in the plenum. The net effect is lower test gas temperature and hence lower test sample surface
temperature.

The "normal" APG limits of pressure, current and power input must also be considered. These,
in general, are less severe than those discussed above and typically can be accommodated through
arc heater and power supply configuration changes. It should be noted that this is especially true
with hydrogen, which is very sensitive to the gas injection configuration and arc heater constric-
tor length. The penalty for use of an improper configuration is usually very unstable arc opera-
tion.

3.2.1.4 Potential Test Gases

As described in Section 3.2.1.2, the potentially important reactants are H_2, H_2O, and CO_2.
In an APG, various concentrations of these gases can be mixed and reacted to form the test stream.
By judicious selection, various reactants and poisons could be isolated in a systematic manner so
that appropriate reaction rate constants could be determined. Possible test gas mixtures are shown
in Table 4. These gases are separated into three groups, reactions which include H_2, H_2O, CO_2,
and CO, reactions with these gases and HCl, and reactions with HF in lieu of HCl. The surface reac-
tion designations are shown in Table 5. The number of test gases to be used in a material charac-
terization test matrix would be selected as a subset of the gases tested in Table 4. This selection
will be based upon a trade-off between the degree to which a particular reactant (or poison) can be
isolated and the operating limitations of the APG. Note that the exhaust gas composition is only
representative and that all gases that contain CO will also have CO_2 in small quantities. At high
temperatures, it is not possible to have large concentrations of CO_2 in the presence of H_2 since
the preferred species would be H_2O and CO.

3.2.2 Test Gas Selection

The gases shown in Table 4 that contain HCl and HF require special toxic gas handling sys-
tems. The current Aerotherm APG facility is equipped to handle HCl, although a number of nontrivial
additions are required before HF can be used. For this reason, test gases that contained HF were
eliminated during the test gas selection.

27

TABLE 4. POTENTIAL APG-MATERIAL CHARACTERIZATION TEST GASES

No.	APG Input Gases Relative Moles							Equilibrium Exhaust Gases Relative Moles							Surface Reactions (See Table 5)
	H_2*	O_2	CO_2	CO	Ar*	HCl	CF_4	R^+	H_2	H_2O	CO	Ar	HCl	HF	
1	1							0	1						1
2	9	4						7	1	8					1,2
3	8	1						2	6	2					1,2,4
4	9		8					20	1	8	8				1,2,3,4
5	2		1	1				11	1	1	1				1,2,3,4
6	8	1						4	6	2	1				1,2,3,4
7	2	1			4			0.2		2		4			2,4
8	2	1		2	4			0.5		2	2	4			2,4
9	10					1		1	10				1		1,5
10	8	1				1		3	6	2			1		1,2,5
11	16		2			8		8	12	4	2		8		1,2,3,4,5
12	9	1	8			1		20	1	8	8		1		1,2,3,4,5
13	12		6			1		12	6	6	6		1		1,2 3,4,5
14	52	7					2	5	36	12	2			8	1,2,3,4,6
15	20	3					2	7	12	4	2			8	1,2,3,4,6
16	11	4	1				1	12	1	8	2			4	1,2,3,4,6
17	16	1					2	4	12		2			8	1,3,4,6
18	18	2	1			4	1	7	12	4	2		4	4	1,2,3,4,5,6

* Arc heated gas

+ Mass ratio of plenum injected to arc heated gases (approximate)

28

TABLE 5. SURFACE REACTIONS

Reaction No.	
1	$2C* + H_2 \rightarrow 2C_2H_2$
2	$C* + H_2O \rightarrow H_2 + CO$
3	$C* + CO_2 \rightarrow 2CO$
4	CO Inhibition
5	HCl Inhibition
6	HF Inhibition

3.2.2.1 Test Gas Evaluation

Test gases 1 through 8 have been evaluated under a wide variety of APG conditions using both water-cooled calorimeters and carbon test sections. These tests clearly show that test gases 2 and 4 resulted in anomalous heating conditions. The probable cause can be defined by considering the schematic of the APG shown in Figure 1. In normal operations, H_2 or an inert gas such N_2, Ar, or He is used as the arc heated column and all other gases are injected between the arc column and the plenum chamber. If we consider test gas 2 as an example, the ratio of injection gas (O_2) to arc column gas (H_2) is 4/9. However, mixing of the two gases will be dependent upon their relative mass rates. A simple conversion shows that the relative mass of injection gas to arc column gas is approximately 7/1. It was originally anticipated that combustion induced turbulence could result in adequate mixing in the plenum, however, measured data suggested a high concentration of low enthalpy injection gases near the walls of the test section. This rather poor mixing of arc heated and injection gases made the test data impossible to adequately analyze. Subsequent trial and error experimentation showed that ratios of injected gas to arc heated gas of less than 5 (by mass) would result in adequate plenum chamber mixing.* Thus test gas number 5 was also eliminated.

Experimentation with test gases 4 and 10 revealed a second difficulty. The kinetic reaction rates of CO_2 with H_2 are much slower than those of H_2 with O_2. In fact, some simple kinetic calculations revealed that there was insufficient residence time in the plenum chamber to attain thermochemical equilibrium. Thus, all gases which would normally inject CO_2 would be replaced by an equivalent combination of CO and O_2.

From the above discussion, HCl test gases 12 and 13 can be eliminated outright, however, gas number 11 can be made acceptable by reducing the relative moles of HCl from 8 to 2.

3.2.2.2 Recommended Test Gases for Full Characterization Studies

Based upon the discussion in Section 3.2.2.1, the test gases for material characterization studies were reduced to the subset shown in Table 6. Note that CO_2 was not used as an injection gas and that it was replaced by an equivalent quantity of O_2 and CO. Note also that HF gases were not included since the advisability of testing with HF has not yet been assessed.

---

*It is assumed that at least one of the injected gases will be O_2 so that there will be combustion induced turbulence.

TABLE 6. RECOMMENDED MATERIAL CHARACTERIZATION TEST GASES

No.	APG Input Gases Relative Moles					$R^\dagger$	Equilibrium Exhaust Gases Relative Moles					Surface Reactions (see Table 5)
	H_2*	O_2	CO	Ar*	HCℓ		H_2	H_2O	CO	Ar	HCℓ	
1	1					0	1					1
2	2	1		4		0.2		2		4		2,4
3	8	1				2	6	2				1,2,4
4	8	1	1			4	6	2	1			1,2,3,4
5	2	1	2	4		0.5		2	2	4		2,4
6	10				1	1	10				1	1,5
7	8	1			1	3	6	2			1	1,2,3
8	8	1	1		1	5	6	2	1		1	1,2,3,4,5
9				1		0				1		Inert Gas

*Arc heated gas

†Mass ratio of plenum injected to arc heated gases (approximate)

31

With the exception of the HF inhibitor, all other surface reactants are represented by this set of reactions. It is clearly not possible to isolate reactions other than H_2 since oxygen-bearing species (CO_2, H_2O) will react with solid carbon to form CO and in gas phase equilibrium, a small quantity of CO_2 will also be present. The reactions shown in Table 6 represent a good compromise between the desire to isolate reactants and still stay within the operating limitations of the APG. An inert gas was also included in Table 6 to test for shear removal affects. Inert gas tests were run at the highest heating conditions compatible with APG limitations. With 3 tests for 5 reacting gas mixtures, 2 tests for 3 mixtures, and 1 for the inert gas test, a minimum of 22 tests were required. Six additional tests were planned as contingency or repeat tests and were performed as required. Thus, a total of 28 tests were planned for each characterization material.

3.2.2.3 Selection of Test Gases for Limited Characterization Studies

Since fewer samples were to be used for the limited characterization materials than the fully characterized materials, more stringent criteria were imposed on the selection of these test gases. Test gases should satisfy the following thermal performances, without exceeding the performance limitations of the arc plasma generator:

- High condition — $q_{c.w.}$ = 1600 Btu/ft²sec, run time = 80 sec

- Medium condition — $q_{c.w.}$ = 1200 Btu/ft²sec, run time = 100 sec

- Low condition — $q_{c.w.}$ = 1000 Btu/ft²sec, run time = 120 sec

Furthermore, these test gases should also be able to characterize the surface reactions as shown in Table 5.

The test gases were selected statistically from the results of the full characterization studies. The probable error for each test gas with respect to the least square curve fit for all test gases was determined in the process of correlating kinetic data. The test gas with the least probable error was considered to be the potential candidate for limited characterization studies. The results of the statistical evaluation of test gases for each generic material are shown in Figures 9 through 11.

Further analyses are required to reach the final set of test gases for limited characterization studies. The reason is that test gases which were selected statistically may serve a similar purpose in characterizing surface reactions. Such redundancy should be avoided if the number of data to be taken are limited. For example, in determining test gases for carbon/carbon materials,
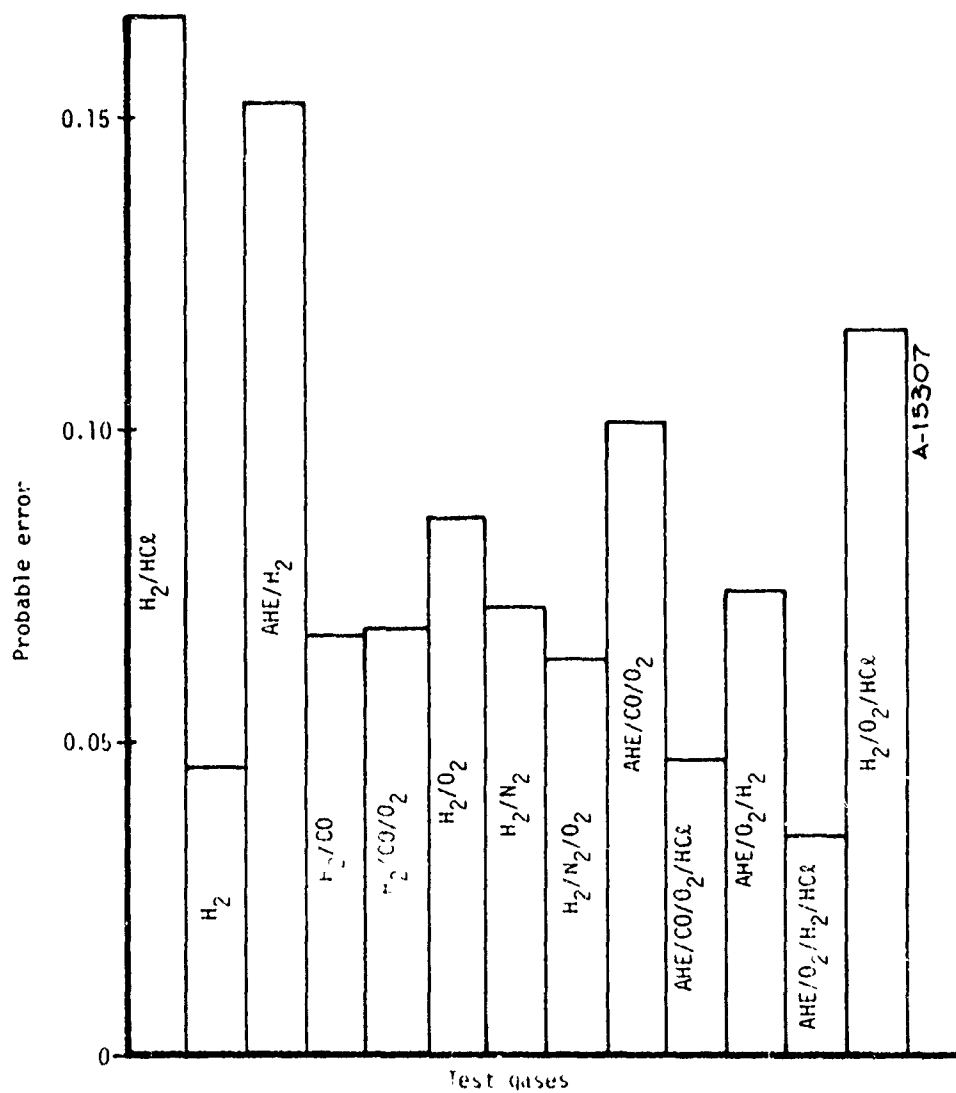
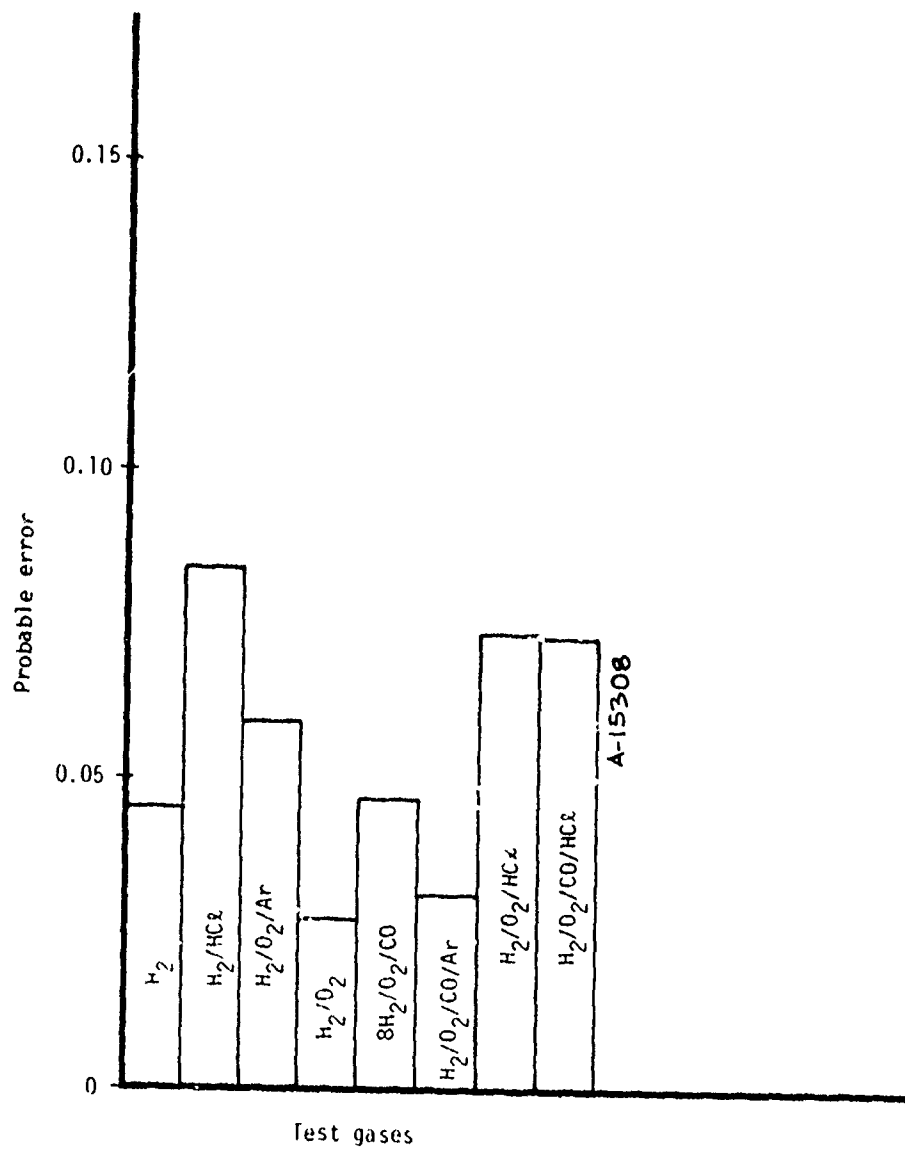Figure 9. Statistical evaluation of test gases, layer pyrolytic graphite.

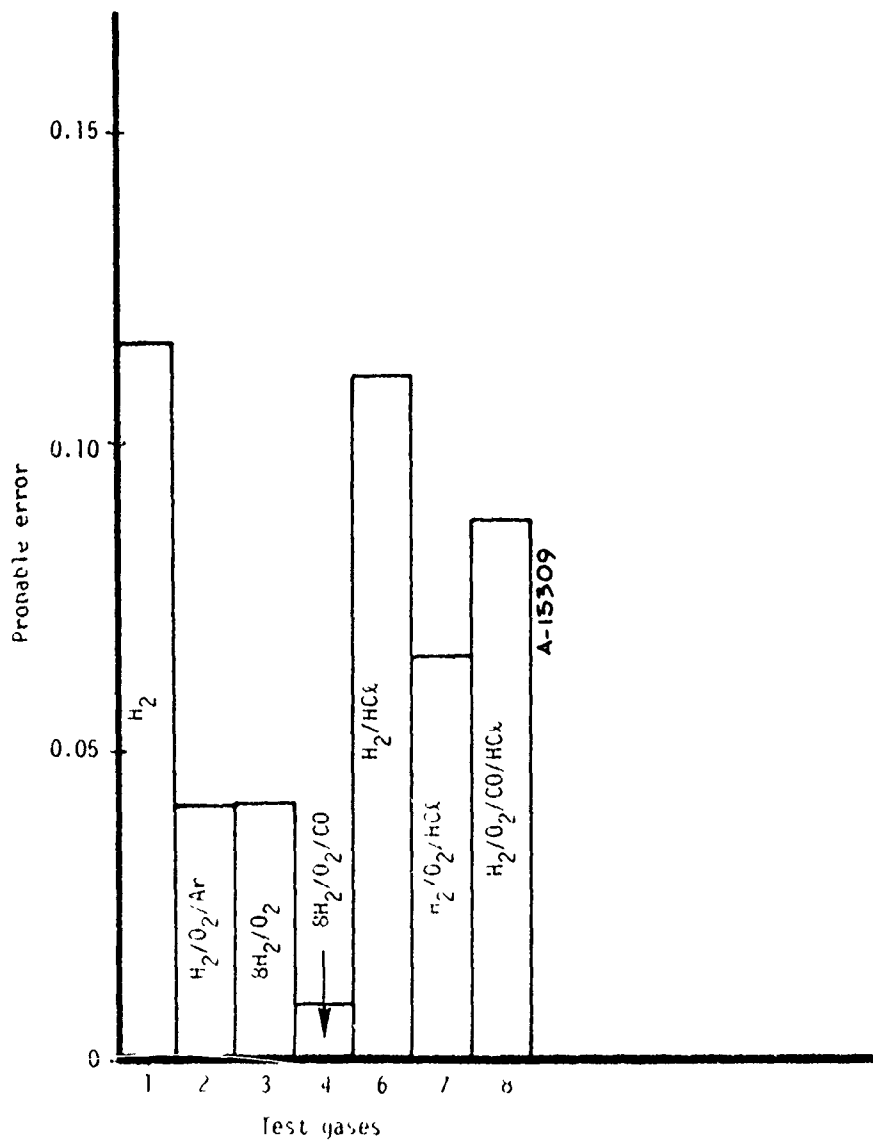Figure 10. Statistical evaluation of test gases, ATJ bulk graphite.

Figure 11. Statistical evaluation of test gases,
Pyrocarb 901 carbon/carbon composite.

from a minimum error standpoint, test gases 2, 3, and 4 (see Figure 11) should be selected. However, they do not provide enough isolation of specific reaction to be a good screening gas set. To arrive at the final screening gas set, gas 2, which is similar to gas 3, was replaced by gas 1 in order to get an isolation of H_2 reaction. Similarly, gas 4 was replaced by gas 7 in order to assess $HC\ell$ inhibition. As for CO inhibition, a test gas with an arbitrary amount of CO is not required for all gas systems with O_2. Thus, the final test gases selected for limited characterization of carbon/carbon are 1, 3, and 7. Similar arguments were used for other generic materials. The resultant sets of limited characterization test gases are shown in Table 7.

3.3 CARBON MATERIALS SURFACE KINETICS CORRELATION PROCEDURE

The ability to achieve a successful empirical formula which describes the reactivity of a carbon surface with propellant gases depends strongly on the selection of the correlation function and the kinetically-controlled reactions. Based on previous Aerotherm experience (Reference 2), the surface kinetics of pyrolytic graphite were correlated by applying the Langmuir-Hinshelwood model and assuming that the following reactions were kinetically controlled:

$$C^* + H_2O \rightarrow H_2 + CO$$

$$C^* + CO_2 \rightarrow 2CO$$

$$2C^* + H_2 \rightarrow C_2H_2$$
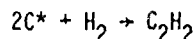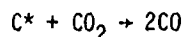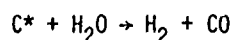
These kinetically controlled reactions can be inhibited by H_2O, CO_2, CO, H_2, $HC\ell$, and HF.

Since it is logical to conclude that all carbon materials have similar kinetic behavior, the same kinetic model was adopted to correlate all the fully characterized materials. In addition, the mass consumption rate due to sublimation is included when surface temperatures exceeding 6000°F are expected.

Carbon surface kinetics based on the Langmuir-Hinshelwood model is given by:

$$\dot{m}_c = \sum_i \frac{A_i T_w^{n_i} e^{-E_i/RT_w} \left(P_i - \frac{1}{K_{P_i}} \Pi P_{prod_i} \right)}{1 + \sum_j A_{ij} P_j} \tag{3}$$

where the subscript i denotes each of the reactants, H_2O, CO_2, and H_2. The numerator of Equation (3) describes the surface reaction with gas phase species, and the denominator describes the

TABLE 7. RECOMMENDED TEST GASES FOR LIMITED CHARACTERIZATION STUDIES

Test Gas No.	Modified Pyrolytic Graphite	Bulk Graphite	Carbon/ Carbon	Surface Reactions (See Table 5)
1	✓	✓	✓	1
3	✓	✓	✓	1, 2, 4
7	✓		✓	1, 2, 3
8		✓		1, 2, 3, 4, 5

surface coverage by gas phase species. As can be seen, the surface reaction can be retarded if the surface is either desorption controlled or is poisoned by species such HCℓ or HF.

The correlation function requires further manipulation before applying an Aerotherm least squares fitting program to determine the coefficients. Usually, the following assumptions are made to simplify the correlation function: the reverse rate is negligible compared to the forward rate, and H_2O and CO_2 surface reactions have the same activation energy and the same inhibiting effect by the gas phase species. These two assumptions can be easily removed if sufficient kinetic data are available. With these two assumptions, Equation (3) can be rewritten as:

$$MC = B_1 e^{-E_1/RT_w} = \frac{\dot{m}_c}{\dfrac{P_{H_2}}{D_1} + \dfrac{B_2 T^{n_2} e^{-E_2/RT_w}\left(P_{H_2O} + B_3 P_{CO_2}\right)}{D_2}} \qquad (4)$$

where

$$D_1 = \left[1 + (AP)_{H_2O} + (AP)_{CO_2} + (AP)_{CO} + (AP)_{H_2}\right]_{H_2} \qquad (5)$$

$$D_2 = \left[1 + (AP)_{H_2O} + (AP)_{CO_2} + (AP)_{CO} + (AP)_{H_2}\right]_{H_2O, \, CO_2} \qquad (6)$$

The coefficients which must be determined from the data analysis are A, B, n, and E.

The data required to correlate carbon material surface kinetics were obtained from arc plasma generator (APG) and motor firing tests. The APG data provides information on total surface recession, surface temperature, experimental time, and reactive gas chamber conditions. These data have a relatively low surface temperature (3000°R - 5500°R) and edge pressure (2 - 7 atm) range, but can be utilized to characterize H_2O and CO_2 surface reactions. The motor firing data provides similar information except that the surface temperature is unknown. However, this surface temperature can be estimated with a semi-infinite slab analytical solution. The motor data generally have higher surface temperatures (5500°R - 6000°R) and edge pressures (30 - 100 atm) than the APG, and can be used to characterize the H_2 surface reaction.

These raw data required further reduction before use to determine the kinetic coefficients. This data reduction procedure is described in the next section. The reduced data contains information on $\dot{m}_c$, T_w, P_e, and surface composition.

Given a sufficient number of data points with $\dot{m}_c$, T_w, P_e, and surface composition known, the coefficients in Equations (4), (5), and (6) can be determined using an Aerotherm least squares fitting program. In principle, the coefficients are adjusted systematically to minimize the residual of the least squares curve fit through a plot of log (MC_i) versus T_{wi}. The systematic adjustments of the coefficients are based upon the method of steepest descent in the vector space of $R(A_i, B_i, E_i)$. Because of the large number of coefficients and the fact that there is no assurance that the residual R is unimodal, there may be several local minimums. Whether or not the true minimum is "discovered" by the optimization search depends largely upon the initial prescribed values of the coefficients.

Because the current data presumes no advance knowledge of the reaction kinetics of the fully characterized graphite materials, the starting point of the optimization search was arbitrarily started with the coefficients determined for c plane oriented pyrolytic graphite (see Reference 6).

Since the surface temperatures for the motor firings were approximated with a best guess solution, it was necessary to analyze the data in the following steps to arrive at the final kinetic coefficients.

1. A correlation of the APG data and the motor firing data (based on approximate surface temperatures) was obtained using the least squares optimum seeking code.

2. The coefficients were input into GASKET for each motor firing data point.

3. CMA solutions were obtained using the GASKET generated surface thermochemistry tables. This yielded a predicted surface response for the fully characterized graphite material.

4. The CMA results were used to update the motor firing data points. An arbitrary choice was made to use the data at the halfway point of the firing duration.

5. A second correlation was obtained from the APG data and the updated motor firing data.

SECTION 4

ANALYSIS OF APG TEST RESULTS

Arc plasma generator test data are shown in Table 8 for the full characterization materials. These data are not in a form compatible with the surface kinetics correlation procedure; hence, further data reduction was required. A procedure was set up to reduce the APG test results (P_o, H_o, K_i, T_w, ΔS, $\theta_{experimental}$) for these kinetic correlations. This procedure is as follows:

- Determine the boundary layer edge condition

- Evaluate the heat and mass transfer coefficients

- Determine the open system surface state chemical equilibrium solution using measured carbon consumption rate and surface temperature

The net effect is a relationship between carbon consumption rate, surface temperature and partial pressures of gases adjacent to the ablating surface. The reduced data before correlation, for all the full characterization carbon materials, are presented in Table 9.

APG test data for the limited characterized materials are shown in Tables 10 through 12. Because no correlations were attempted, no further reduction of this data was required.

4.1 CARBON CONSUMPTION RATE

The carbon consumption rate can be calculated from the expression:

$$\dot{m}_c = 12 \, \rho \, \frac{\Delta S}{\theta} \tag{7}$$

where ρ is the carbon density, Δs is the total measured recession (in.), and θ is the actual reaction time. However, the determination of $\dot{m}_c$ is not straightforward because θ is unknown without a prior knowledge of the surface kinetics.

One way to estimate the reaction time is to assume the tested carbon material has a kinetic response similar to edge PG. Substitution of the measured surface temperature history into the edge PG surface kinetics expression allows a recession rate history to be obtained. The reaction time is approximately the time interval between the final time and the time where the recession rate suddenly increases.

41

TABLE 8. ARC PLASMA GENERATOR DATA FOR FULL CHARACTERIZATION MATERIALS

Test Number	Model Number	Test Gas	P_o (atm)	H_o (Btu/lbm)	T_w (°R)	$\dot{m}$ (lb/ft²sec)	Δs (mils)	θ_{exp} (sec)
G-90								
2809-1	178 C	1	3.25	35,700	4300	0.0007788	1.58	39.0
2810-1	169 C	1	3.48	46,230	5000	0.002214	7.30	59.0
2811-1	177 C	1	3.55	55,500	5358	0.002370	11.80	52.0
2813-1	196 C	3	5.20	8,470	4150	0.009755	56.40	62.0
2814-1	176 C	3	5.18	10,930	4400	0.01214	35.10	32.0
2815-1	168 C	3	4.825	14,630	4899	0.01126	59.40	39.5
2817-1	167 C	4	5.13	6,300	4300	0.008424	28.20	49.0
2818-2	194 C	4	5.10	6,970	4850	0.009599	48.20	55.0
2820-2	195 C	2	5.00	2,590	4800	0.007652	39.20	-56.0
2821-2	187 C	2	4.95	2,060	4750	0.009083	41.00	59.0
2823-3	163 C	5	6.25	1,440	4800	0.01046	40.30	59.0
2823-5	172 C	5	6.25	980	4350	0.007058	31.50	59.0
2826-2	186 C	6	5.60	14,950	5200	0.004946	14.80	42.5
2828-1	171 C	6	5.70	12,750	4900	0.003918	15.70	58.0
2829-2	185 C	6	5.40	10,210	4350	0.0007746	2.75	56.5
2831-2	162 C	7	4.32	12,880	4850	0.005305	26.10	59.5
2832-2	170 C	7	3.98	12,480	4850	0.004878	24.00	61.5
2833-2	161 C	7	4.00	10,260	4600	0.006103	19.50	47.5
2836-2	190 C	8	5.30	12,340	5000	0.004929	23.50	56.5
2838-2	184 C	8	5.05	12,140	4800	0.004667	21.30	59.0
ATJ								
2585-1	003 C	1	4.48	64,000	4900	0.000999	6.71	61.0
2589-2	004 C	3	5.50	8,190	3860	0.00770	33.90	40.0
2591-1	005 C	3	5.50	13,700	4500	0.0110	47.80	39.5
2592-1	006 C	3	5.70	16,700	4750	0.0117	52.80	41.0
2593-1	007 C	1	4.20	55,130	4900	0.00102	4.38	39.0
2594-1	009 C	3	5.00	9,520	4100	0.00908	53.00	52.0
2597-1	010 C	4	5.85	9,300	4600	0.00830	44.30	48.5
2607-1	008 C	2	7.70	911	3720	0.0166	89.00	48.5
2609-1	011 C	2	4.80	4,030	3980	0.01903	84.80	40.5

TABLE 8. Continued

Test Number	Model Number	Test Gas	P_o (atm)	H_o (Btu/lbm)	T_w (°R)	$\dot{m}$ (lb/ft²sec)	Δs (mils)	θ_{exp} (sec)
ATJ (Concluded)								
2617-1	013 C	2	5.35	2,930	3860	0.00810	39.20	38.0
2619-1	014 C	5	6.40	1,800	4000	0.00733	34.70	44.5
2619-2	015 C	5	6.40	1,660	4200	0.00896	43.40	43.0
2620-2	016 C	5	7.15	1,460	3580	0.00395	10.00	24.0
2620-3	017 C	5	6.45	905	3720	0.00540	26.40	44.5
2815-3	019 C	3	5.10	14,700	4950	0.01325	52.50	40.0
2817-3	028 C	4	5.30	5,560	4500	0.01998	82.50	48.0
2818-1	029 C	4	5.00	6,430	4450	0.010991	48.40	45.0
2818-4	030 C	4	5.25	7,000	4800	0.00903	50.70	54.0
2820-1	027 C	2	5.00	2,550	4900	0.01075	50.30	55.0
2823-1	020 C	5	5.45	1,470	4750	0.008819	53.40	59.0
2826-1	021 C	6	5.70	14,710	5300	0.004192	15.00	37.0
2827-1	022 C	6	5.63	13,250	5050	0.003292	14.50	57.0
2829-3	023 C	6	5.16	[10,280]	4600	0.0008054	2.66	--
2831-3	024 C	7	4.30	13,280	4850	0.004814	26.50	59.0
2832-3	025 C	7	4.30	11,810	4850	0.004723	27.30	60.0
2834-1	031 C	7	4.05	9,290	4500	0.004704	24.60	38.5
2837-1	018 C	8	4.85	12,940	5000	0.004872	20.25	48.5
2838-3	026 C	8	4.95	12,640	4850	0.005450	30.00	63.0
15% SiC PG								
2668-1	104 C	4'	6.60	11,780	4850	0.01014	26.00	32.0
2669-1	105 C	4'	6.20	6,209	4000	0.00369	9.45	31.0
2672-1	106 C	1	3.35	36,590	4250	-0.0002645	-0.52	33.0
2674-1	107 C	1	3.15	31,370	4050	0.0000272	0.05	34.0
2676-1	108 C	2	6.08	2,650	3720	0.002111	2.67	32.0
2678-1	109 C	3	5.62	8,550	4150	0.004179	11.25	34.0
2679-1	110 C	3	5.50	11,880	4775	0.01493	31.90	31.0
2680-1	111 C	3	5.65	15,470	4900	0.01525	40.40	32.0
2705-1	114 C	7	4.32	9,890	3760	0.0002457	1.05	58.0

TABLE 8. Continued

Test Number	Model Number	Test Gas	P_0 (atm)	H_0 (Btu/1bm)	T_W (°R)	$\dot{m}$ (1b/ft²sec)	Δs (mils)	θ_{exp} (sec)
15% SiC PG (Concluded)								
2707-1	115 C	7	4.58	12,180	3900	0.001577	5.73	55.5
2709-1	116 C	7	4.60	14,140	4350	0.005113	23.60	59.0
2711-1	117 C	7'	5.13	7,860	3960	0.008093	16.60	30.0
2712-1	118 C	7'	5.53	8,430	4000	0.006700	27.20	57.5
2715-1	119 C	8	4.80	10,040	4200	0.004235	20.45	60.0
2716-1	120 C	8	4.48	10,190	4150	0.003978	27.20	90.0
2719-1	121 C	3	5.28	11,680	4300	0.01086	39.90	44.0
2721-1	122 C	3	5.40	9,730	3920	0.007406	31.65	55.0
2723-1	123 C	1	3.30	31,580	4400	0.001009	4.40	57.0
2725-1	124 C	1	4.00	45,450	5050	0.004020	13.40	42.5
2727-1	125 C	4'	5.85	7,180	3780	0.002808	9.00	50.5
Pyrocarb 901								
2809-2	140 C	1	3.25	36,630	4350	0.0005241	3.08	55.0
2810-2	142 C	1	3.55	49,320	5000	0.001997	16.75	52.5
2811-2	158 C	1	3.50	55,430	5358	0.005077	21.70	59.0
2813-2	149 C	3	5.00	8,880	4150	0.009770	42.80	36.5
2814-2	150 C	3	5.00	10,300	4700	0.01116	44.70	37.5
2815-2	159 C	3	5.00	14,200	5100	0.01147	51.50	39.5
2817-2	151 C	4	5.00	6,140	4700	0.009489	58.80	56.0
2818-3	160 C	4	5.00	7,060	5100	0.01329	63.90	45.0
2820-3	137 C	2	5.00	2,540	5200	0.008035	49.80	58.0
2821-1	146 C	2	4.90	2,020	4950	0.009405	59.30	59.0
2823-2	138 C	5	6.20	1,530	5000	0.02257	72.30	60.0
2823-4	147 C	5	5.90	950	4700	0.01856	58.50	59.0
2825-1	139 C	6	4.35	14,850	5750	0.01402	47.20	38.0
2826-3	156 C	6	5.50	15,910	5500	0.006820	26.60	50.0
2828-2	157 C	6	5.65	13,250	5500	0.005640	22.60	50.0
2829-1	152 C	6	5.50	10,420	4800	0.0006405	1.54	42.0

TABLE 8. Concluded

Test Number	Model Number	Test Gas	P_0 (atm)	H_0 (Btu/lbm)	T_w (°R)	$\dot{m}$ (lb/ft²sec)	Δs (mils)	θ_{exp} (sec)
Pyrocarb 901 (Concluded)								
2831-1	143 C	7	4.75	14,010	4900	C.008084	40.60	58 5
2832-1	134 C	7	4.15	12,940	5000	0.008564	33.40	45.0
2833-1	153 C	7	3.82	9,820	4950	0.007745	24.00	48.0
2836-1	144 C	8	5.30	11,600	5000	0.009186	37.30	55.0
2838-1	154 C	8	5.00	12,170	5050	0.007721	39.60	60.5

TABLE 9. REDUCED ARC PLASMA GENERATOR DATA FOR FULL CHARACTERIZATION MATERIAL

Test ID	Test Model	Test Gas	Plenum State H_o (Btu/lbs)	P_o (atm)	T_o (°K)	$\dot{m}_{flow}$ (lb/sec)	Edge State P_e (atm)	T_e (°K)	$\rho_e u_e c_M$ (lb/ft²sec)	$\dot{m}_c$ (lb/ft²sec)	B'_{meas}	Surface State T_w (°K)	$1/T_w$ (1/°K)	Aver T_w (°K)	B'_{diff}	B'/B'_{diff}	Surface Mole Fractions XH_2O	XH_2	$XHCL$	XCO_2	XCO
C-90 2809	178 C	1	35,700	3.25	6164	0.007044	1.864	5833	0.02406	7.786-04	0.03237	2389	4.19-04	4300	0.04756	0.6807		0.98353			
2810	169 C	1	46,230	3.475	6605	0.007044	1.993	6263	0.02430	2.214-03	0.29111	2778	3.60-04	5000	0.2824	0.3226		0.93425			
2811	177 C	1	55,500	3.550	6915	0.007044	2.034	6555	0.02422	2.37-03	0.09862	2977	4.72-04	5358	0.7105	0.1380		0.88856			
2813	196	3	8,470	5.200	6358	0.02217	2.999	6052	0.0804	0.009755	0.1213	2306	4.34-04	4150	0.4216	0.2877	0.10003	0.77624			0.11587
2814	176 C	3	10,935	5.175	6556	0.02217	2.985	6288	0.0838	1.214-02	0.1449	2444	4.09-04	4400	0.4345	0.3334	0.13462	0.76871		0.002697	0.08397
2815	168 C	3	14,620	4.825	6860	0.02217	2.781	6545	0.0792	1.126-02	0.1422	2722	3.67-04	4899	0.5067	0.7806	0.05494	0.76474		0.0015734	0.14624
2817	167 C	4	6,300	5.125	6346	0.02714	2.949	5924	0.08490	8.424-03	0.05922	2389	4.19-04	4300	0.3184	0.3117	0.13271	0.69921		0.0051045	0.15541
2818	194 C	4	6,970	5.10	6452	0.02714	2.936	6131	0.06832	9.599-03	0.1087	2694	3.71-04	4850	0.3676	0.2956	0.12396	0.68471		0.004374	0.15990
2820	195 C	2	2,590	5.00	7219	0.0496	2.854	6811	0.1580	7.652-03	0.04843	2667	3.75-04	4800	0.1398	0.3465	0.14953	0.16514		0.013056	0.093780
2821	187 C	2	2,060	4.95	6888	0.04967	2.833	6516	0.1713	9.083-03	0.05302	2639	3.79-04	4750	0.385	0.3828	0.14162	0.15483		0.014723	0.10365
2823	163 C	5	1,440	6.25	6776	0.06289	3.578	6398	0.1903	1.04e-02	0.05497	2667	3.75-04	4800	0.1071	0.5131	0.07255	0.14629		0.023078	0.30279
2823	172 C	5	980	7.25	6419	0.06269	3.581	6059	0.2075	7.058-03	0.03401	2417	4.14-04	4350	0.1039	0.3300	0.10638	0.11895		0.039266	0.25720
2826	186 C	6	14,950	5.60	6738	0.02292	3.207	6376	0.0738	4.946-03	0.06702	2589	3.46-04	4200	0.043	0.3290		0.82694	0.093365		
2828	171 C	6	12,750	5.70	6476	0.02292	3.208	6120	0.0809	3.918-03	0.04843	2722	3.67-04	4900	0.1007	0.4810		0.85255	0.099473		
2829	185 C	6	10,210	5.40	6094	0.02292	3.089	5739	0.0619	7.746-04	0.009458	2417	4.14-04	4350	0.02696	0.3508		0.88022	0.10685		
2831	162 C	7	12,880	4.325	6535	0.01857	2.486	6206	0.03364	4.365-03	0.1332	2694	3.71-04	4850	0.2948	0.4516	0.03747	0.81183	0.046709	0.00046071	0.075043
2832	170 C	7	12,480	3.975	6465	0.01857	2.285	6140	0.05361	4.875-03	0.09099	2694	3.71-04	4850	0.2952	0.3082	0.055607	0.80758	0.048514	-0.0055434	0.052895
2833	161 C	7	10,260	4.00	6201	0.01857	2.298	6386	0.04140	5.123-03	0.1474	2556	3.91-04	4600	0.254	0.5817	0.026471	0.82242	0.047541	0.00042959	0.083155
2836	190 C	8	12,340	5.3	6616	0.022245	2.871	6274	0.07164	4.929-03	0.06880	2778	3.60-04	5000	0.2748	0.2504	0.043565	0.79545	0.038143	0.00066228	0.081764
2836	184 C	8	12,140	5.00	6590	0.022265	2.842	6249	0.07528	4.667-03	0.06200	2667	3.75-04	4800	0.2291	0.2706	0.048011	0.80620	0.039038	0.00071799	0.078446

46

TABLE 9. Continued

Test ID	Test Model	Test Gas	W₀ (Btu/lbm)	P₀ (atm)	T₀ (°R)	ṁ_flow (lb/sec)	P_e (atm)	T_e (°R)	ρ_e u_e C_M (lbm/ft²sec)	ṁ_c (lb/ft²sec)	B'_meas	T_w (°R)	1/T_w (1/°K)	Aver T (°R)	B'_diff	B'/B'_diff	CH₂O	AH₂	AHCL	XCO₂	XCO
ATJ Graphite																					
2584	002 C	1	43,400	3.90	6544	0.0704	2.24	6199	0.0189	—	0	2722	3.67-04	4900	0.2164	0.2583	0.14533	0.95413			
2585	003 C	2	64,000	4.80	7297	0.0704	2.74	6902	0.0232	.1267	0.0559	2144	4.67-04	3860	0.4130	0.3262	0.13189	0.77018		0.002984	0.07946
2589	004 C	3	8,190	6.13	6266	0.0222	3.53	5943	0.0661	0.015	0.1347	2500	4.00-04	4500	0.4408	0.3308	0.13189	0.76871		0.002375	0.08425
2589	005 C	3	13,700	6.50	6377	0.0222	3.74	6043	.0950	0.0140	0.1458	2639	3.79-04	4750	0.4720	0.3699	0.11067	0.76681		0.002195	0.09795
2591	006 C	3	16,700	6.63	6729	0.0222	3.84	6781	0.0945	0.0165	0.746	2722	3.67-04	4900	0.2163	0.3250		0.9522			
2592	007 C	1	25,730	6.63	6975	0.0704	2.42	6607	0.0236	0.00165?	0.0703	2278	4.39-04	4100	0.4184	0.3250	0.14302	0.76969		0.002728	0.08000
2594	009 C	3	9,520	6.07	6434	0.0271	3.49	6311	0.0831	0.0113	0.1360	2556	3.91-04	4600	0.3345	0.2758	0.10779	0.70451		0.004138	0.16854
2597	010 C	4	9,300	6.81	7373	0.0271	3.92	6531	0.1002	0.0126	0.1257	2067	4.84-04	3720	0.3282	0.3437	0.24606	0.17809		0.03747	0.12914
2607	008 C	2	911	10.00	6007	0.0762	4.43	5699	0.1933	0.0278	0.1128	2211	4.52-04	3980	0.3402	0.4565	0.22776	0.29484		0.3123	0.21183
2609	011 C	2	4,050	5.74	7126	0.0400	3.30	6791	0.1500	0.033	0.1553	2144	4.66-04	3860	0.2532	0.2887	0.27235	0.22602		0.02669	0.11129
2617	013 C	2	2,930	6.08	6986	0.0497	3.50	6641	0.1409	0.0103	0.0731	2222	4.50-04	4070	0.1026	0.6614	0.5975	0.16171		0.02202	0.31441
2619	014 C	5	1,800	7.54	7021	0.0629	3.66	6619	0.1767	0.0106	0.0617	2222	4.50-04	4070	0.1026	0.4995	0.07103	0.15038		0.02678	0.29363
2619	015 C	5	1,660	7.59	6909	0.0629	3.65	6517	0.1946	0.0100	0.0514	2333	4.29-04	4230	0.1029	0.4995	0.07103	0.15038		0.02678	0.29363
2620	016 C	5	1,460	7.47	6899	0.0629	4.09	6423	0.2373	0.0076	0.0320	1989	5.03-04	3580	0.1018	0.3143	0.10654	0.13469		0.04347	0.24663
2620	017 C	5	995	7.26	6326	0.0629	3.69	5965	0.2222	0.00799	0.0350	2067	4.84-04	3720	0.1012	0.3550	0.09897	0.1243		0.04318	0.25827
2615	019 C	3	14,700	5.10	6887	0.02217	2.939	6568	0.06622	0.01325	0.1537	2750	3.64-04	4950	0.5198	0.2957	0.12290	0.75195		0.0021227	0.08700
2817	028 C	4	5,560	5.30	6224	0.02714	3.046	5899	0.08969	0.01998	0.1290	2500	4.00-04	4500	0.3306	0.6746	0.046553	0.71010		0.0024632	0.22963
2818	029 C	4	6,430	5.00	6360	0.02714	2.878	6239	0.08519	0.01099	0.1290	2472	4.04-04	4450	0.3765	0.3951	0.10990	0.70063		0.0045335	0.17369
	030 C	4	7,000	5.25	6465	0.02714	3.022	6143	0.08855	0.00903	0.020	2667	3.75-04	4800	0.3604	0.2830	0.12839	0.68634		0.0044822	0.15590
2820	027 C	2	2,550	5.00	7363	0.04967	2.855	6788	0.576	0.01075	0.0682	2722	3.67-04	4900	0.1415	0.4825	0.10927	0.17881		0.12299	0.13354
2823	020 C	5	14,0	5.45	6757	0.06289	2.12	6383	0.1706	0.00362	0.0517	2639	3.79-04	4750	0.1063	0.4362	0.07694	0.13954		0.0253C	0.29614

47

TABLE 9. Continued

Test ID	Test Model	Test Gas	Plenum State				Edge State			Surface State								Surface Mole Fractions				
			H_o (Btu/lbm)	P_o (atm)	T_o (°R)	$\dot{m}_{flow}$ (lb/sec)	P_e (atm)	T_e (°R)	$\rho_e c_e u_e$ (lb/ft²sec)	$\dot{m}$ (lb/ft²sec)	B_{meas}	T_w (°K)	$1/T_w$ (1/°K)	Aver T_w (°R)	B_{diff}	B'/B'_{diff}	XH_2O	XH_2	$XHCl$	XCO_2	XCO
ATJ Graphite (Concluded)																					
2826	021 C	6	14,710	5.70	6719	0.02292	3.265	6357	0.0705	0.04192	0.0563	2544	3.60-04	5300	0.2582	0.2180		0.8193	0.093692		
2827	022 C	7	-3,250	5.625	6540	0.02292	3.222	6184	0.0814	0.03293	0.0410	2806	3.56-04	5050	0.1432	0.2963		0.8437	0.099432		
2829	023 C	6	[10,280]	5.160	6092	0.02292	2.952	5739	0.0781	0.0008054	-0.01031	2555	3.91-04	4600	0.0496	0.2081		0.8724	0.10567		
2831	024 C	7	12,285	4.3	6574	0.01657	2.471	6244	0.03959	0.004814	0.1216	2694	3.71-04	4850	0.2948	0.4126	0.038688	0.81134	0.047072	0.00050097	0.059029
2832	025 C	7	11,810	4.3	6418	0.01857	2.471	6091	0.05724	0.004723	0.08251	2694	3.71-04	4850	0.2951	0.2796	0.060745	0.80757	0.049171	0.00055388	0.048381
2834	031		9,293	4.05	5926	0.01857	3.0	5622	0.04134	0.004704	0.1138	2500	4.00-04	4500	0.2423	0.4696	0.044903	0.82337	0.049458	0.0005913	0.065977
2837	018 C	8	12,940	4.87	6674	0.022444	3.099	6331	0.07054	0.004872	0.06956	2778	3.60-04	5000	0.2754	0.2526	0.042868	0.79458	0.037895	0.0005332	0.081904
2838	02C	7	12,640	4.95	6632	0.022265	2.77	6291	0.07254	0.00545	0.07573	2694	3.71-04	4850	0.2384	0.3176	0.040174	0.80469	0.03285	0.0004895	0.085405
2668	104 C	4	.780	6.60	6975	0.0277	3.791	6624	0.432	7.014-02	0.2347	2694	3.71-04	4850	0.5623	0.4174	0.11259	0.72851		0.29119-2	0.12379
2669	105 C	4	6,210	6.20	6379	0.0272	3.566	6056	0.2532	3.69-03	0.0654	2222	4.50-04	4000	0.3265	0.2123	0.15852	0.69959		0.56096-2	0.13062
2672	106 C	1	36,590	3.35	6414	0.0007044	2.922	5681	0.0270	-2.645-04	-0.0098	2381	4.24-04	4250	0.04669	-0.2099		0.99059			
2674	107 C	1	31,370	3.15	5947	0.022044	1.855	5667	0.0255	2.72-05	0.00107	2250	4.44-04	4050	0.32699	0.0396	0.40272	0.99430			
2676	108 C	2	2,650	6.06	6886	0.4967	3.497	6555	0.1128	2.11-03	0.0187	2067	4.84-04	3720	0.2694	0.0694	0.19319	0.16746		0.11614-1	0.23003-1
2678	109 C	5	8,550	5.625	6291	0.02217	3.237	5971	0.0609	4.179-03	0.0686	2306	4.34-04	4150	0.4495	0.1526	0.94733-1	0.75984		0.17442-2	0.37971-1
2679	110 C	3	11,880	5.50	6650	0.02217	3.167	6329	0.0670	1.493-02	0.2226	2653	3.7-04	4775	0.5204	0.4281	0.21143-2	0.76254		0.21143-2	0.65917-1
2680	111 C	3	15,470	5.65	6966	0.01854	3.250	6635	1.36	1.525-02	0.1290	2722	67-04	4900	0.5488	0.2350	0.14327	0.75297		0.19189-2	0.18096-2
2705	114 C	7	9,890	4.32	6164	0.01854	2.639	5856	0.0986	2.457-04	0.00317	2083	5.79-04	3760	0.2242	0.01414	0.11516	0.82342	0.57150-1	0.52305-4	0.14869-1
2707	115 C	7	12,180	4.58	6482	0.01854	2.632	6150	0.0986	1.577-03	0.0269	2167	4.61-04	3902	0.2240	0.1701	0.96716-1	0.83056	0.53879-1	0.33955-3	0.53417-1
2709	116 C	7	14,140	4.60	6662	0.01854	2.643	6348	0.049	5.113-03	0.1029	2417	4.-04	4350	0.2457	0.4189	0.52672-1	0.83111	0.49146-1	0.57681-3	

48

TABLE 9. Continued

Test ID	Test Wr	Test Gas	Q (Btu/lb)	C str				Case State ρe (atm)	e (L)	ρe/0 ser	b̄ sec	ρe V̄ lb/ft·sec	Bmeas	T (°K)	ā (1/°R)	Aver T (°R)	Bdiff	B/Bdiff	XH2O	XH2	XHCL	XCO2	XCO
2711	117	7	7,426	5.22		6450	0.0246	2.95	6132	0.0636	8.29-03	0.1272	2290	4.55-04	3960	0.3519	0.3615	0.12577	0.73556	0.49842-1	0.25811-2	0.78590-1
2712	118	7	8,433	5.525		6552	0.02448	3.181	6231	0.0679	6.70-03	0.1000	2206	4.55-04	4000	0.3513	0.2846	0.14429	0.73411	0.49823-1	0.23725-2	0.62836-1
2715	119	8	10,040	4.80		6316	0.0203	2.755	5975	0.0456	4.235-03	0.0929	2333	4.29-04	4230	0.2794	0.3325	0.81855-1	0.81694	0.41526-1	0.38196-3	0.49431-1
2716	120	8	10,150	4.88		6342	0.0203	2.801	6004	0.0504	3.978-03	0.0789	2306	4.34-04	4150	0.2766	0.2853	0.89792-1	0.81658	0.42049-1	0.84213-3	0.42391-1
2719	12		11,860	5.275		6617	0.0222	3.038	6398	0.0467	7.086-02	0.2325	2369	4.19-04	4300	0.4550	0.5110	0.93797-1	0.77778		0.23197-3	0.11494
2721	122		5,170	5.40		6427	0.0222	3.10	6103	0.0368	7.406-03	0.1351	2178	4.59-04	3920	0.4392	0.3076	0.14849	0.77102		0.26636-3	0.71178-1
2723	123	1	31,580	3.36		5980	0.0704	1.891	5629	0.0239	1.097-03	0.0422	2444	4.09-04	4400	0.06938	0.0608		0.97698			
2725	124	1	45,410	4.00		6626	0.0704	2.243	6281	0.0285	4.323-03	0.1410	2806	3.56-04	5050	0.3604	0.3913		0.92538			
2727	125	4	110	5.85		6318	0.0272	3.361	5983	0.0720	2.808-03	0.0390	2100	4.76-04	3780	0.4747	0.3822	0.25598	0.7157		0.17312-2	0.23603-1
Pyroceram 901																						
2809	140		34,600	3.250		6206	0.007044	1.864	5875	0.02400	0.0007467	0.02096	2417	3.72-04	4350	0.05433	0.3858		0.98388			
2810	142		44,370	3.55		6739	0.007044	2.035	6370	0.02587	0.001997	0.0779	2778	3.60-04	5000	0.28149	0.2737		0.93671			
2811	136		54,430	3.52		6900	0.007544	2.065	6546	0.02454	0.005077	0.2112	3056	3.27-04	5356	0.3211	0.2971		0.85039			
2813	149	3	3,690	5.00		6389	0.02217	2.864	6065	0.0790	0.009770	0.1237	2306	4.34-04	4150	0.4211	0.29374	0.15065	0.76836		0.002569	0.07310
2814	150	3	13,500	5.04		6527	0.0222	2.864	6227	0.07688	0.01116	0.1452	2611	3.83-04	4700	0.4734	0.3086	0.13404	0.75825		0.002331	0.9402
2815	159	3	14,200	5.00		6843	0.0222	2.84	6527	0.03483	0.009469	0.1352	2833	3.53-04	5100	0.5706	0.237	0.13314	0.73877		0.002024	0.077267
2817	151	4	6,140	5.00		6	0.0274	2.877	5993	0.0450	0.009469	0.1123	2611	3.83-04	4700	0.3483	0.3224	0.12194	0.68984		0.0045311	0.16329
2818	164	4	7,660	5.00		6450	0.0274	2.879	6130	0.08394	0.01329	0.1583	2633	3.53-04	5100	0.4200	0.3769	0.085971	0.67627		0.003786	0.18829
2820	37		7,440	5.00		7184	0.0496	2.855	6766	0.054	0.006035	0.05171	2889	3.46-04	5200	0.1507	0.3431	0.13709	0.73817		0.012431	0.10037
282?	146		2,???	4.90		6595	0.0496	2.854	6500	0.1084	0.009405	0.05585	2750	3.54-04	4950	0.149	0.3335	0.13396	0.15301		0.014318	0.10956

49

TABLE 9. Concluded

TABLE 10. ARC PLASMA GENERATOR DATA FOR LIMITED CHARACTERIZATION MATERIAL (CARBON/CARBONS)

Test Number	Nodel Number	Test Gas	P_0 (atm)	H_0 (Btu/lbm)	T_w (°R)	$\dot{m}$ (lb/ft²sec)	Δs (mils)	θ (sec)
903 Pyrocarb								
2851-1	218 S	1	3.60	55,470	5500	0.003259	16.875	49.0
2855-5	216 S	1	3.50	46,630	5300	0.002393	22.00	87.0
2860-4	219 S	1	3.33	36,820	4800	0.00046	4.76	98.0
2863-1	220 S	3	5.15	13,100	5250	0.00975	44.30	43.0
2867-6	214 S	3	4.93	7,480	4550	0.00825	40.54	46.5
2869-1	223 S	7	4.05	12,490	4800	0.00467	32.78	66.5
2872-5	217 S	7	4.10	9,710	4750	0.00454	35.55	74.0
903 HD								
2854-1	250 S	1	3.40	34,700	4700	0.000303	2.9C	99.0
2856-3	243 S	1	3.48	44,280	5200	0.001258	10.90	82.0
2858-2	247 S	1	3.48	53,980	5600	0.00309	17.00	57.0
2864-5	244 S	3	5.10	11,740	5050	0.01171	50.90	45.0
2865-3	246 S	3	5.00	6,200	4200	0.00604	36.80	63.0
2871-2	248 S	7	4.50	12,660	5100	0.00533	32.40	63.0
2874-1	249 S	7	4.60	12,840	4750	0.000802	33.32	43.0
2876-3	245 S	7	4.18	9,280	4800	0.00398	30.78	80.0
HRX-5125								
2852-1	229 S	1	3.50	40,460	4950	0.001064	13.38	100.0
2856-1	232 S	1	3.45	44,900	5250	0,001683	18.40	87.0
2859-2	228 S	1	3.65	54,630	5600	0.001684	12.38	58.5
2860-3	231 S	1	3.60	54,030	5650	0.001751	12.98	59.0
2863-2	230 S	3	4.80	12,930	5400	0.01156	52.30	36.0
2870-1	225 S	7	4.12	12,080	4950	0.00525	37.60	57.0
2875-1	226 S	7	4.35	9,760	4850	0.00391	29.70	60.5
HRX-5875								
2857-3	239 S	1	3.50	50,270	5250	0.002934	17.89	59.0
2858-1	238 S	1	3.48	50,880	5450	0.003903	23.80	59.0
2864-3	241 S	3	5.0	11,740	5150	0.004624	16.25	34.0
2870-2	240 S	7	4.08	11,830	5000	0.00420	25.60	59.0

TABLE 10. Concluded

Test Number	Model Number	Test Gas	P_o (atm)	H_o (Btu/lbm)	T_w (°R)	$\dot{m}$ (lb/ft²sec)	Δs (mils)	θ (sec)
MDAC 3-D C/C								
2854-2	199 S	1	3.40	34,120	4300	0.0001004	0.958	99.0
2861-1	198 S	1	3.68	53,470	5450	0.0007621	4.625	58.0
2864-4	200 S	3	5.15	11,520	5050	0.01255	53.71	44.5
2866-1	202 S	3	5.12	6,100	4300	0.002574	14.85	60.0
2870-3	197 S	7	4.35	11,910	5100	0.00469	26.62	59.0

TABLE 11. ARC PLASMA GENERATOR DATA FOR LIMITED CHARACTERIZATION MATERIAL (BULK GRAPHITES)

Test Number	Model Number	Test Gas	P_o (atm)	H_o (Btu/lb)	T_w (°R)	$\dot{m}$ (lb/ft²sec)	Δs (mils)	θ (sec)
PO 3								
2584-2	034 S	1	3.68	41,900	4450	0.0002138	1.33	59.0
2585-2	035 S	1	4.55	61,900	3200	0.002931	13.60	44.0
2585-3	036 S	1	4.60	62,200	—	0.001810	9.54	50.0
2589-1	037 S	3	5.35	7,950	3700	0.00946	46.90	47.0
2592-2	038 S	3	5.95	16,350	5000	0.01027	39.20	36.2
2596-1	039 S	4	5.55	6,570	4100	0.00763	37.80	47.0
2617-2	068 S	2	5.40	2,680	4200	0.00808	39.20	46.0
2855-3	070 S	1	3.53	45,520	5150	0.05900	7.64	83.0
2878-2	071 S	8	4.95	10,740	4800	0.00241	17.16	67.5
2878-4	069 S	8	4.75	8,630	4150	0.00258	21.77	80.0
ATJ-S								
2617-4	076 S	2	5.70	2,520	3800	0.00582	1.864	46.0
2853-1	084 S	1	3.38	37,520	4800	0.00057	5.88	98.0
2855-2	077 S	1	3.53	44,960	5000	0.0008184	6.375	74.0
2855-4	085 S	1	3.70	55,100	5350	0.0016198	10.06	59.0
2861-3	082 S	1	3.48	54,040	5500	0.001685	10.64	60.0
2863-3	078 S	3	5.15	12,130	5150	0.009112	46.04	48.0
2867-3	081 S	3	4.92	7,560	4250	0.00562	35.50	60.0
2878-1	079 S	8	5.30	10,080	4600	0.00269	17.29	61.0
2878-3	080 S	8	4.75	8,330	4100	0.00244	20.81	81.0

TABLE 12. ARC PLASMA GENERATOR DATA FOR LIMITED CHARACTERIZATION MATERIAL (PYROLYTIC GRAPHITES)

Test Number	Model Number	Test Gas	P_o (atm)	H_o (Btu/lb)	T_w (°R)	$\dot{m}$ (lb/ft²sec)	ΔS (mils)	θ (sec)
HITCO a-b PG								
2853-2	094 S	1	2.88	38,980	4800	.000883	7.525	98.0
2857-2	093 S	1	3.20	44,780	5100	.00111	8.58	89.0
2859-4	099 S	1	2.88	56,260	5250	.001503	7.71	59.0
2861-2	098 S	1	3.25	54,780	5500	.001755	8.85	58.0
2865-1	100 S	3	4.73	11,640	5000	.005377	17.30	37.0
2867-2	096 S	3	5.60	7,660	4500	.0006469	3.38	60.0
2872-2	092 S	7	4.23	12,680	5000	.00309	16.25	60.5
2872-4	097 S	7	4.00	13,710	4850	.003069	15.48	58.0
2874-2	091 S	7	4.00	9,940	4600	.00104	7.35	81.0
Supertemp PG								
2584-1	040 S	1	3.75	44,200	4550	.000647	3.35	59.5
2586-1	041 S	1	4.28	65,400	5050	.00342	16.79	56.5
2592-3	043 S	3	6.10	16,500	4700	.01292	40.10	35.7
2596-2	044 S	4	5.25	7,260	4650	.01888	46.80	28.5
2597-3	051 S	4	6.45	8,930	4750	.00557	23.50	48.5
2617-5	072 S	2	6.20	2,630	4500	.00477	18.67	45.0
2854-4	074 S	1	3.45	34,850	4750	.0002218	1.89	98.0
2867-1	073 S	3	3.30	9,560	4100	.000104	0.542	60.0
2870-4	075 S	7	4.62	11,940	5050	.00295	15.50	60.5
Pfizer PG								
2584-4	045 S	1	3.80	42,400	4450	.0001278	0.667	60.0
2586-2	046 S	1	4.30	64,600	4450	.000341	13.80	46.5
2590-1	047 S	3	6.12	9,130	3650	.00636	16.60	30.0
2592-4	048 S	3	5.78	16,600	4800	.01624	60.00	42.5
2596-3	049 S	4	6.45	6,770	4550	.01095	55.70	58.5
2597-2	050 S	4	5.90	9,242	5000	.01126	48.00	49.0
2584-5	087 S	1	3.38	34,330	4250	.000170	1.45	98.0
2860-1	086 S	1	3.75	54,900	5600	.003127	15.50	57.0

TABLE 12. Concluded

Test Number	Model Number	Test Gas	P_o (atm)	H_o (Btu/lb)	T_w (°R)	$\dot{m}$ (lb/ft²sec)	ΔS (mils)	θ (sec)
Pfizer PG (Concluded)								
2872-1	089 S	7	4.52	12,611	5350	.00939	50.60	62.0
2876-2	088 S	7	4.62	9,123	5150	.00657	45.72	80.0
5% SiC PG								
2860-2	235 S	1	3.73	54,730	5550	.00287	14.58	59.0
2864-1	234 S	3	5.45	11,980	5000	.01013	38.00	43.5
2867-4	233 S	3	5.25	7,920	4250	.00447	23.92	62.0
23% SiC PG								
2617-3	052 S	2	6.20	2,540	3600	.0000179	.0667	45.0
2854-3	053 S	1	3.28	33,270	4850	.001057	8.68	99.0
2856-4	065 S	1	3.22	45.620	5250	.00680	38.3	68.0
2859-3	060 S	1	3.40	55,080	5450	.010575	34.8	53.0
2864-2	059 S	3	5.25	12,400	5100	.0231	51.8	28.0
2867-5	055 S	3	4.90	7,500	4550	.01163	53.0	55.0
2872-3	066 S	7	4.18	12,810	4900	.00924	49.0	64.0
2876-1	062 S	7	3.92	9,850	4600	.00503	32.11	77.0
HCF PG								
2853-3	203 S	1	3.20	38,820	4850	.001689	3.5	97.0
2865-2	208 S	3	5.50	11,050	5250	.02915	25.54	41.0
2867-7	209 S	3	5.45	6,960	4500	.00117	13.75	55.0
2871-1	206 S	7	4.50	13,280	4850	.01674	2.11	59.0
2874-3	210 S	7	4.50	9,080	4950	.00203	3.04	70.0

4.2 BOUNDARY LAYER EDGE SOLUTIONS

The free stream conditions at various locations within the nozzle were calculated based on the assumption of one-dimensional isentropic flow. This calculation can be easily performed with the isentropic expansion option in the GASKET program. In order to determine the entropy for the isentropic expansion calculations, the thermodynamic state of the plenum chamber was first calculated based on the measured or evaluated parameters (P_o, h_o, K_i).

4.3 EVALUATION OF HEAT AND MASS TRANSFER COEFFICIENTS

The heat transfer coefficient $(\rho_e u_e C_H)$ was evaluated directly from experimental measurements through the following relationship:

$$(\rho_e u_e C_H)_{cw} = \frac{q_{cw}}{h_o - h_{cw}} \tag{8}$$

Where q_{cw} is the cold wall heat flux measured from a calibration run prior to each ablation test, h_o is the total enthalpy which is known from the APG operating conditions, and h_{cw} is the cold wall enthalpy which is merely the sum of the heat of formation multiplied by the mole fraction of each species in the test gas.

In order to account for hot wall effects, the Bartz equation was used as a scaling function. For a given geometry, the Bartz equation has the form:

$$(\rho_e u_e C_H)_B \sim (\rho_{ref} u_e)^{0.8} \mu_{ref}^{0.2} Pr^{-0.6} \tag{9}$$

Thus, the hot wall heat transfer coefficient can be determined from

$$\rho_e u_e C_H = \frac{(\rho_e u_e C_H)_{B,hw}}{(\rho_e u_e C_H)_{B,cw}} \times (\rho_e u_e C_H)_{cw} \tag{10}$$

Through the Reynold's analogy, the mass transfer coefficient can also be determined. The correlation frequently employed is (Reference 18).

$$\frac{C_M}{C_H} = Le^{2/3} = (\frac{Pr}{Sc})^{2/3}_{ref} \tag{11}$$

For the above computations, all properties are determined from the GASKET program. The subscript ref denotes the values at the reference enthalpy state, defined as:

$$h_{ref} = 0.36 \ h_e + 0.19 \ h_o + 0.45 \ h_w \tag{12}$$

The calibration results and the evaluated transfer coefficients are shown in Tables 13 and 14.

TABLE 13. CALIBRATION DATA SUMMARY — PLANAR CONFIGURATION

Test Set	Test Level	Test Gas Composition	Mass Fraction/Flowrate (C/A)ᵢ	Mass Fraction/Flowrate (C/A)ᵢ	Mass Fraction/Flowrate (E/A)ᵢ	(E/A)ᵢ	Ẇ total (lb/sec)	Q̇₀ (Btu/lbm)	P₀ (atm)	Q̇cw (Btu/ft²sec)	Arc Current (amps)	Arc Voltage (volts)	Eff(c) (%)	Reference (Test No.)	Cold Wall Heat Transfer Coefficient (lbm/ft²sec)	Remarks
1	Low	N₂	1.0/0.00704				0.00794	31,320	3.25	973	493	966	47.9	2673.01	0.0303	
	Med							35,000	3.46	1077	633	971	42.2	2671.01	0.0219	●
	High							30,500	3.42	845	684	927	38.1	2722.01	0.0288	
								41,380	4.00	1354	1306	960	31.6	2724.01	0.0333	
2	Low	H₂/O₂/Ar	0.020/0.000944	0.1506/0.00748	0.0295/0.0412		0.04967	2,590	6.48	725	1422	702	13.5	2675.02	0.1601	
3	Low	H₂/O₂	0.334/0.00731	0.644/0.01476			0.02217	8,230	6.87	1258	571	1214	27.7	2677.01	0.1038	
	Med							10,640	6.33	1628	794	1145	27.3	2682.01	0.1121	
								9,230	4.80	947	800	1032	26.2	2720.01	0.0722	
	High							14,960	6.96	1853	798	1213	27.7	2683.01	0.1016	
								11,450	6.09	1156	1001	1150	23.8	2718.01	0.0754	
4	Low	H₂/C₂/CO	0.222/0.00605	0.447/0.01215	0.324/0.00893		0.0272	5,960	6.29	901	577	1154	27.0	2676.01	0.0986	
	Med		0.253/0.00689	0.400/0.01388	0.347/0.00943			7,250	5.52	1020	791	1781	26.3	2726.01	0.0909	
	High							11,940	7.62	1232	935	1457	26.3	2665.01	0.0735	
7	Low	H₂/C₂/NC₄	0.323/0.00599	0.332/0.00595	0.356/0.00661		0.0714	9,640	4.49	1443	677	1082	26.8	2702.02	0.1235	
	Med							10,400	4.51	1060	848	1027	23.1	2706.01	0.0853	
								13,370	4.76	1223	956	1099	24.6	2708.01	0.0794	
			0.245/0.00599	0.446/0.01199	0.270/0.00661		0.02448	7,100	5.99	1148	1078	987	24.6	2713.01	0.1119	Revised Gas Composition
8	Low	H₂/Ar/CO/HCl	0.216/0.00699	0.234/0.00480	0.204/0.00414	0.264/0.00637	0.0093	10,700	4.61	1018	981	1019	26.3	2737.01	0.0776	
	Med							10,490	5.48	1070	998	1068	23.2	2717.02	0.0816	

TABLE 14. CALIBRATION DATA SUMMARY — AXISYMMETRIC CONFIGURATION

*For screening tests transfer coefficient not needed

TABLE 14. Concluded

Test Set	Test Level	Test Gas Composition	(x/A)_i	Mass Fraction(s)/x-rate i K_i	(x/A)_f	(x/A)_f	m (lb/sec)	Q (Btu/lbm)	P_o (atm)	Q_av (Btu/ft²sec)	Arc Current (amps)	Arc Voltage (volts)	Effic (%)	Reference (Test No.)	Cold Wall Heat Transfer Coefficient (lbm/ft²sec)	Remarks
1	low	N₂/O₂/CO	0.223/0.00605	0.445/0.01215	0.130/0.0094		0.0271	6,660	7.75	1634	625	1296	26.3	2595.02	0.1682	
			0.241/0.0644	0.425/0.0118	0.333/0.0093		0.07678	6,010	6.59	1786	637	1372	24.5	2814.01	0.1744	-
	high		0.233/0.00605	0.448/0.01215	0.330/0.0099		0.0271	7,400	7.78	2116	759	1310	22.9	3595.04	0.1820	
			0.241/0.0644	0.425/0.01138	0.333/0.0093		0.02680	7,480	7.14	2145	735	1270	27.1	2816.02	0.1833	
3	low	N₂/O₂/CO/Ar	0.0158/0.00094	0.1189/0.00748	0.2102/0.01322	0.6551/0.0412	0.0629	1,100	8.36	974	738	787	16.4	2829.04	0.3811	
								1,210	7.84	886	750	739	18.7	2822.01	0.3420	
	high							1,530	8.43	1026	1215	752	13.7	2818.01	0.3300	
								660	8.41	1044	1417	744	12.2	2818.03	0.3495	
								700	8.09	966	1413	743	12.9	2822.02	0.3208	
4	low	H₂/HCl	0.307/0.0704	0.692/0.1587			0.2292	10,670	5.59	1678	739	1126	33.1	2824.03	0.1527	
	high							13,570	6.41	2141	981	1199	23.4	2824.02	0.1542	
								14,850	6.31	2128	1211	1120	27.8	2824.21	0.1403	
5	low	N₂/O₂/HCl	0.322/0.00599	0.322/0.00595	0.357/0.0664		0.01857	10,230	5.20	955	650	1054	29.0	2830.03	0.0779	Cal Data Noisy
								9,940	5.24	1877	690	1050	27.9	2873.01	*	
	high							12,410	5.30	1552	907	1047	26.4	2830.02	0.1074	Cal Data Noisy
								12,780	5.23	1090	995	1039	24.9	2830.01	0.0736	
								12,260	5.53	2273	894	1020	25.9	2873.02	*	
6	low	N₂/O₂/CO/HCl	0.296/0.00599	0.237/0.0048	0.206/0.00416	0.263/0.00533	0.02265	12,320	5.23	1897	894	1081	28.7	2835.02	0.1787	
	high							6,800	5.34	1766	665	1033	28.5	2877.02	*	
								12,520	5.53	1942	982	1116	25.6	2826.01	0.1200	
								11,660	5.86	2123	1005	1040	25.0	2877.01	*	

*For screening tests transfer coefficient not needed

59

4.4 OPEN SYSTEM SURFACE STATE SOLUTIONS

The final step of the data reduction procedure is to calculate the mole fraction of reactive species at the carbon surface. By specifying the edge gas thermodynamic state, Tw, and B', the surface state solution can be determined using the Aerotherm Chemical Equilibrium (ACE) computer program. B' is the nondimensional ablation variable and is defined as

$$B' = \frac{\dot{m}_c}{\rho_e u_e C_m} \tag{13}$$

The results of this calculated data were presented in Table 9.

SECTION 5

ROCKET MOTOR TEST RESULTS

Previous sections have described how both arc plasma generator and motor firing data were incorporated into the kinetics model. The basic data used was in the form of mass removal rate, wall temperature, and wall partial pressures. This data is readily available from arc plasma generator tests but not from nozzle test firings. For a typical test firing of a full or subscale nozzle, only the pressure history and final total recession are reported. To deduce the appropriate data, an iterative procedure for correlating the data was adopted. This was described in a five-step process at the end of Section 3.3. This section will summarize the nozzle test data and how it was derived for the five steps. Step 1 of the correlating procedure requires approximate values of surface recession rate, surface temperature, and species partial pressures at the wall. These were obtained by performing a complete in-depth conduction solution at the nozzle location of interest using the standard Aerotherm procedure (to be described in Section 7). Since the kinetics constants needed for GASKET are unknown at this time, a best guess is used. Previously developed constants for materials roughly similar to the material of interest are typically used. Figure 12 illustrates a typical surface response prediction. A complete history of surface temperature, surface recession rate, and cumulative surface recession is obtained from the CMA computer code. Notice that the data needed for the correlation varies with time. To deduce only one data point per firing, it was assumed that the conduction prediction procedure accurately predicted the relative time variation of surface temperature and recession rate. New kinetics constants were felt to improve the accuracy of the total surface recession only. For this reason, the point in time used for data in all cases was chosen to be the midpoint of the firing. Surface mass removal rate was deduced from the surface recession rate as follows:

$$\dot{m} = \dot{S} * \rho \tag{14}$$

where $\dot{m}$ = mass removal rate

$\dot{S}$ = surface recession rate

ρ = material density

With this data for one or more motor firings, Step 1 of the correlation procedure could be completed.
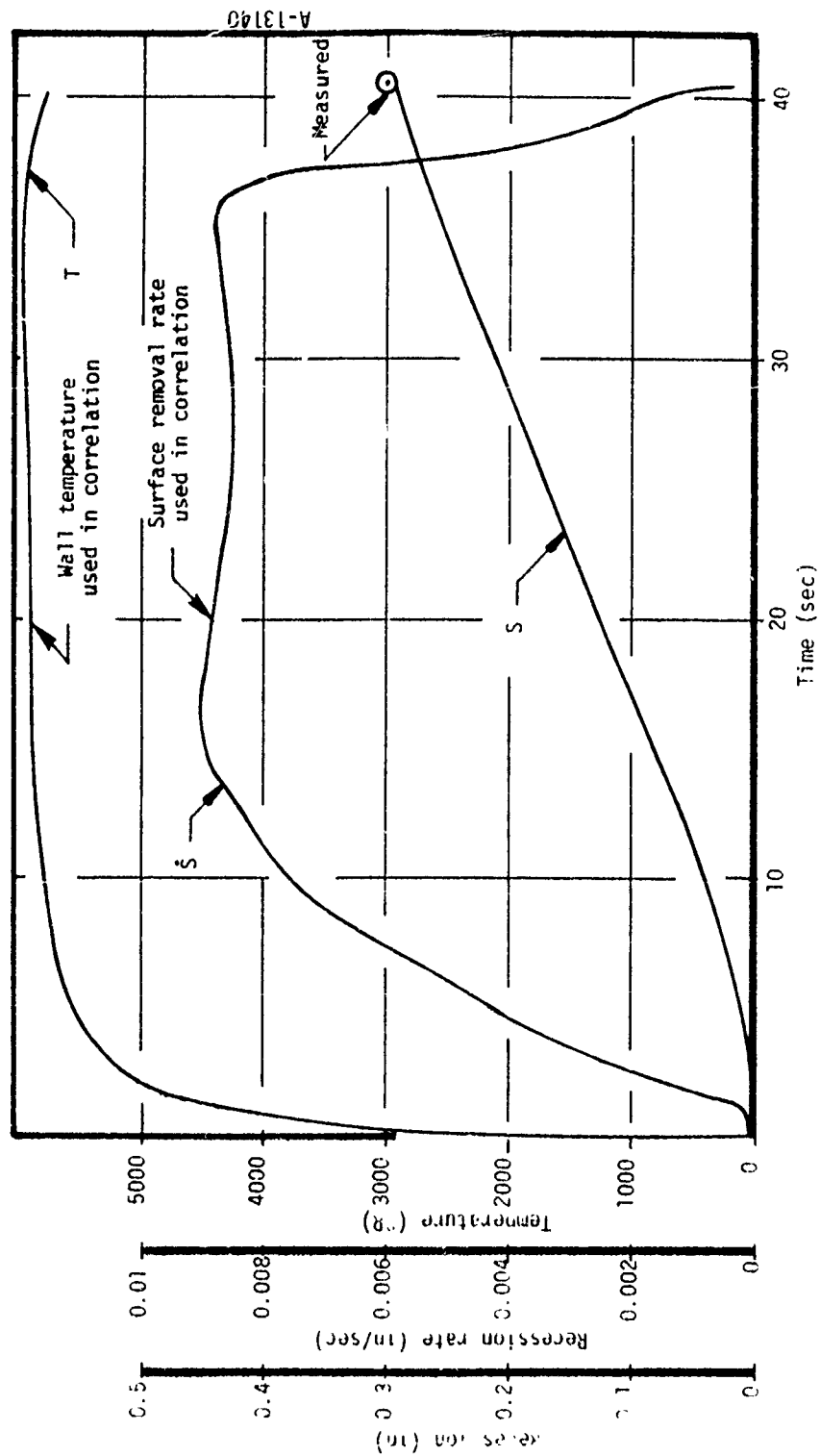
Figure 12. Typical surface response prediction for motor firing.

A second prediction was then run with the resulting kinetics model. First, a GASKET prediction was made (Step 2) and then a new CMA prediction was run (Step 3). This second prediction was identical to the first except for the more refined kinetics constants. Depending on the accuracy of the first guess, the total predicted recession may or may not match the measured recession. If not, the newly predicted surface temperature and a modified surface recession rate was used to update the data used in the correlation (Step 4). The modified surface recession rate was defined as:

$$\dot{S}_{Modified} = \dot{S}_{predicted} * \frac{S_{measured}}{S_{predicted}} \tag{15}$$

With this information the final kinetics correlation model was determined (Step 5). The final motor firing data used for all of the kinetics models are summarized in Table 15.

A final complete prediction was made for each motor firing to verify the kinetics model. In most cases the model was verified by predicting the measured total surface recession within 25 percent. These verification predictions are referred to as correlation studies and are presented briefly in Section 7 and in full detail in a second final report (AFRPL-TR-76-71).

TABLE 15. SUMMARY OF CORRELATION DATA OBTAINED FROM MOTOR FIRINGS

Carbon Type	Study	P_e (atm)	T_w (°K)	$\dot{m}_c$ (lb/ft²sec)	Reactant Partial Pressures					
					P_{H_2O}	P_{H_2}	P_{HCl}	P_{CO_2}	P_{CO}	P_{HF}
Edge PG	2	37.20	3228.6	0.0776	0.0383	13.5594	3.0950	0.0050	13.5036	0
	3	43.28	3416.7	0.0624	0.0039	12.7952	0.8994	0.0006	16.1246	0.3246
	4	40.05	3441.0	0.1245	0.0012	10.1967	0.2083	0.0002	15.8598	0
	5	35.35	3500.0	0.0300	0.2424	10.2904	0.7553	0.0382	12.9614	0.2817
	6	54.936	3500.0	0.0510	0.1057	16.4965	1.1793	0.0164	20.5406	0.4381
	7	94.03	3016.0	0.0430	8.8858	31.1239	13.3523	1.1754	29.8075	0
	8	72.3	2981.0	0.0384	7.3023	24.0036	10.7727	0.9254	21.8346	0
15% SiC/PG	9	26.18	2975	0.0377	0.7004	9.4473	3.4550	0.0991	9.5766	0
	10	39.02	3144	0.0474	1.4991	13.7378	5.1604	0.2015	13.8002	0
	11	44.52	3529	0.0351	0.5089	12.9803	0.9742	0.0777	15.9404	0.3695
G-90	12	41.78	2347.2	0.0228	8.3681	8.1580	6.4888	2.3626	13.0303	0
	13	27.37	2777.8	0.0224	2.1609	9.6137	3.8707	0.2884	8.6752	0
ATJ Graphite	14	13.76	3111.1	0.0287	0.0002	2.3648	0.1490	0.0001	7.9942	0
Pyrocarb 901 C/C	15	48.21	3152.8	0.0839	0.0015	13.3267	0	0.0003	18.2417	0

SECTION 6

EVALUATION OF KINETIC CONSUMPTION RATES

Two procedures were applied to evaluate kinetic consumption rates of carbon materials. The first procedure, namely full characterization studies, correlated the carbon consumption rate data from both APG and motor firing testings as a function of the following parameters:

- Surface temperature

- Boundary layer edge pressure

- The chemical composition of the propellant gas

The correlation function used was based on the Langmuir-Hinshelwood model. This model takes into account such detailed mechanisms as chemadsorption, desorption, and heterogeneous reactions. Thus, not only is the obvious ablation performance evaluated, but significant physical insights may be obtained on the competition of active sites by reactive species and poisoning effects by halogen species This correlation procedure was described in Sections 3 and 4.

The second procedure, namely limited characterization studies, used the APG to evaluate the relative ablation performance of the screening carbon materials. This procedure included the following items:

- Selection of test gases that characterized the actual motor firing surface kinetics

- Extrapolation of the APG results to determine the relative ablation performance at actual motor-firing conditions (T_w = 5500°R - 6000°R)

Fully characterized materials were used as a baseline material for the screening materials for the same generic class in order to determine their relative ablation performance.

6.1 RESULTS OF FULL CHARACTERIZATION STUDIES

Kinetic constants and inhibition coefficients of the following materials were determined from the APG and motor firing data using an Aerotherm least squares data optimization program:

- Supertemp Edge PG

- 15% SiC/PG

- ATJ Bulk Graphite

- G-90 Bulk Graphite

- Pyrocarb 901 Carbon/Carbon

Carbitex 700 data was available from previous work and its correlation functions were reassessed in this study. The quality of the data optimization are shown in Figures 13 through 17 and numerical results are presented in Table 16.

The maximum standard deviation obtained in these correlations is $\sigma = 0.16$. From a statistical point of view, these correlations are considered to be satisfactory. The accuracy of these correlations, however, must be further tested by comparing predictions with the motor firing data. The results of these comparisons will be discussed in Section 7.

The following conclusions were reached from the full characterization studies:

- The H_2 - C* reaction has a high activation energy and a relatively large number of active sites. This kinetic reaction becomes significant at surface temperatures above 5500°R and is a major contributor to carbon surface recession at motor firing conditions.

- The H_2O and CO_2 - C* reactions have relatively low activation energies and relatively small numbers of active sites compared with the H_2 - C* reaction. These reactions play a dominant role in carbon surface recession at temperatures between 4000°R and 5500°R. Their effects, however, diminish due to the dissociation of H_2O and CO_2 as the surface temperature increases.

- HCℓ retards the CO_2 and H_2O - C* reactions, but has no effect on the H_2 - C* reaction.

- G-90 graphite is slightly more active with respect to reactants of H_2O and CO_2 than the other three full characterization materials.

- Carbon sublimation results in a nonnegligible rate of carbon consumption at anticipated rocket motor temperatures. The significance of sublimation becomes increasingly important as propellant and surface temperature increase, especially for materials with low carbon ablation rates.

Because of the complexity of the kinetic formulations, it is not possible to make general comments about the magnitudes of each reaction for a given material. However, one can compare the reaction rate coefficients, as presented in Table 16, as a function of temperature. These comparisons are shown in Figures 18 through 22 for the materials characterized in this study. In addition, results from earlier studies for Carbitex 700 and Atlantic Research Corporation layer PG are shown

66

A-15190

MC_-

1/T$_W$ x 10^4 (°K^{-1})

o = .16

□ H$_2$ APG data

⊙ H$_2$, H$_2$O, CO$_2$, CO APG data

△ H$_2$, H$_2$O, CO$_2$, CO, HCℓ APG data

❁ Motor firing data

No of APG data: 17

Date of correlation: 7/16/75
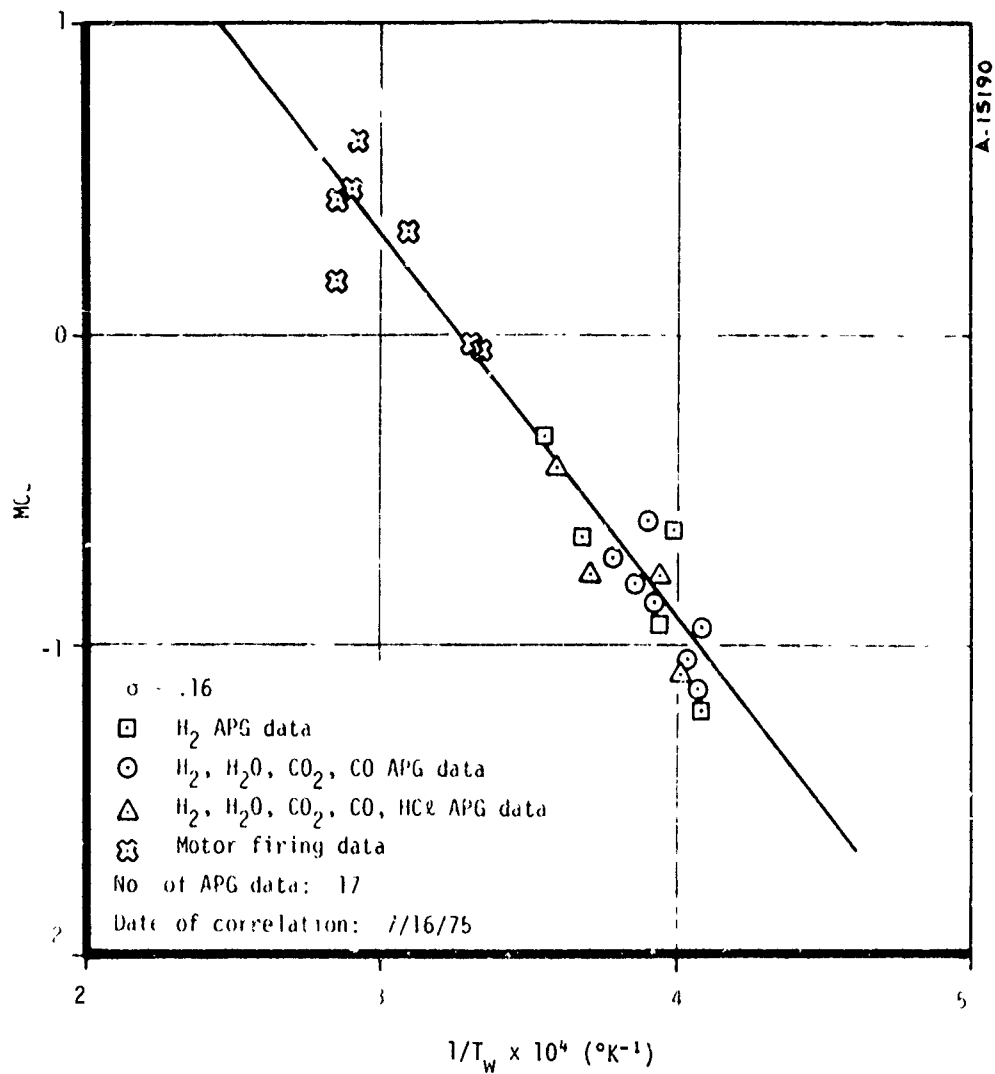
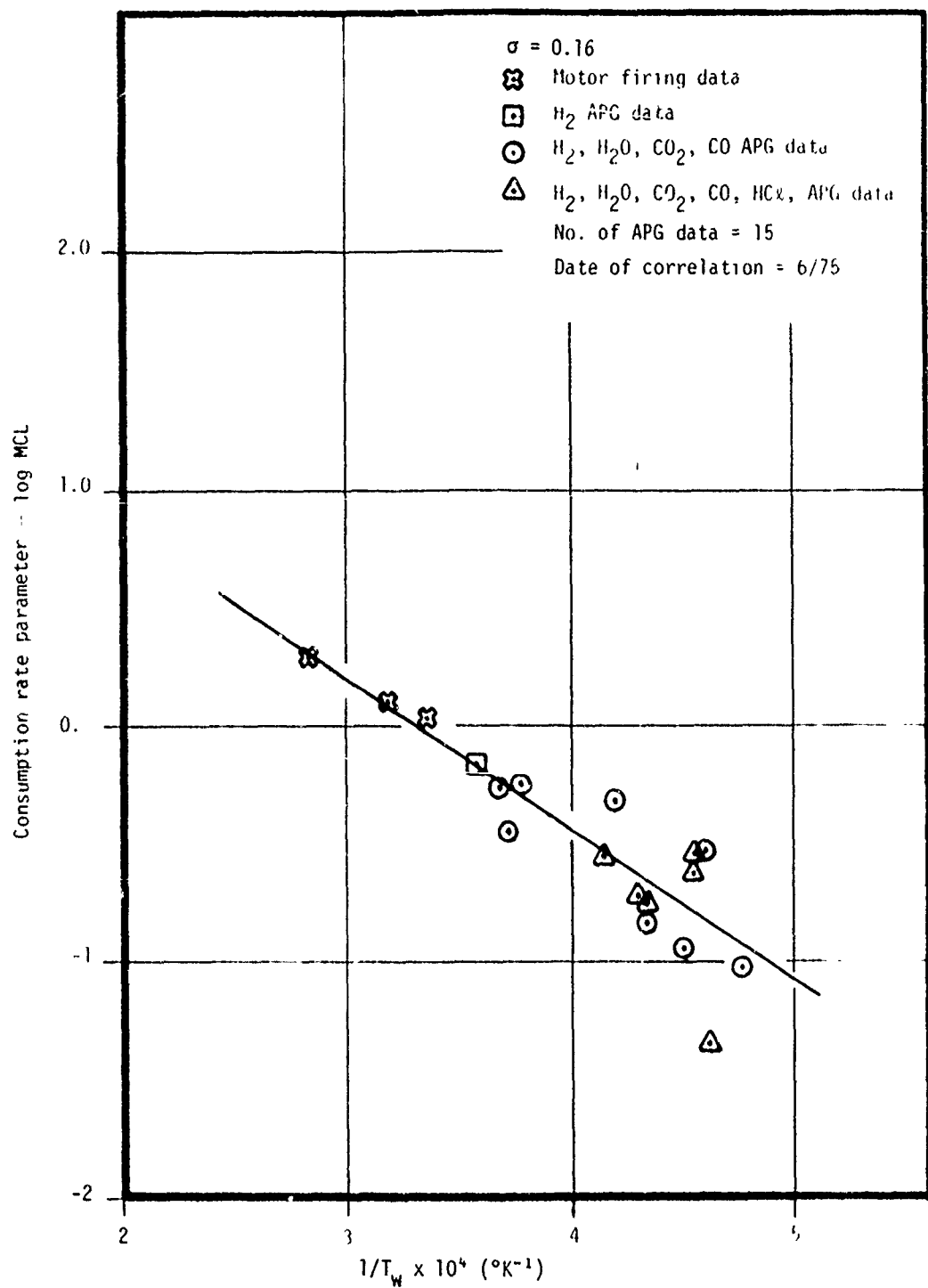Figure 13. Supertemp PG, c plane surface kinetics.
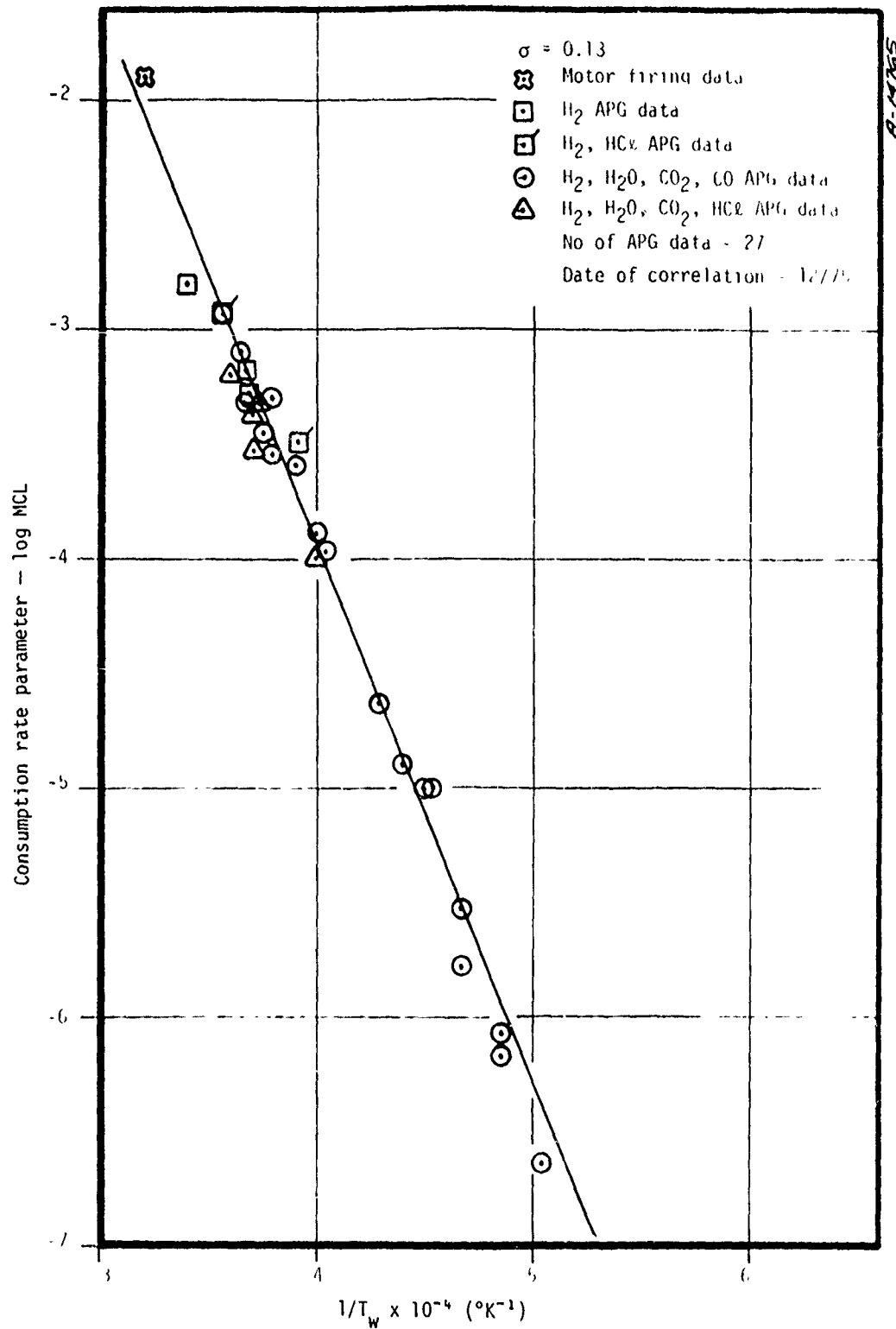
Figure 14. Results of 15% SiC/PG kinetic correlation.

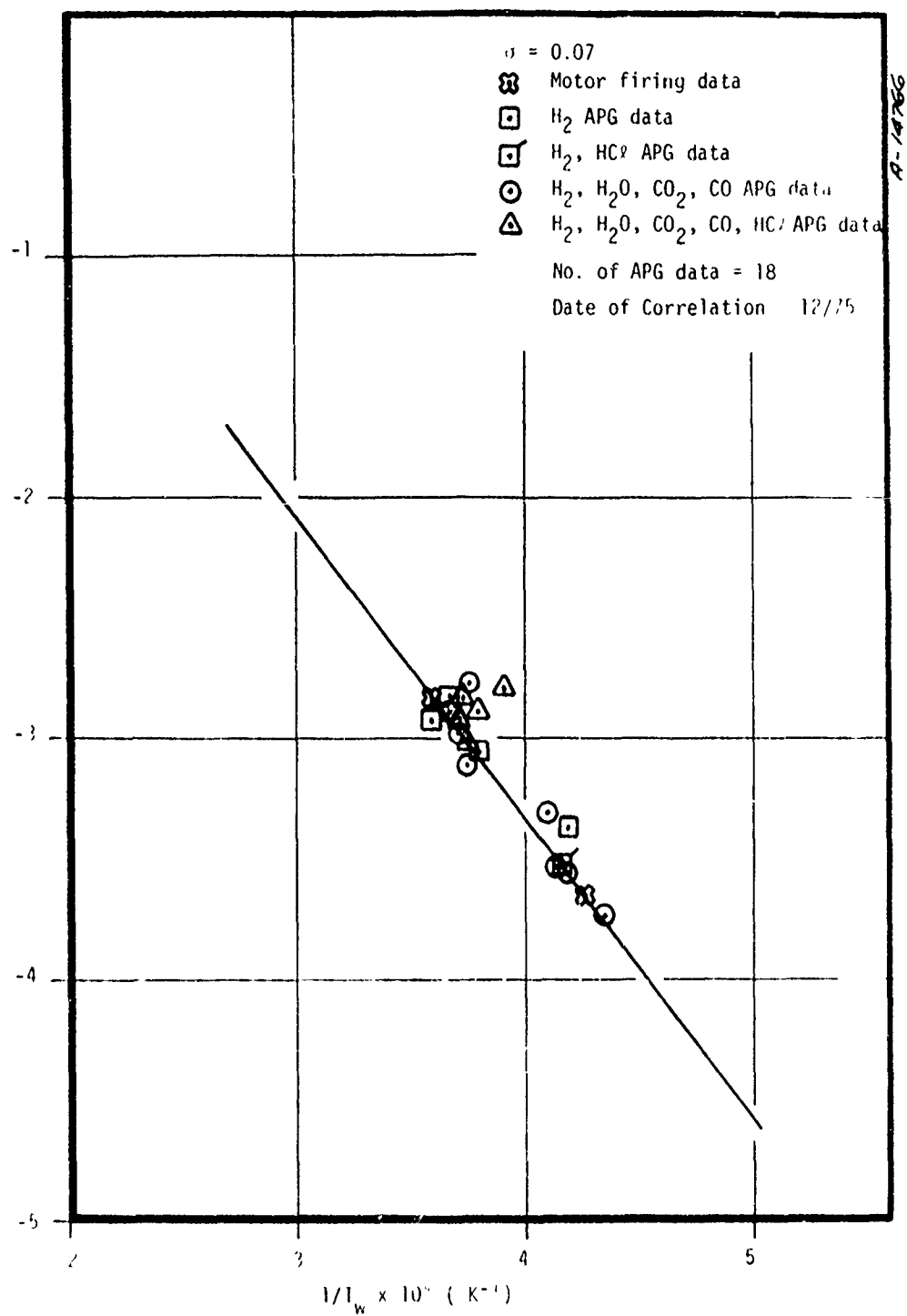Figure 15. Results of ATJ graphite kinetic correlation.

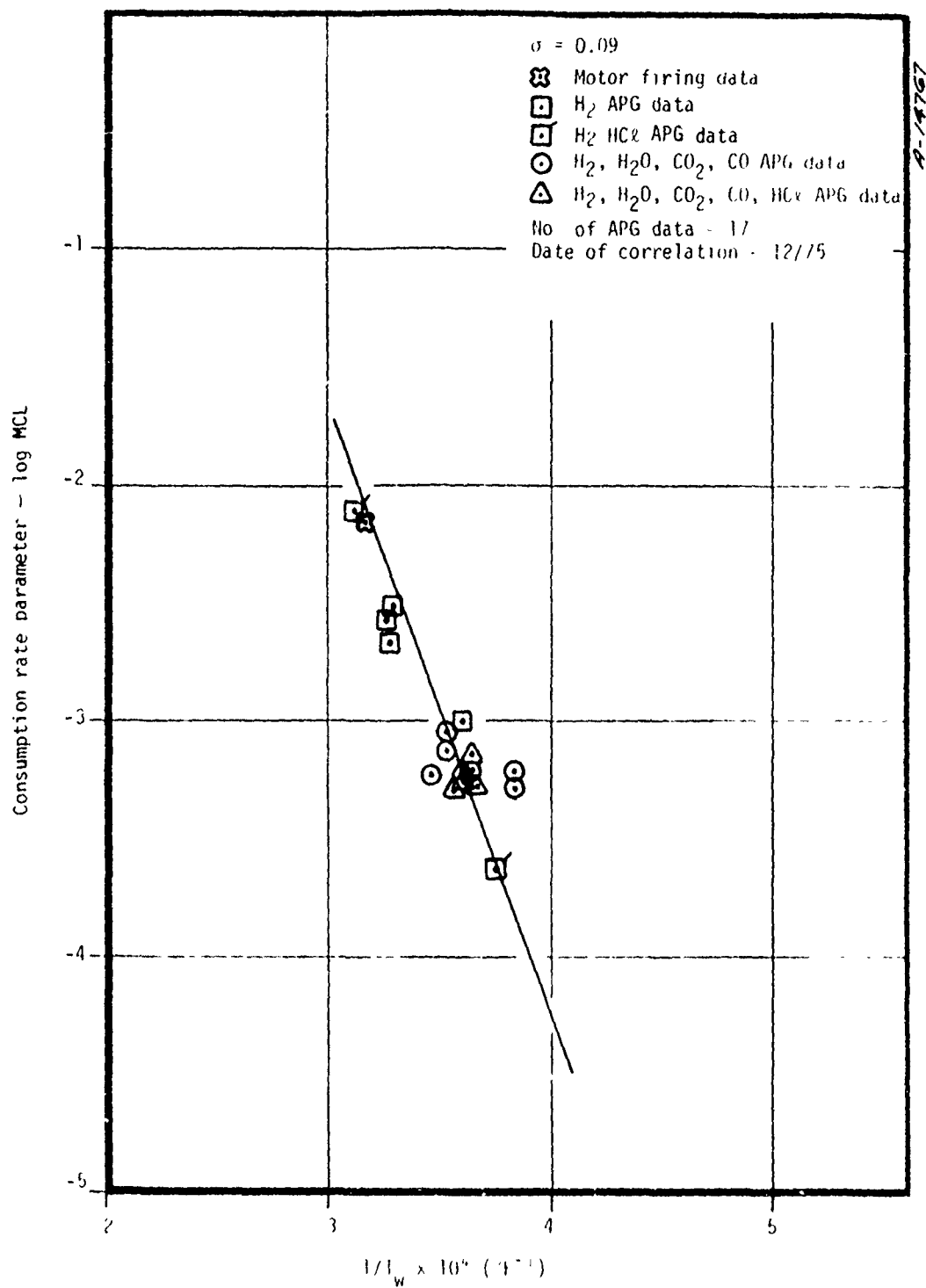Figure 16. Results of G-90 kinetic correlation.

Figure 17. Results of Pyrocarb 901 kinetic correlation.

TABLE 16. CARBON KINETICS COEFFICIENTS FOR FULL CHARACTERIZATION MATERIALS

ATJ BULK GRAPHITE

Reaction	A_i (lbmole/ft²sec-atm)	E_i (cal/gmole)	n_i	Ψ_{ji} H_2O	CO_2	CO	H_2	$HC\ell$	HF
H_2O	0.74	4,551	0	164	399	167	13.1	100	0
CO_2	3.45	4,551	0	164	399	167	13.1	100	0
H_2	1.96×10^4	110,500	0	0	0	0	0	0	0

BULK GRAPHITE

Reaction	A_i (lbmole/ft²sec-atm)	E_i (cal/gmole)	n_i	Ψ_{ji} H_2O	CO_2	CO	H_2	$HC\ell$	HF
H_2O	3.87×10^{-2}	4,175	-0.29	0.03	0.06	0.02	0.00	0	1.0
CO_2	$1.50 \times 10^-$	4,175	-0.29	0.03	0.06	0.02	0 CO	0	1.0
H_2	1.91	57,175	0	0	0	0	0	0	0

LAYER PG

Reaction	A_i (lbmole/ft²sec-atm)	E_i (cal/gmole)	n_i	Ψ_{ji} H_2O	CO_2	CO	H_2	$HC\ell$	HF
H_2O	12.67	46,000	0	1.0	1.0	1.0	1.0	3.0	3.0
CO_2	12.67	46,000	0	1.0	1.0	1.0	1.0	3.0	3.0
H_2	1.53	55,500	0	1.0	1.0	1.0	0	0	0

TABLE 16. Continued

SUPERTEMP EDGE FC

Reaction	A_i (lbmole/ft²sec-atm)	E_i (cal/gmole)	n_i	Ψ_{ji}					
				H_2O	CO_2	CO	H_2	HCℓ	HF
H_2O	2.64×10^3	61,918	0	151	26	2.16	0	93	0
CO_2	3.43×10^6	69,431	0	47	166	30	0	1325	0
H_2	5.14×10^5	124,460	0	0	0	0.56	0	0	53

15% SiC/PG

Reaction	A_i (lbmole/ft²sec-atm)	E_i (cal/gmole)	n_i	Ψ_{ji}					
				H_2O	CO_2	CO	H_2	HCℓ	HF
H_2O	11.09	29,387	0	29	374	0	1.72	0.01	2500
CO_2	2.09×10^2	29,387	0	29	374	0	1.72	0.01	2500
H_2	7.00×10^{-1}	50,640	0	88	20.2	13.7	0	0	0

PYROCARB 901

Reaction	A_i (lbmole/ft²sec-atm)	E_i (cal/gmole)	n_i	Ψ_{ji}					
				H_2O	CO_2	CO	H_2	HCℓ	HF
H_2O	6.89×10^5	101,677	0.43	253	5418	0.05	0	0	0
CO_2	1.32×10^7	101,677	0.43	253	5418	0.05	0	0	0
H_2	4.42×10^4	117,283	0	54	18.8	0.06	0	0	0

TABLE 16. Concluded

CARBITEX 700

Reaction	A_i (lbmole/ft²sec-atm)	E_i (cal/gmole)	n_i	ψ_{ji}					
				H_2O	CO_2	CO	H_2	$HC\ell$	HF
H_2O	0.48	34,308	0.62	16.6	142	76	21.8	0.10	0
CO_2	14.48	34,308	0.62	16.6	142	76	21.8	0.10	0
H_2	0.02	34,884	0	0	0	0	0	0	0

$$m_c'' = \sum_i \frac{A_i T^{n_i} e^{-E_i/RT_w}}{1 + \sum_j \psi_{ji} P_j} \left(P_i - \frac{1}{K_{P_i}} \prod_{prod} P_{prod} \right) \quad \frac{lbm}{ft^2 sec}$$

Kinetically Controlled Reactions:

1. $H_2O + C^* \rightleftarrows CO + H_2$

2. $CO_2 + C^* \rightleftarrows 2CO$

3. $H_2 + 2C^* \rightleftarrows C_2H_2$
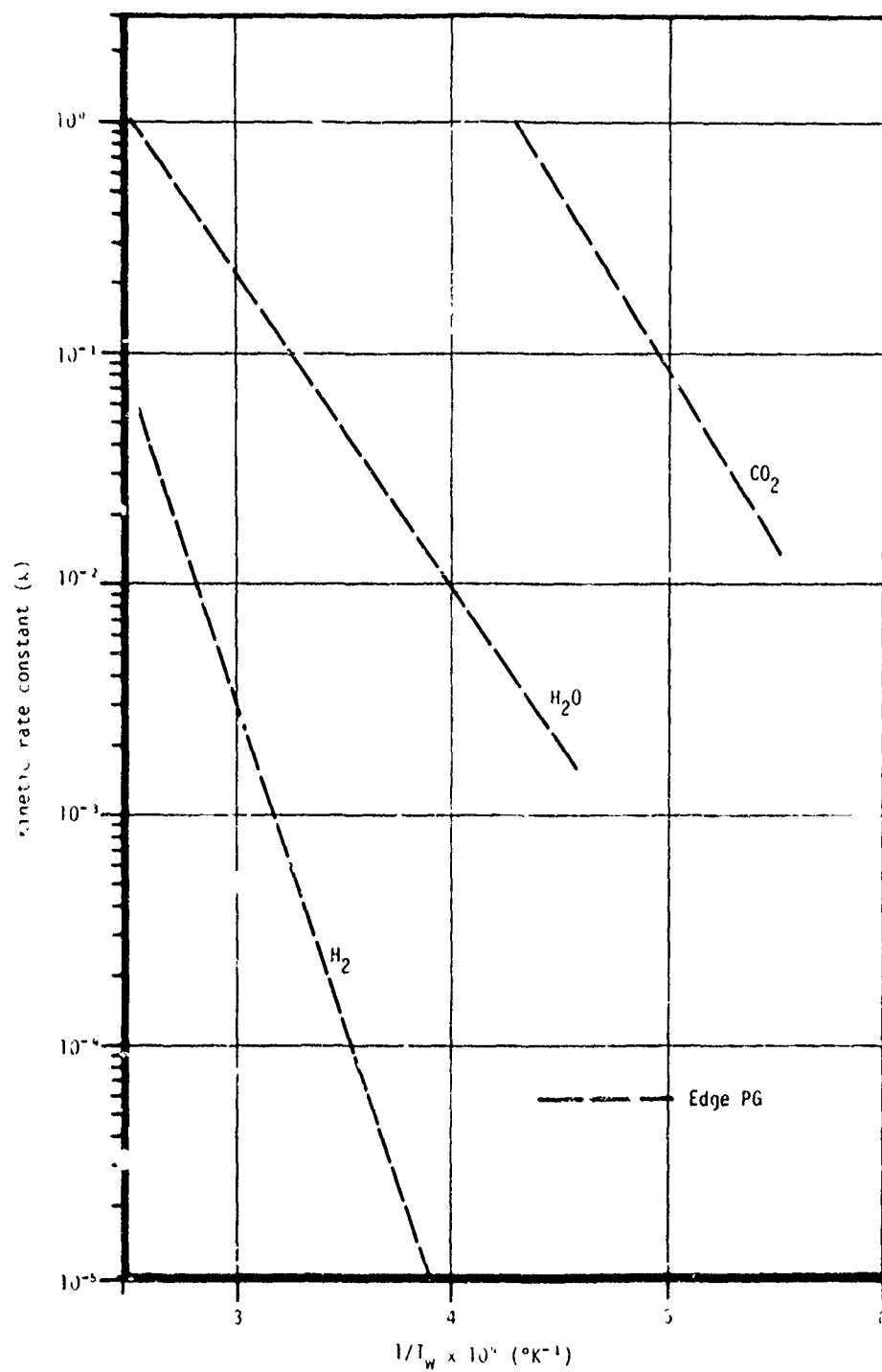
Figure 18. Reaction rate coefficients for
Supertemp edge pyrolytic graphite.
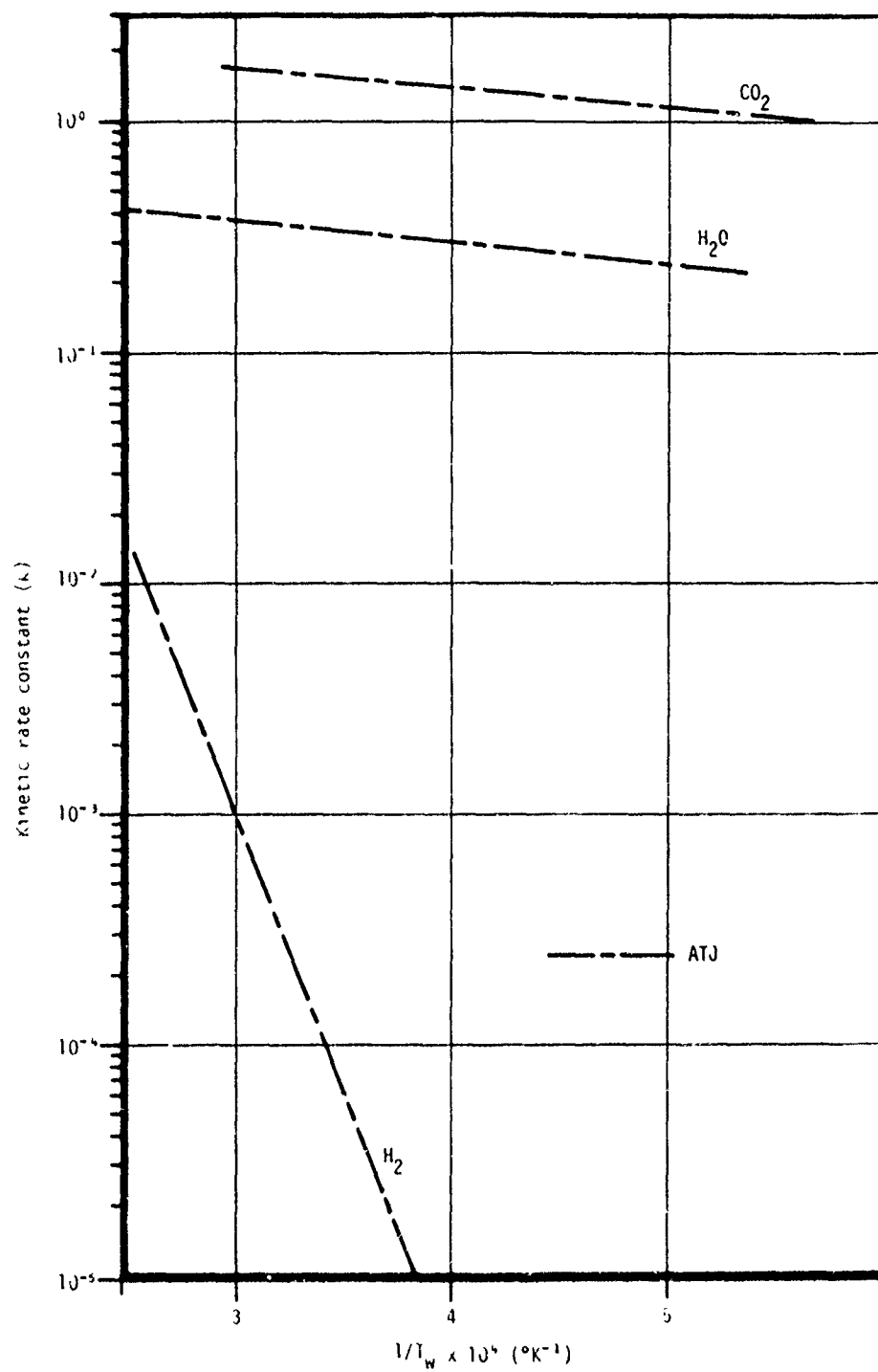
Figure 19. Reaction rate coefficients for ATJ graphite.
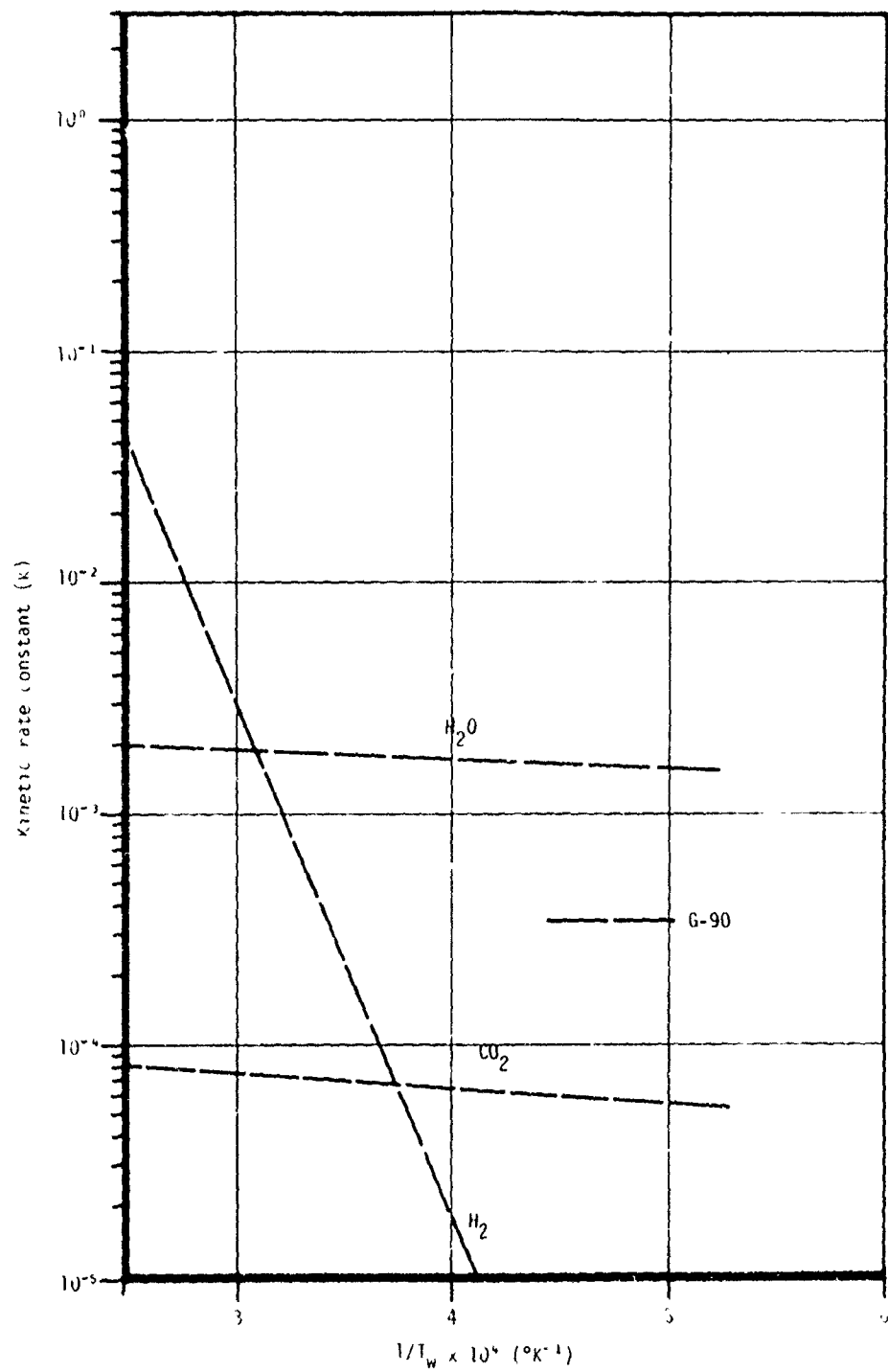
Figure 20. Reaction rate coefficients for G-90 graphite.

77
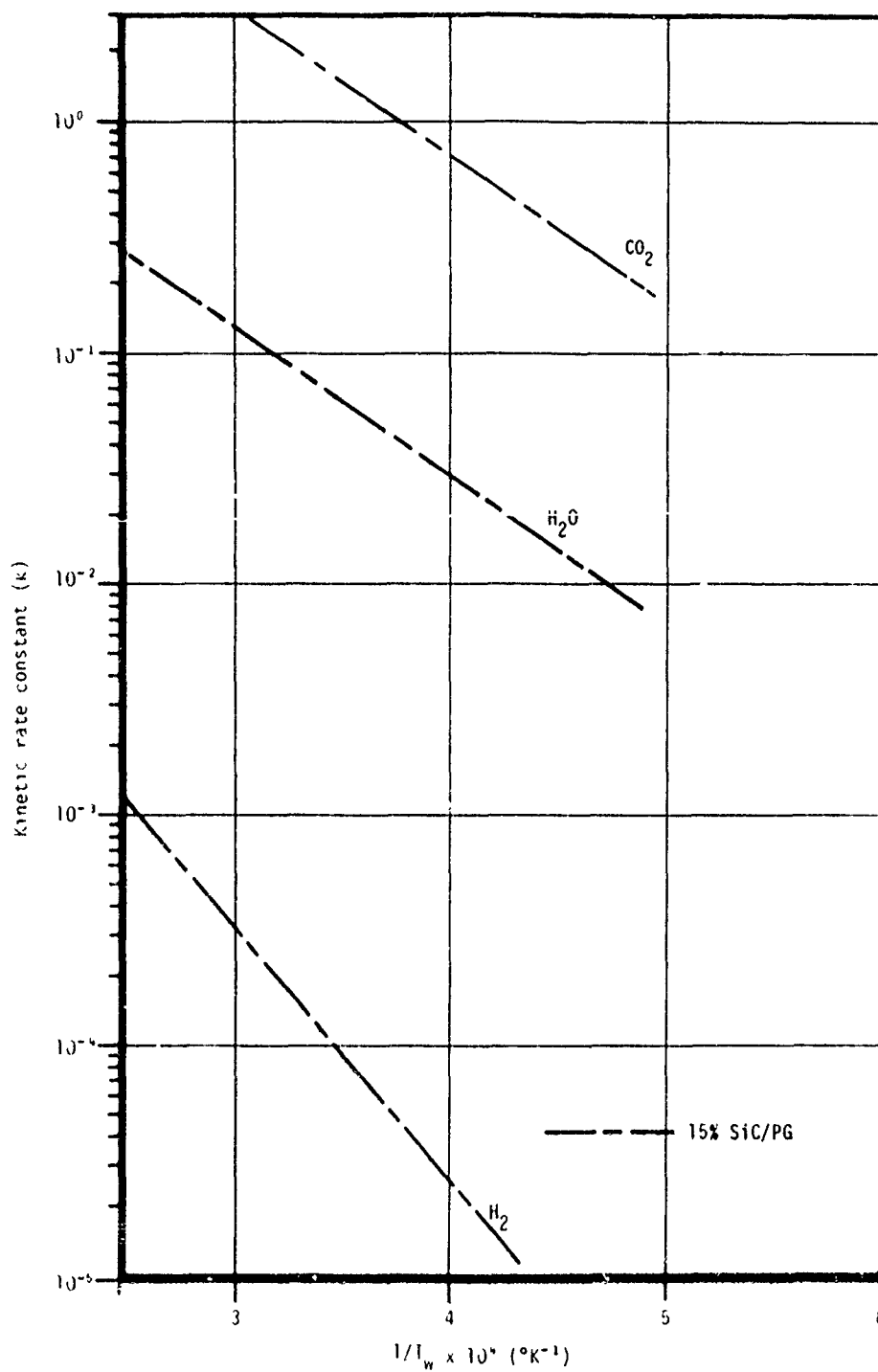
Figure 21.   Reaction rate coefficients for 15% SiC/PG.
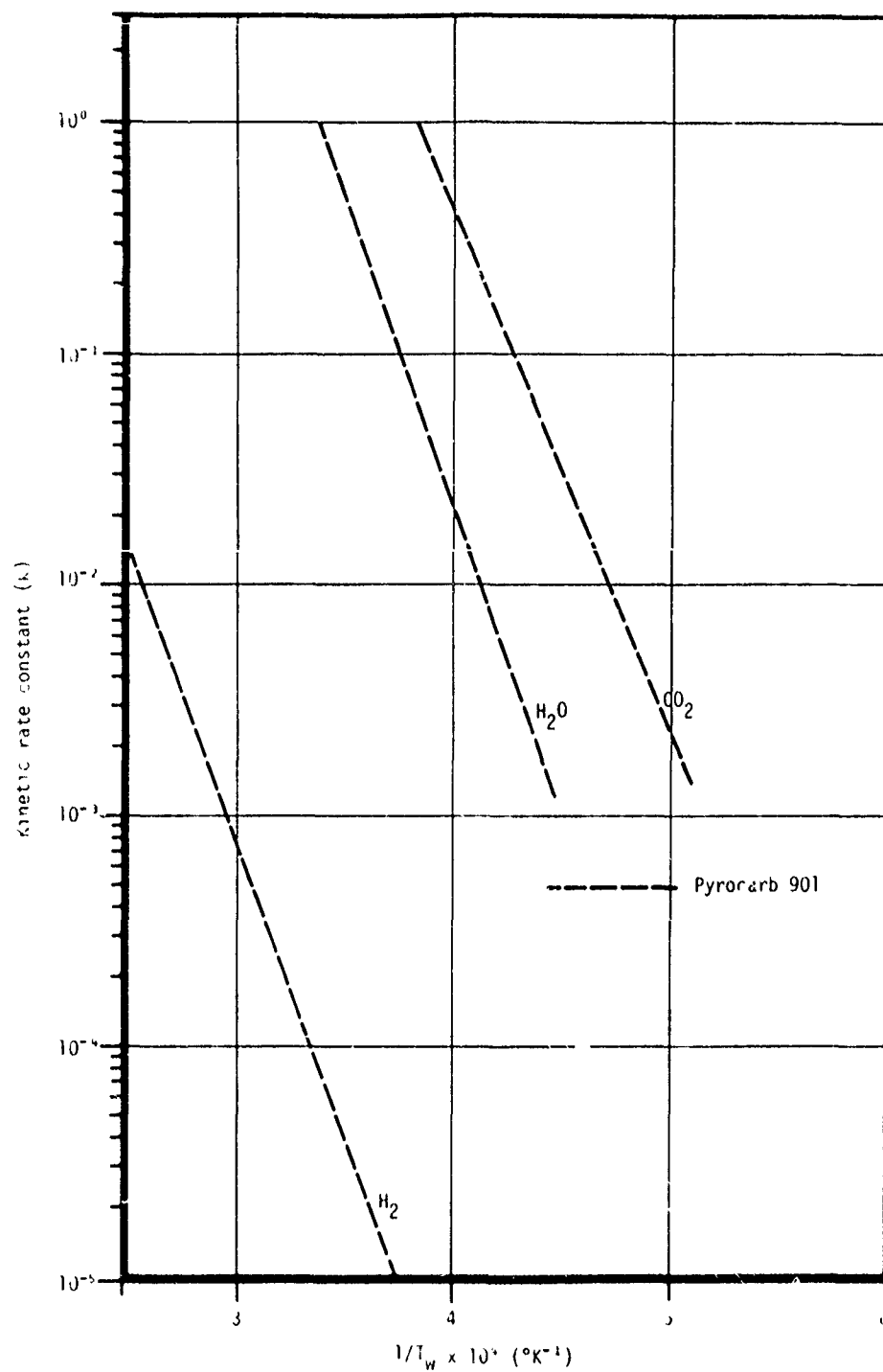
Figure 22.   Reaction rate coefficients for
Pyrocarb 901 carbon/carbon.

79

in Figures 23 and 24. For the Carbitex 700 material, data from Reference 19 (Thiokol) were re-correlated to be consistent with first-order kinetics. For layer PG, the results were taken directly from Reference 6 (Schaefer).

Before the reader draws any conclusions from these figures, he is cautioned to qualitatively account for the facts that:

1. Figures 18 through 24 do not include the effects of inhibitors and poisons

2. The actual carbon consumption rate is the product of the reaction rate coefficient (modified by inhibitor terms) and the local partial pressure of the reactant at the reacting surface

Because of these two constraints, valid comparisons of the reaction rates can only be made for specific propellants. Conclusions based only on Figures 18 through 24 can be very misleading. For instance, the edge PG results of Figure 18 indicate that the reaction rate for H_2O at 6000°R ($1/T_w = 3 \times 10^{-4} K^{-1}$) is about two orders of magnitude greater than that for H_2. However, GASKET code calculations show that the mole fraction of H_2O is about four orders of magnitude less than that of H_2 (Figure 8). Hence the carbon consumption rate for the H_2O - C* reaction will about two orders of magnitude less than that for the H_2 - C* reaction.

6.2 RESULTS OF LIMITED CHARACTERIZATION STUDIES

H_2 Test Gas

From the results of the full characterization studies, it was concluded that H_2 is the major contributor for carbon consumption in the temperature range corresponding to typical motor firing conditions. H_2O and CO_2 are somewhat less reactive in this same temperature range. In fact, their significance diminishes due to the disappearance of both species by dissociation. These findings suggest that H_2 is the most appropriate test gas for material screening in the APG.

An H_2 test gas simplifies the interpretation of data. The reason is that the H_2 - C* reaction is not strongly inhibited by other gas species, halogens included. Thus, the kinetic rate of this reaction closely obeys the Arrhenius expression, i.e.,:

$$\dot{m}_c = A\, e^{-E/RT_w}\, P_{H_2}$$

By plotting log ($\dot{m}_c/P_0$) versus $1/T_w$ with the APG data, a straight line should be obtained. This straight line can then be extrapolated to the motor firing temperature range to estimate the ablation performance of the screening materials. Some engineering judgment must then be used to include the effect of H_2O and CO_2 reaction.
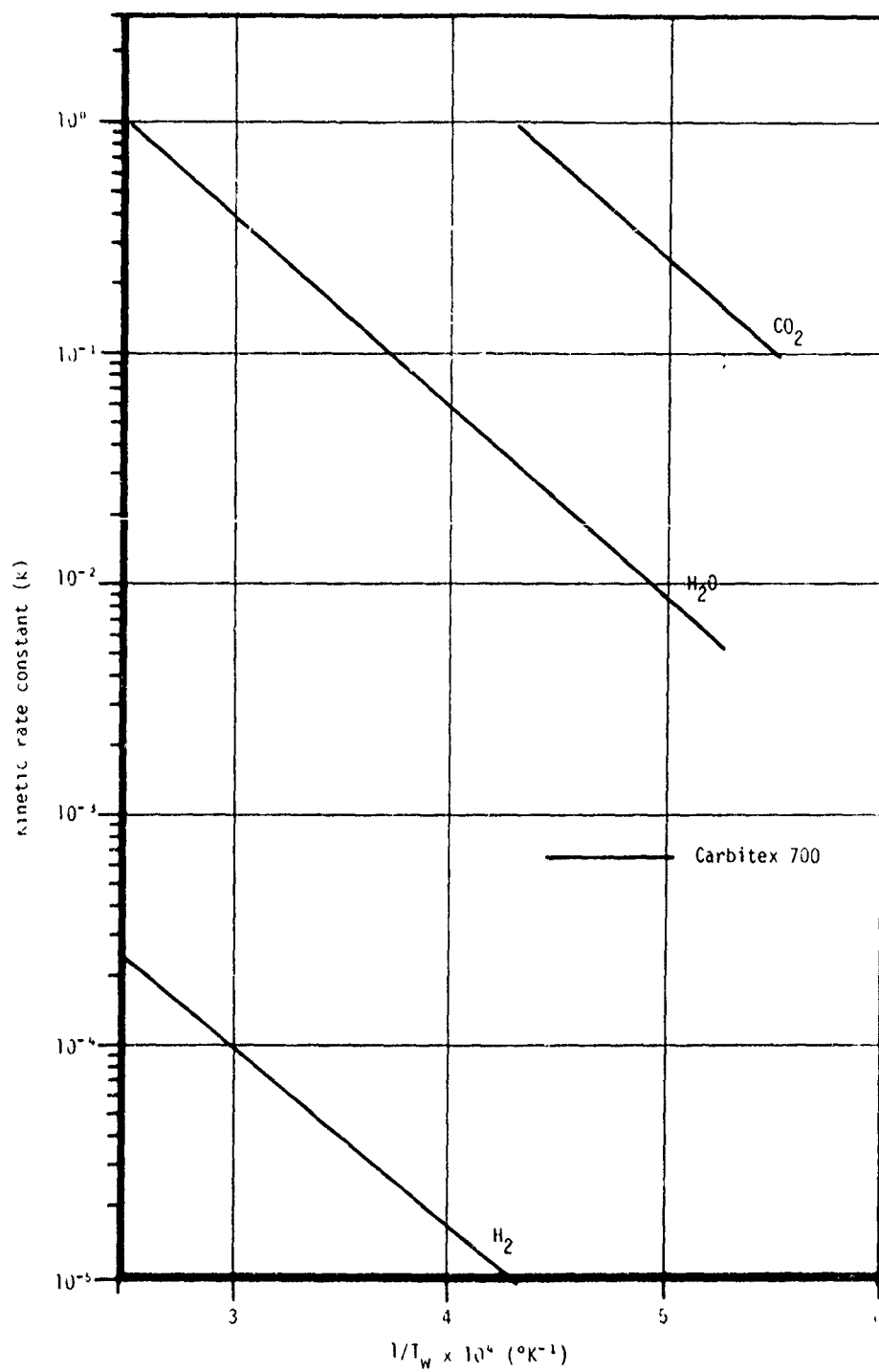
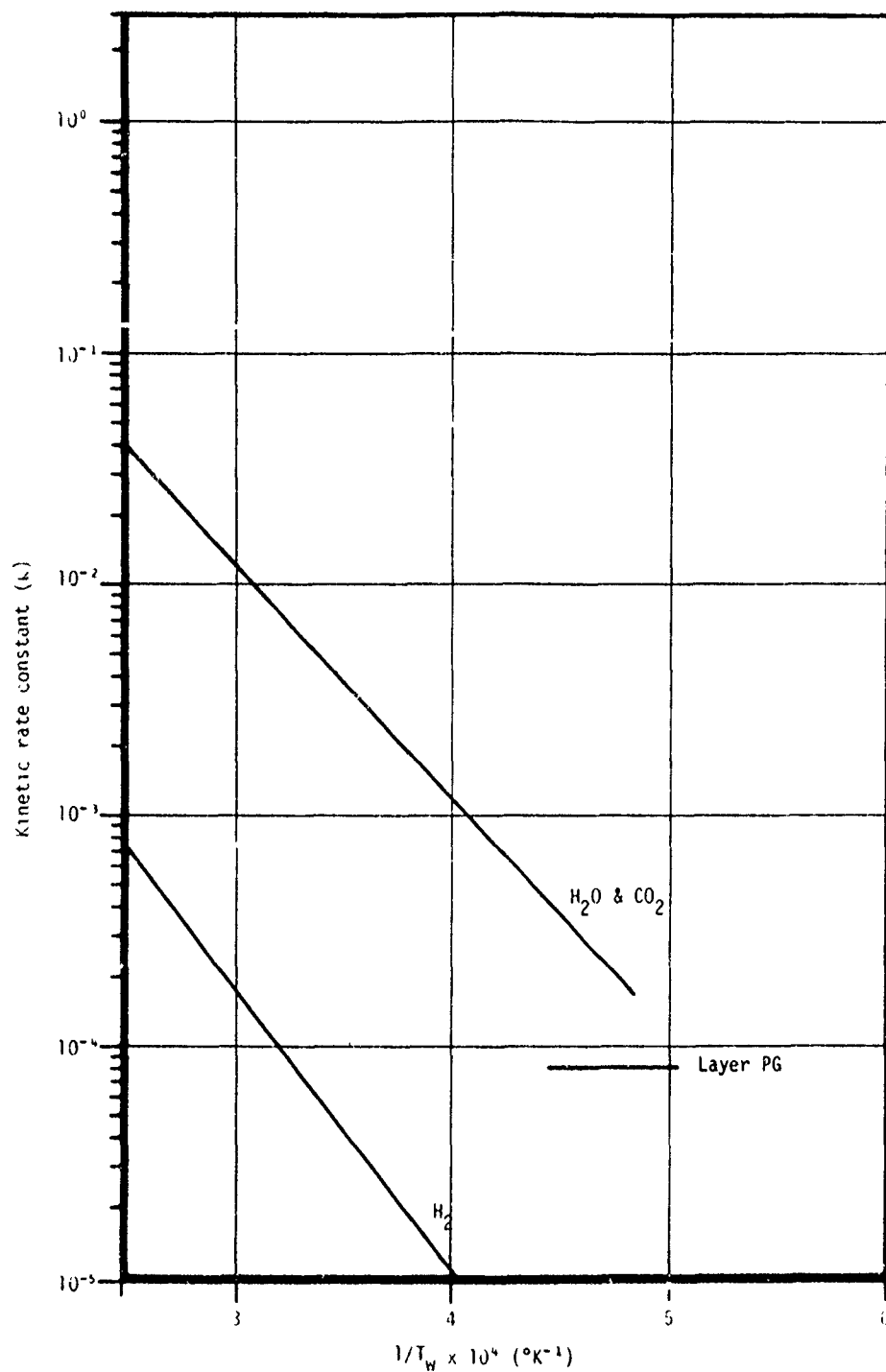Figure 23. Reaction rate coefficients for Carbitex 700 carbon/carbon.

81

Figure 24. Reaction rate coefficients for Atlantic
Research Corporation layer pyrolytic graphite.

Figures 25 and 26 show the relative ablation performance of the following carbon/carbon materials in the APG.

- HRX 5125

- HRX 5875

- MDAC 3-D C/C

- Pyrocarb 903

- Pyrocarb 903 HD

These are compared to the full characterization material, Pyrocarb 901. Based on these results, the ranking of ablation performance at motor firing conditions was determined and is presented in Table 17.

TABLE 17. RANKING OF CARBON/CARBONS BASED
ON MASS CONSUMPTION PERFORMANCE

Ranking	Material Designation	Source	Measured Density (gm/cc)	Reinforcement Precursor
1	3-D C/C	MDAC	2.0	Rayon yarn 3D orthogonal weave
2	HRX 5125	Haveg	1.55	Rayon fabric 0°-22°-45° ply orientation
3	Pyrocarb 903 HD	Hitco	1.90	PAN fabric 0°-45°-90° ply orientation
3	Pyrocarb 903	Hitco	1.84	Same as Pyrocarb 903 HD
4	HRX 5875	Haveg	1.82	PAN fabric 0°-22°-45° ply orientation
5	Pyrocarb 901	Hitco	1.65	Rayon fabric 0°-45°-90° ply orientation

From the carbon/carbon data, an attempt was made to relate the measured relative performance to the construction of the composite. In particular, the relative orientation of the adjacent plies, the reinforcement precursor and the composite density were considered. No ply orientation relationship was observed; however, some general relationships were found for the reinforcement precursor and the composite density.

Generally, it was found that:

- Rayon precursor composites are superior to PAN precursor composites of equal density

- Within classes of materials that have the same precursors, high density materials perform better than low density materials
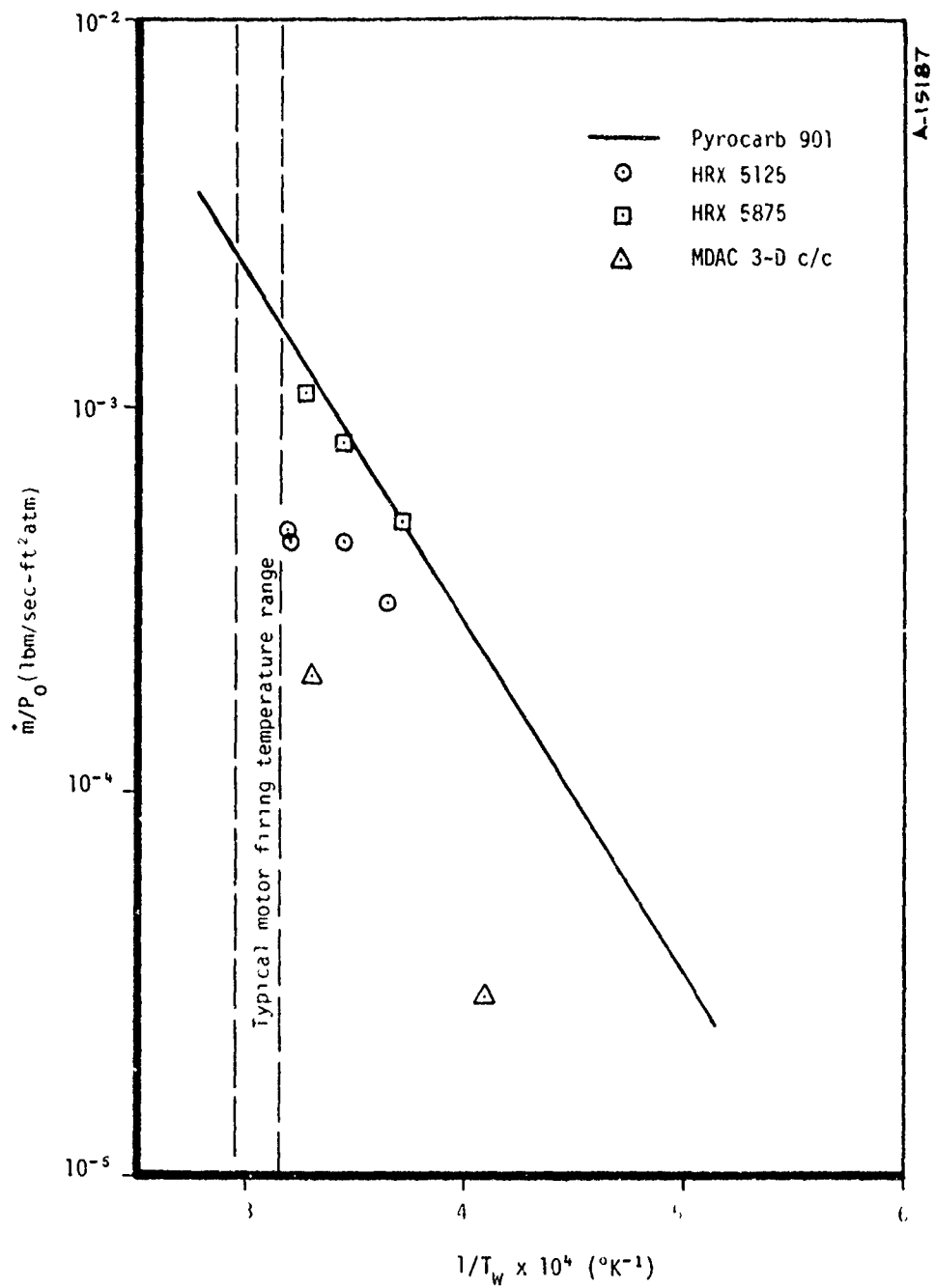
Figure 25. Carbon/carbons, APG test gas — H_2.

10^{-2}

——————— Pyrocarb 901

⊙   Pyrocarb 903

⊡   Pyrocarb 903 HD

10^{-3}

Typical motor firing temperature range

$\dot{m}_i/P_O$ (lbm/sec-ft^{2}atm)

10^{-4}

10^{-5}

3   4   5   6

$1/T_W \times 10^4$ (°K^{-1})
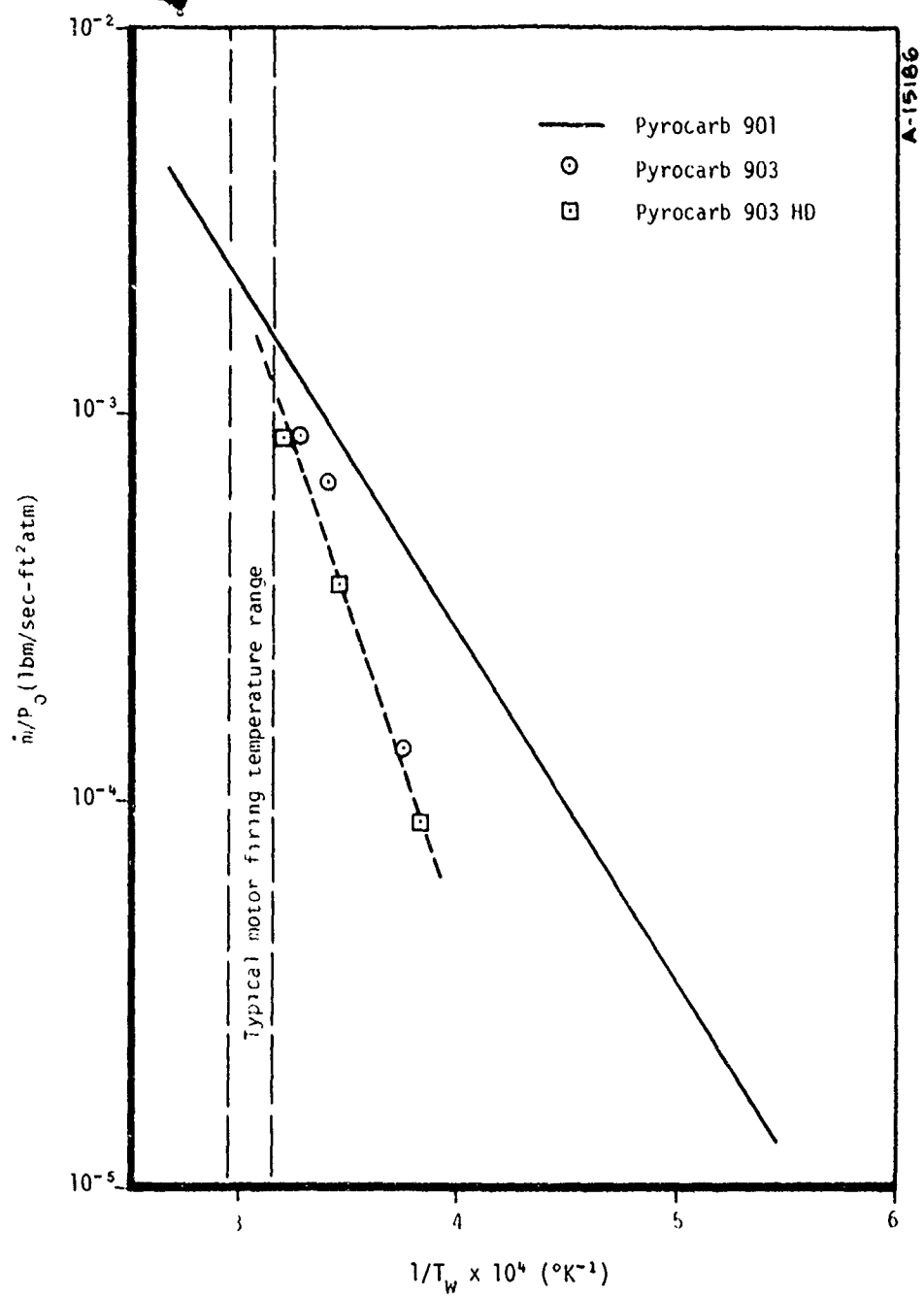
Figure 26.   Carbon/carbons, APG test gas — H_2.

These conclusions were made based on the results presented in Table 17 and Figure 27. Figure 27 was constructed from the results of Figures 25 and 26 by extrapolation of a mean line through the APG data. For reference, these lines are shown in Figure 28.

Figure 29 shows the performance variations of pyrolytic graphite materials in a hydrogen environment. These materials were fabricated by:

- Hitco and Atlantic Research Corp. (ARC) for a-b plane

- Supertemp and Pfizer for c plane

The ARC and Supertemp materials were used as references and are shown in Figure 29 as lines. It is apparent from this figure that the material source is not important for the ablation performance of pyrolytic graphites.

The relative performance of modified pyrolytic graphite materials in a hydrogen environment are shown in Figure 30. These materials included:

- 5, 15 and 23 percent (by weight) silicon carbide codeposited pyrolytic graphite

- 65 percent (by weight) hafnium carbide codeposited pyrolytic graphite

Although it is presumptuous to reach any conclusions from the limited amount of APG data, it appears that:

- 23 percent SiC/PG performs similarly to edge oriented PG

- 5 percent SiC/PG performs marginally better than 15 percent SiC/PG, which performs noticeably better than 23 percent SiC/PG. It should be noted that the 23 percent SiC/PG was highly nonuniform so the 23 percent is merely a nominal indication of the SiC content.

- 65 percent HFC/PG material performs similarly to edge-oriented PG; however, when the mass loss is transformed to surface recession, the performance of this material is quite good since it has a density of about 9 gm/cc compared to 2.2 gm/cc for PG

Figure 31 shows the relative ablation performance of PO3 and ATJ-S graphite relative to the full characterization material, G-90 graphite. The ablation performance of these three materials is in the order ATJ-S, PO3, and G-90, although the differences between these materials is not significant.

$H_2 - O_2$ Test Gas

APG results for $H_2 - O_2$ gas mixtures are presented without further discussions in Figures 32 through 35.
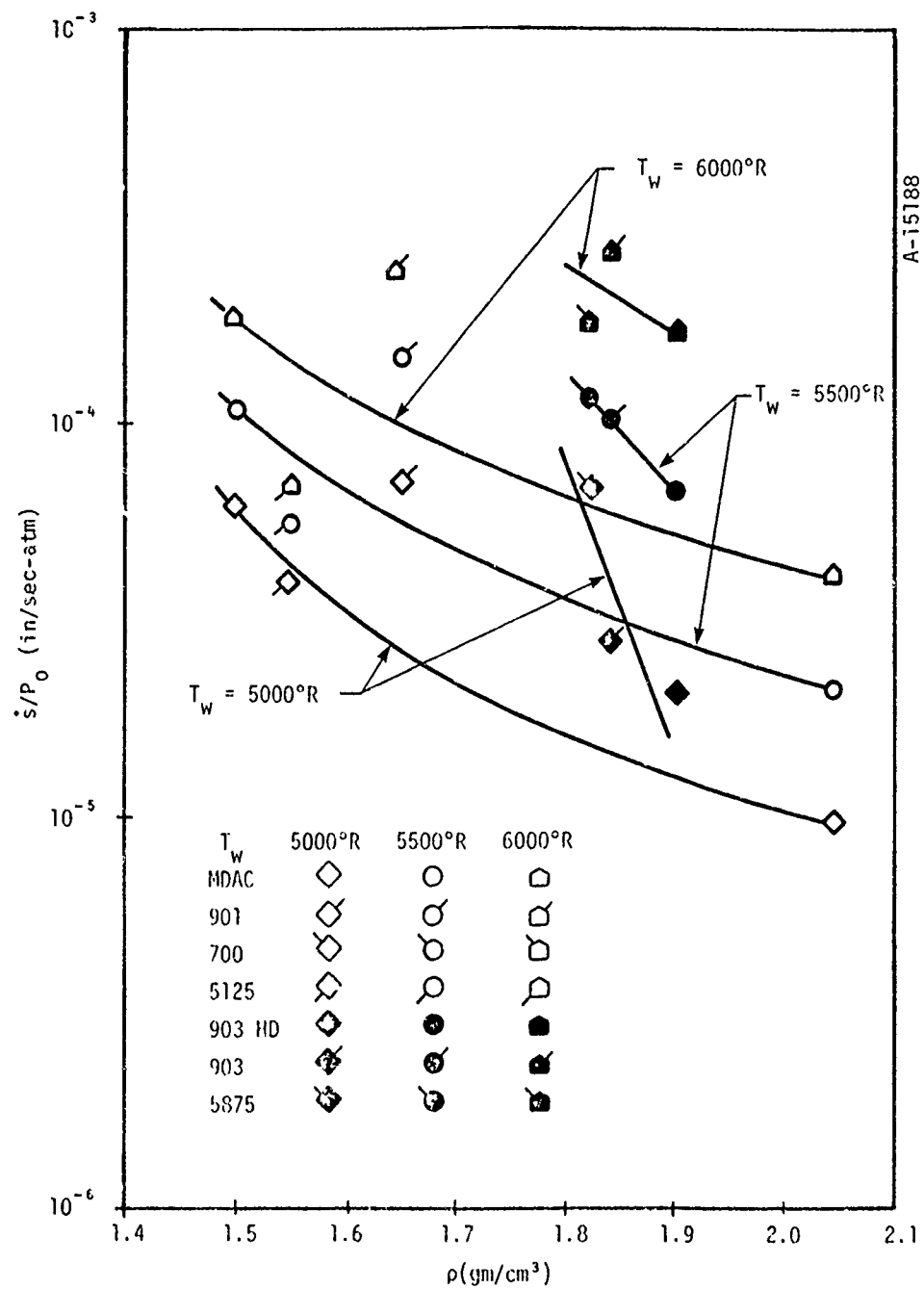
Figure 27. Measured ablation rates in a hydrogen environment.
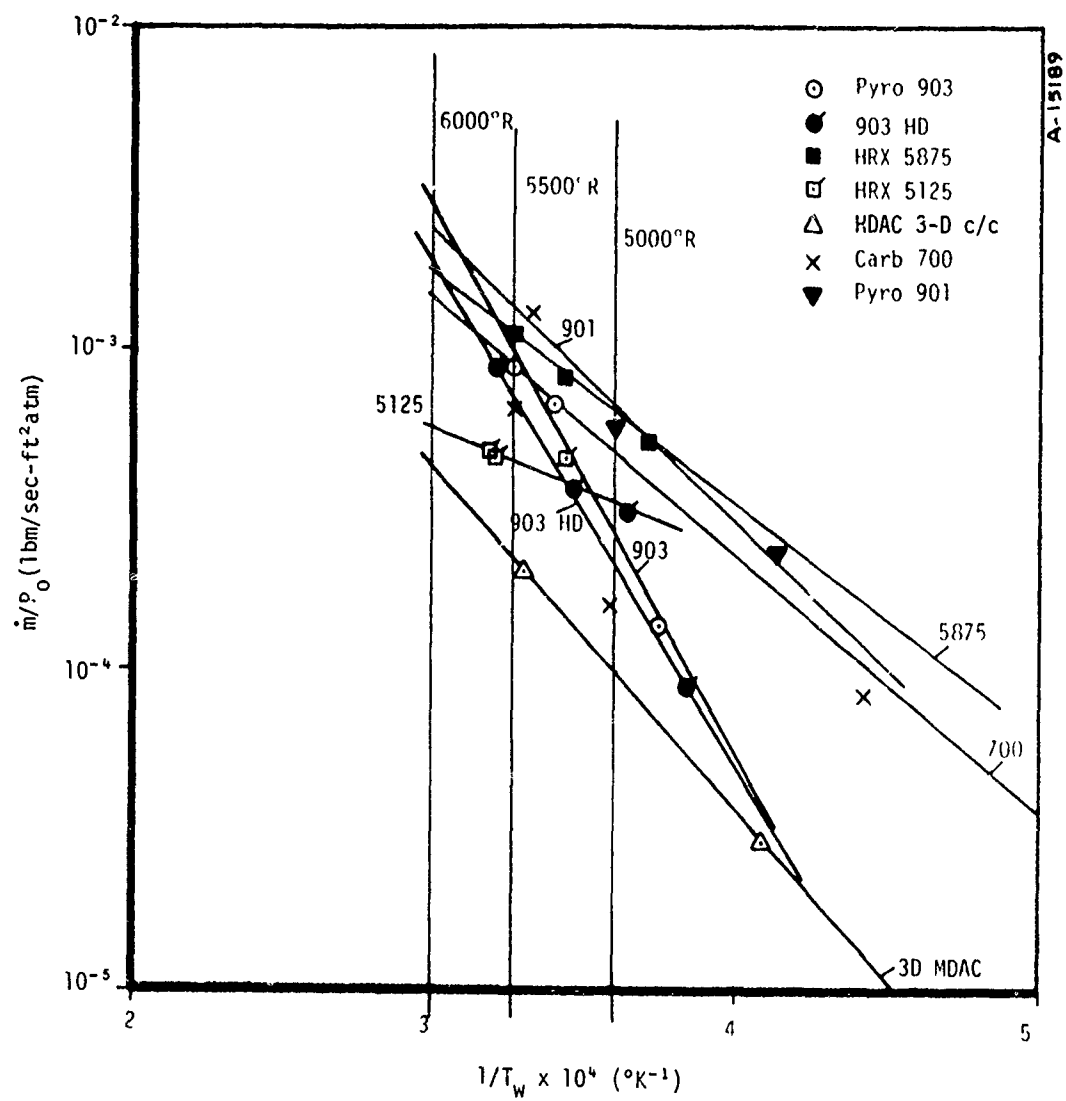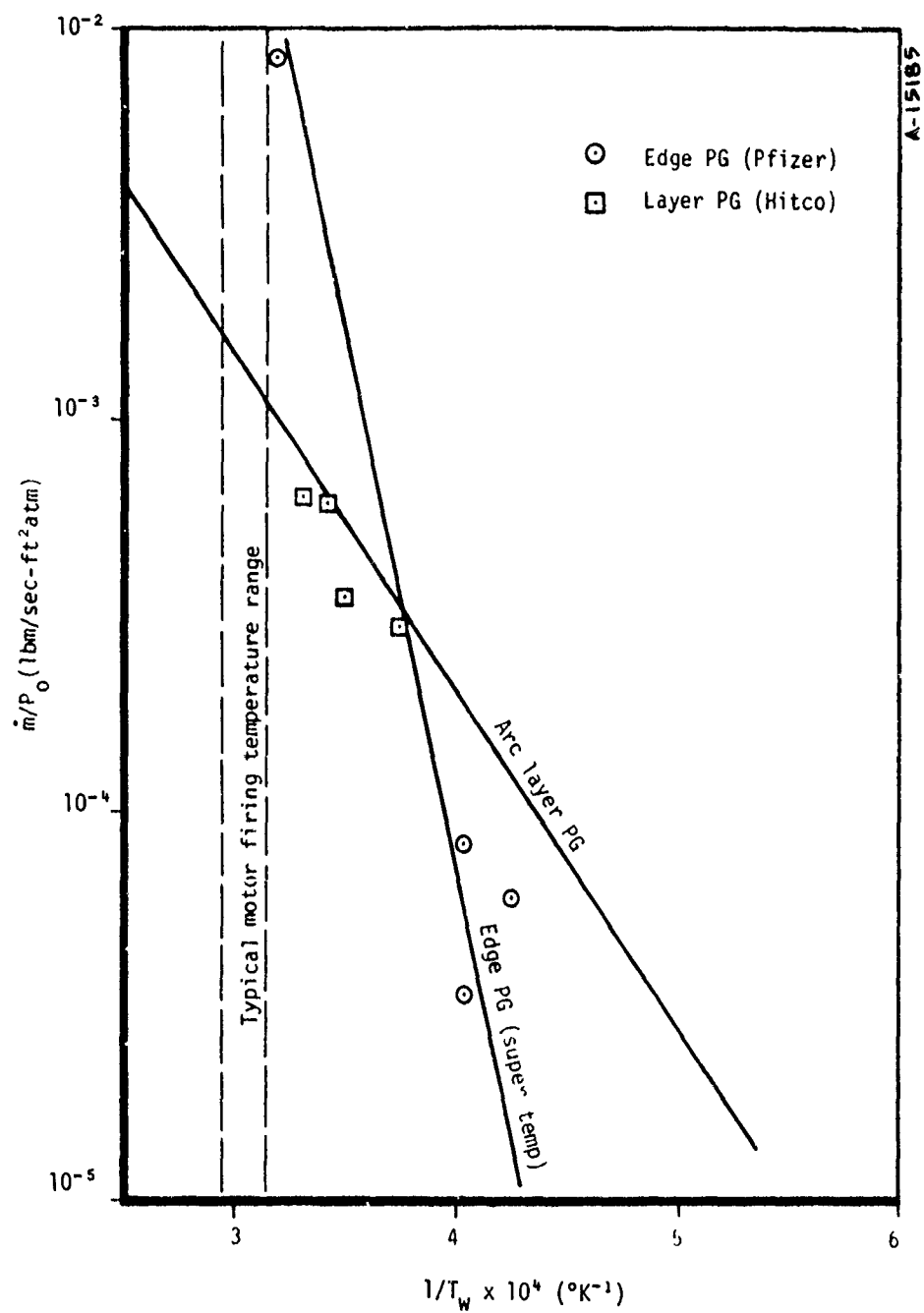
Figure 28. Data for construction of Figure 27.

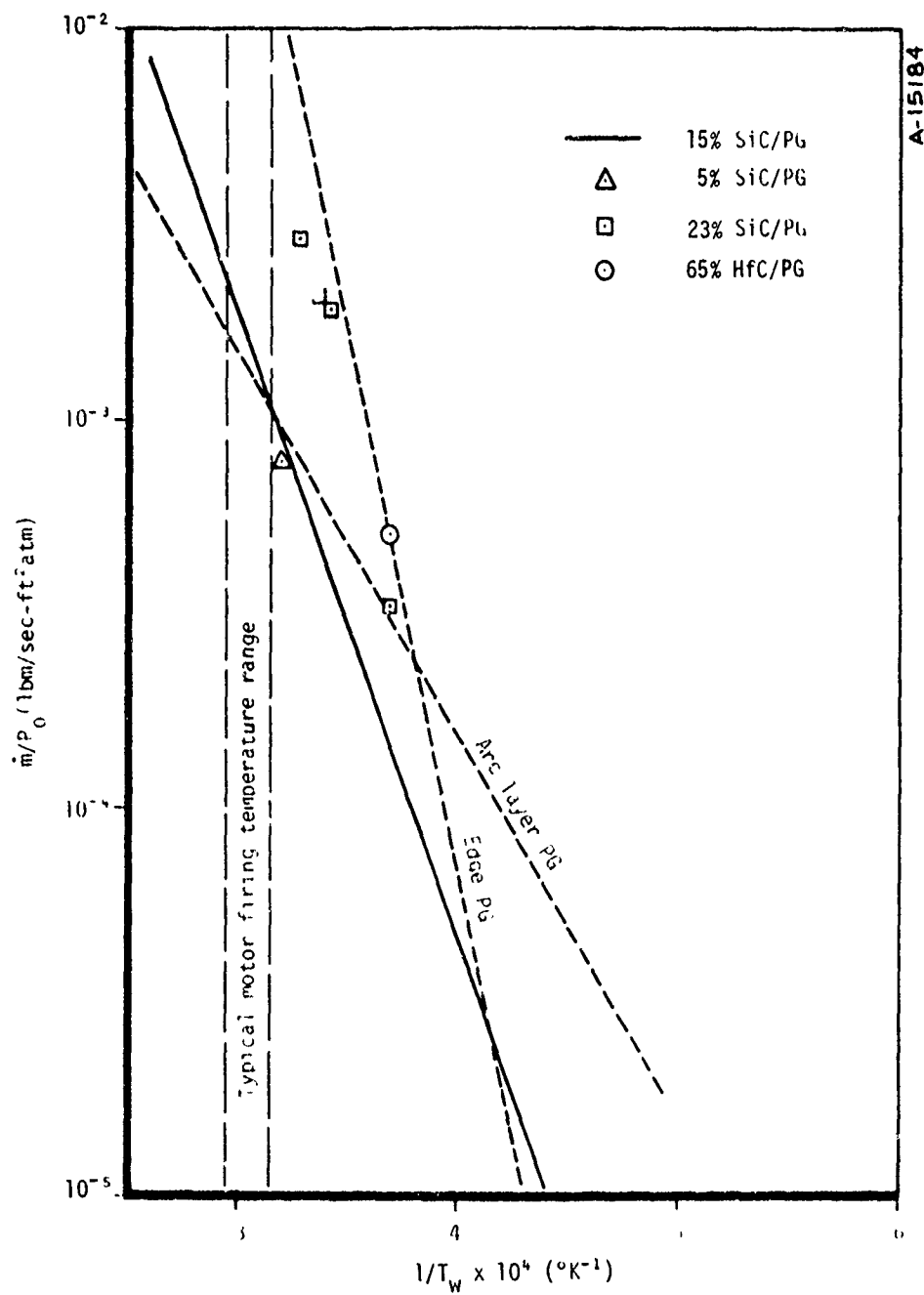Figure 29. Ablation data, pyrolytic graphites, APG test gas — H_2.

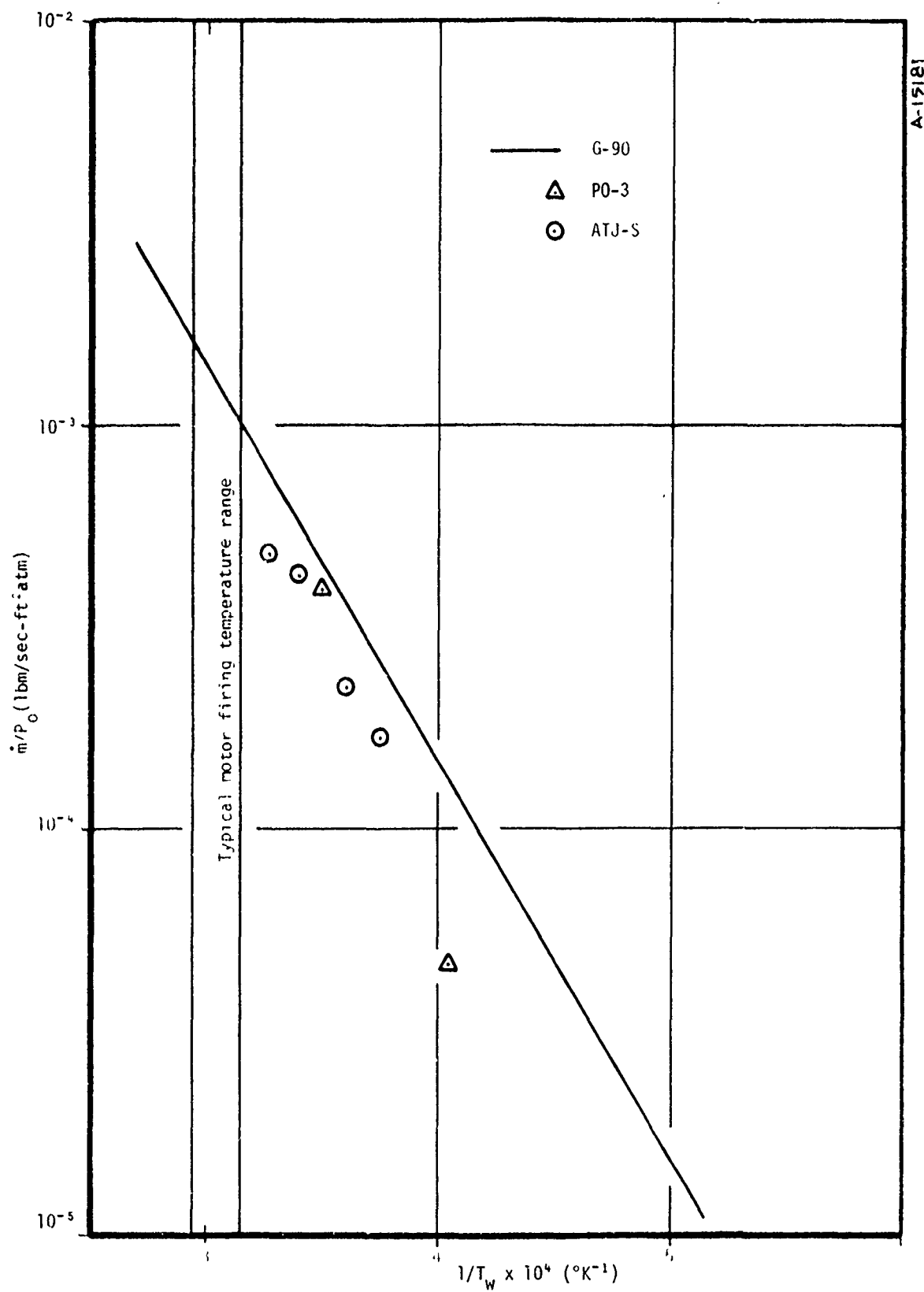Figure 30. Ablation data, modified pyrolytic graphites, APG test gas — H_2.

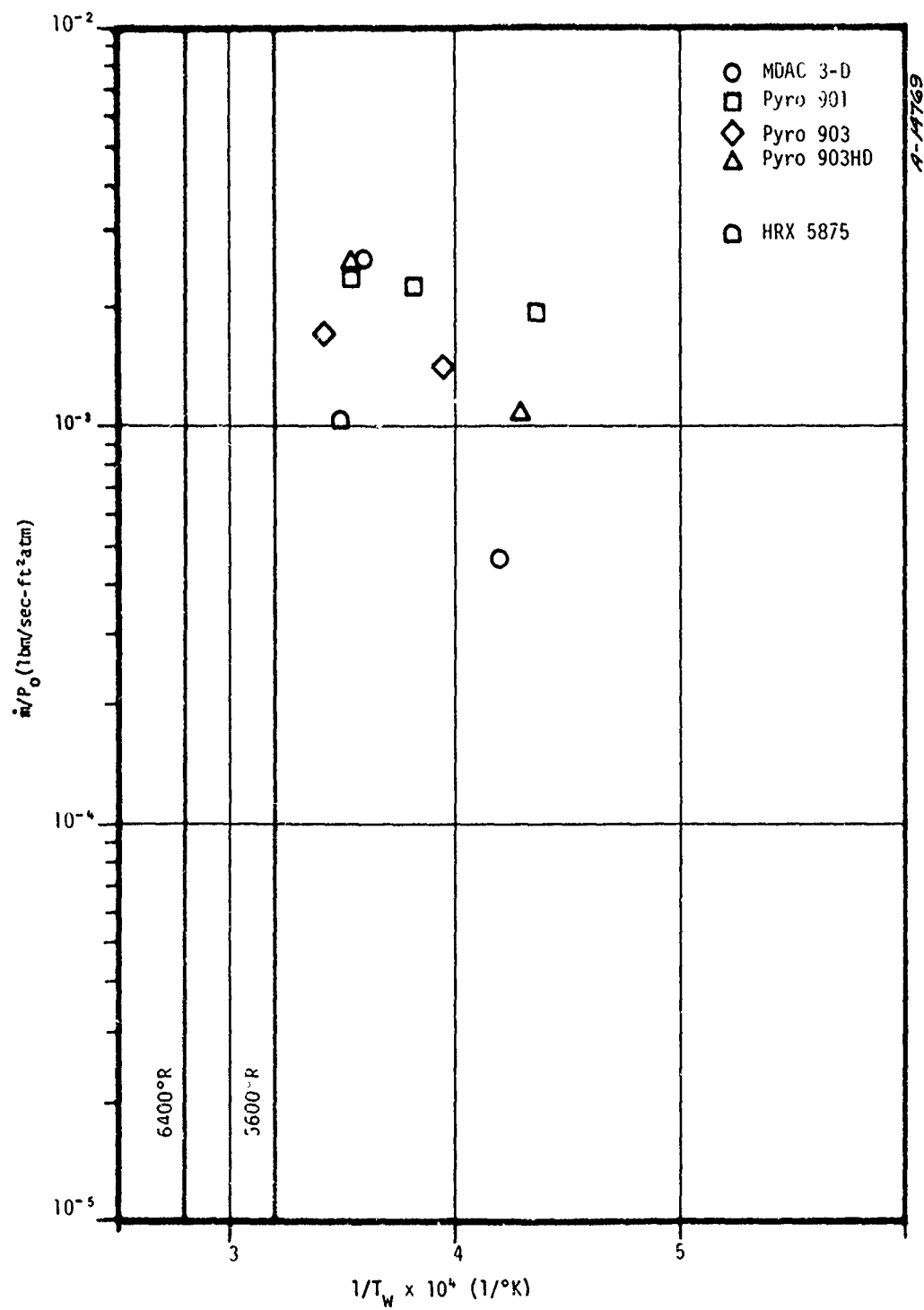Figure 31. Ablation data, bulk graphites, APG test gas — H_2.

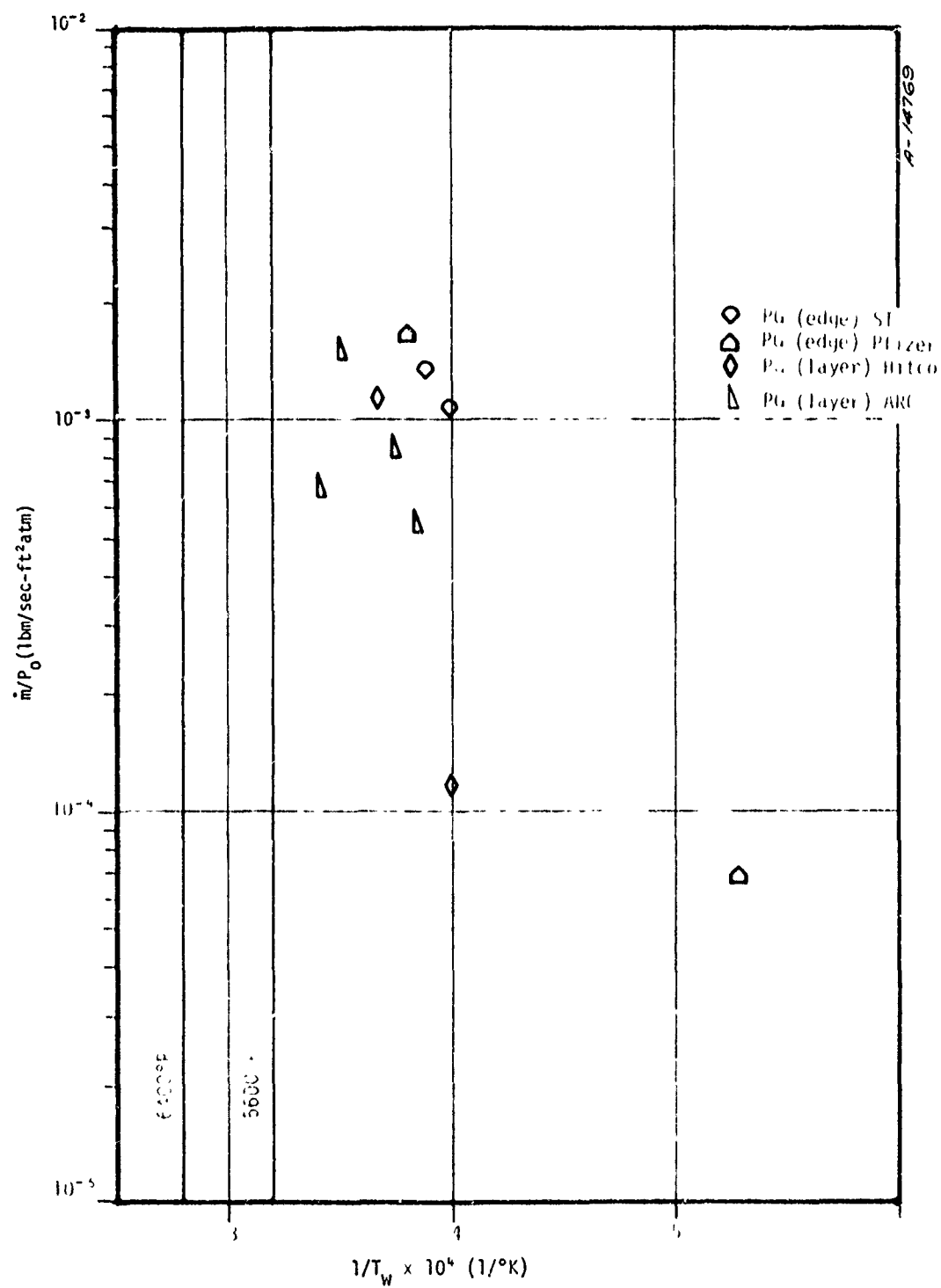Figure 32. Ablation data, carbon/carbons, APG test gas — H_2/O_2.

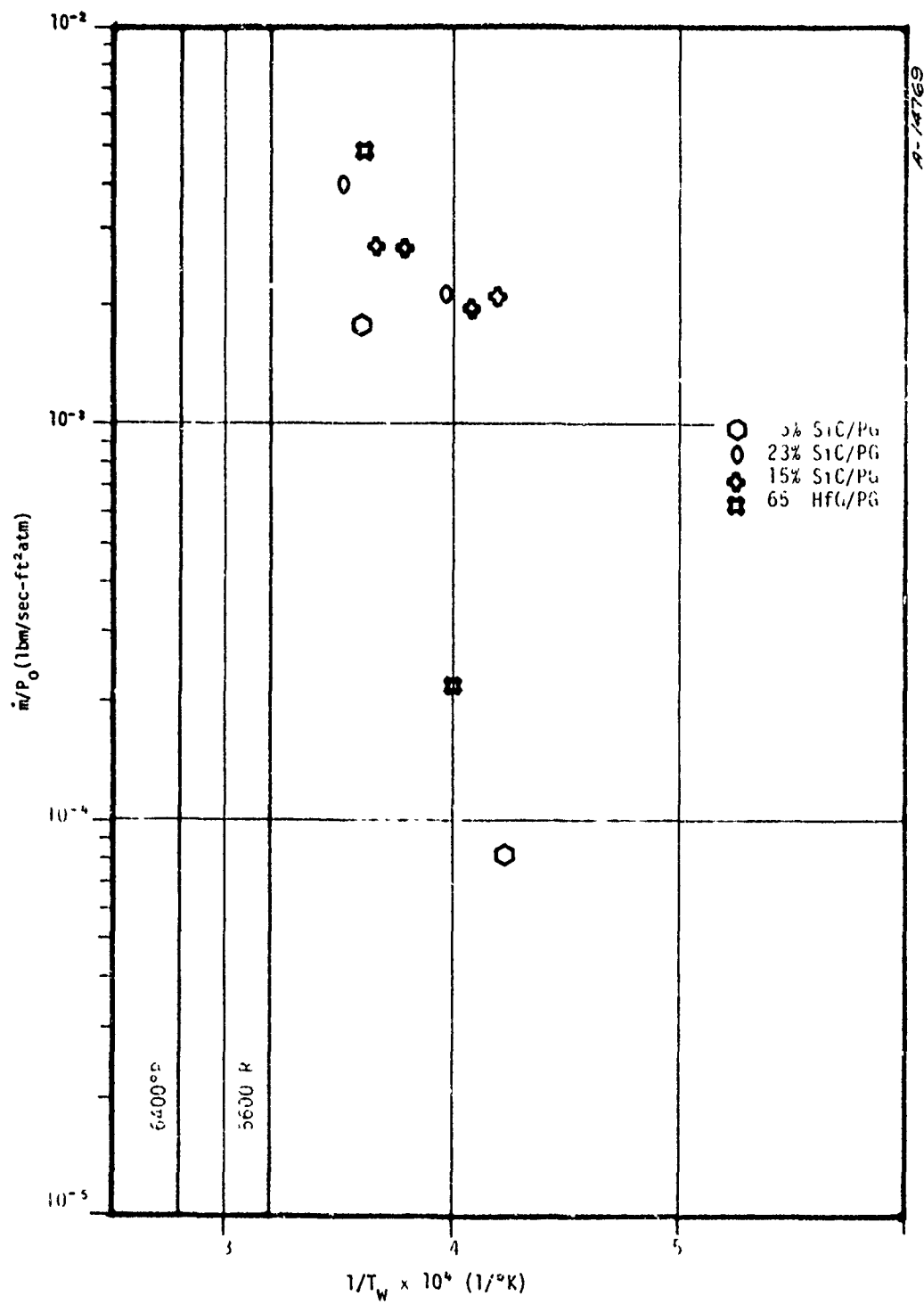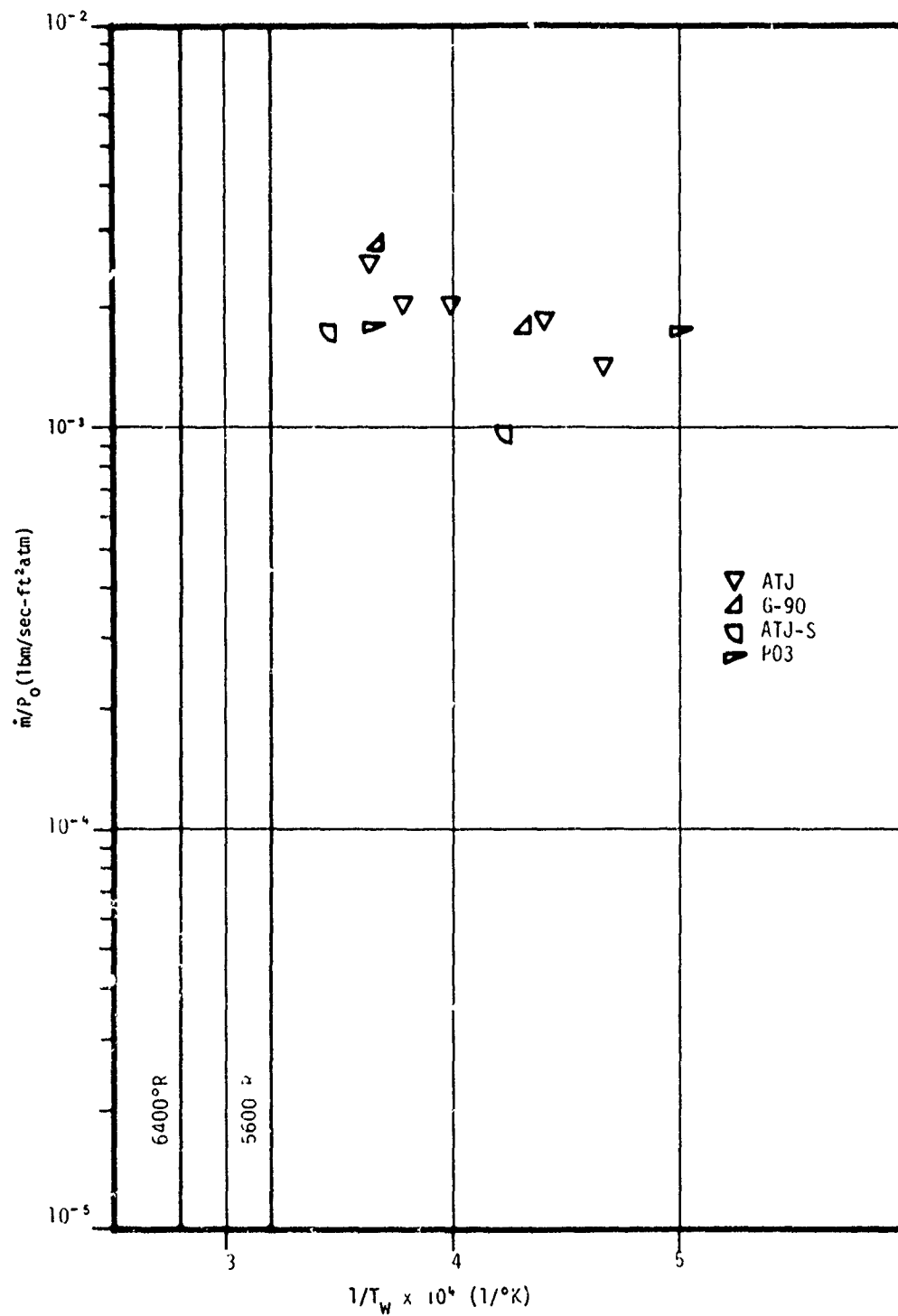Figure 33. Ablation data, pyrolytic graphites, APG test gas H_2/O_2.

Figure 34. Ablation data, modified pyrolytic
graphites, APG test gas H_2/O_2.

94

Figure 35. Ablation data, bulk graphites, APG test gas — H_2/O_2.

SECTION 7

PREDICTED ROCKET NOZZLE PERFORMANCE

The GASKET2 code (Reference 9), which includes the kinetic models presented in Table 16, was used to predict many actual motor firings. Specifically, 15 correlation studies and 6 performance studies were performed. The purpose of the correlation studies was to provide basic motor firing data to be incorporated in the kinetics correlation. Once this data was provided, the correlation studies were used to verify the resulting model. These verification calculations, along with performance studies in support of AFRPL technology programs, have been performed and will be summarized in this section.

7.1 ANALYSIS PROCEDURE

The analysis procedure used to predict motor firings is described in this section. The events which occur near the internal surface of an ablative rocket nozzle are illustrated in Figure 36. An inviscid flow field comprises the bulk of the flow of propellant gases through the nozzle. Typically, the propellant contains less than 21 percent (by weight) of aluminum, which forms liquid alumina particles that flow with the other products of combustion through the nozzle. Near the surface, the flow field is represented by a boundary layer in which alumina particles are not considered to be present. Chemically reactive species diffuse through this boundary layer and cause surface ablation. The nozzle thermal protection material must respond to three sources of energy transfer the convection and diffusion of energy across the boundary layer and the radiation or energy from high temperature alumina particles in the inviscid case flow. All of these energy events result in a given amount of energy being conducted into the material to cause internal component heating.

The procedure used for ablation predictions treats the inviscid flow field, the boundary layer and the radiant energy transfer separately. Although the analyses are separate, the final solution is properly coupled as illustrated in Figure 37. Each area will be discussed individually in the following paragraphs.

Flow Field

The flow field was analyzed with the "Aerotherm Chemical Equilibrium (ACE)" computer code (Reference 20). This is a chemical equilibrium code which is used to compute the local thermodynamic
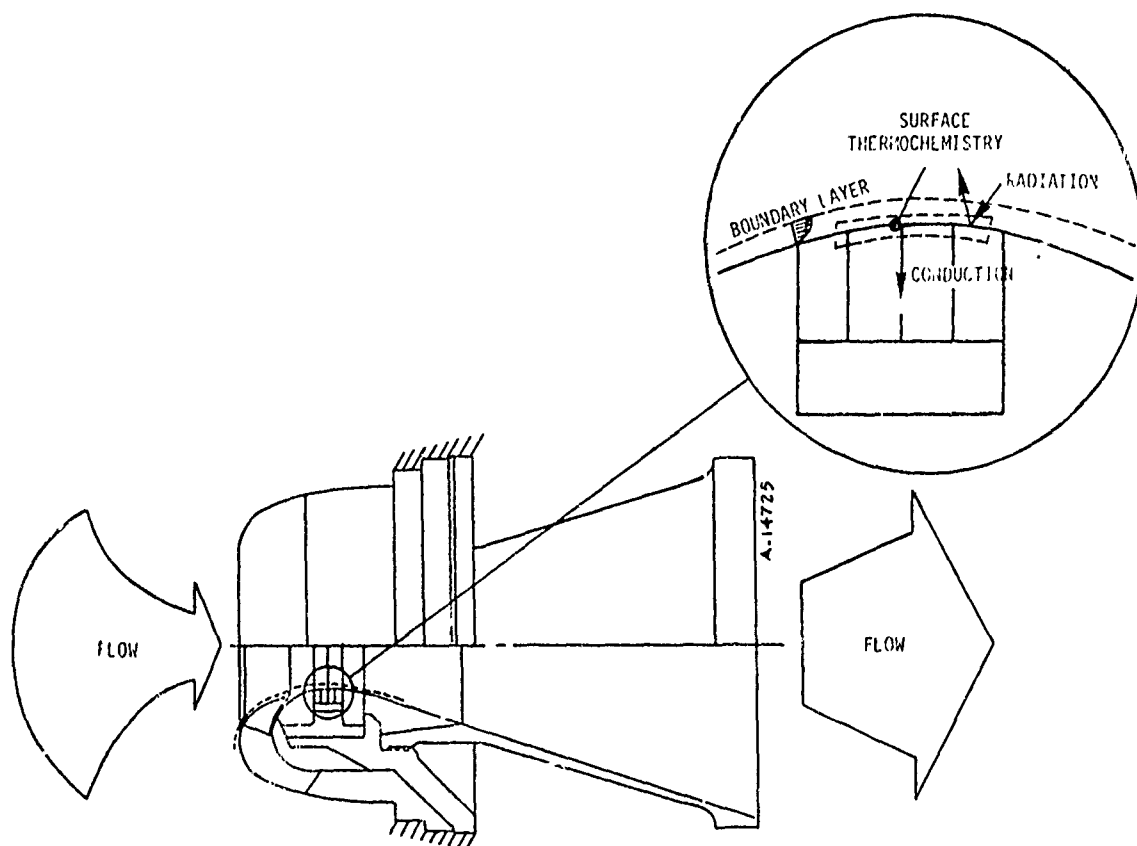
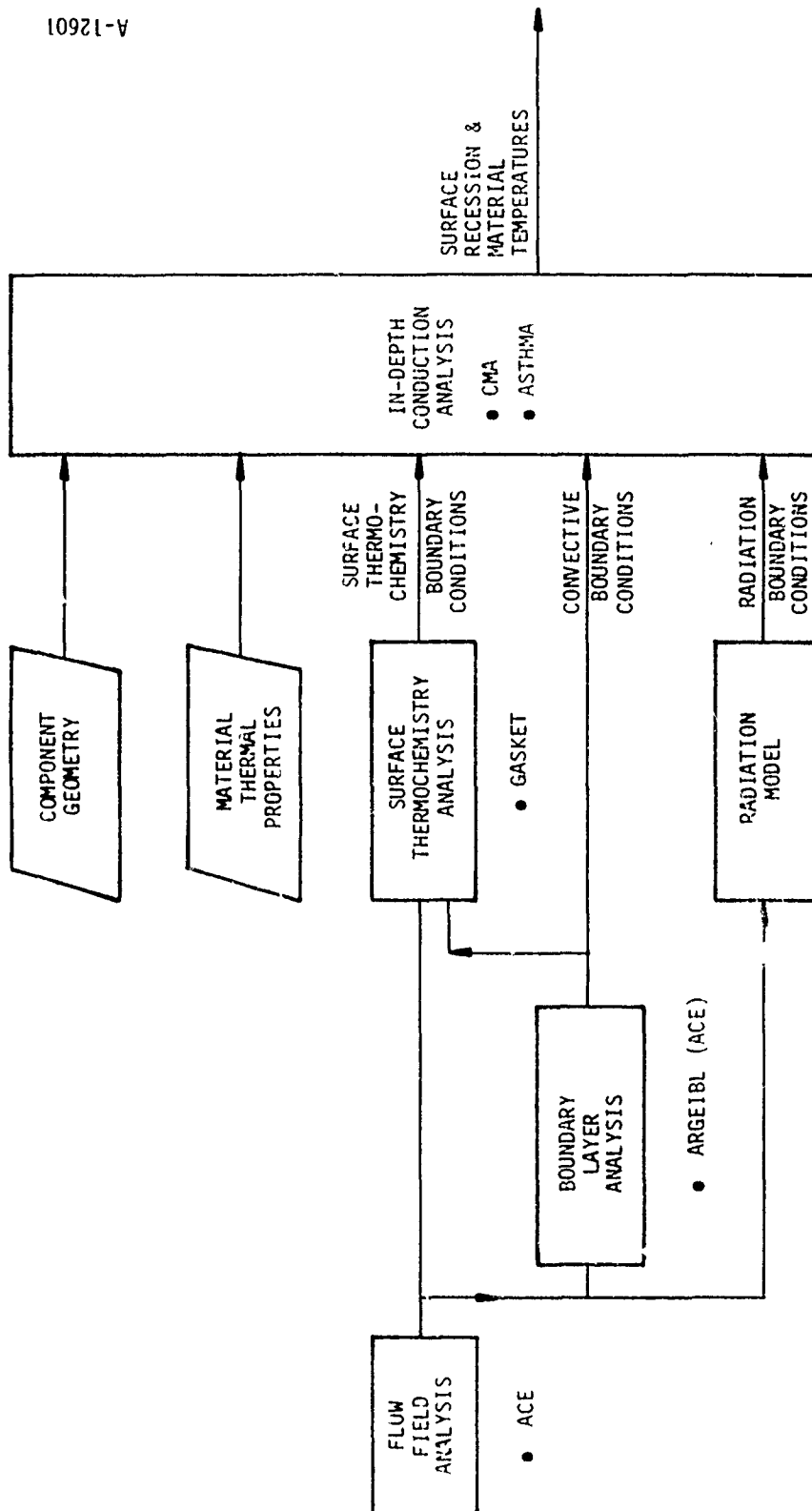Figure 36. Major areas of analysis in prediction procedure.

Figure 37. Thermal analysis flow chart.

state throughout the nozzle. The primary variables of concern are the local pressures, temperatures and chemical species. These are determined by performing many isentropic closed-system equilibrium solutions throughout the nozzle. The ACE code can handle any arbitrary real gas by knowing the chamber state (temperature and pressure) and the propellant elemental composition. Both gaseous and liquid phases are computed, but no thermal or velocity lags are accounted for. The closed system solutions are associated with given positions in the nozzle by assuming one-dimensional flow and using conservation of mass relations.

Boundary Layer

The analysis of the boundary layer is performed by using the "Aerotherm Real Gas Energy Integral Boundary Layer (ARGEIBL)" computer code (Reference 21). This is an energy integral technique which can handle any arbitrary real gas with the input of general Mollier-type tables generated by the ACE computer code. Since no alumina particles are in the boundary layer, these properties are for the gas phase only. Other input consists of edge state variables (P_e and T_e) generated by the flow field analysis. Arbitrary wall temperatures are also handled by this code. Since these are not predicted until a conduction analysis is performed, an estimation of the wall temperature is required. If this estimation proves to be far in error, an iteration back through the boundary layer analysis is necessary.

Turbulent flow is assumed and the boundary layer is started (with zero energy thickness) at the nose of submerged nozzles and at the base of the aft closure for conventional nozzles. The nose of a submerged nozzle is defined as that point furthest axially upstream of the throat and the base of an aft closure is considered as the point where the nozzle insulation mates to the insulation in the propellant case.

To compute the heat transfer coefficient for ablating surfaces, a blowing correction is made to the ARGEIBL results. This is a multiplying factor which is a function of the mass injected into the boundary layer. The correction is made internal to the CMA code and a detailed discussion can be found in Reference 22.

Previous experience has shown that the heat transfer coefficient predicted by the ARGEIBL code is high and should be multiplied by 0.75; that is:

$$\rho_e u_e C_H = 0.75 \, (\rho_e u_e C_H)_{ARGEIBL} \tag{16}$$

where $(\rho_e u_e C_H)_{ARGEIBL}$ is the convective heat transfer coefficient predicted by the ARGEIBL code. This factor has been included in all of the predictions reported. For the transient in-depth thermal

analysis presented in subsequent sections, Equation (16) is modified further to account for the actual chamber pressure history by using the relationship:

$$\rho_e u_e C_H = 0.75 \left(\frac{P_o}{P_{o_{ave}}}\right)^{0.8} (\rho_e u_e C_H)_{ARGEIBL} \tag{17}$$

where P_o is the instantaneous measured (or predicted) chamber pressure and $P_{o_{ave}}$ is the average chamber pressure assumed for the flow field analysis.

Surface Thermochemistry

The surface thermochemistry analysis is performed by using the Aerotherm "Graphite Surface Kinetics (GASKET2)" computer code (Reference 9). It computes the surface state (complete wall gas thermodynamic and chemical make-up) of many graphitic materials exposed to a corrosive rocket nozzle environment. The reactions which occur between the graphite material and the propellant gases are considered kinetically-controlled and are modeled by Arrhenius-Langmuir type reaction rate equations. This code can handle arbitrary propellant gases and arbitrary surface reaction kinetic constants. Kinetics constants used for the predictions discussed in this section are currently included in the GASKET2 code for the following graphitic materials:

- a-b plane PG

- c plane PG

- 15% SiC/PG

- Pyrocarb 901 carbon/carbon

- Carbitex 700 carbon/carbon

- ATJ bulk graphite

- G-90 bulk graphite

As input, the GASKET2 code requires the local thermodynamic edge state (P_e and T_e) and the elemental composition of the gas, which are obtained directly from the ACE generated flow field analysis. The mass transfer coefficient is also required and is obtained directly from the heat transfer coefficient computed by ARGEIBL from the following relationship:

$$\rho_e u_e C_M = \left(\frac{Pr}{Sc}\right)^{2/3} \rho_e u_e C_H \tag{18}$$

where
$\quad$ Pr = Prandtl number
$\quad$ Sc = Schmidt number

The Prandtl and Schmidt numbers are both obtained from the ACE generated Mollier input to the ARGEIBL code. For nozzles whose pressure traces are far from constant throughout a firing, Equation (17) shows that the heat transfer coefficient (and thus mass transfer coefficient) will vary with time. For these cases, up to three surface thermochemistry analyses are performed for a given firing. The conduction solution procedure then interpolates between these solutions to obtain instantaneous firing and boundary conditions.

To model the radiative boundary conditions during nozzle firings, a parallel plate model was used. This model applies to aluminized propellants and assumes that the particle laden stream of combustion products is optically thick and that it exchanges radiant energy with the surface as if the stream and wall were parallel plates. In this way, multiple reflections between the wall and stream were taken into account. In addition, the assumption was made that both the stream and wall behave as gray bodies and that they emit and reflect radiant energy diffusely. Based on the above assumptions, the net radiant heat flux relation is given as

$$\dot{q}_{net\ rad} = \varepsilon_{eff}(\sigma T_s^4 - \sigma T_w^4) \tag{19}$$

where

ε_{eff} — Effective emissivity $= \dfrac{1}{1/\varepsilon_w + 1/\varepsilon_s - 1}$

ε_w — Wall material emissivity

ε_s — Particle laden stream emissivity

σ — Stefan-Boltzmann constant

T_s — Free stream (edge) temperature

T_w — Wall temperature

To determine the effective emissivity using Equation (19), the stream emissivity was defined as

$$\varepsilon_s = 1 - exp\ (-C\frac{n}{16}\ \rho D) \tag{20}$$

where

C — Empirical constant (0.808)

n — Percentage of aluminum loading

ρ — local density of propellant combustion species (lb/ft^3)

D — Local beam length, usually taken as the diameter (in.)

In-Depth Conduction

Both the Aerotherm "Axisymmetric Transient Heating and Material Ablation (ASTHMA)" (Reference 23) and the Aerotherm "Charring Material Ablation (CMA)" (Reference 22) computer codes were used for the in-depth conduction analyses. Bascially, the ASTHMA code is two-dimensional and CMA is one-dimensional. Both have the capability of handling temperature dependent material properties. CMA also has the capability of modeling materials which internally decompose. This capability was not exercised in the motor firing predictions since only graphitic surface materials were considered.

Figure 37 shows that the flow field (H_r), boundary layer ($\rho_e u_e C_H$), surface thermochemistry (B' map), and radiation (net radiation flux) analyses are all used as input to CMA and ASTHMA. Also shown as input are the component geometry and material properties. Material properties are referenced for each nozzle firing analyzed, but a majority of the properties were obtained from the "Aerotherm Graphitic Material Handbook of Thermophysical Properties" (Appendix B).

7.2 CORRELATION STUDIES

This section summarizes the 15 correlation studies which were performed. The following five kinetics models were verified by these studies:

- c plane PG

- 15% SiC/PG

- G-90 bulk graphite

- ATJ bulk graphite

- Pyrocarb 901 carbon/carbon

Predictions were made for test nozzles fired by several companies, using various propellants. The firings were both fullscale and subscale, with both submerged and conventional nozzles. Those chosen in most cases were typical of advanced ICBM conditions.

The motors used for the 15 correlation studies are as follows:

C Plane PG

1. TCC, MMIII, HTPB Demo

2. CSD, C-4, 3rd Stage Demo

3. ASPC, C-4, 1st Stage Demo

4. TCC, C-4, 1st Stage Demo (FST-002)

5. ASPC, Nimrod 14, Subscale

6. ASPC, Nimrod 15, Subscale

7. CSD, MX, Lower Stage, Subscale

8. TCC, C-4, 30-inch Material Evaluation (3SF-24)

15% SiC/PG

9. ARC, 7-inch

10. ARC, 3.5-inch

11. ASPC, Nimrod 6, Subscale

G-90

12. Rocketdyne Condor

13. CSD, FW-5

ATJ

14. Hercules, X259 Antares II

Pyrocarb 901

15. TCC, C-4, 30-inch Material Evaluation (3SF-24)

Complete details of all of the predictions are given in a second final report (AFRPL-TR-76-71). Since much of the work is classified, only a brief summary of the results will be presented here.

Figure 38 shows that 12 of the studies predicted total surface recession within 25 percent. The three that fell beyond the ±25 percent band were studies 1, 5, and 6. The second final report discusses in detail the comparisons between the predictions and the data.

7.3 PERFORMANCE STUDIES

As mentioned previously, the performance studies were done in support of AFRPL technology programs. A total of six were performed and are summarized as follows:

1. Hercules 3rd Stage MX (Carbitex 700) (Reference 10)

2. Rocketdyne Condor (Reference 11)

3. Hercules 3rd Stage MX (Pyrocarb 901) (Reference 12)

4. Standard 7-inch Nozzle (Throat Sensitivity) (Reference 13)
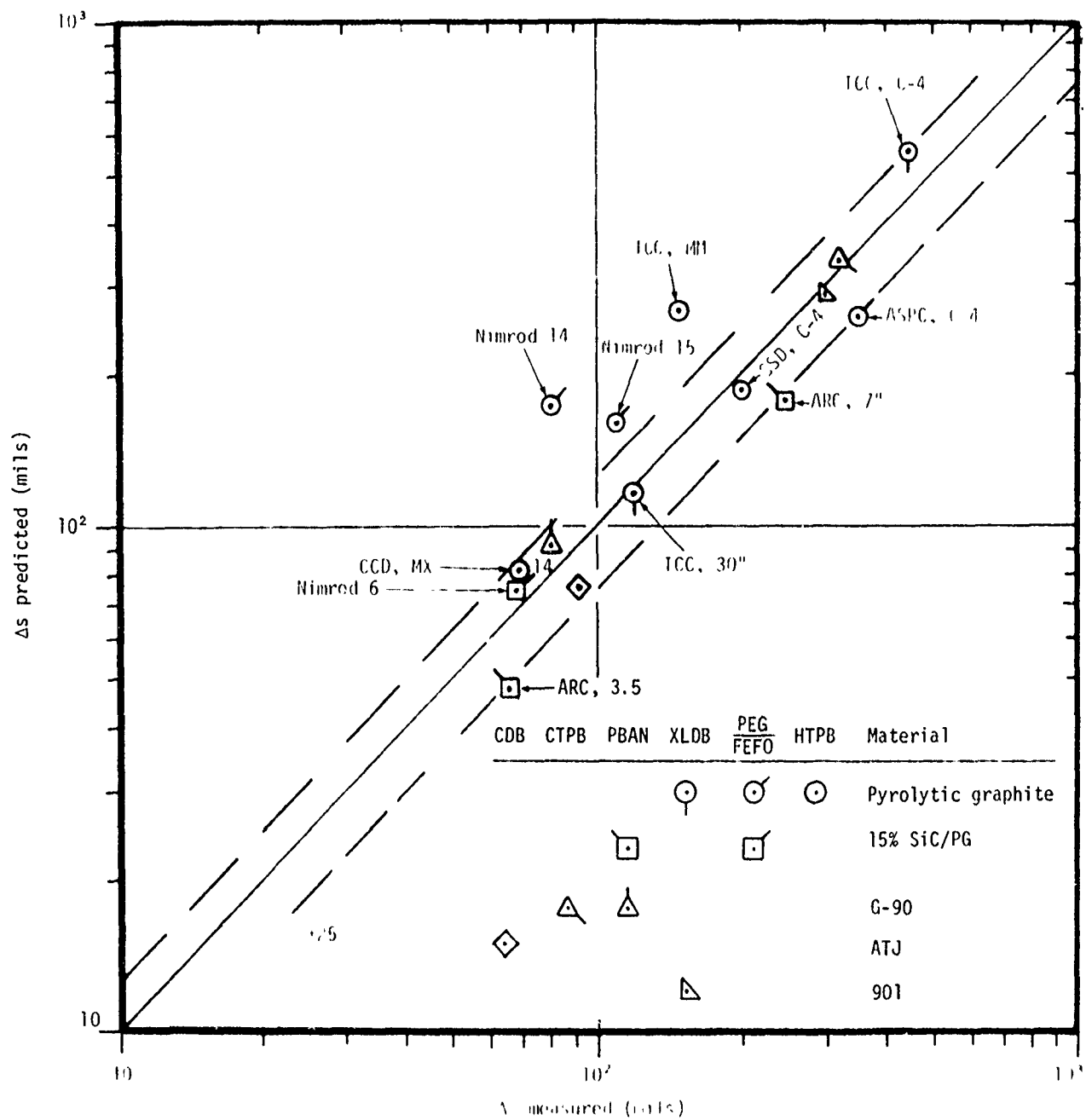
Figure 38. Comparison of measured and predicted ablation
for correlation studies.

5. Standard 7-inch Nozzle (Nosecap Sensitivity) (Reference 14)

6. BATES Motor (Thermostructural) (Reference 15)

Each study was reported in detail as individual nozzle bulletins published under this contract. In the following paragraphs a brief overview is given of each study.

Study 1 — Hercules 3rd Stage MX (Carbitex 700) (Reference 10)

The purpose of this study was to compare the predicted performance of a Hercules 3rd Stage MX test nozzle fired in an HTPB propellant environment (AFRPL, January 1976) versus the original design environment of an 18.5 percent Al XLDB propellant. The results of the Aerotherm performance study were used to select a firing time for the nozzle test.

A complete two-dimensional thermal analysis, including surface recession, was performed for two carbon/carbon components upstream and downstream of the throat and five pyrolytic graphite washers which formed the throat pack. Another complete thermal analysis was performed assuming a 21 percent Aℓ, 90 percent solids HTPB propellant. The chemical compositions and ideal chamber conditions for the propellants are listed in Table 18. The chamber pressure history used is presented in Figure 39. The nozzle geometry, obtained from Hercules, is presented in Figure 40.

Typical internal temperatures predicted by the ASTHMA code are shown in Figure 41. This particular prediction is for the HTPB propellant after 60 seconds. Conclusions reached from this study were that the HTPB propellant was more corrosive than the XLDB propellant and that the nozzle was expected to withstand a 60-second firing in the HTPB environment. Figure 41 shows that approximately 50 percent of the leading PG washer has receded by 60 seconds. Although it was felt that this nozzle could sustain a 60-second firing, it was recommended that it be fired in the HTPB propellant for 40 seconds.

This test occurred in March 1976 and was successful. A detailed comparison of measured and predicted recession has not been performed to date.

Study 2 — Rocketdyne Condor (Reference 11)

For this performance study, a one-dimensional ablation analysis of the throat was used to compare the accuracy of the newly developed edge PG kinetics model to Condor firing data. This motor was chosen to demonstrate the applicability of the kinetics modeling to conditions other than that of typical ICBM type motors. The Condor firing durations were on the order of 200 seconds in a low aluminum, low flame temperature propellant. The nozzle is a blast tube type with a throat diameter of 1.1 inches. The ICBM type test motors (which were primarily used for developing the current kinetics model) typically have firing durations of less than 60 seconds in high performance

TABLE 18.   PROPELLANT DATA

| Designation — XLDB (18.5% Al)		
Formulation —	Element	Gm Atoms/100 Gms
	Hydrogen	2.3475
	Carbon	1.2745
	Nitrogen	1.8271
	Oxygen	2.3897
	Aluminum	0.6857
Ideal Chamber Conditions — Pressure = 800 psia		
	Temperature = 6700°R	
Designation — HTPB (21% Al, 90% solids)		
Formulation —	Element	Gm Atoms/100 Gms
	Hydrogen	3.4864
	Carbon	0.6933
	Nitrogen	0.5933
	Oxygen	2.3766
	Aluminum	0.7784
	Chlorine	0.5873
Ideal Chamber Conditions — Pressure = 800 psia		
	Temperature = 6649°R	
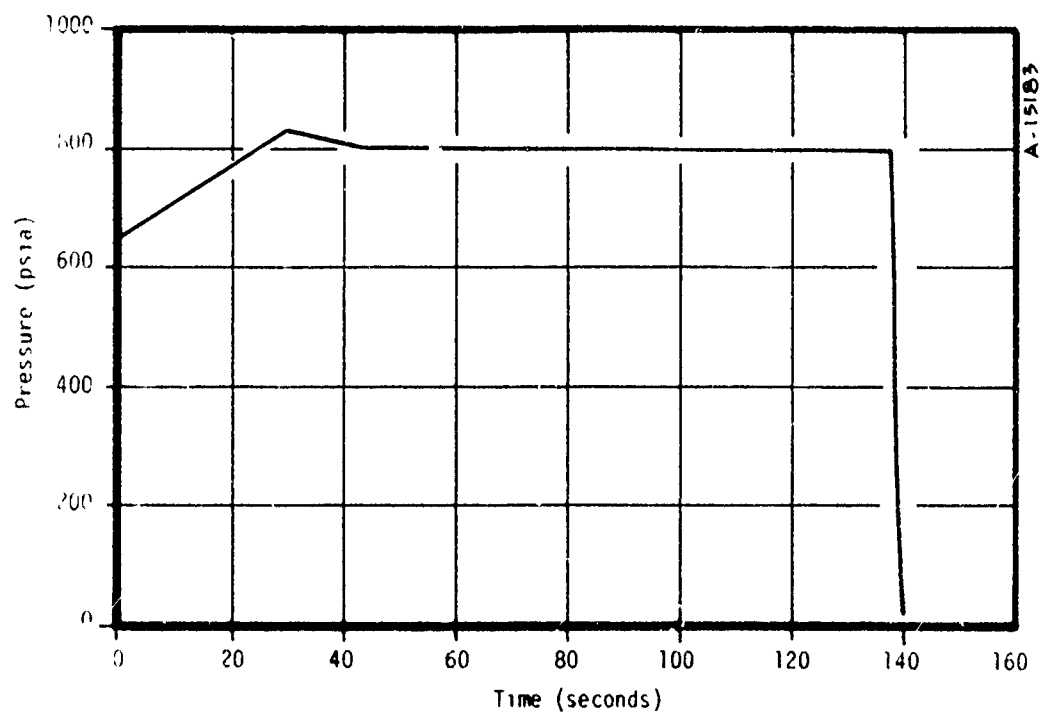
Figure 39. Chamber pressure history.
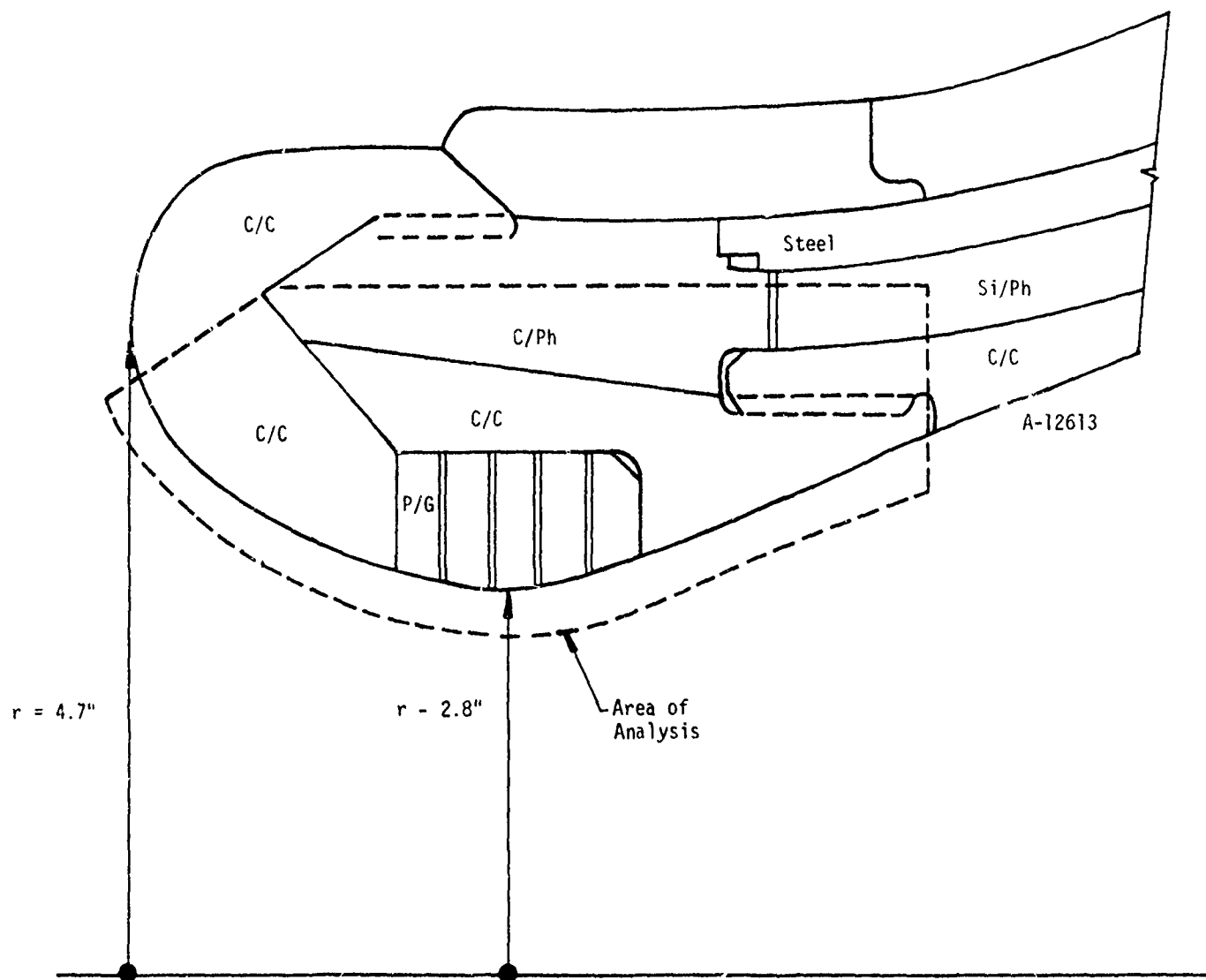
Figure 40. Nozzle geometry, Hercules test nozzle.
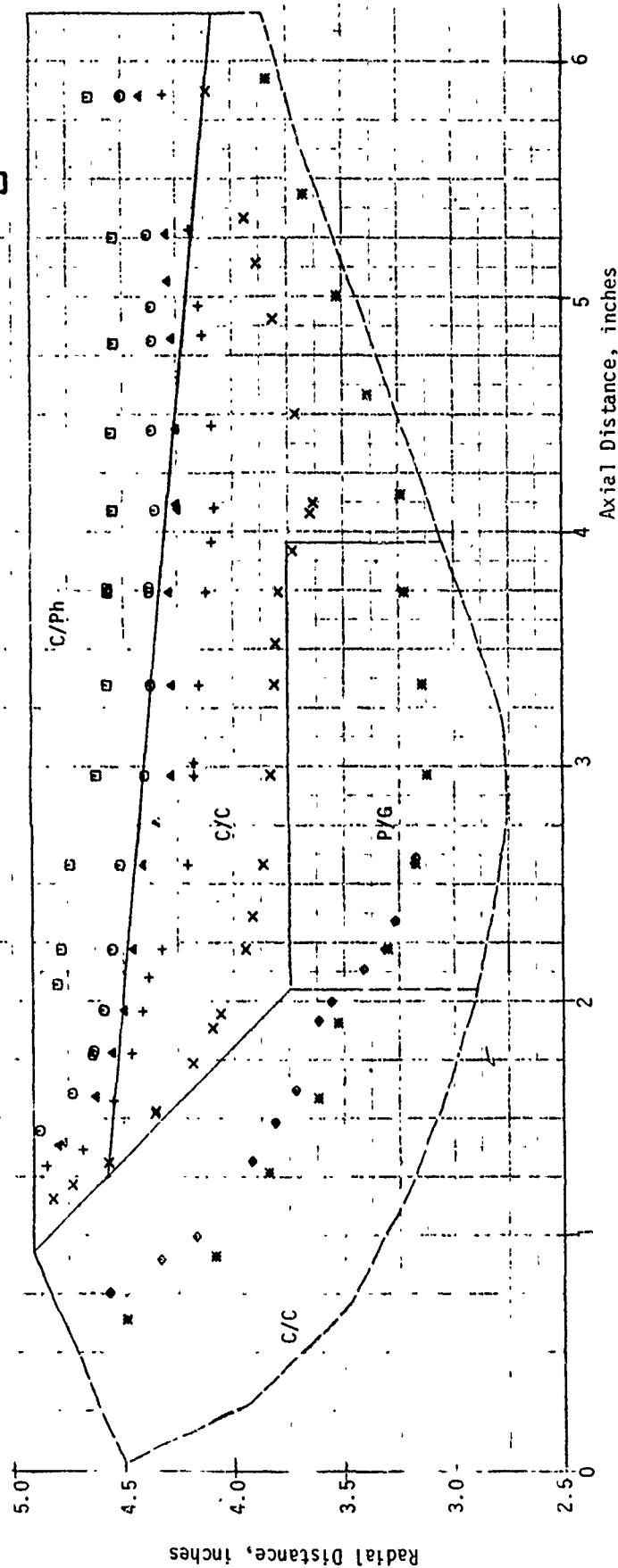
Figure 41. Predicted nozzle response to HTPB propellant, 60.0 seconds.

(a) 60.0 seconds

propellants (18 - 21 percent aluminum and 6000°R - 6900°R flame temperatures). These motors are usually submerged and have throat diameters from 4 to 15 inches.

The firing data used was obtained from Rocketdyne Solid Rocket Division in MacGregor, Texas. A series of seven firings were given, each of which differed mainly in the prefire temperature of the motor. The resulting throat erosion rate was more than an order of magnitude less than that exhibited by typical ICBM type motors and varied considerably among the seven firings. Both the propellant and firing data are confidential and are not included in this report. The geometry is given in Figure 42.

Figure 43 shows the predicted surface recession as a function of time. The predictions were found to be approximately 80 percent higher than the average measured recession. This is an acceptable prediction for the following reasons:

- Firing data indicates that alumina condensed out on PG washers

- Data scatter was large

- Measured recession was very small (making a percentage comparison invalid as an indication of accuracy)

Study 3 — Hercules 3rd Stage MX (Pyrocarb 901) (Reference 12)

This performance study is almost identical to Study 1. Recall that Study 1 incorporated PG washers in the throat and carbon/carbon components up and downstream of the washers. The carbon/carbon material has a specific gravity of 1.60 and was made by Kaiser. At the time of the prediction, the only carbon/carbon kinetics model available was one developed by Aerotherm for Thiokol Corporation (P.O. 414011). This kinetic model was specifically developed for Carbitex 700 (S.G. = 1.5) and was used for this prediction by adjusting the material to a 1.6 specific gravity.

After Study 1 was performed a kinetics model for Pyrocarb 901 (S.G. = 1.83) was developed under this contract. Preliminary indications showed that the kinetics model was markedly different from that developed for Carbitex 700. With the indication that some carbon/carbon materials behave differently from others, it was of interest to rerun the prediction of Study 1 with the newly developed Pyrocarb 901 model (S.G. = 1.83).

As in performance Study 1, two complete ASTHMA analyses were performed for the carbon/carbon components and PG washers in the region of the throat. One was for an 18.5 percent Aℓ XLDB propellant and the other was for a 21 percent Aℓ, 90 percent solids HTPB propellant.
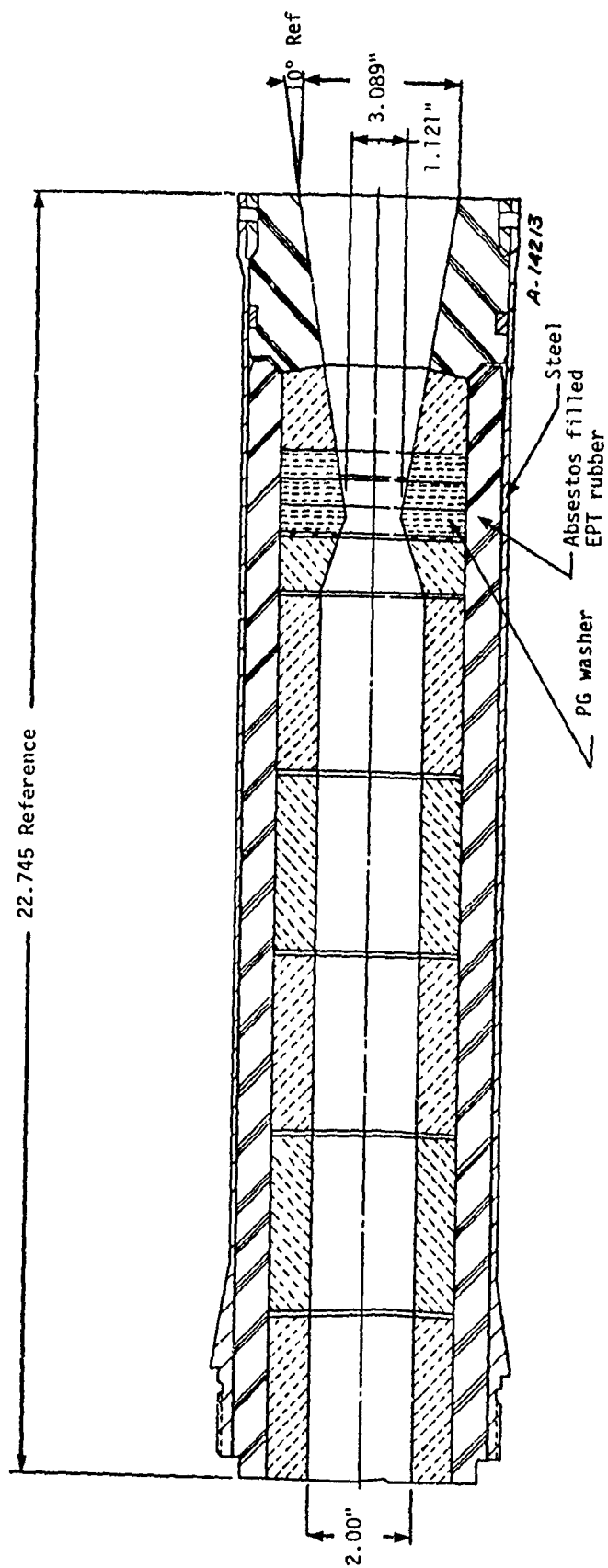
Figure 42. Nozzle geometry, Rocketdyne Condor nozzle.
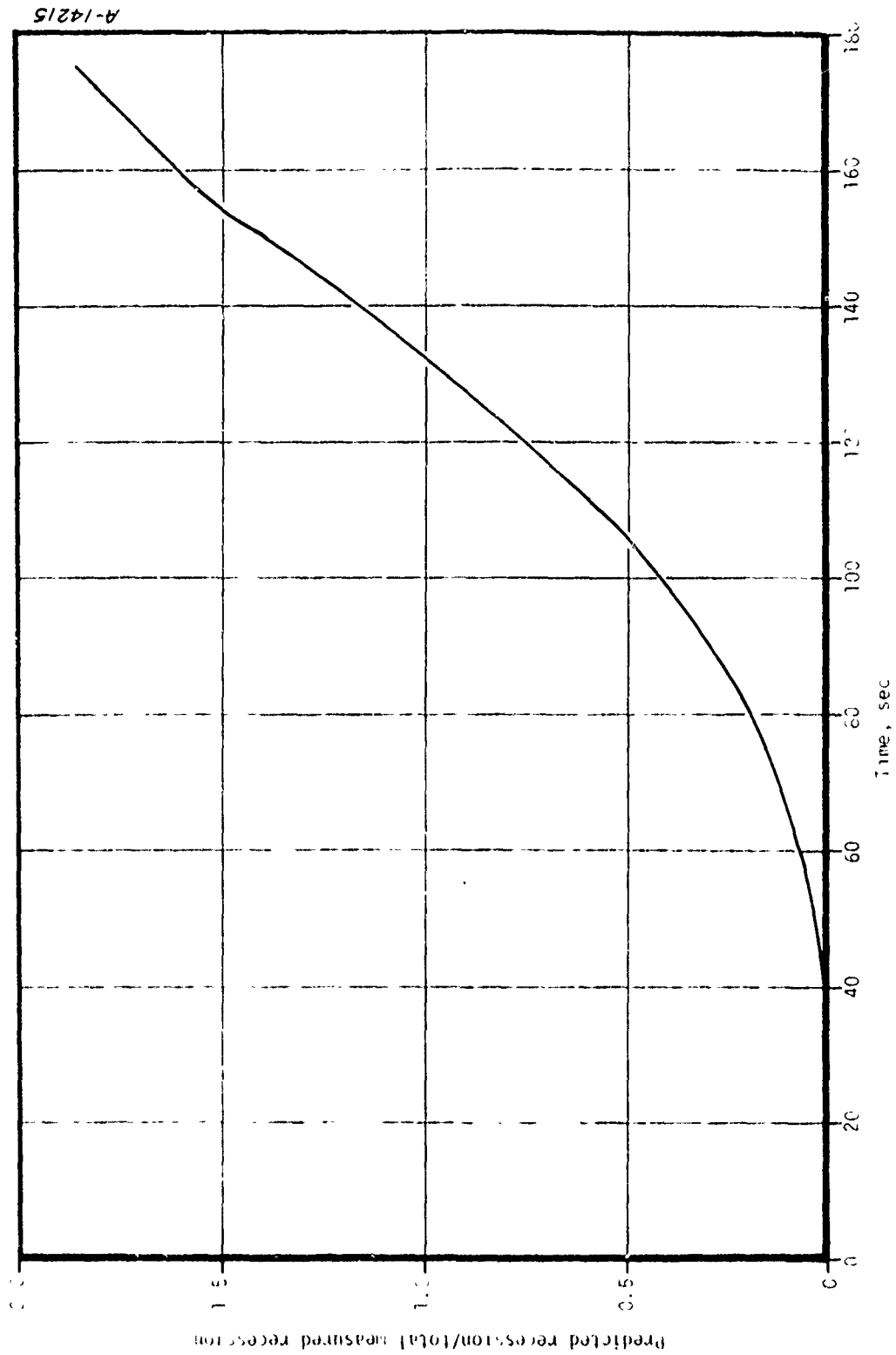
Figure 43. Surface recession history, Rocketdyne Condor nozzle.

113

Figure 44 shows the predicted isothermal profiles after 60 seconds of exposure to the HTPB environment. As expected from the kinetics data, the predictions indicated more recession for the Pyrocarb 901 than the Carbitex 700. This can be seen by a comparison between Figures 41 and 44. This study showed that the Pyrocarb 901 could not sustain a 60-second firing without severe undercutting of the PG washers.

Table 19 is included as a further comparison of Studies 1 and 3. Basically, this shows that the XLDB propellant is not as severe as the HTPB and that predicted recession for Pyrocarb 901 is more than Carbitex 700 for comparable conditions.

Study 4 — Standard 7-Inch Nozzle (Throat Sensitivity) (Reference 13)

The purpose of this study was to compare the predicted performance of four possible throat materials in the standard 7-inch test nozzle configuration, namely:

- Pyrocarb 901 carbon/carbon (density = 1.83 g/cc)

- c plane pyrolytic graphite (edge)

- a-b plane pyrolytic graphite (layer)

- 15% SiC/PG

For each material, three propellant environments were considered.

- HTPB

- XLDB

- PEG/FEFO

For each propellant/material combination, a complete one-dimensional thermal analysis including surface recession was carried out at the throat. A total of 12 nozzle analyses were performed.

The chemical composition and actual chamber conditions for the propellants considered are summarized in Table 20. The firing duration was 60 seconds at a chamber pressure of 1000 psia. The nozzle geometry is shown in Figure 45(a). Figures 45(b) and 45(c) show the geometries of the throat insert depending on whether a coated or solid component is used.

Of most interest in this study is a comparison of the predicted surface recession for all of the material/propellant combinations. The predicted total recessions and average recession rates are tabulated in Table 21. The average recession rates are illustrated in Figure 46. This shows that the Pyrocarb 901 recedes at least a factor of two or more than the other materials in a given
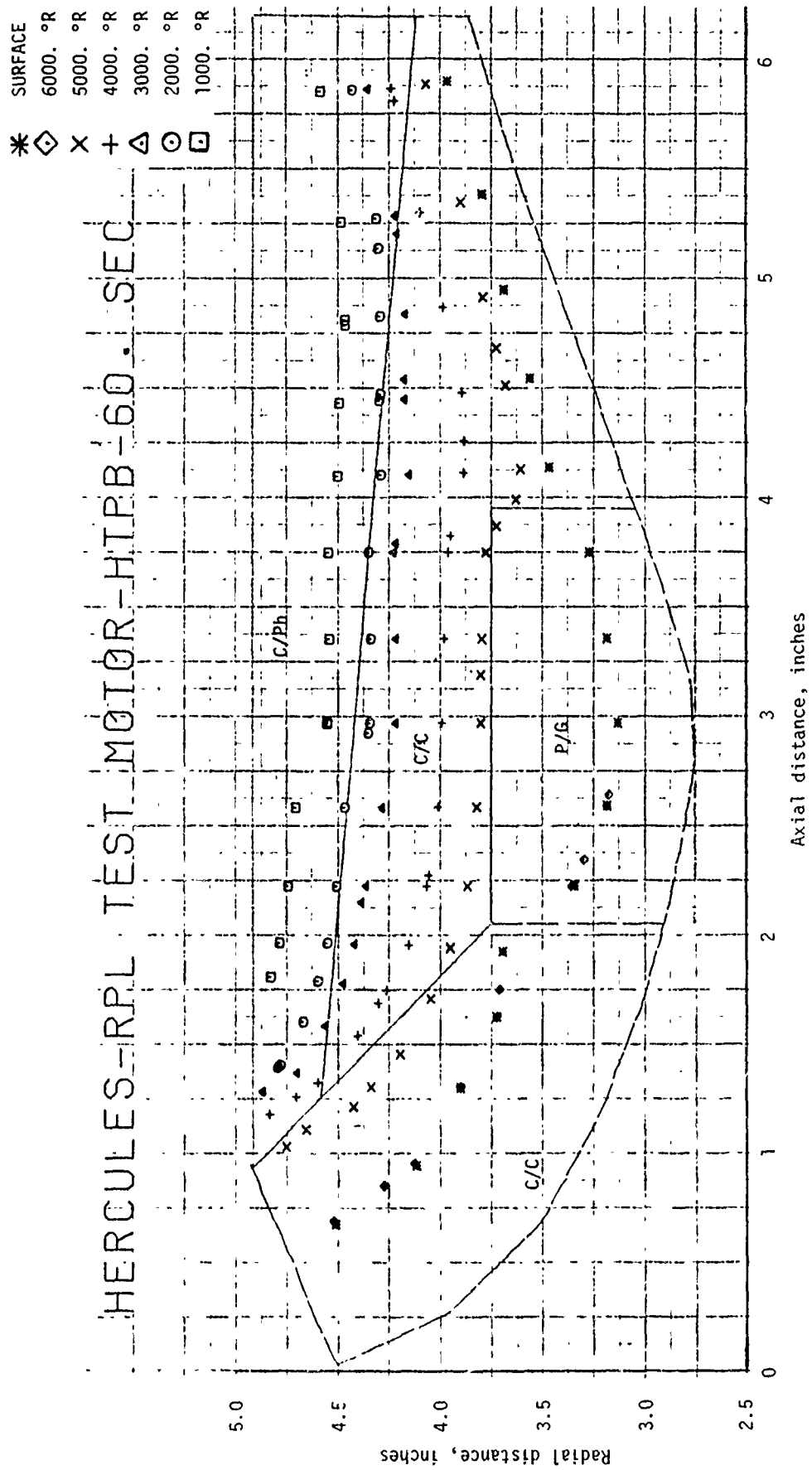
Figure 44. Predicted nozzle response to HTPB propellant, 60 seconds.

TABLE 19. RECESSION RATE SUMMARY, HERCULES 3RD STAGE MX NOZZLE

Location	Propellant	Material	Average Recession Rate @ 60 secs (mils/sec)
Upstream Throat	XLDB	Carbitex 700	6.6
"	"	Pyrocarb 901	8.9
"	HTPB	Carbitex 700	9.5
"	"	Pyrocarb 901	12.2
Throat	XLDB	PG Washers	3.8
"	HPB	"	5.9
Downstream Throat	XLDB	Carbitex 700	2.1
"	"	Pyrocarb 901	3.3
"	HTPB	Carbitex 700	1.8
"	"	Pyrocarb 901	5.5

TABLE 20. PROPELLANT DATA, STUDY 4

Propellant	XLDB (19% Al)	HTPB (21% Al, 90% Solids)	PEG/FEFO (20% Al)
Hydrogen ($\frac{GMATOMS}{100\ GMS}$)	2.3885	3.4864	2.5416
Carbon	1.2348	0.6933	1.0967
Nitrogen	1.6779	0.5933	1.5528
Oxygen	2.4224	2.3766	2.2753
Fluorine	—	—	0.0750
Aluminum	0.7042	0.7784	0.7417
Chlorine	0.0423	0.5873	0.1320
Pressure (psia)	1000.	1000.	1000.
Temperature (°R)	6808.	6699.	6772.
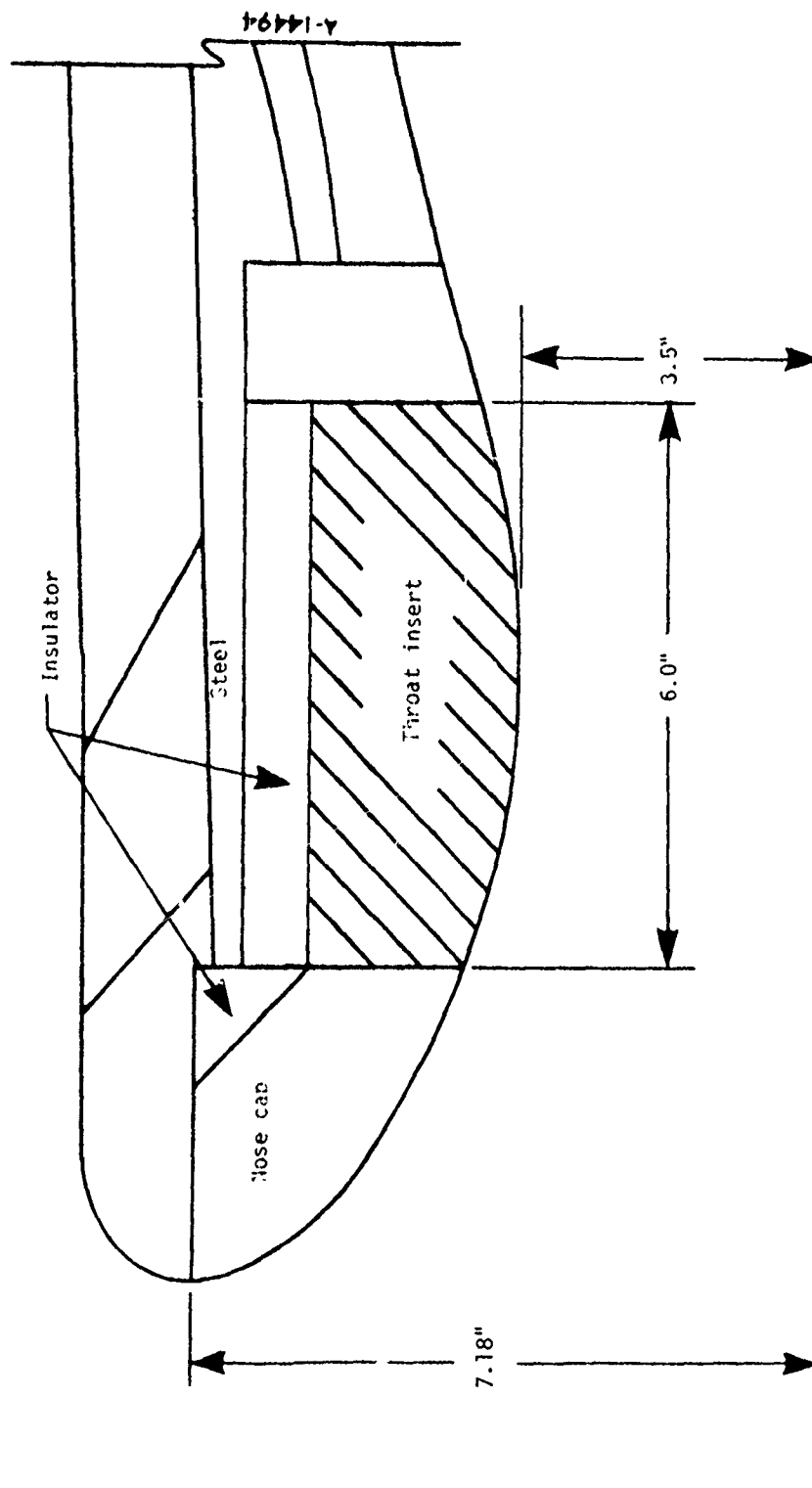
(a) Location of throat insert

Figure 45. Nozzle geometry, Study 4.

Layer PG or SiC/PG

(b) Layered throat insert

Pyrocarb 901
or edge PG

(c) Solid throat insert
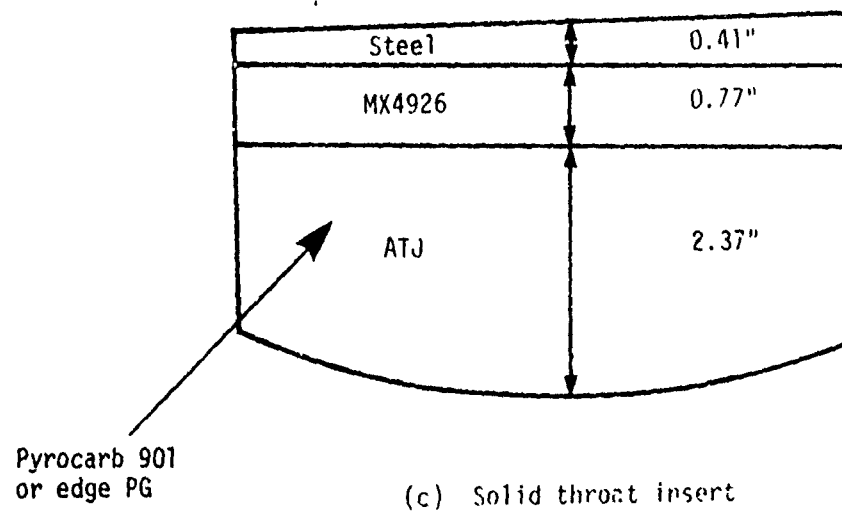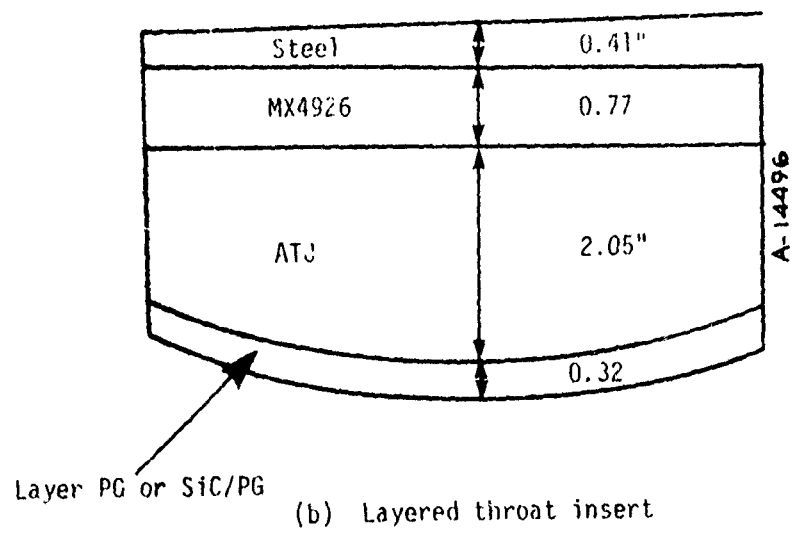
Figure 45. Concluded.

119

TABLE 21. MATERIAL RESPONSE SUMMARY, STUDY 4

Propellant	Throat Material	Total Recession[a] (in)	Average Recession Rate (mils/sec)
XLDB	C/C 901	0.444	7.4
	Edge PG	0.203	3.4
	Layer PG	0.119	2.0
	15% SiC PG	0.145	2.4
HTPB	C/C 901	0.588	9.8
	Edge PG	0.289	4.8
	Layer PG	0.104	1.7
	15% SiC PG	0.325[b]	5.4
PEG/FEFO	C/C 901	0.383	6.4
	Edge PG	0.156	2.6
	Layer PG	0.112	1.9
	15% SiC PG	0.095	1.6

[a] 60-second firing

[b] Extrapolated (coating burned through at 59 secs.)
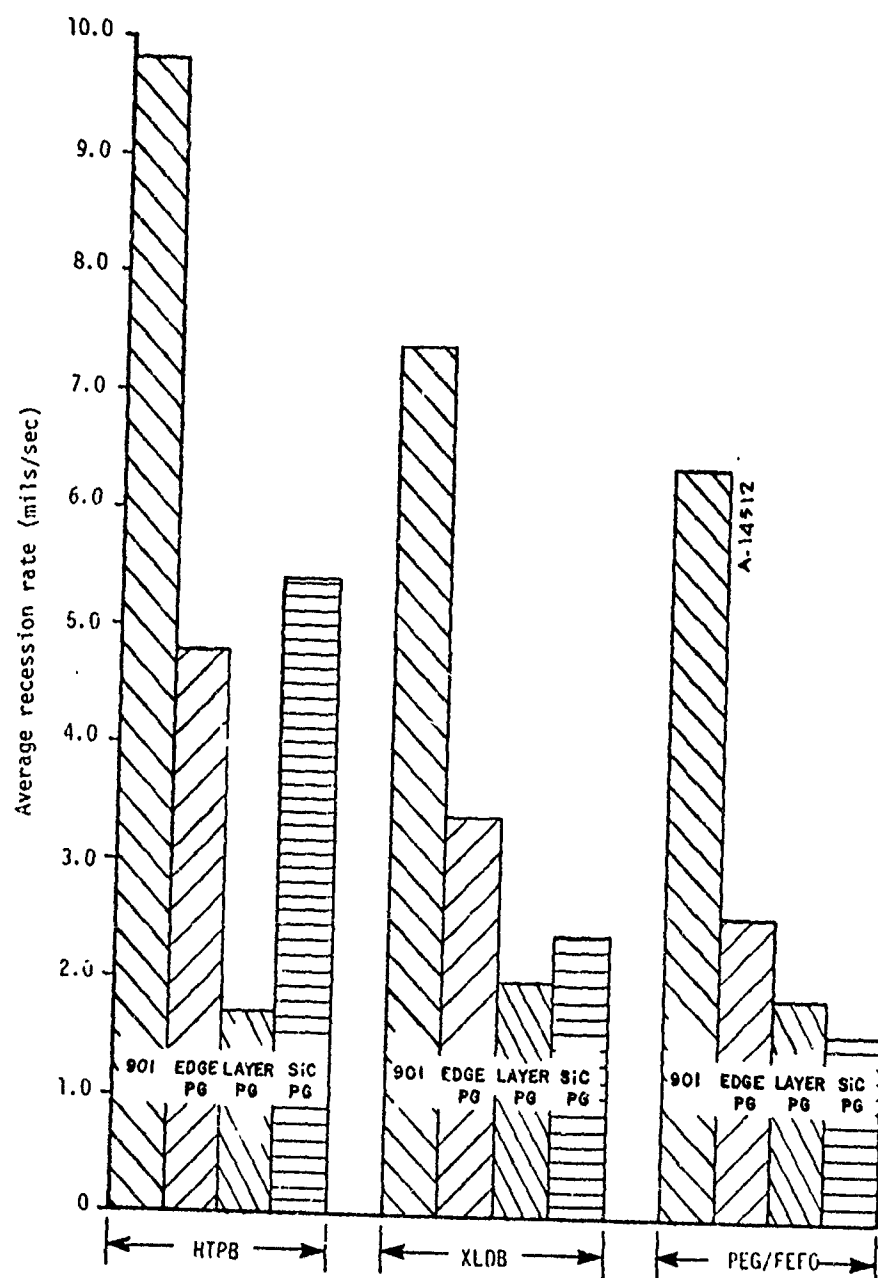
Figure 46.   Predicted average recession rates, Study 4.

propellant group. It is also evident that HTPB, XLDB, and PEG/FEFO, respectively decrease in corrosivity for all materials except layer PG.

Study 5 — Standard 7-Inch Nozzle (Nosecap Sensitivity) (Reference 14)

The purpose of this study was to compare the predicted performance of five possible nosecap materials in the standard 7-inch test nozzle. The five materials are:

- ATJ graphite

- G-90 graphite

- Pyrocarb 901 carbon/carbon (density = 1.83 gr/cc)

- Carbitex 700 carbon/carbon (density = 1.50 gr/cc)

- 15% SiC/PG

A one-dimensional thermal analysis including surface recession was performed for each material in an HTPB propellant environment. This propellant is identical to the HTPB used in Study 4, as are the firing duration (60 seconds) and average chamber pressure (1000 psia). The nozzle geometry is shown in Figure 47.

Table 22 summarizes the predicted total recession and average recession rate for the five materials. A more graphic presentation of the average recession rates is given in Figure 48. This shows that the materials can be ranked by their resistance to ablation as follows:

1. 15% SiC/PG

2. Carbitex 700 carbon/carbon

3. G-90 bulk graphite

4. Pyrocarb 901 carbon/carbon

5. ATJ bulk graphite

Study 6 — BATES Nozzle (Reference 15)

Previous studies were to predict the ablation performance of rocket nozzle materials. Since the Air Force Rocket Propulsion Laboratory (AFRPL) has experienced numerous failures of the one piece graphite nozzle utilized in various versions of the BATES rocket motor, the purpose of this study was to perform a preliminary structural analysis of the BATES nozzle to understand the reasons for failure and to recommend solutions to the problem.
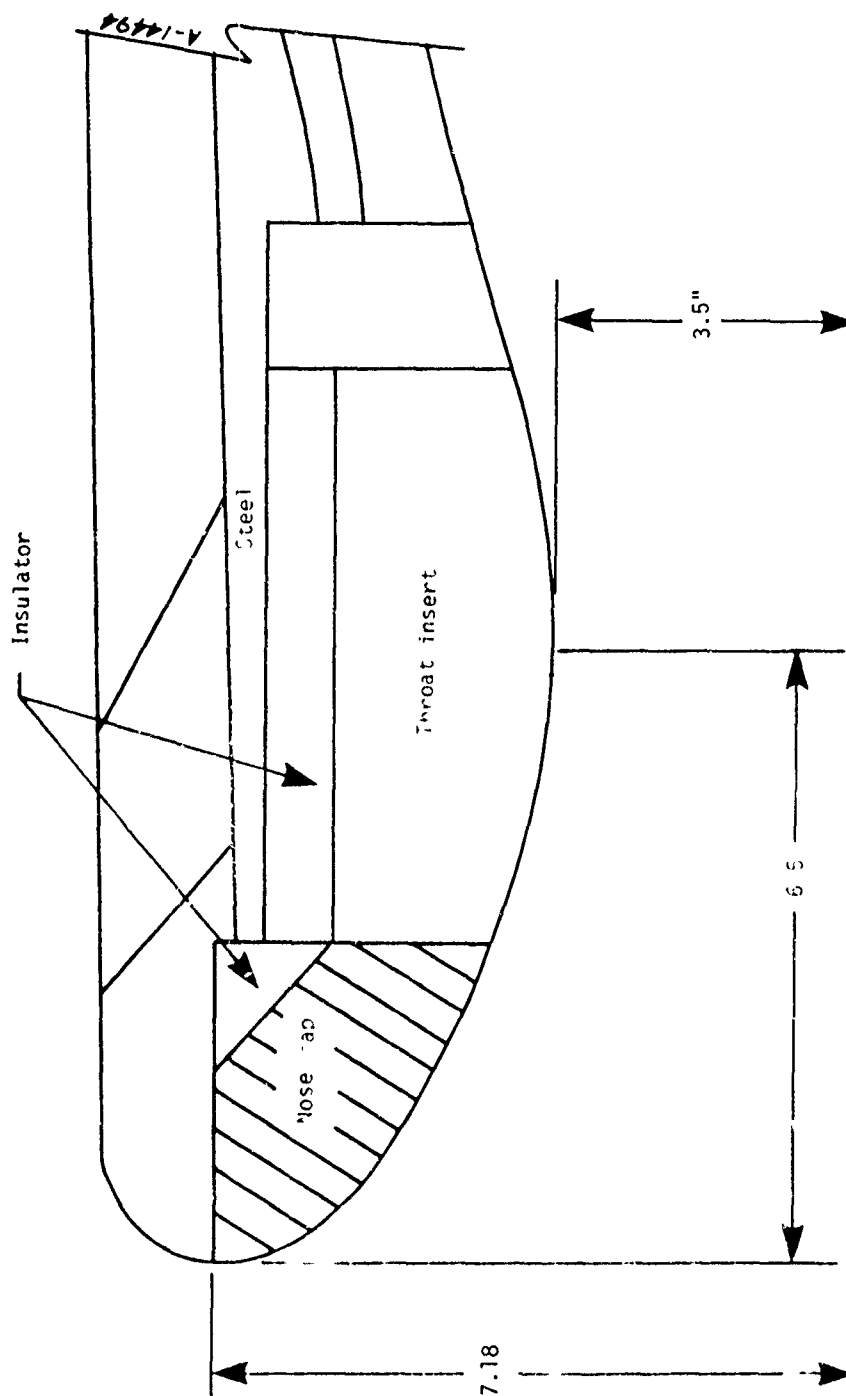
Figure 47. Nozzle geometry, Study 5.

123
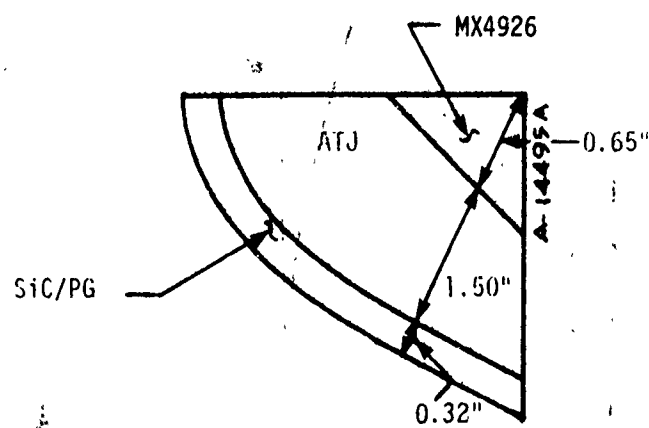
(b) Layered nose cap
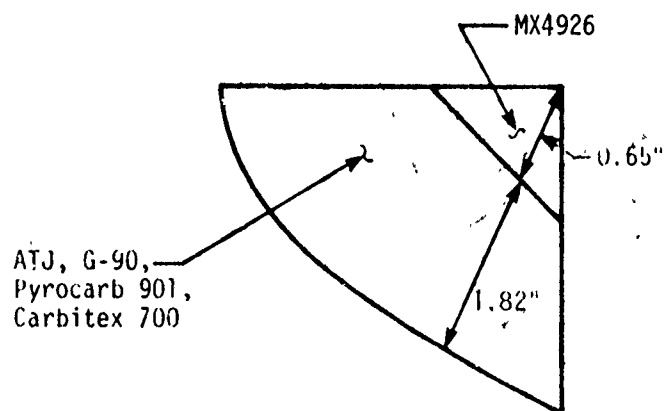
(c) Solid nose cap

Figure 47. Concluded.

TABLE 22. MATERIAL RESPONSE SUMMARY

Propellant	Material	Total Recession[a] (in)	Average Recession Rate (mils/sec)
HTPB	ATJ	0.645	10.8
	G-90	0.505	8.4
	Pyrocarb 901	0.568	9.5
	Carbitex 700	0.456	7.6
	15% SiC/PG	0.309	5.2

[a]60-second firing
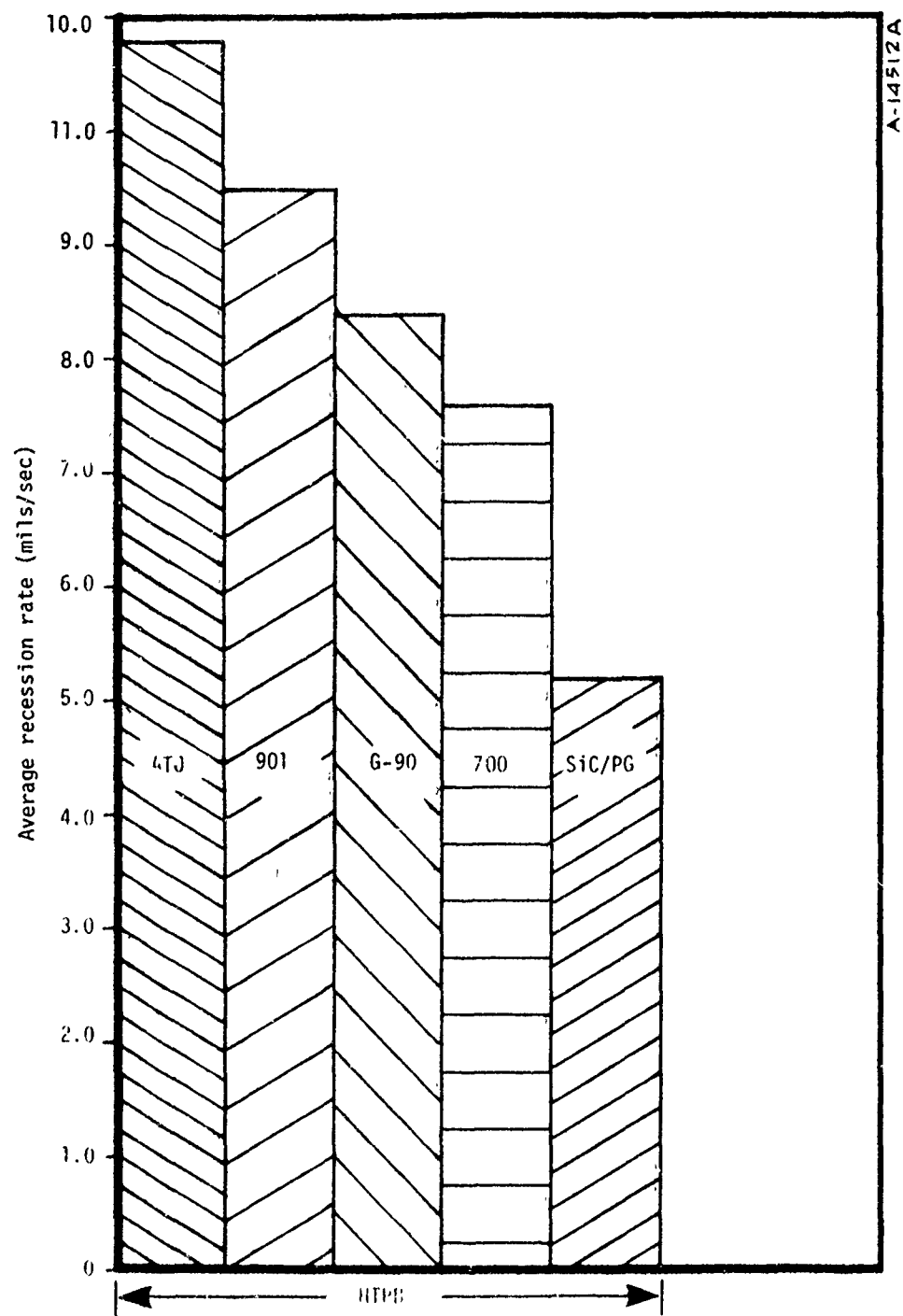
Figure 48.   Predicted average recession rates.

Three basic classes of BATES motors are in use at AFRPL: a 15-pound motor, a 70-pound motor, and a high pressure (approximately 80-pound) motor. A drawing of the high pressure BATES configuration is shown in Figure 49. The nozzle is of single piece construction, specified as HLM 85 or equivalent graphite. The nozzle is held in place by 16 steel bolts torqued to 600 inch-pound. This preloads the graphite between a retaining ring and the motor aft closure. An O-ring seal prevents gas leakage at the entrance region of the nozzle.

The BATES motors exhibit an essentially flat pressure-time characteristic, reaching full chamber pressure quite rapidly. Typical run times are only a few seconds, with 9 or 10 seconds being a maximum. A worst case propellant assumption would be a high solids loaded, high aluminum content formulation such as 90 percent solids – 20 percent aluminum formulation.

Nozzle failures have occurred with all three motor types, particularly when operating at pressures greater than 1500 psia. The mode of failure is consistent, involving radial fracture planes as a result of hoop stresses. Generally the nozzle fractures into two nearly equal pieces. However, three radial fracture planes producing three essentially 120° segments are sometimes observed. Occasionally, a transverse fracture is also observed at the juncture of the forward nozzle flange and the motor aft closure. It is felt that this fracture may occur subsequent to the previously described hoop failure. All failures are felt to occur quite early, possibly upon reaching full chamber pressure.

Many different graphites including Great Lakes HLM 85, Stackpole 2020, Airco Speer 8882 and 873, Union Carbide ATJ, and Carborundum G83 have failed. Although a grain direction is not specified on the nozzle insert drawing, it is safe to assume that the grain direction was perpendicular to the nozzle centerline for molded graphites and along the nozzle centerline for extruded graphites.

Per AFRPL request, the analysis was initially concentrated on the high pressure BATES design. For approximately a dozen firings up to the onset of this study, the high pressure nozzle had exhibited approximately a 75 percent success rate for pressures up to 2000 psia and essentially no success beyond 2000 psi.

In addition to the nozzle failures occurring during actual motor firings, a hydrostatic test has also resulted in nozzle failure. A special hydrostatic test nozzle was fabricated of HLM 85 with the internal features of the exit cone left unmachined (solid). The nozzle was mounted in a fixture identical to the aft closure of the motor and pressurized hydrostatically to failure at ambient temperature. Failure in two nearly equal halves identical to actual firing failures occurred at 1700 psia.
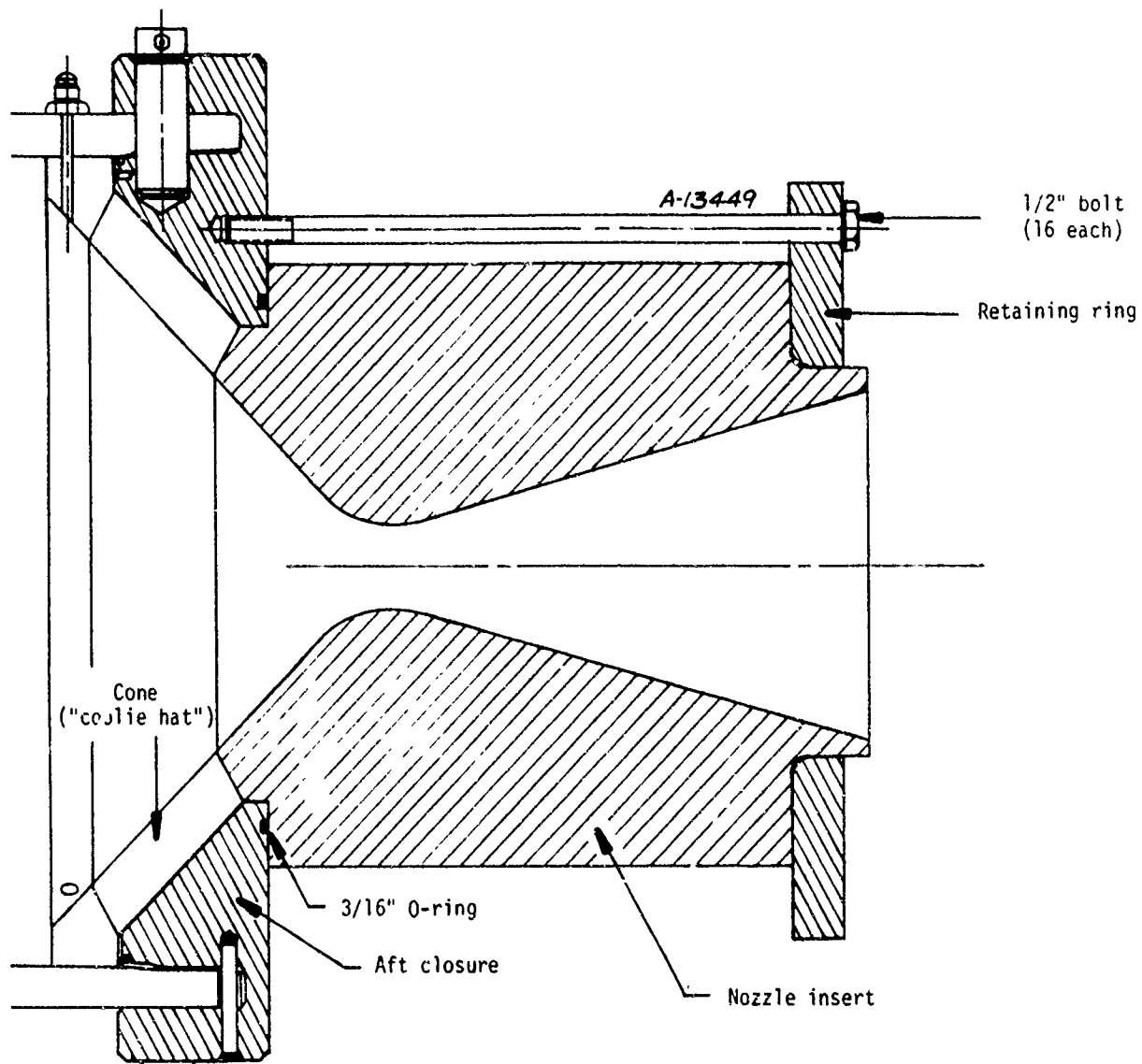
Figure 49. BATES high pressure motor.

Labels in figure:
A-13449
1/2" bolt (16 each)
Retaining ring
Cone ("coolie hat")
3/16" O-ring
Aft closure
Nozzle insert

The general approach to the problem consisted of first conducting a structural analysis of the existing BATES high pressure configuration in both the hydrostatic test and motor firing modes to see if the observed failures could be correlated. Once a correlation was established, these same analytical techniques were used to examine various potential fixes. The DOASIS finite element computer code was used (Reference 24) to solve the displacements, strains and stresses in the nozzle using orthotropic properties and axisymmetric pressure and thermal loading. All motor calculations were performed for a chamber pressure of 2000 psia, which appears to be the threshold level for relatively consistent nozzle failure.

As a result of the finite element calculations, it was concluded that the failure of the BATES nozzle probably occurs as a result of circumferential tensile stresses in a region just forward of the nozzle throat. It was further concluded that the failure occurs very early in the burn and is almost solely the result of pressure loading on the inner contour at a time when the interface leading to the O-ring is essentially sealed.

Assuming the above failure mode is indeed correct, the most promising fix to the problem involves intentional design features to assure that chamber pressure reaches the O-ring rapidly. In this way the nozzle is in effect "self-healing". A reduction in maximum hoop tensile stress of greater than a factor of two is realized from this change alone.

Another fix with the potential of increasing nozzle capability by more than a factor of two is the use of ATJ or equivalent strength graphite rather than HLM 85 quality graphite. Several of the graphites that have failed in the BATES testing are quite inferior to ATJ.

A slip-fit sleeve does not appear promising as a fix to the problem for two reasons. First, the radial expansion of the baseline design with no sleeve is only about 2 mils, which is probably the same order-of-magnitude as the gaps present in a slip-fit sleeve of this large diameter. Second, the calculations for a zero gap indicate only about a 30 percent reduction in hoop tensile stress due to the sleeve.

Pressurization of the nozzle OD appears to be quite beneficial in reducing hoop tensile stresses. The benefits are nearly as great in the region of major interest, the entrance/throat region, if pressurization is applied only to the forward portion of the OD.

There appears to be a tendency for the couple produced by the offset action lines of the net pressure force and the reaction force at the aft end of the nozzle to splay the aft end, producing hoop tensile stresses. Although the failures are not felt to originate in this region,

angling the aft end of the nozzle somewhat will alleviate this situation. Although it was not ex-
amined, it might be possible to design the forward end of the nozzle in a similar fashion so that
the bolting force would produce a compressive hoop prestress in the entrance region.

All of these conclusions were presented to AFRPL as recommendations for solving the failure
problems of the high pressure BATES nozzle. Further recommendations were also made to solve similar
problems on the lower pressure BATES motors.

SECTION 8

CONCLUSIONS AND RECOMMENDATIONS

Kinetic expressions for ATJ, G-90, c oriented PG, 15% SiC/PG, and Pyrocarb 901 were obtained from correlations of APG data and rocket motor firing data. These expressions, along with expressions from previous results for a-b oriented PG and a recorrelation of previous Carbitex 700 data, were incorporated into the former GASKET code for thermochemical ablation analysis. The new code, GASKE12, also includes an improved accounting of sublimation kinetics, additional gas phase species (Duff-Bauer), and a generalized procedure for specification of kinetic reactions.

Using the GASKET2 code and the Aerotherm rocket nozzle prediction procedure, the ablation performance of 15 motor firings was predicted. All but three of these predictions were within ±25 percent of measured results. From these predictions, which included a wide range of propellants and nozzle designs, it was concluded that the kinetic expressions were acceptably accurate. However, additional verifications are required since in several cases only one motor firing was used to validate the kinetic expressions for a particular material.

In addition to the data used for kinetic correlations, ablation data for 13 other materials were obtained in the Aerotherm APG. These data were compared within a generic class of materials to determine qualitative performances. Data obtained to date show that some materials are sensitive to manufacturing source and others are not.

Significant conclusions from this investigation, including discussions from the appendix, are:

1. The GASKET2 code and the Aerotherm rocket nozzle prediction procedure can accurately predict the ablation performance of a rocket nozzle which uses materials that have been characterized.

2. If propellant temperatures increase beyond current values of about 6800°R, carbon sublimation kinetics will become important. In anticipation of this, the new GASKET2 code includes appropriate sublimation terms.

3. At surface temperatures representative of MX nozzles, the H_2 - C* reaction is the domi-
    nant carbon removal mechanism. Although the reaction rate constants are large for H_2O
    and CO_2, their reaction rates at motor temperatures are usually small because of low re-
    actant partial pressures.

4. Pyrolytic graphite ablation rates are not sensitive to the material suppliers.

5. Bulk graphite and carbon/carbon composite ablation rates are sensitive to the material
    suppliers. In general, density alone is not a performance scaling parameter; however,
    for carbon/carbon composites it was observed that a nonlinear density dependence could
    exist, if the material is separated according to the reinforcement precursor. That is,
    rayon precursor composites and PAN precursor composites each exhibit a density dependence.
    It is highly probable that the matrix precursor should also be a correlating parameter.

6. For equal densities, rayon precursor composites performed better in the APG than PAN
    precursor composites. As shown in Appendix A, PAN precursor composites show evidence of
    fiber cleavage whereas rayon precursor composites do not.

7. At very high temperatures all materials seem to approach an asymptotic mass removal rate.

8. No correlations of ablation performance were observed for material porosity.

9. Chemadsorption measurements show no surface adsorption of reaction species, namely,
    CO_2, H_2O, and H_2.

10. Significantly more data and data analysis will be required to relate ablation performance
    to processing or material microstructure.

The following are recommended in order to improve rocket nozzle ablation performance predic-
tions and to obtain an understanding of the relationship between ablation performance and material
processing.

1. APG data should be obtained for additional carbon/carbon composites which include a wide
    range or processing variables. Ideally, the composites should be processed with a sys-
    tematic variation in these variables.

2. The microstructure of each material should be carefully examined and recorded. This ex-
    amination should include, as a minimum, metallographs, SEM's, porosity, and chemoadsorp-
    tion.

3. Thermophysical properties should also be measured and include, as a minimum, local density, thermal expansion coefficients and thermal conductivity.

4. Additional motor firings should be examined and predicted to improve the prediction accuracy of the GASKET2 code.

5. Alternate procedures should be examined for obtaining accurate high temperature kinetic ablation data.

REFERENCES

1. Khitrin, L. N. and Golovina, E. S., "Interaction Between Graphite and Various Chemically Active Gases at High Temperature," Proceedings of an International Symposium on High Temperature Technology, September 1963.

2. Lewis, J. C., Floyd, I. J., and Cowlard, F. C., "A Comparative Study of the Gaseous Oxidation of Vitreous Carbon and Various Graphites at 1500 - 3000°K," Allen Clark Research Centre, Plessey Co. Ltd., England, and Beckwith Carbon Corporation, Van Nuys, California.

3. Maahs, Howard G., "Oxidation of Carbon at High Temperatures: Reaction-Rate Control or Transpost Control," NASA Technical Note D-6310, June 1971.

4. Thackray, R. W., "A Survey of Carbon/Gas Reaction Rates Applicable to Rocket Nozzles," Rocket Propulsion Establishment Westcott Technical Memorandum No. 600, June 1972.

5. "Principles Governing the Behavior of Solid Materials in Severe High Temperature Environments," Union Carbide Research Institute Final Report UCRI-388, May 31, 1966.

6. Wool, M. R., Schaefer, J. W., Murphy, A. J., Clark, K. J., and Reese, Jr., J. J., "Kinetic Response of Pyrolytic Graphite to Combustion Product Environments," Aerotherm Final Report 72-48, April 1972.

7. "User's Manual, Aerotherm Graphite Surface Kinetics Computer Program, Volume I — Program Description and Sample Problems," Aerotherm User's Manual UM-72-25, January 1972.

8. Murphy, A. J., Chu, E. K., and Kesselring, J. P., "Interim Report — AFRPL Graphite Performance Prediction Program, Vol. 1, Recommendations for a Standardized Analytic Procedure for MX Nozzle Throat Recession Calculations," Aerotherm Report 75-143, May 1975.

9. Chu, E. and Tong, H., "Aerotherm Graphite Surface Kinetics Computer Program (GASKET2)," Aerotherm Report TR-76-13, May 1976.

10. Murphy A. and Kwong, K., "Nozzle Performance Bulletin #1, Performance Study #1: — 3rd Stage Hercules MX Nozzle Analysis," Aerotherm Report TM-75-86, November 1975.

11. Murphy, A., and Kwong, K., "Nozzle Performance Bulletin #2, Performance Study 2: Rocketdyne Condor Test Nozzle Analysis," Aerotherm Report TM-76-197, April 1976.

12. Murphy, A., Kwong, K., "Nozzle Performance Bulletin #3: 3rd Stage Hercules MX Nozzle Analysis Using Pyrocarb 901 Kinetics," Aerotherm Report TM-76-117, April 1976.

13. Murphy, A. and Kwong, K., "Nozzle Performance Bulletin #4, Performance Study #4: Material/ Propellant Sensitivity Stuo, for the Throat Location of the Standard 7" Test Nozzle," Aerotherm Report TM-76-121, May 1976.

14. Murphy, A. and Kwong, K., "Nozzle Performance Bulletin #5, Performance Study #5: Material Sensitivity Study for the Nose Cap of the Standard 7" Test Nozzle," Aerotherm Report TM-76-122, May 1976.

15. Kulkarni, V. S. and McClellan, R. E., "Structural Analysis of BATES Nozzle," Aerotherm Report TM-76-98, February 1976.

16. Tong, H., Hartman, J. C., and Chu, E. K., "Interim Report — AFRPL Graphite Performance Prediction Program, Volume 2, Arc Plasma Generator Evaluation of Graphite Reaction Kinetics in Rocket Propellant Environments," Aerotherm Report 75-143, May 1975.

17. Unpublished data for Aerotherm APG obtained by Lockheed Missile and Space Division.

18. Dorrance, W. H., *Viscous Hypersonic Flow*, McGraw-Hill Book Co., Inc., New York, New York, 1962, p. 226.

19. Tong, H., Hartman, G. J., Chu, E. K., and Keyes, K. A., "Kinetic Mass Consumption Rate for C-4 Trident Nozzle Material — Carbitex 700," Aerotherm Final Report 74-126, November 1974.

20. "User's Manual, Aerotherm Chemical Equilibrium (ACE) Computer Program," Aerotherm Corporation, Mountain View, California, May 1969.

21. "User's Manual, Aerotherm Real Gas Energy Integral Boundary Layer Program (ARGEIBL)," Aerotherm User's Manual, UM-75-69, December 1975.

22. "User's Manual, Aerotherm Charring Material Thermal Response and Ablation Program, Version 3," Aerotherm Corporation, Mountain View, California, Report UM-70-14, April 1970.

23. "User's Manual — Aerotherm Axi-Symmetric Transient Heating and Material Ablation Computer Program (ASTHMA3), AFRPL-TR-72-24, Aerotherm Report UM-72-26, January 1972.

24. "DOASIS — A Computer Code for the Deformation Plastic, Orthotropic, Axisymmetric (and Plane) Solution of Inelastic Solids," Volumes I, II, and III, Weiler Research, Inc., Air Force Materials Laboratory Technical Report AFML-TR-75-37, October 1975.

APPENDIX A

MICROSTRUCTURAL EXAMINATIONS

A.1 INTRODUCTION

Surface kinetic constants depend on the microstructure of the material. This was shown by the large difference in measured ablation rates of a-b plane and c plane pyrolytic graphite. Because of this, parameters such as relative fiber/matrix content, composite density and porosity, and the degree of graphitization are potentially important variables. In addition, the orientation of carbon platelets, which depend on the precursor materials and their processing, is important. For instance, PAN and rayon precursors yield fibers with platelet orientations as shown in Figure A-1. For ablation along the cylindrical face, PAN fibers appear like layered PG and rayon fibers appear like random carbon edges. Thus the ablation kinetics will also depend on the relative fabric orientation and the orientation of the fabric relative to the ablation surface.

Processing of carbon/carbon rocket nozzle materials is quite proprietary; hence, only general information is available. Some of the information for materials used in this investigation is described in Section A.2. However, greater details are required before a meaningful relationship can be established between materials processing and ablative performance. Figure A-2 shows the interdependence between:

- Fabrication and processing

- Pretest microstructure

- Ablation performance

- Post-test microstructure

The ideal situation is to be able to obtain a desired ablation performance by prescribing fabrication and processing variables. Unfortunately, the current state-of-knowledge is only sufficient to provide simple guidelines which may have many qualifiers or exceptions.

With the current engineering approach to determining reaction kinetics, it is not possible to define the fundamental mechanisms for carbon consumption. Thus, it would not be unexpected for
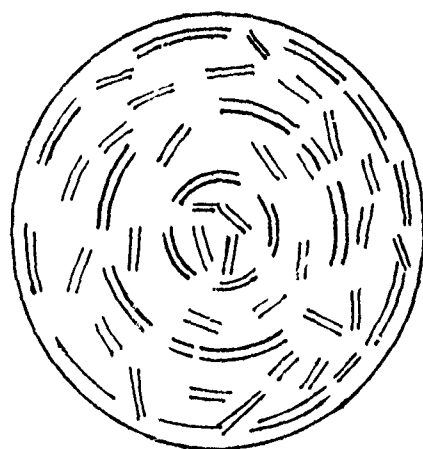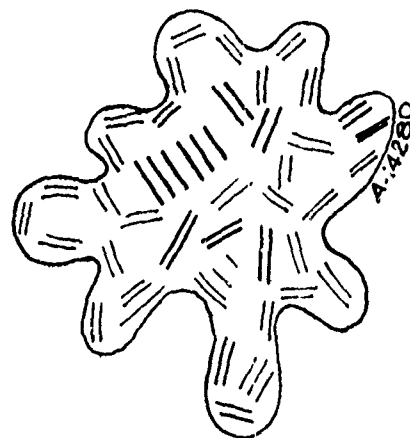
PAN base   Rayon base

Figure A-1. Schematic of observed carbon fiber structures.
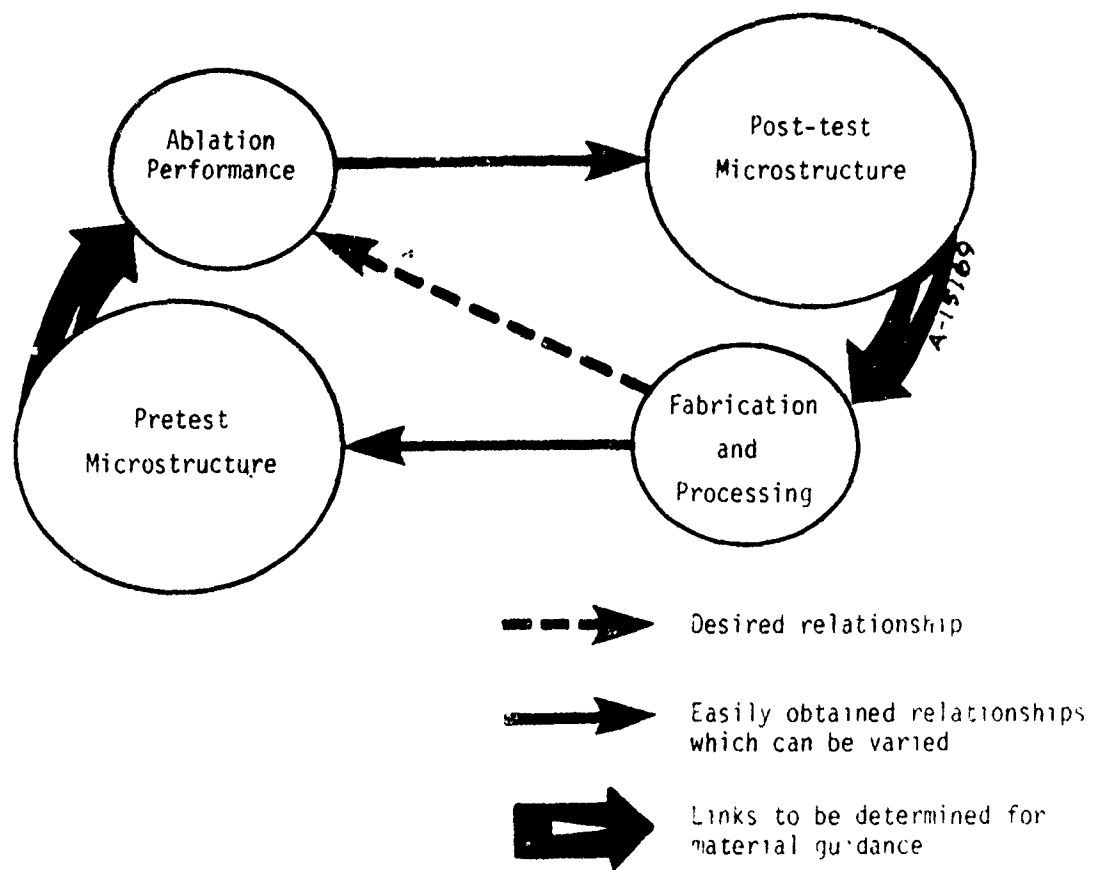
Figure A-2. Relationship between ablation and fabrication.

each form of carbon (e.g., bulk graphite, pyrolytic graphite, etc.) to be represented by a different reaction rate expression. This behavior has in fact been verified by this investigation. For instance Figure A-3 is a theoretical prediction based on the empirical correlations described in Section 6. This figure shows that the mass removal rate is dependent upon the type of carbon under consideration. It also implies that preferential attack will occur in carbon composites which are heterogeneous mixtures of different carbons. This implication has been verified by the ablation tests described in Section 4. Figure A-4 shows the results of some of these measurements for carbon/carbon materials in a hydrogen environment. Different precursor materials are apparently attacked more or less vigorously by hot hydrogen gases. Preferential ablation can also be seen in SEM's of post-test surfaces. For example, Figures A-5 and A-6, respectively, show the ablated surfaces of rayon and PAN precursor composites. Rayon is apparently attached preferentially, leaving a visible surface which is virtually all matrix material. PAN composites, however, show surfaces which are mixtures of fibers and matrix. Significant micromechanical breakage of fibers is observed and apparently enhances the ablation rates. This fiber cleavage is more evident in Figure A-7.

Two tentative conclusions can be reached from a preliminary examination of the carbon/carbon pre- and post-test microstructures. First, for a resin (or pitch) impregnated c/c at a given density, the recession rate performance of rayon precursor reinforcements is superior to that of PAN precursor reinforcements (Figure A-4). Second, post-test SEM's show that the reinforcement in a rayon precursor c/c recedes below the surface of the matrix (Figure A-5). This second conclusion suggests that the matrix is a better ablator than the rayon reinforcement. Thus, a potentially good material would use a low volume content of rayon precursor reinforcement and a high density graphitized matrix.

It is recognized that continuous filament rayon material will soon be unavailable so that a first impression would be to avoid the use of rayon. However, there is a mounting effort to develop low density PAN and pitch precursor reinforcements with physical properties similar to that of rayon. Hence, basic information obtained with rayon precursor c/c materials will be valuable for providing ablation and microstructure relationships to guide material development.

Fiber volumes for two-dimensional c/c materials are typically 45 to 55 percent. Fiber volumes for 3-D materials are around 30 to 35 percent. Thus, 3-D materials offer two advantages. First, they are structurally better than 2-D materials and second, they have inherently lower fiber volumes. The disadvantage of 3-D materials is their higher fabrication cost and potentially greater scale-up problems. If 3-D materials prove to be ablation-wise superior, then these disadvantages can be tolerated.
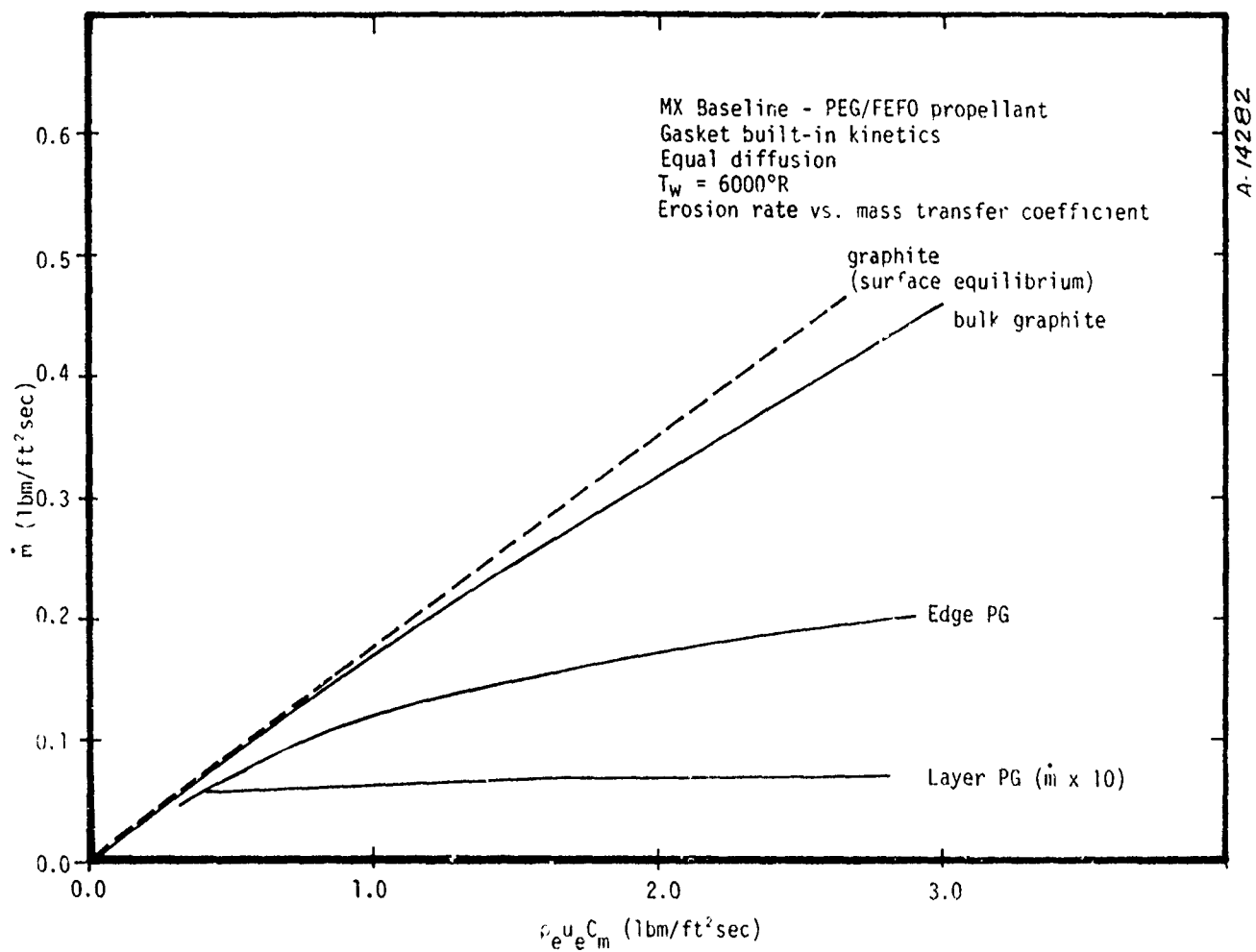
Figure A-3. Relationship between mass transfer coefficient and ablation
rate for various carbon materials.
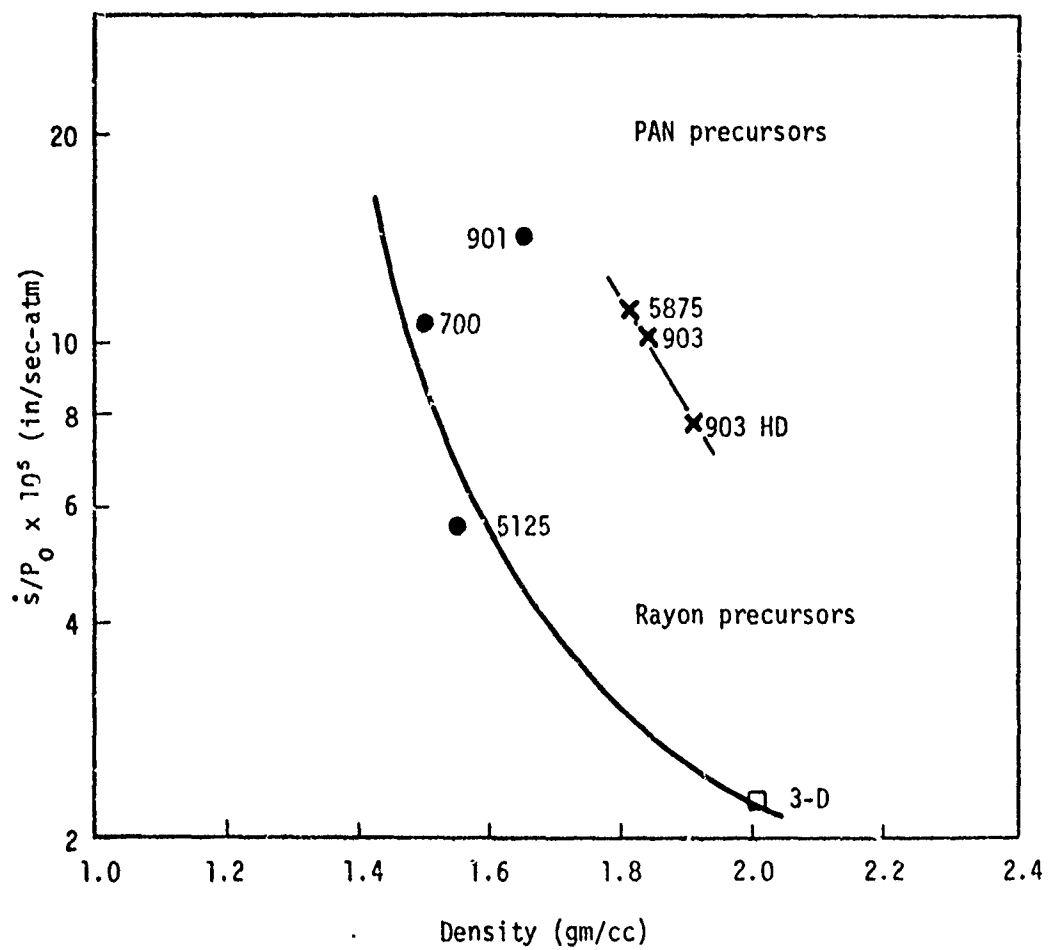
Figure A-4. Measured ablation rates in hydrogen environment, $T_w \simeq 5500°R$.

ht 24p8

Hrx 5125

.005"
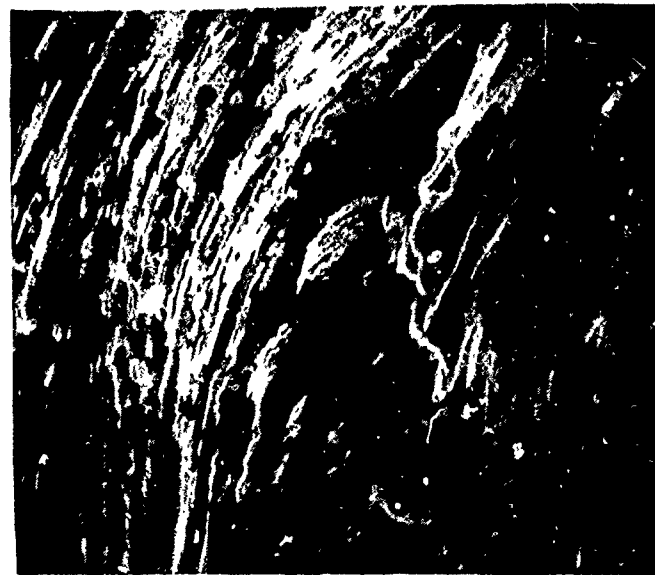
Carbitex 700
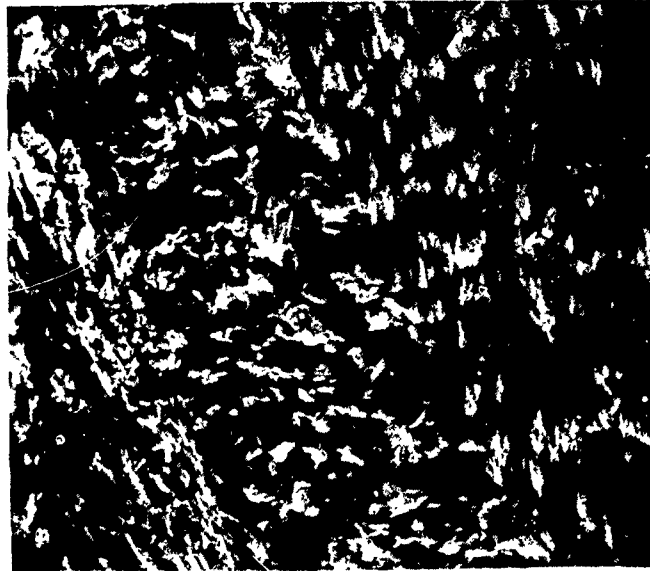
Figure A-5
Exposed matrix at surface of rayon precursor composite.
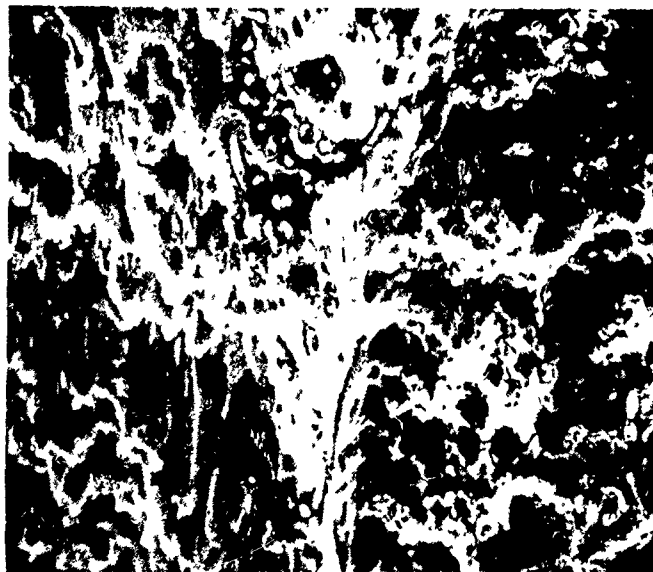
ht 23pa
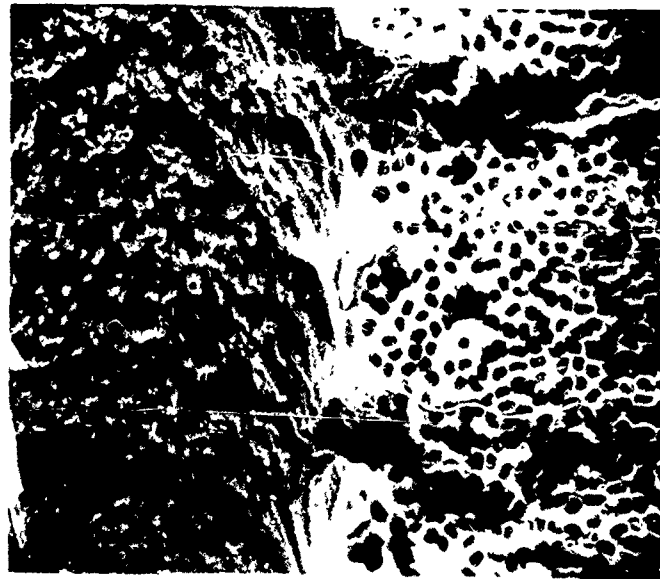
Hrx 5875

Pyrocarb 903

.005"

Figure A-6

Exposed matrix and fibers of PAN precursor composite

hx 22pa

cleaved
fibers

Hrx 5875
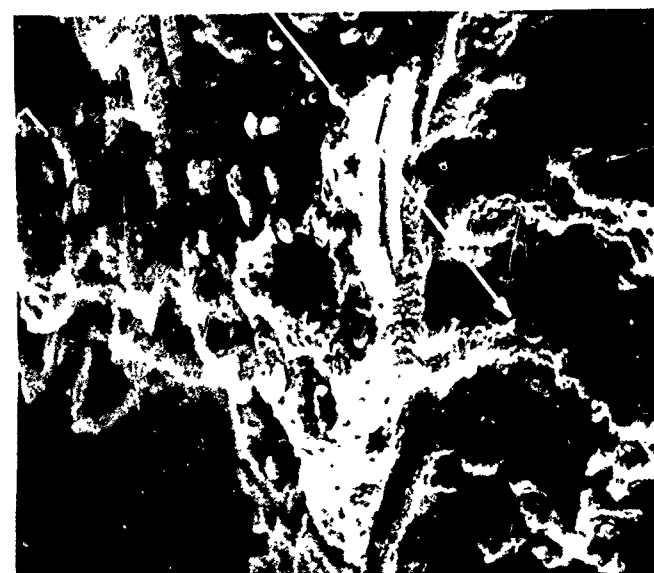
Pyrocarb 903

|— .002" —|

Figure A-7

Evidence of fiber cleavage in PAN precursor composite.

147/148

As part of this investigation, pre- and post-test microstructural characteristics were examined for two purposes. First, it was hoped that some obvious relationships would be observed to relate microstructure to ablation performance and material fabrication. Believing, however, that there would not be sufficient data to establish firm relationships, the second purpose was to collect this microstructure data as a "data bank" for future reference. As additional data is added to this data bank, the relationships between fabrication and ablation performance should become more obvious. Eventually, the kinetic behavior of a graphitic material can be determined by a detailed knowledge of its fabrication or by examination of its pretest microstructure. This, of course, is a very ambitious objective and may take a decade to realize.

The microstructural characterization measurements performed in this study are tabulated in Table A-1. All characterizations, with the exception of ordinary photography and scanning electron microscopy, were performed by Mr. Jay Baetz of the Aerospace Corporation, El Segundo, California.

A.2   MICROSTRUCTURAL EXAMINATION

Microstructural examination was conducted to characterize both virgin and tested material conditions. The primary areas of interest in this examination included in-depth assessment of untested material structure and the surfaces resulting from exposure to arc test conditions. The principal microstructural features of interest for tested specimens included response of reinforcements and matrices to the imposed test conditions.

Selected specimens were examined by photomicrographic and scanning electron microscopy (SEM) techniques. Representative selected materials were examined in the tested and untested states by both techniques. However, primary emphasis in the photomicrographic studies was directed toward untested material examination. This emphasis was maintained so that high resolution definition of polished material samples would be obtained. The SEM was primarily used for arc tested material analysis, which permitted utilization of the SEM large depth of focus to assess tested surfaces without surface modifications.

Materials Summary

Three classes of materials were examined. These classes included carbon/carbon composites, bulk graphites, and vapor-deposited carbons. Within the carbon/carbons both two- and three-dimensionally reinforced materials were analyzed. The bulk graphites included aerospace grade, fine grained systems and commercial grade graphites. Vapor deposited carbon material systems examined included conventional pyrolytic graphites, a-b oriented graphites and graphites codeposited with metal carbides. A summary of the materials examined is provided in Table A-2.

TABLE A-1. MICROSTRUCTURAL CHARACTERIZATION MEASUREMENTS

Material Description	Pretest							Post-Test					
	Metallograph	SEM	C_o	L_a	CTE	Porosity	Chemadsorption	Metallograph	SEM	C_o	L_a	Porosity	Chemadsorption
G-90	X				X	X	X	X	X			X	X
ATJ	X					X		X	X			X	
ATJ-S	X					X		X	X			X	
PO-3	X							X	X				
Hitco a-b PG	X		X	X				X	X				
Pfizer c PG	X		X	X	X			X	X			X	
Supertemp c PG	X		X	X	X			X	X	X	X		
ARC 23% SiC/PG	X							X	X				
ARC 15% SiC/PG	X						X	X	X			X	X
ARC 5% SiC/PG	X							X	X				
Raytheon 65% HfC/PG	X							X	X				
Pyrocarb 901	X	X			X	X	X	X	X			X	X
Pyrocarb 903	X	X			X	X	X	X	X			X	
Pyrocarb 903 HD	X				X	X		X	X			X	
MDAC 3-D c/c	X				X	X	X	X	X			X	
Haveg 5125 c/c	X				X	X		X	X			X	
Haveg 5875 c/c	X				X	X		X	X			X	

TABLE A-2. SUMMARY OF MATERIALS EXAMINED

Material Class	Manufacturer	Identity
Carbon/carbon	Hitco/Defense Products Division	Pyrocarb 901
	Hitco/Defense Products Division	Pyrocarb 903
	Haveg	HRX 5125
	Haveg	MRX 5875
	McDonnell-Douglas	MDAC 3-D c/c
	Carborundum	Carbitex 700
Bulk Graphite	Union Carbide	ATJ
	Pure Carbon	PO-3
	Carborundum	G-90
	Union Carbide	ATJ-S
Vapor Deposited Carbons	Pfizer	Standard pyrolytic graphite
	Supertemp	Pyrolytic graphite (101-B)
	Hitco/Defense Products Division	a-b oriented pyrolytic graphite
	Atlantic Research Corporation	5% SiC/pyrolytic graphite
	Atlantic Research Corporation	15% SiC/pyrolytic graphite
	Atlantic Research Corporation	23% SiC/pyrolytic graphite
	Raytheon	HfC coated pyrolytic graphite

151

These materials constitute a representative cross-section of all classes of materials currently considered for nozzle application. Within each materials class, a number of constituents or processing techniques are considered proprietary by the respective manaufacturers. A summary of each material examined is provided within the above cited proprietary restrictions as follows.

Pyrocarb 901

Pyrocarb is a two-dimensional reinforced composite with a rayon precursor square weave carbon fabric. The laminate is initially formed by fabric impregnation with a phenolic resin. Individual plys are rotated within the billet plane as specified by the customer. Details of processing and densification are considered proprietary by the manufacturer.

Pyrocarb 903

This material is also a two-dimensional reinforced carbon/carbon. The reinforcement is an eight harness satin weave with a PAN precursor. Laminates are fabricated with the fabric impregnated with a phenolic matrix. Multiple density levels are available depending upon the customer requirements. In this program two density levels were tested. Ply rotation is as specified by the customer.

HRX 5125

HRX 5125 is a two-dimensional carbon/carbon fabricated from a rayon precursor fabric such as WCA. The initial densification is accomplished with H-resin. This matrix is carbonized at 800°C. Redensification is accomplished with the H-resin for an unspecified number of cycles. Subsequent densification is accomplished with Allied Chemical's new coal tar pitch. The final processing step performed is at 2800°C graphitization. Adjacent plys are rotated to obtain quasi-isotropic, in-plane properties.

HRX 5875

HRX 5875 is a two-dimensional reinforced carbon/carbon composite. The reinforcement consists of a PAN precursor carbon fabric with an eight harness satin construction. A typical yarn used is Thornel 300. Prior to use in laminates, the fabric is heat treated to the graphitization temperature. H-resin is used as the initial impregnating matrix and is carbonized at 800°C. At the midpoint of densification processing, the laminate is graphitized. Continued densification is accomplished with 15 V coal tar pitch. The final processing step is graphitization at 2800°C. Ply rotation is performed.

Carbitex 700

Carbitex 700 is a two-dimensional reinforced carbon/carbon. The reinforcement is a square weave rayon precursor graphitized in fabric form. The matrix utilizes a resin precursor. Graphitization is conducted at a minimum temperature of 2700°C.

MDAC 3-D C/C

The single three-dimensionally reinforced material was MDAC 3-D c/c. This composite utilized orthogonal reinforcements of Thornel 50 yarns. Weave construction was 224. The preform was woven by FMI and carried the identity of 173B. Densification was accomplished with 15 V pitch and a thermosetting resin. Graphitization between densification cycles was conducted at 2800°C. The final thermal treatment was a 1000°C pyrolysis. No definition of the pitch/resin impregnating sequence is available.

ATJ-S

ATJ-S was the initial bulk graphite considered. This product, the best characterized of the aerospace grade graphites, is fine grained (0.006 inch maximum) with a density of 1.83 gm/cm^3 and an ash level of 193 ppm.

ATJ

ATJ is a molded graphite with a grain size equivalent to an ATJ-S. However, its density (1.74 gm/cm^3) is somewhat lower and its ash level (1200 ppm) is somewaht higher than ATJ-S. The specific material utilized in this program was obtained from the center of a 15-inch diameter billet.

PO-3

PO-3 is a commercial grade molded graphite, stated by the manufacturer to be somewhat porous. Specific information regarding manufacturing processes has not been obtained. A number of grades are produced including some with carbide additions.

G-90

G-90 is an aerospace grade graphite. It has a 1.9 gm/cm^3 minimum density and is manufactured as an extruded product. Ash content is 0.06 percent. The maximum grain size is 0.037 inch.

Supertemp PG

Pyrolytic graphite was obtained from Supertemp in accordance with their specification 101-B. No information as to source gases, deposition temperatures, or other processing conditions were available.

HfC/PG

This product consists of pyrolytic graphite codeposited with hafnium carbide. Codeposition ʳformed at approximately 10 Torr pressure and a temperature between 1800°C to 1850°C. The resulting deposition rate is approximately 10 mils/hour on a graphite mandrel substance. The resulting product is characterized as reasonably fine grain renucleated.

A-B PG

This product was obtained by deposition of pyrolytic graphite on premachined ATJ substrates. The material was not machined prior to testing so that the initial ablation surface was the as-deposited surface.

Pfizer PG

Pfizer pyrolytic graphite is deposited as pure carbon to obtain a continuously nucleated structure. Further details are not known.

5, 15, and 23 Percent SiC PG

Silicon carbide is codeposited with graphite to obtain this product. Fabrication information is contained in Reference A-I.

A.2.1 Metallographs

Representative samples of pre- and post-test materials were photographed using a metallograph. These metallographs yielded qualitative information on the structure and uniformity of each material. Select post-test samples were also photographed to reveal the roughness of the ablation surface. Magnifications of 40 to 1000X were used although the preponderance of photographs were for magnifications less than 200. A list of the materials and magnification levels is shown in Table A-3.

No noticeable changes were observed for the in-depth microstructure between pre- and post-test states. Some differences were noted, however, in the characteristic surface roughness of different materials. Since surface roughness metallographs also show the in-depth structure, there

154

TABLE A-3. PRE- AND POST-TEST METALLOGRAPHS

Material	Pretest Magnifications						Post-Test Magnifications			
	20-90	100-190	200-290	300-490	500-1000	2000-4000	40-90	100-190	200-290	300-490
G-90		4						2	2	
ATJ		1		1				2	2	
ATJ-S		2						2		
PO-3		1		1				2		
Hitco a-b PG			5					1		
Pfizer c PG	2						2		3	
Supertemp c PG		5						2		
UK PG		20								
23% SiC/PG	7	2					2	3		
15% SiC/PG	1	1						2	2	
5% SiC/PG								2	2	
65% HfC/PG		2		2				2		
Pyrocarb 901	1	1			2	1		2	2	
Pyrocarb 903		2						1	2	
Pyrocarb 903 HD		4						2	1	
MDAC 2-D		2	2				1	8	2	
Haveg 5125		1						1	2	
Haveg 5825	6	10						2	1	

would be little value in showing pretest microstructures. Thus, only representative post-test metallographs will be shown.

Metallographs for the bulk graphites, PO-3 and G-90 are shown in Figures A-8 and A-9, respectively. These photographs show the effect of grain size on the texture or roughness of the ablated surface. PO-3, being a very fine grain material, has a virtually smooth ablation surface, while G-90, which has a large grain size, has a rough surface.

ATJ and ATJ-S have grain sizes between PO-3 and G-90 and although not shown have an ablation surface with a roughness between that of PO-3 and G-90.

Metallographs for Pyrocarb 903 and HRX 5875 are shown in Figures A-10 and A-11, respectively. These are both PAN precursor reinforcements; however, there are some obvious differences in fabrication. The HRX 5875 apparently uses a heavier carbon yarn or is processed at lower pressures. This is evidenced by the uniformity of the plys compared with those of Pyrocarb 903. The latter shows significantly more yarn distortion. Surface roughness of these two materials are about the same with roughness heights of about 3 to 5 mils.

Figures A-12 and A-13 show the microstructure of Pyrocarb 901 and HRX 5125, respectively. The differences in ablation surface roughness are apparent although both are fabricated from rayon precursor fabric. The "evenness" of the Pyrocarb 901 surface is unusual when compared with the other carbon/carbon composites.

A metallograph for the 3-D carbon/carbon is shown in Figure A-14. The carbon yarns are clearly thicker than those of 2-D composites and because of the orthogonal weave, there are distinct and systematic matrix pockets.

A.2.2 SEM Analysis

As stated above, primary emphasis in the SEM studies was placed on post-test examination of the eroded nozzle surfaces. Sections were removed from the tested models and viewed as shown in Figure A-15. In all SEM photos of tested models taken, the entrance of the throat is to the left of the picture. All specimens were examined without surface preparation. A number of magnification levels were taken; however, only 50 and 500 magnification levels will be shown. As with the metallographs, only representative SEM photographs will be shown.

A summary of the models and test conditions for which SEM analysis was conducted is provided in Table A-4.
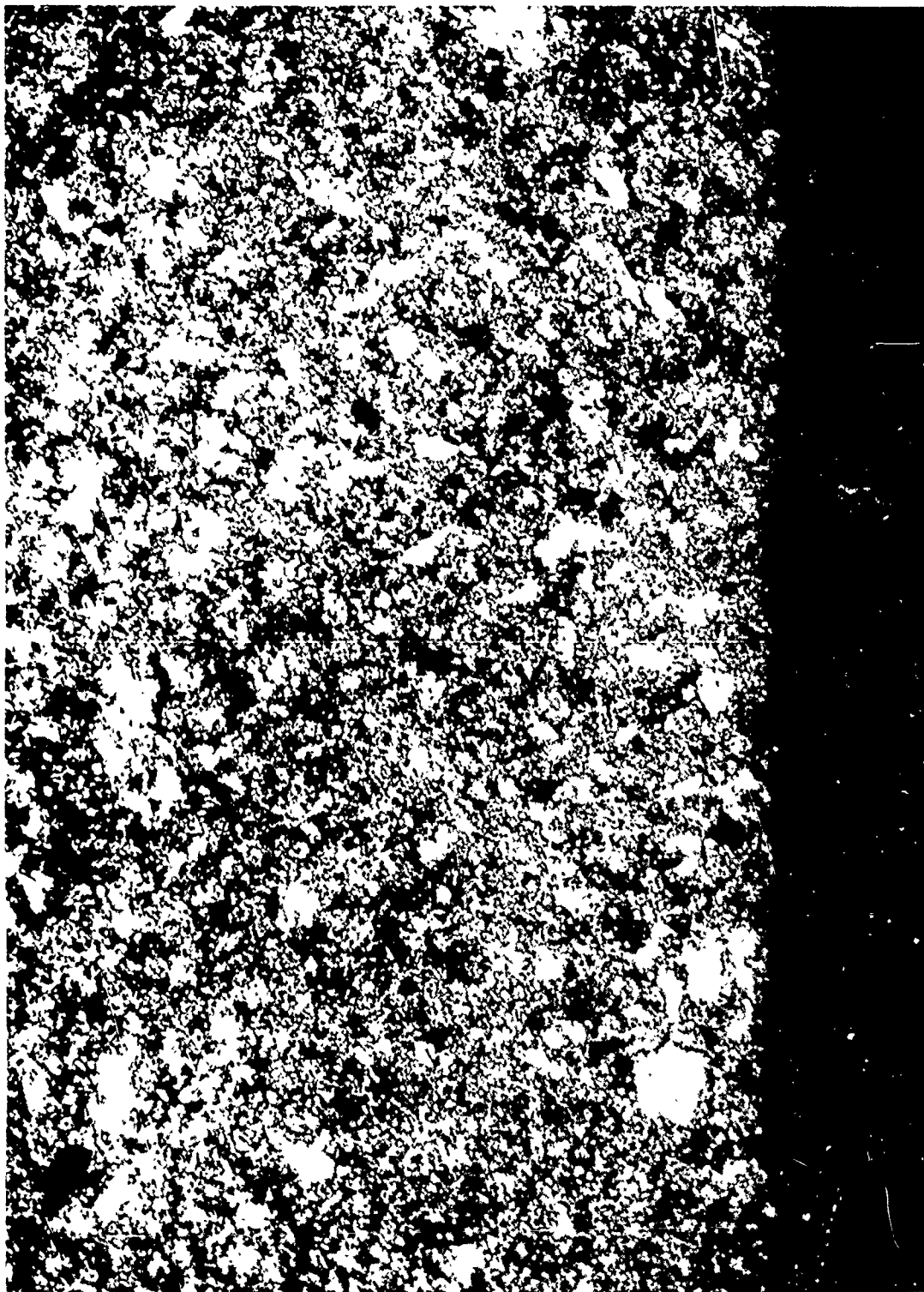
Figure A-8. Post-test microphotographs for PO3 100X.

Figure A-9. Post-test microphotographs for G-90 100X.

Figure A-10.   Post-test microphotographs for Pyrocarb
                   903   100X.

Figure A-11. Post-test microphotographs for
HRX 5875   100X

Figure A-12. Post-test microphotographs for Pyrocarb
901 100X.

Figure A-13. Post-test microphotographs for 52X
5125   100X

Figure A-14. Post-test microphotographs for MDAC
3-D — 50X.
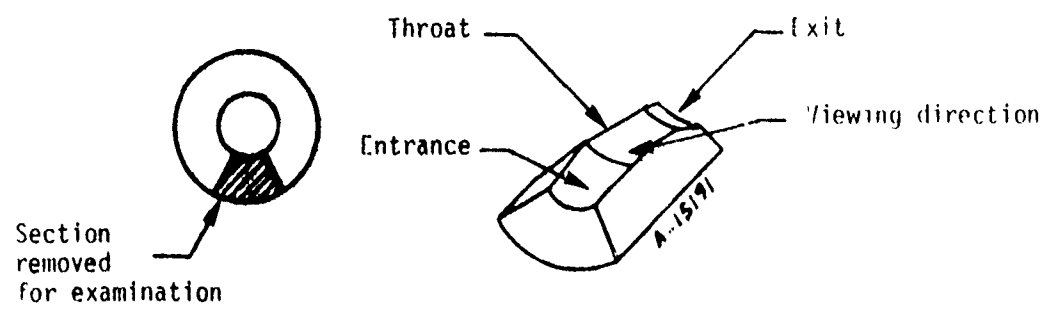
Figure A-15.   SEM sample orientation.

TABLE A-4. SUMMARY OF BULK GRAPHITES EXAMINED BY SEM

Model Identity	Test Conditions							Average Recession Rate (mils/sec)	Material Identity
	P_o Total Supply Pressure (atm)	T_s Maximum Surface Temp (°R)	$\dot{H}$ Bulk Enthalpy Rate (Btu/sec)	t Test Time (sec)	H Total Bulk Enthalpy (Btu)	Test Gas Composition	No.		
078 S	5.25	5263	268.9	48	12,907	H_2/O_2	3	0.9592	ATJ-S
079 S	5.62	4788	219.6	61	13,394	$H_2/C_2/CO/HC\ell$	8	0.2834	ATJ-S
081 S	5.76	4258	167.7	50	10,062	H_2/O_2	3	0.5917	ATJ-S
084 S	3.35	4814	264.3	98	25,901	H_2	1	0.0600	ATJ-S
006 C	5.70	4750	370.7	41	15,200	H_2/O_2	3	1.288	ATJ
007 C	4.20	4900	388.1	39	15,113	H_2	1	0.1123	ATJ
070 S	3.44	5202	320.6	83.0	26,613	H_2	1	0.0920	PO-3
168 C	4.825	4899	324.2	52.0	16,860	H_2/O_2	3	1.142	G-90
177 C	3.55	5358	390.7	49.0	19,143	H_2	1	0.241	G-90
184 C	5.32	4999	245.9	—	—	$H_2/O_2/CO/HC\ell$	8	—	
154 C	5.28	5132	246.6	48	11,836	$H_2/O_2/CO/HC\ell$	8	0.825	Pyrocarb 901
158 C	3.50	5358	390.5	40	15,618	H_2	1	0.5425	Pyrocarb 901
159 C	5.00	5100	314.8	33	10,389	H_2/O_2	3	1.226	Pyrocarb 901
218 S	3.75	5514	390.7	49	19,146	H_2	1	0.3444	Pyrocarb 903
220 S	5.66	5309	290.4	43	12,487	H_2/O_2	3	1.0302	Pyrocarb 903
223 S	4.56	4873	232.0	66.5	15,425	$H_2/O_2/HC\ell$	7	0.4929	Pyrocarb 903
244 S	4.44	5118	269.8	45.0	12,140	H_2/O_2	3	1.1311	Pyrocarb 903 HD
246 S	5.64	4199	137.4	63.0	8659	H_2/O_2	3	0.5841	Pyrocarb 903 HD
247 S	3.57	5611	380.2	57.0	21,673	H_2	1	0.2982	Pyrocarb 903 HD

TABLE A-4. Continued

Model Identity	Test Conditions							Average Recession Rate (mils/sec)	Material Identity
	P_o Total Supply Pressure (atm)	T_s Maximum Surface Temp (°R)	$\dot{H}$ Bulk Enthalpy Rate (Btu/sec)	t Test Time (sec)	H Total Bulk Enthalpy (Btu)	Test Gas Composition	No.		
229 S	3.43	5075	285.0	100.0	28,500	H_2	1	0.1338	HRX 5125
230 S	5.52	5527	286.6	36.0	10,319	H_2/O_2	3	1.4528	HRX 5125
240 S	4.68	5056	219.7	59.0	12,962	$H_2/O_2/HC\ell$	7	0.4339	HRX 5875
241 S	4.48	5225	260.3	34.0	8,849	H_2/O_2	3	0.4779	HRX 5875
242 S	3.54	5225	291.0	76.0	22,115	H_2	1	0.1872	HRX 5875
007	6.6; 5.6	4965	233.1	40	9,324	H_2/O_2	3	1.252	Carbitex 700
236 S	3.88	54.59	391.2	55	21,513	H_2	1	0.6291	Carbitex 700
200 S	4.91	5151	255.4	44.5	11,364	H_2/O_2	3	1.207	MDAC 3-D c/c
201 S	3.78	5412	387.8	18.25	7,077	H_2	1	0.2181	MDAC 3-D c/c
073 S	3.22	4112	211.9	60	12,716	H_2/O_2	3	0.0090	Supertemp PG
074 S	3.38	4733	245.5	98	24,057	H_2	1	0.0193	Supertemp PG
075 S	4.74	5095	221.7	60.5	13,416	$H_2/O_2/HC\ell$	7	0.2562	Supertemp PG
086 S	3.74	5622	386.7	57	22,043	H_2	1	0.2719	Pfizer PG
089 S	4.91	5379	234.2	62	14,520	$H_2/O_2/HC\ell$	7	0.8161	Pfizer PG
074 S	2.99	4851	274.6	98	26,908	H_2	1	0.0768	Hitco a-b PG
100 S	4.81	5097	258.0	37.0	9,547	H_2/O_2	3	0.4676	Hitco a-b PG
234 S	5.65	5177	265.6	43.5	11,552	H_2/O_2	3	0.8736	ARC 5% SiC/PG
235 S	3.59	5624	385.5	58.5	22,552	H_2	1	0.2471	ARC 5% SiC/PG

TABLE A-4. Concluded

| Model Identity | Test Conditions | | | | | | | Average Recession Rate (mils/sec) | Material Identity |
| | P_o Total Supply Pressure (atm) | T_s Maximum Surface Temp (°R) | $\dot{h}$ Bulk Enthalpy Rate (Btu/sec) | t Test Time (sec) | H Total Bulk Enthalpy (Btu) | Test Gas | | | |
						Composition	No.		
111 C	5.65	4900	342.9	31.0	10,630	H_2/O_2	3	1.303	ARC 15% SiC/PG*
124 C	4.00	5050	320.0	39.0	12,479	H_2	1	0.3436	ARC 15% SiC/PG
059 S	5.60	5168	274.9	28.0	7697	H_2/O_2	3	1.850	ARC 23% SiC/PG
010 S	3.67	5478	388	53	20,563	H_2	1	0.6566	ARC 23% SiC/PG
203 S	3.32	4871	273.4	97	26.524	H_2	1	0.0361	HfC/PG
205 S	2.49	5093	317	90	28,528	H_2	1	0.2500	HfC/PG
209 S	5.55	5173	154.3	55	8486	H_2/O_2	3	0.2500	HfC/PG

Vapor Deposited Carbons

SEM photographs of Supertemp pyrolytic graphite specimens tested in hydrogen, hydrogen/
oxygen, and hydrogen/oxygen/hydrogen chloride mixtures are shown in Figures A-16, A-17, and A-18.
The low magnification hydrogen tested model exhibited three primary features. These features in-
cluded the formation of cavities, microcracks perpendicular to the throat axis and apparent waviness
of structure as shown in Figure A-16(a). The waviness is also evident at higher magnification
(Figure A-16(b)) as is the presence of a nodular structure on the cavity walls.

Exposure of Supertemp pyrolytic graphite to the hydrogen/oxygen test gas at somewhat lower
temperatures resulted in the grainy, near fibril appearance shown in Figure A-17(a). At high
magnification, these features are plainly shown. As indicated in Table A-4, a lower recession rate
was found with the hydrogen/oxygen mixture than the pure hydrogen environment. This apparently
anomalous condition may be related to the lower test temperatures employed in the hydrogen/oxygen
environment.

The structure resulting from hydrogen, oxygen, and hydrogen chloride closely represents the
more severe recession conditions normally seen in oxygen-containing environments on other materials.
This is shown in Figure A-18. It should be noted that the temperature employed in this test approx-
imated that used on other oxygen-containing environments. Small cracks are again evident in a
generally scalloped macrostructure. At higher magnification, the generally layered structure is
evident outside the crack region.

The a-b pyrolytic graphite in a hydrogen environment exhibited the presence of partially de-
laminated layers parallel to the throat and the presence of a nodular structure at low magnifica-
tions. This is shown in Figure 19(a). At higher magnification, the detail nodular structure is
apparent. Some alignment of the nodule peaks parallel to the test gas flow is also observed in
Figure A-19(b).

Compared to the Supertemp material, the Pfizer pyrolytic graphite material exhibited a
similar but more extreme case of cavity formation in hydrogen environments. Surface pitting and
a-b plane delaminations were also more severe.

The codeposited pyrolytic graphites are typified by SiC/PG. Figures A-20 and A-21 illustrate
the structures observed for the 23% and 5% silicon carbide materials. A definite nodular structure
is evident at the low magnification in both the 23% and 5% SiC specimens tested in hydrogen (Figure
A-20(a) and A-21(a)). Additionally, these figures show the cavity structure observed on other pyrol-
ytic graphite. A higher magnifications, small cracks at the base of the nodules are evident in the
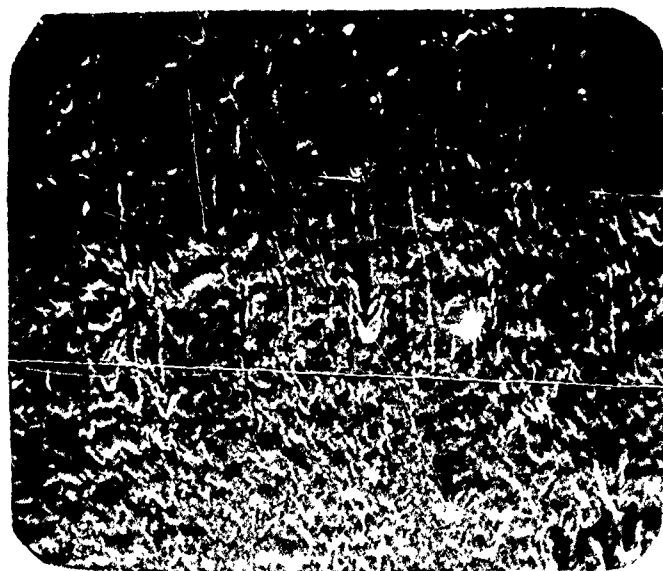
50X

500X

Figure A-16. SEM of Supertemp PG tested
in H_2, T_w = 4733°R.

169

G16

50X
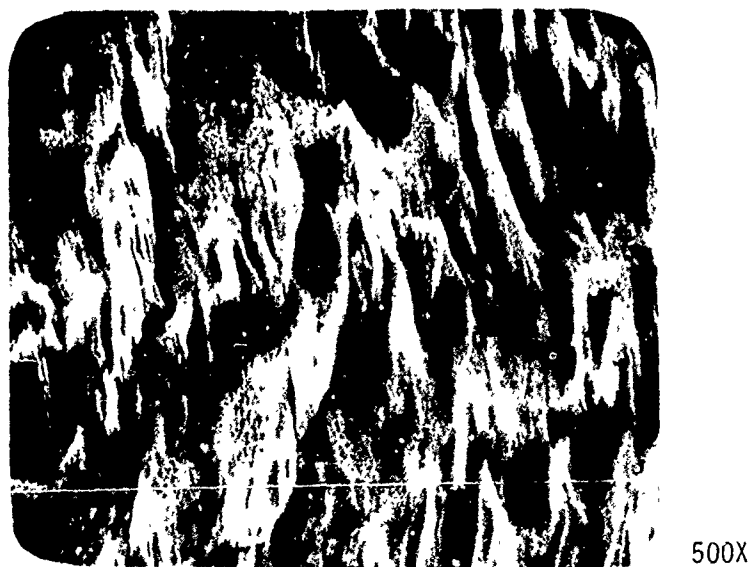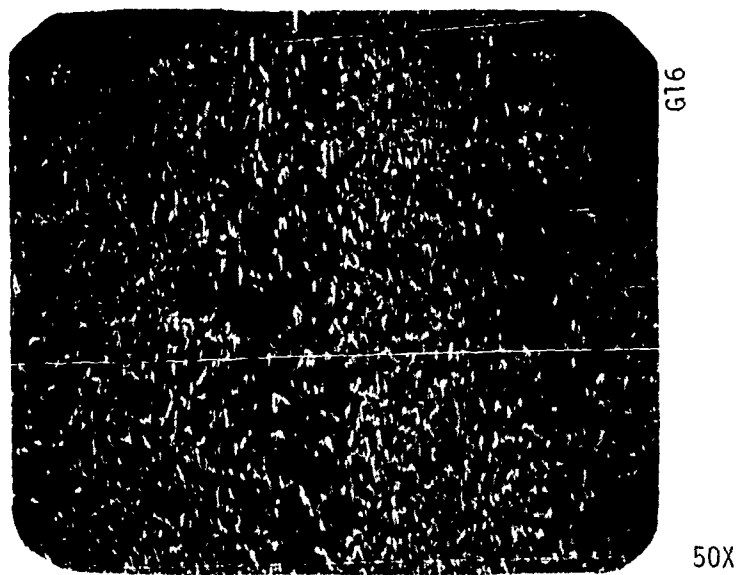
500X

Figure A-17. SEM of Supertemp PG tested in H_2/O_2, $T_w = 4112°R$.

G17
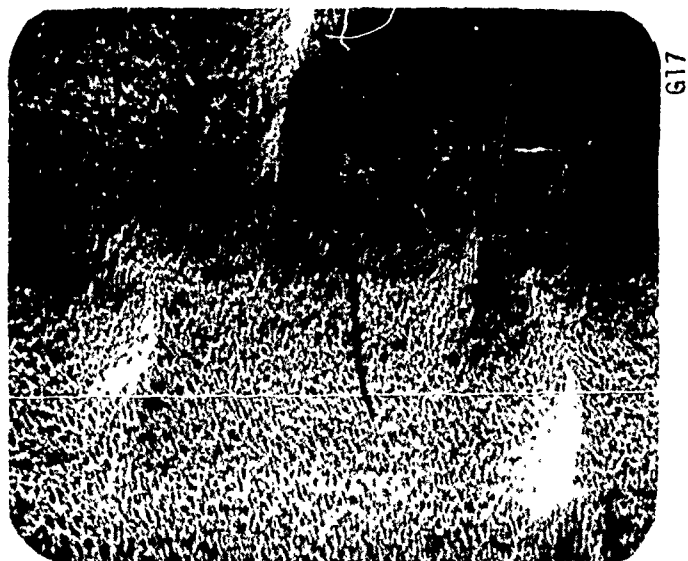
50X
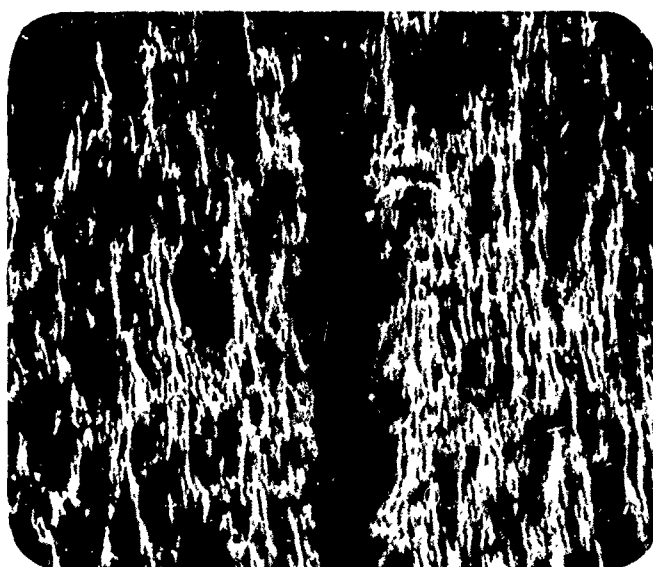
500X

Figure A-18. SEM of Supertemp PG tested
in $H_2/O_2/HC\ell$, T_w = 5095°R.

171
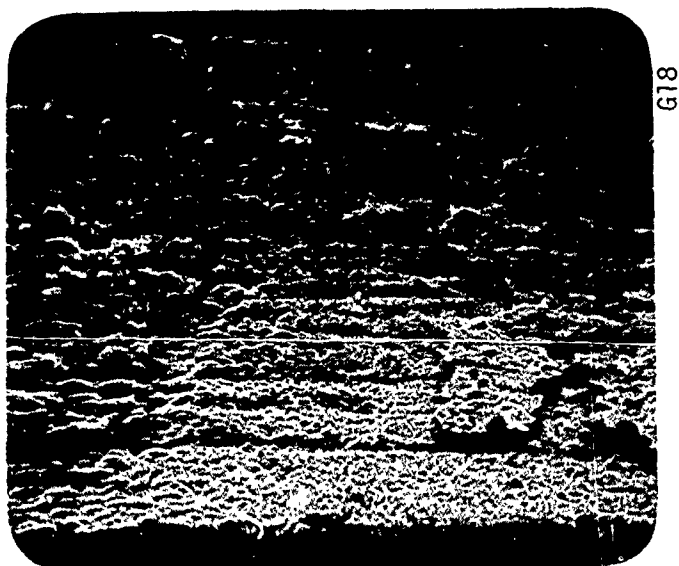
50X
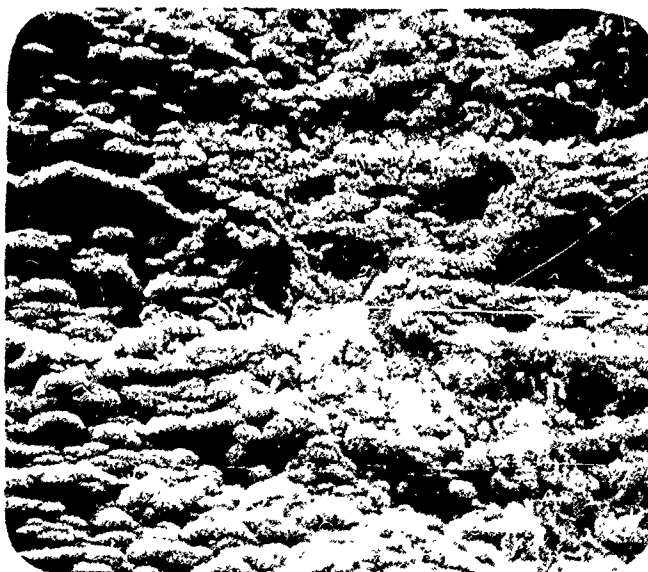
500X

Figure A-19.   SEM of a-b pyrolytic graphite,
tested in H_2, T_w = 4851°R.

50X
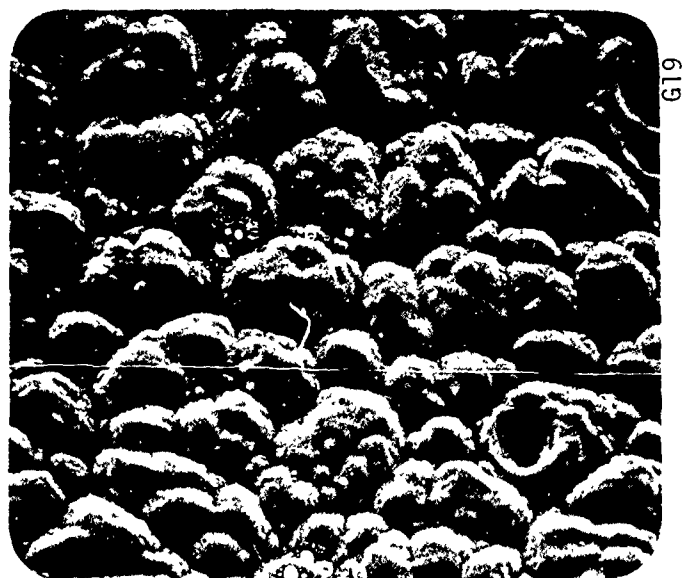
5COX

Figure 20. SEM of 15% SiC/PG tested in
H_2, T_w = 5478°R.

173

G20

50X

500X
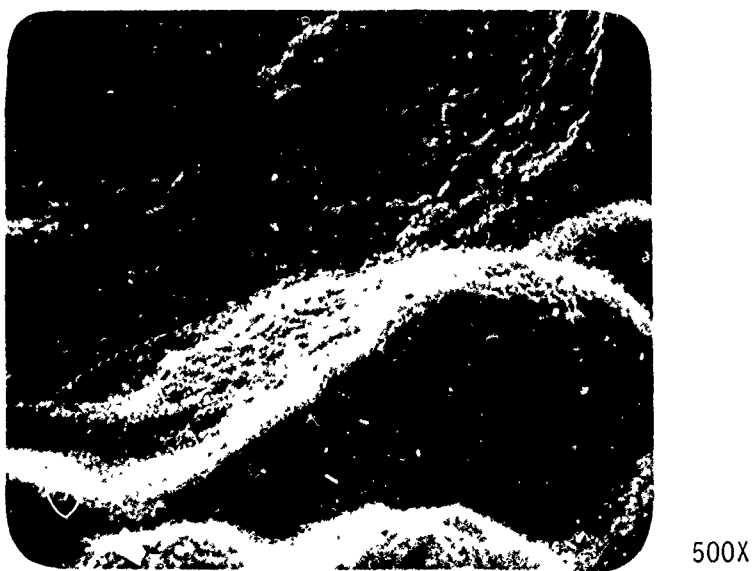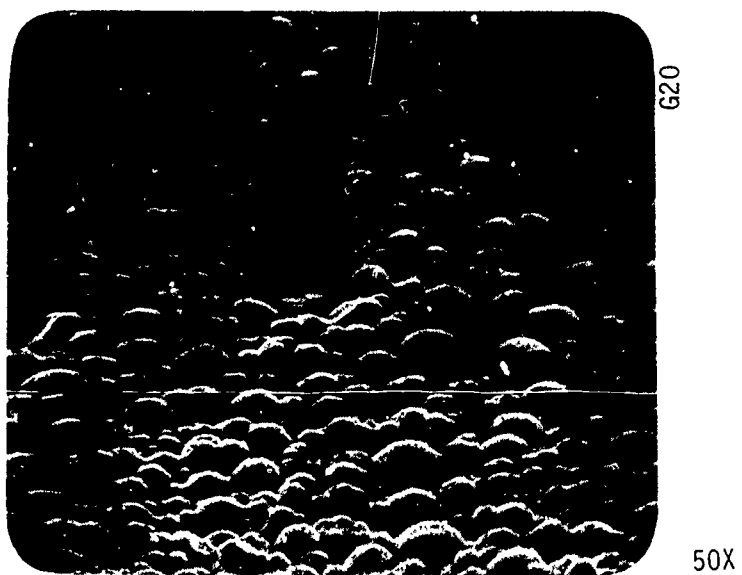
Figure A-21.   SEM of 5% SiC/PG in H_2,
                T_W = 5624°R.

23% silicon carbide material (Figure A-20(b)). In both the 5% and 23% SiC materials, the high magnification shows the nodules to have a fine grained appearance (Figures A-20(b) and A-21(b)).

For both the 5% and 23% SiC specimens, introduction of oxygen produced a significantly different appearance. At low magnification, the 23% silicon carbide model formed a white coating (probably S_1O_2) interrupted by holes. At high magnification, this coating is observed to consist of ceramic type globules. The 5% SiC model exhibited a similar coated nodul:r structure; however, coating density was less complete. Although tested at almost identical temperatures, high magnification views of the 5% silicon carbide coating showed a fiberous, needle-like structure compared to the globular structure for the 23% material.

Hafnium carbide pyrolytic graphite tested in hydrogen gas showed a relatively dense uniform coating. Presence of Hafnium in this coating is indicated by darkened areas whicn changed while in the SEM unit. At high magnification, minor evidence of a substrate structure was evident below the coating cracks.

Bulk Graphites

ATJ-S is representative of the bulk graphites considered in the SEM analysis. Introduction of oxygen in the test gas results in progression of the microstructure from a comparatively smooth, fine-grained appearance to a roughened, coarse structure. This is shown in Figures A-22 and A-23. Roughening corresponded to a large recession rate increase as indicated in Table A-4. This change was not due to temperature differences used in the test. This is jased upon the increased erosion rate and coarsened 50X microstructure which was obtained at the approximately 600°R lower H_2/O_2 temperature. The coarsened microstructure is retained in the H_2/O_2 test environment with an increase of 1000°R but with less recession rate increase than the change in test gas from H_2 to H_2/O_2. No significant change in 500X microstructure is evident with introduction of oxygen into the environment as shown comparing Figures A-22 and A-23. No significant changes occurrel either in macro or microstructure with CO/HCl introduction.

The effect of oxygen was also observed in somewhat larger grain-sized graphites. For example, ATJ progressed from an essentially uniform, relatively smooth macrostructure to the coarse, rough structure with the introduction of oxygen. Again, no significant change in 500X microstructure was observed.

The PO-3 graphite presented a uniçue feature among the molded or extruded graphites. This feature was the formation of macro level cavities within the hydrogen environment. However, at 500X no significant difference in macrostructure is noted compared to the ATJ-S on ATJ systems.
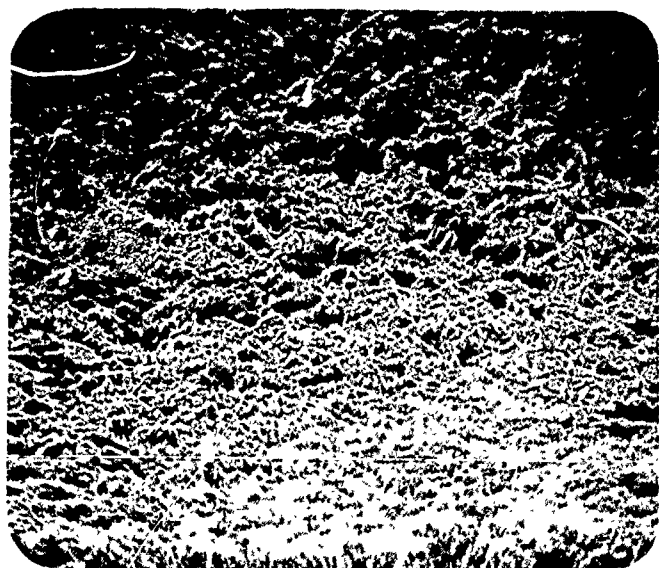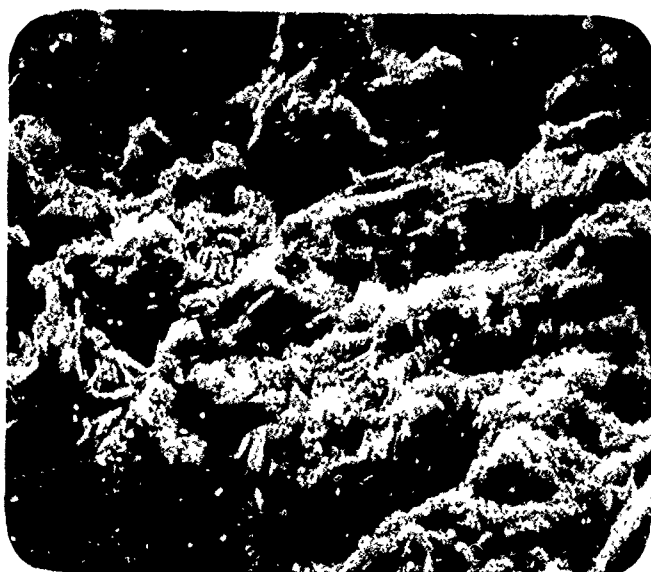
Figure A-22. SEM of ATJ-S tested in H_2, $T_w = 4814°R$.
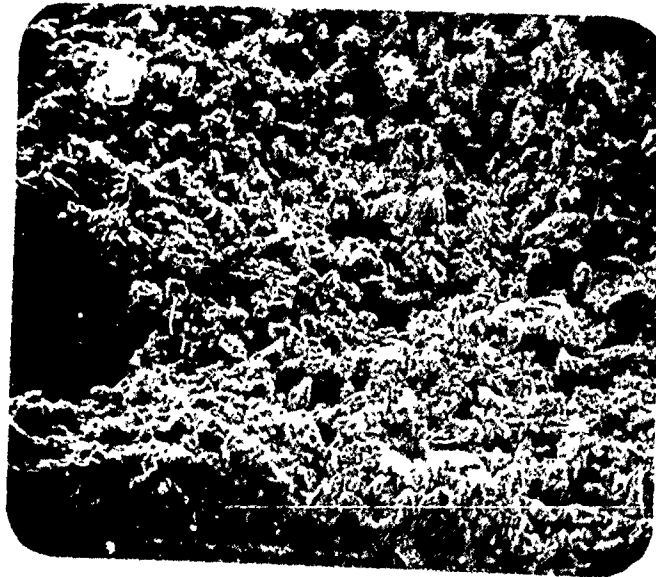
Figure A-23. SEM of ATJ-S in H_2/O_2,
$T_w = 4258°R$.

Carbon/Carbons

The progressive microstructure change in carbon/carbons from untested material through exposures in typical environments was demonstrated by Pyrocarb 903. This progression is shown in Figures A-24 through A-27 for Pyrocarb 903. Progression from untested material to a hydrogen exposed material results in a moderate amount of recession. This recession is evidenced by the initial observation of peaks and valleys around the PAN based yarns parallel to the film plane (Figures A-24(a) and A-25(a)). At higher magnifications, the structure changes from thoroughly intermixed fibers and matrix to exposure of some filaments with a majority of the matrix retained.

Introduction of oxygen results in much higher yarn definition as shown in Figure A-26. This definition resulted from the approximately threefold increase in ablation rate (see Table A-4). It should be noted that this change with H_2/O_2 introduction occurred at a slightly lower temperature than H_2 only. The ply rotation characteristics of this material is shown by filaments approximately perpendicular to the film plane both in the low and high magnifications of Figure A-26. As observed in Figure A-26(a), introduction of oxygen resulted in removal of significant amounts of matrix from the filament groups.

HRX 5125 was examined as another representative two-dimensionally reinforced carbon/carbon. This rayon precursor reinforced, H-resin/15 V pitch densified material exhibited the same dependence on oxygen presence in appearance as did the preceding material. All of the features previously cited including fiber exposure, ply rotation, and matrix loss with oxygen, were observed to some degree.

HRX 5785 presented an anomaly to the above cited microstructure trend. Although tested at similar or lower temperatures, the specimen exposed to hydrogen showed an apparently more severe loss in both low and high magnifications.

The single three-dimensionally reinforced material examined was MDAC 3-D c/c. This material was examined at three locations for the specimen tested in hydrogen. Two of these positions were orthogonal while the third was at 45° to the previous two. No relationship to the throat circumferential position was noted. In all cases, the surface exhibited distinct fiber exposure and retained matrix in the low and high magnifications. Progressive fiber exposure and smoothness were evident in the H_2/O_2 specimen.

Although tested at approximately the same temperature as the H_2/O_2 environment, introduction of CO and HCℓ resulted in better retention of the fibers parallel to the film plane. This is accounted for by the CO and HCℓ producing a less severe environment than H_2/O_2 and was confirmed by the reported recession rates.
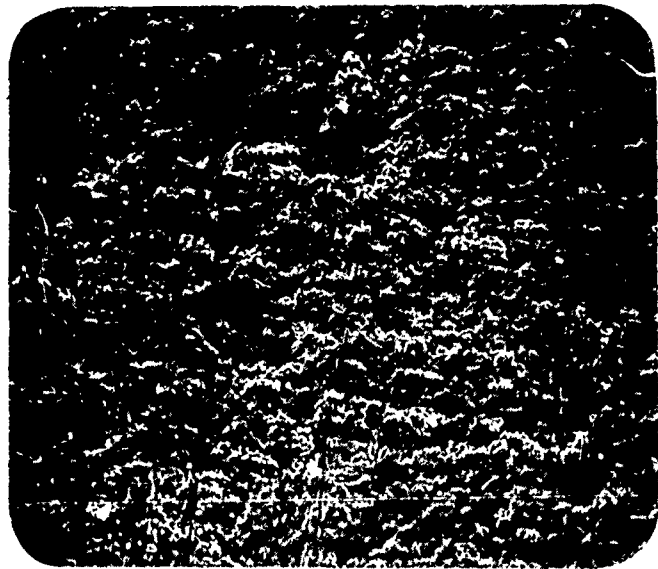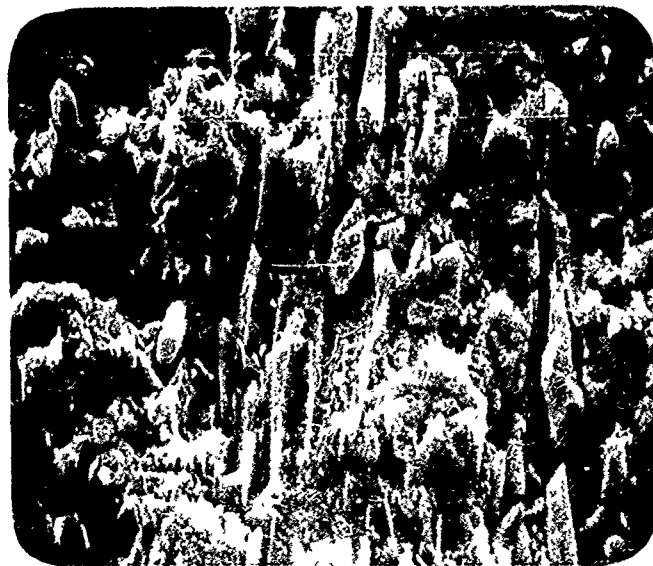
Figure A-24. SEM of Pyrocarb 903, as
machined.
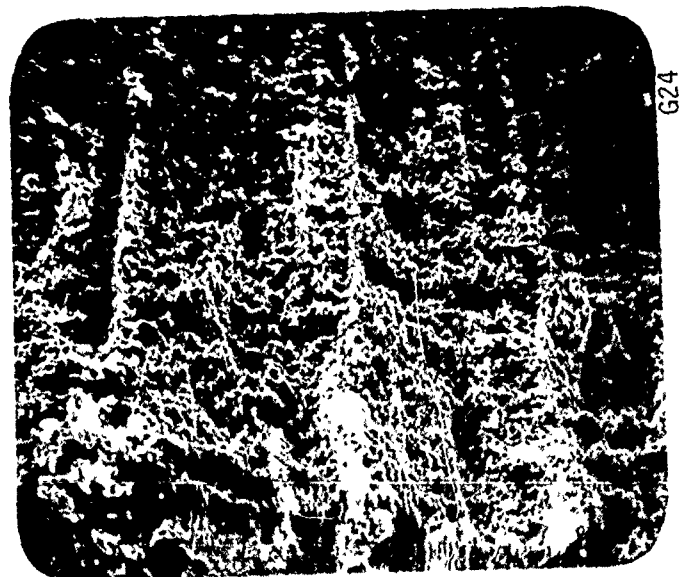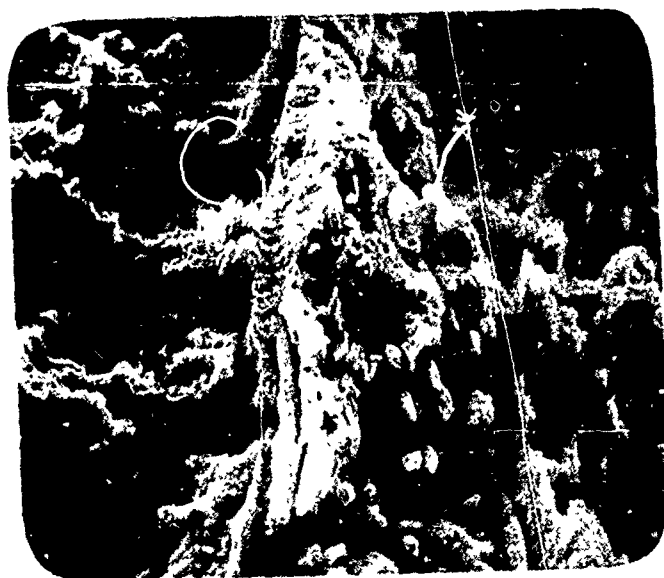
Figure A-25. SEM of Pyrocarb 903 tested in H_2, T_w = 5514°R.
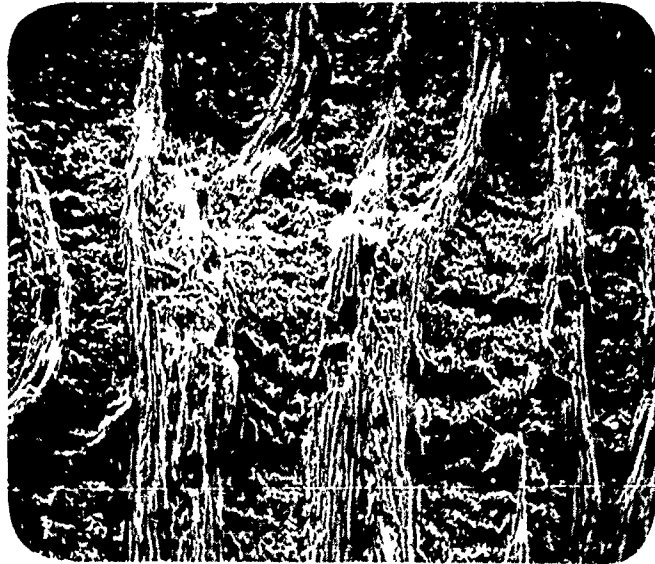
Figure A-26. SEM of Pyrocarb 903 tested in H_2/O_2, $T_w = 5309°R$.
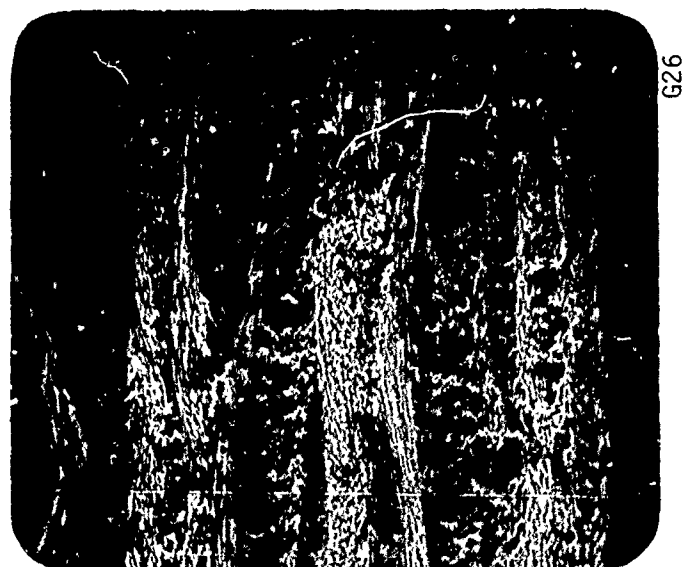
Figure A-27.   SEM of Pyrocarb 903
tested in $H_2/O_2/HC\ell$,
$T_w = 4873°K$.

From the standpoint of microstructure, changes in density for the same material (over the density levels tested) provide no significant alterations. This is determined by comparing Pyrocarb 903 HD (high density) with the Pyrocarb 903 previously discussed. Both were tested in H_2/O_2 environments at similar temperatures. At low magnifications the same roughened, exposed fiber appearance is evident. At high magnifications loss of matrix around filaments is evident for both materials. Somewhat more matrix retention may be present in the "HD" version, and this may be when measured recession rates for the HD version were slightly lower than the standard Pyrocarb 903 version.

The roughened surface, fiber exposure, ply rotations, and matrix removal features were retained with the introduction of HCl into the H_2/O_2 test gas. It should be noted that the depth of recession between yarns is somewhat less for this case than for H_2/O_2 only, which is in accordance with the lower recession rate reported.

Pyrocarb 901 showed the same general trends. The reported recession rates in all test environments were higher for this material than for Pyrocarb 903. It should be noted, however, for Pyrocarb 901, definite fiber exposure and ply exposure was observed in the hydrogen test environment. Introduction of oxygen resulted in severe removal of the exposed yarns. This removal is evidenced by a "smoothing" of the rayon based yarns.

Examination of the high magnification views of Pyrocarb 901 in both H_2 and H_2/O_2 is somewhat less informative. Here, matrix was retained intermixed with the fibers in both environments.

A.2.3 Thermal Expansion Coefficients

Materials and specimens on which thermal expansion coefficients were determined are summarized in Table A-5. The specimens have been divided into the following three material classes:

- Carbon/carbon (c/c)

- Pyrolytic graphite (PG)

- Bulk graphite

Except as noted below, all the specimens listed in Table A-5 were machined out of discs of approximately 2-1/4-inch diameter and 1/4 inch thickness. The blackened portion of sketches drawn in Column 7 of Table A-5 shows the location of specimen within the disc and the specimen shape as it was submitted for testing. Specimen L-1 was machined out of a G-90 billet and its location in the billet is shown in Figure A-28.

In the following discussion, c direction refers to the cross-ply direction and a-b to the with-ply direction.

TABLE A-5. TEST MATERIALS

No.	Sample ID	Material		Class	Density (g/c/c)	Specimen Made From ↓	Specimen Location and Shape
		No.	Name				
1	R-1	26	HRX 5125 (Haveg)	c/c	1.86	Disc	☺
2	L-2	34	MDAC 3-D	c/c		Disc	☺
3	L-3	26	HRX 5875	c/c	1.86	Disc	☺
4	D-8	28	Pyrocarb 901 (Hitco)	c/c	1.80	Disc	◉
5	D-9	28	Pyrocarb 903	c/c	1.84	Disc	◉
6	D-10	26	HRX 5125 (Haveg)	c/c		Disc	◉
7	D-3	12	Supertemp PG	PG		Disc	◉
8	J-7	28	Hitco PG	PG		Disc	☺
9	L-1	41	G-90	Bulk Graphite		Billet G-90 (Figure 1)	

Figure 28. Cutting diagram for G-90 samples.

185
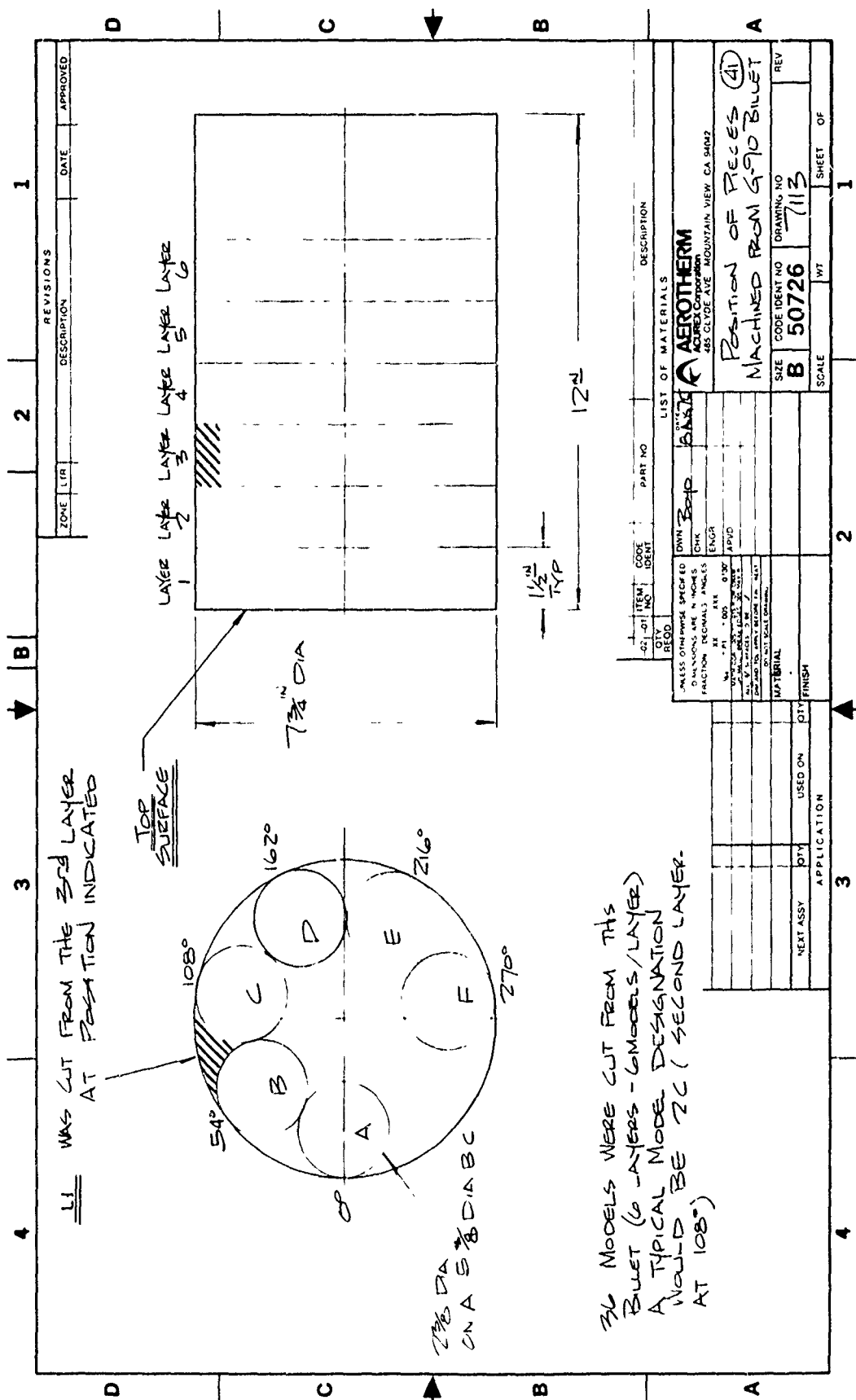
Carbon/Carbon Materials

Thermal expansion data as a function of temperature for two-dimensionally reinforced carbon/carbon materials tested is summarized in Figure A-29. Thermal expansion is lower in the a-b direction, which is a result of carbon fibers not expanding as much as the matrix material. In the c-direction at a temperature of 1800°F, the highest value of thermal expansion is 9.4×10^{-3} inch/inch for the Pyrocarb 903 material. The corresponding lowest value is 7.1×10^{-3} inch/inch for HRX 5125.

In the a-b direction at a temperature of 1800°F, the highest value is 3.2×10^{-3} inch/inch for HRX 5125 and the corresponding lowest value is 0.02×10^{-3} inch/inch for HRX 5875. The increase in the thermal expansion values is approximately linear with temperatures over the temperature range shown.

Thermal expansion data for the single 3-D c/c material is shown in Figure A-30. As expected, the values of thermal expansion in the z-direction are considerably lower than those in the x- or y-direction since the z-direction has a higher volume of c/c fibers. There is a nonlinear relationship between the thermal expansion and temperature at higher temperatures for this material.

Vapor Deposited Carbons

For pyrolytic graphite, the thermal expansion values are much higher in the c direction than in the a-b direction. This is shown in Figure A-31. Both specimens (Hitco a-b PG and Supertemp PG) exhibit similar thermal expansion characteristics in their respective c and a-b directions. However, the increase in the thermal expansion values with temperature in the c direction is much greater than that in the a-b direction. The increase in the a-b direction expansion values becomes nonlinear with temperatures above about 3600°F.

Bulk Graphites

The only thermal expansion measurements of bulk graphites were for G-90. These results are shown in Figure A-32. Some anisotropy in this material is reflected in the two different curves. This is a result of the preferential grain orientation induced by processing forces.

A.2.4 Ion Microprobe Mass Analysis (IMMA)

IMMA data was obtained for representative materials in pre-test and post-test states. Post-test samples were selected on a basis of the measured surface temperature and exposure gas. Ideally these conditions would be representative of those found in rocket nozzles, however, these conditions
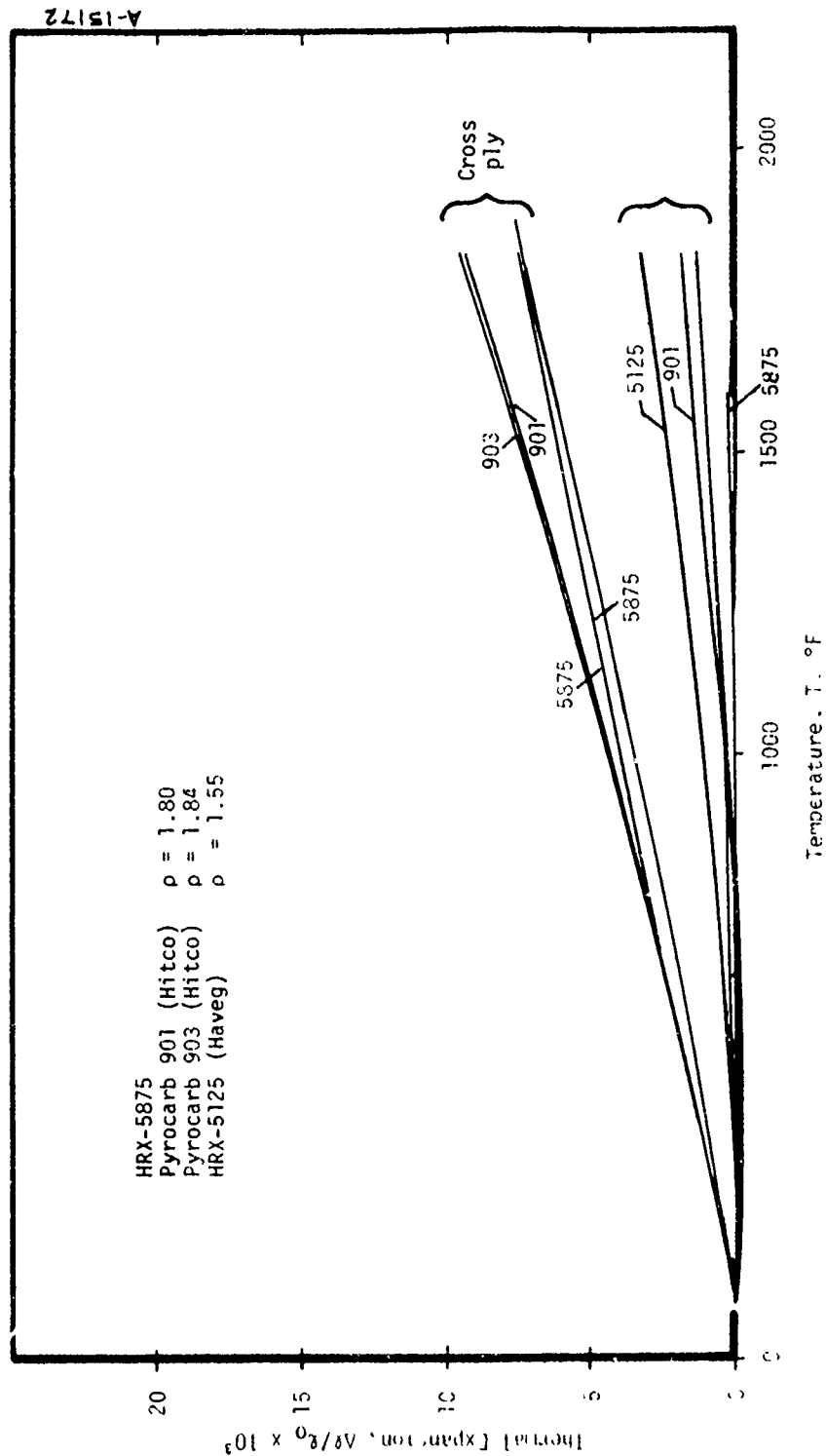
Figure A-29. Thermal expansion for 2-D carbon/carbons.
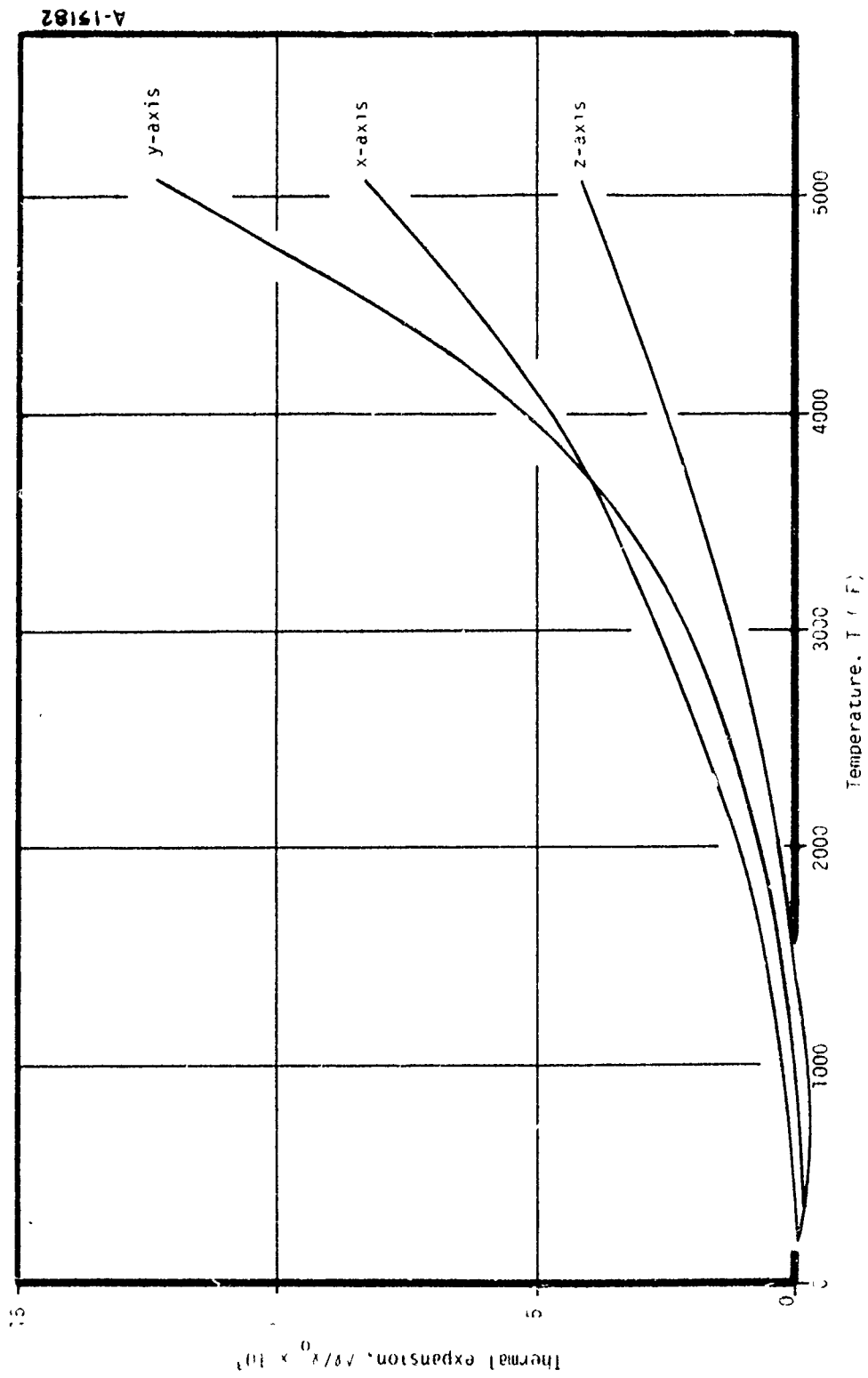
Figure A-30. Thermal expansion for MDAC 3-D carbon/carbons.
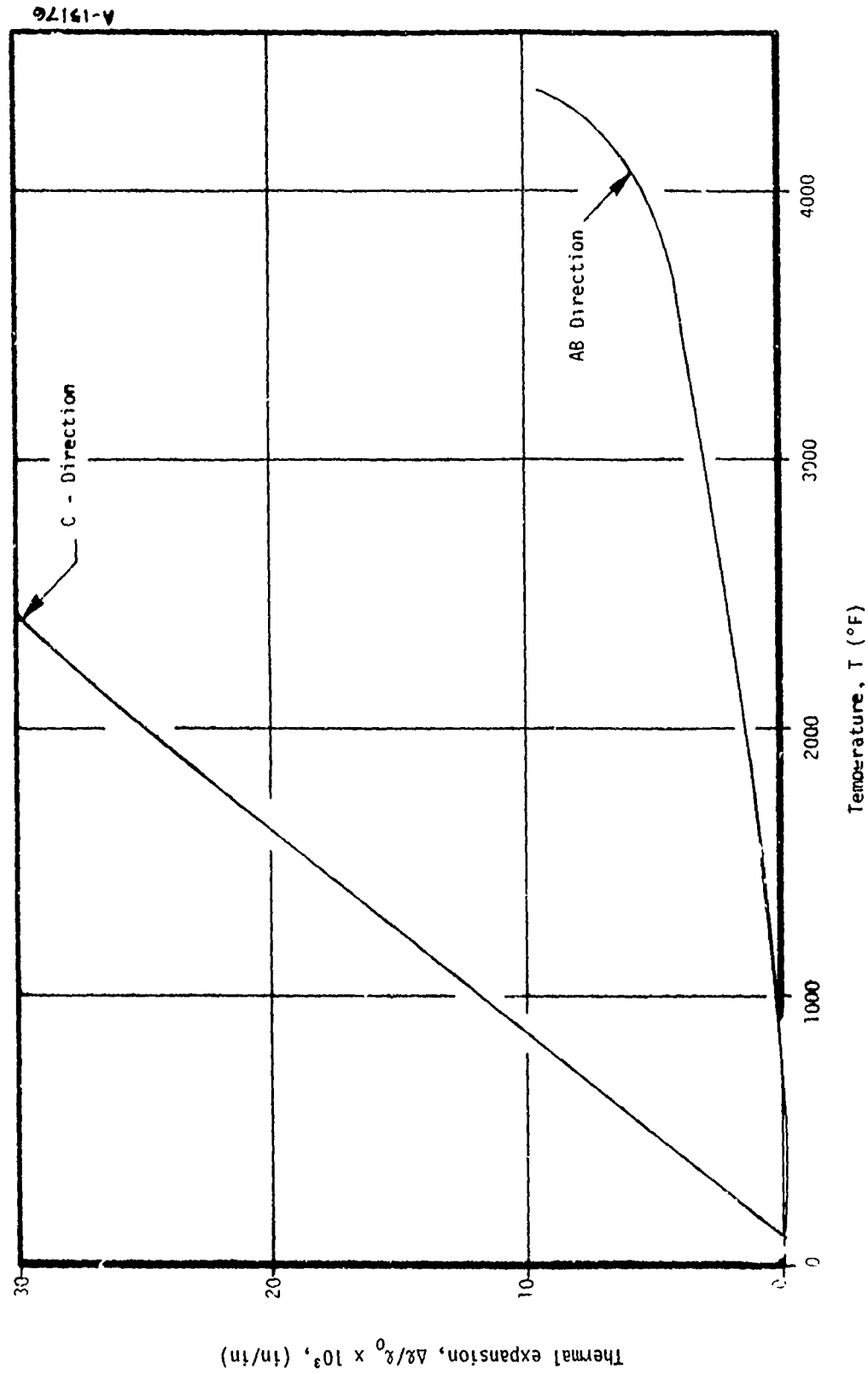
Figure A-31. Thermal expansion of pyrolytic graphite, Supertemp and Hitco.
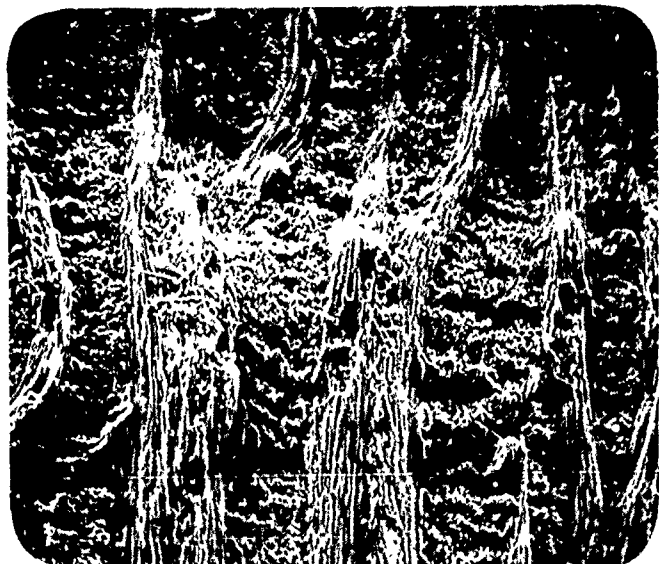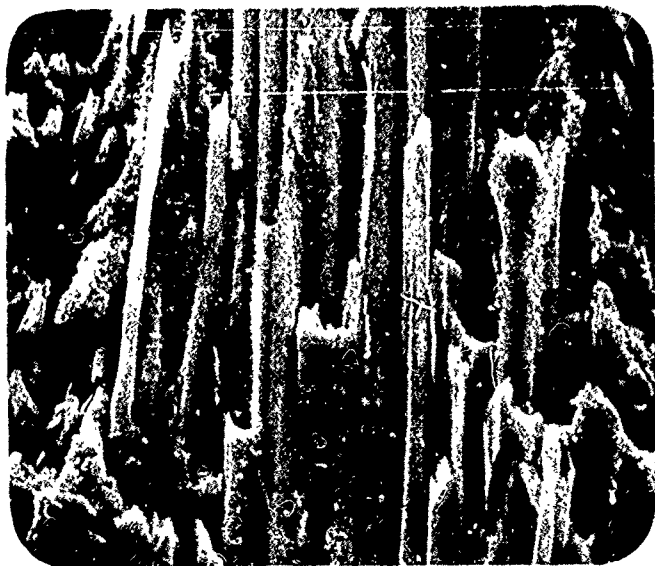
Figure A-26.   SEM of Pyrocarb 903 tested
                in H_2/O_2, T_w = 5309°R.
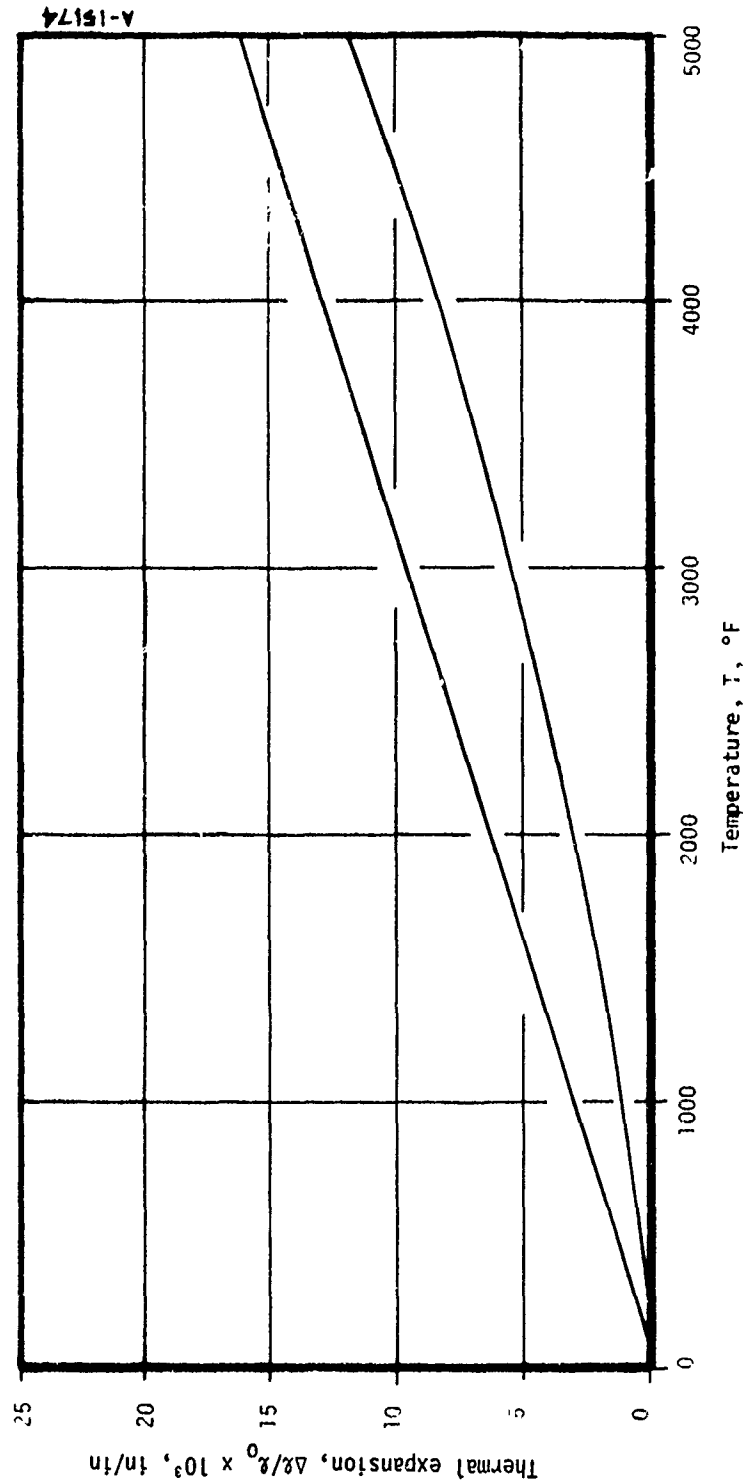
Figure A-32. Thermal expansion of G-90 bulk graphites.

A-15174

could not be duplicated in the APG. The IMMA post-test samples were therefore selected as a compromise between test gas and high surface temperatures. Identification information on the selected IMMA samples is shown in Table A-6.

IMMA scans were made for both positive and negative ions. Typical surface scans are shown in Figures A-33 and A-34. Since only the molecular weight of molecules are shown, it is not always possible to unequivically identify the molecule. For instance, a molecular weight at 28 may be a molecule of N_2, CO, or Si. In addition, the concentration of each surface species can not be determined from the IMMA data. Thus, the scans are largely qualitative.

Rather than presenting all of the IMMA scans, the dominant lines from each scan were identified and are presented in tabular form in Table A-7. Also shown in this table are possible chemical species that could be represented by each molecular weight. Only molecular weights up to 50 are shown.

Two samples of one of the materials, namely Pyrocarb 901, were scanned to gain an appreciation of the repeatability of the material. These samples were at slightly different reported densities but were presumably otherwise identical. The positive ion scans showed a noticeable difference, which may be attributed to impurities from handling or to material processing. The former appears more likely since most of the differences are from elements of salts which are contained in human perspiration.

Comparisons of post-test surface scans with (1) pre-test scans and (2) post-test subsurface scans show that the surface may contain a large number of hydrocarbon species. These would be natural by-products of the reaction between APG gases and the surface. A known poison species, HCℓ, is observed only in one case, whereas Cℓ is observed in almost all materials. This again may possibly be attributed to sample handling.

From the amount and quality of data taken, no firm conclusions can be reached about the value of the IMMA scans, either in terms of guidance for material development or as aids in interpreting kinetic reaction rates. However, it can be concluded that future samples must be handled much more carefully and the IMMA scans should be conducted very shortly after testing. New procedures should also be used to identify adsorbed species. In addition, future samples should be scanned at a number of positions to reduce the uncertainties of local impurities or contamination.

A.2 5 Porosity

A mercury porosimetry was used to determine pore size, pore size distribution and density of selected materials. Data obtained by the mercury penetration technique includes pore size and

TABLE A-6.   IMMA SAMPLES

Material	Identification	Pre-test	Density gm/cc	Post-test	Exposure Conditions			
					T_W (°R)	Gas	Time (sec)	Recession (in.)
Pyrocarb 901 (J2)	Hitco 919946-2	X	1.72					
Pyrocarb 901 (J1)	Hitco 919950-6	X	1.84					
Pyrocarb 901 (PA4)	Hitco 919951-1		1.83	X	5000	7	36.5	0.0334
Pyrocarb 903 (PA4)	Hitco 919957-3 Aerotherm 7113-134	X	1.84					
MDAC 3-D (C2)		X	2.02					
G-90	Aerotherm 41 Layer 3, 54°/108°	X						
SG-90	Aerotherm 7113-170			X	4850	7	48.5	0.024
15% SiC/PG	ARC 8328-10 003-23							
15% SiC/PG	Aerotherm 7113-116			X	4350	1	54.0	0.024
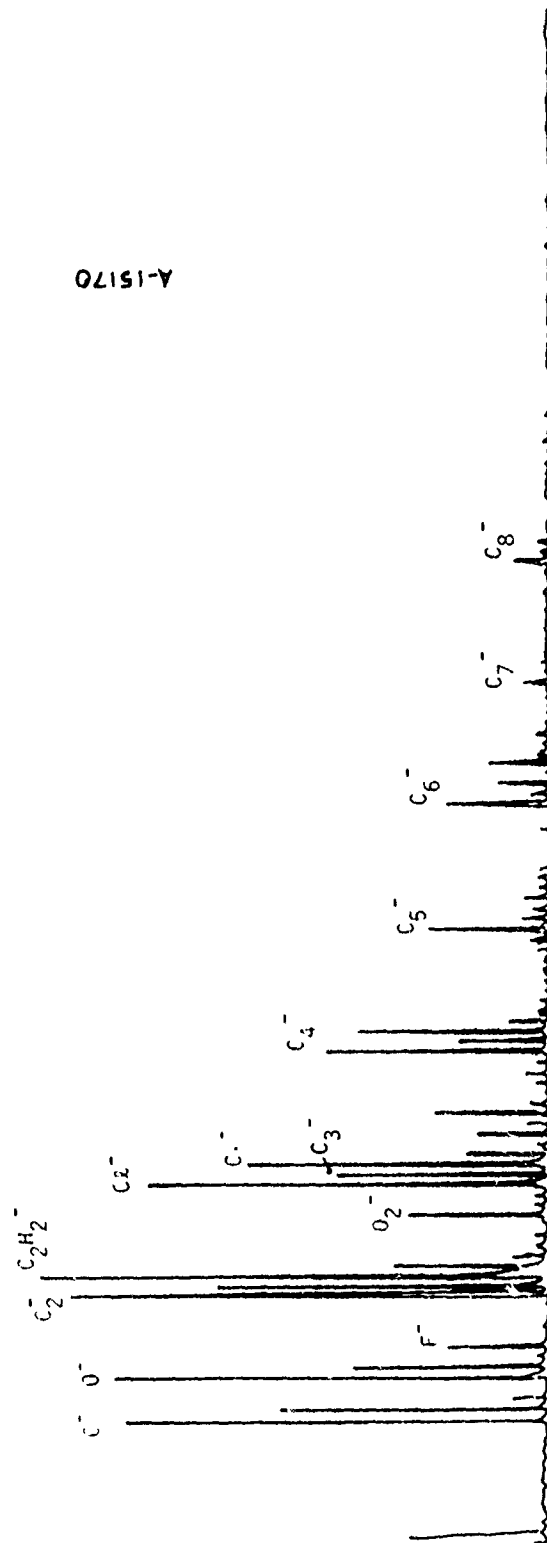
Figure A-33. Typical IMMA scan for post-test Pyrocarb 901 surface, negative ions.
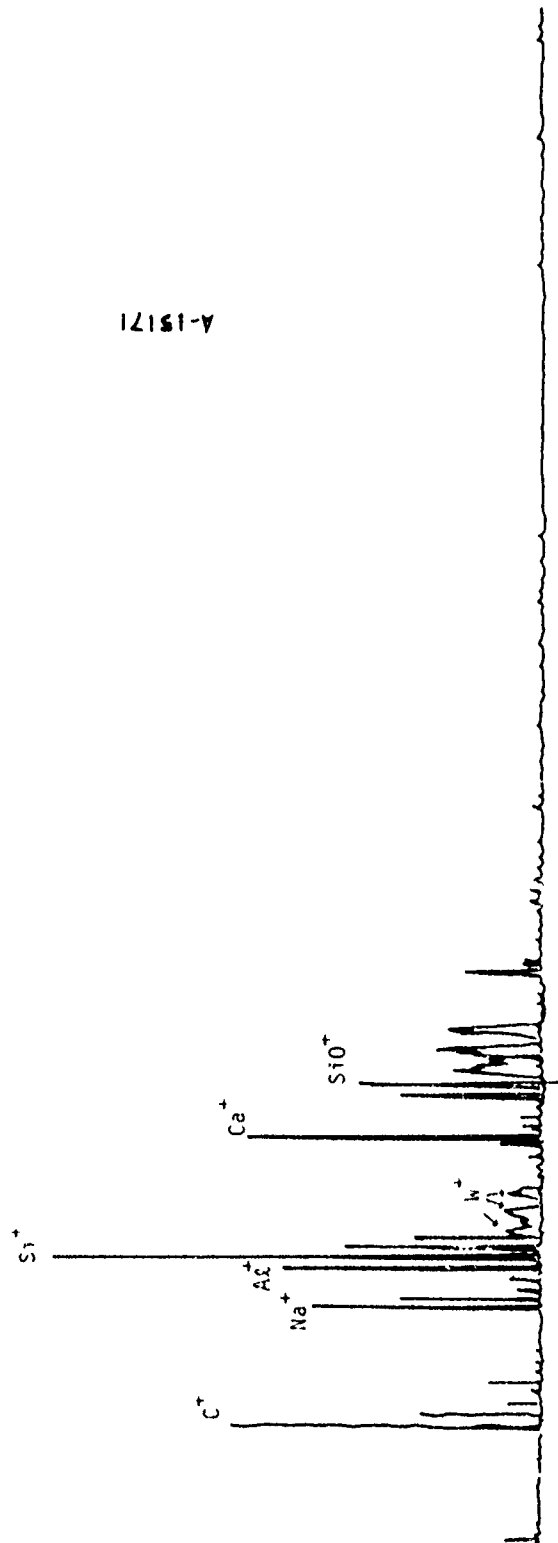
Figure A-34. Typical IMMA scan for post-test Pyrocarb 901 surface, positive ions.

TABLE A-7. RESULTS OF IMMA SCANS

Line No.	Material	Pre	Post	Ion Scan	Location
1	901	X		+	SURF
2	901	X		–	SURF
3	901	X		+	SURF
4	901	X		–	SURF
5	901		X	+	SURF
6	901		X	–	SURF
7	901		X	+	SUB
8	903	X		+	SURF
9	903	X		–	SURF
10	MDAC	X		+	SURF
11	MDAC	X		–	SURF
12	MDAC		X	+	SURF
13	MDAC		X	–	SURF
14	MDAC		X	+	SUB
15	G-90	X		+	SURF
16	G-90	X		–	SURF
17	G-90		X	+	SURF
18	G-90		X	–	SUB
19	G-90		X	+	SUB
20	16% SiC	X		+	SURF
21	16% SiC	X		–	SURF
22	16% SiC		X	+	SURF
23	16% SiC	X		–	SURF
24	16% SiC		X	+	SUB

Atomic Weight scale (15–50) with species labels:
C; CH; O, CH_4; OH; H_2O; F; HF; Na; C_2; C_2H; CN; C_2H_2, HCN; Ar, HCN; N_2, CO, Si; NO; O_2, S; C_2; HC_2; C_3H; C_2N; K; SiC; CNO; CO_2, SiO; NO_2; Ti

volume. Density is calculated from the results obtained. These data are determined by measuring the quantity of mercury which can be forced into the pores of the test material at various increasing pressures. Evidence of pore shape is obtained by determining the amount of mercury expelled from the pores at various decreasing pressures.

The theoretical basis for the mercury penetration method is negative capillary action: this effect results from the nonwetting nature of mercury. Since mercury exhibits a contact angle of greater than 90° with most materials, it will not penetrate pore openings in a material unless forced by an applied pressure. Mercury will then penetrate the pores in accordance with the force applied and the size of the openings.

The relationship describing penetration of mercury into circular openings under pressure is:

$$PD = -4\sigma \cos \Theta \qquad\qquad\qquad (A-1)$$

where:

P = applied pressure

D = diameter of smallest pore, filled at pressure P

σ = surface tension of mercury

Θ = contact angle or wetting angle

Reported measurements of contact angle between mercury and a large number of materials range from about 112° to 142°, with a contact angle of 130° as the most frequent value. Accordingly, taking Θ = 130° and surface tensin of mercury σ = 474 dynes/cm (vacuum, 25°C), the following relationship is obtained for cylindrical pores:

$$PD = 177 \qquad\qquad\qquad (A-2)$$

where pressure P is in psia and diameter D is in microns.

As the pressure is increased, the amount of liquid mercury forced into the pores increases. From Equation (A-2), the diameter of the pore is obtained for that particular pressure. The volume of mercury forced into a pore is a direct function of the volume of the pore. Thus a penetration-volume versus applied-pressure curve can be drawn and analyzed for particle size. Material density can be calculated with pores larger than any limiting size excluded.

Table A-8 lists the measured physical properties of different materials by material state, i.e., virgin, backface or fired. The virgin state refers to the as-received material, the fired state refers to the fired surface, and the backface state refers to the material a small distance below the fired surface. Within a state, the materials are divided into three groups by material class. These three groups are:

1. Bulk graphite

2. Carbon/carbon (c/c)

3. Pyrolytic graphite (PG)

In order to make a comparison between different material classes at various material states, average material properties are plotted in Figures A-35 through A-37.

In preparing these figures, only those materials for which data was available in all three states were utilized.

Density values of the virgin state are greater than those at the fired state as seen in Figure A-35. As expected, the porosity values show just the reverse behavior as seen in Figure A-36. As observed in Figure A-2, while the total porosity of c/c materials is greater than the others, its open porosity is smaller than that for bulk graphite.

Figure A-37 presents the average specific open pore volume by material class for various materials conditions. The shapes of the curves are similar to those of the open porosity curves. Data for pyrolytic graphite is insufficient to draw any convincing conclusions regarding the properties behavior.

Figures A-38 through A-40 show typical pore size spectrums for selected materials. There was no consistent pore size occurrence within a given material class for a given material state. For example, the pore size distribution for G-90 shows that about 22 percent of the pores fall in the diameter range from 0.069 to 0.035 microns. The remaining porosity is scattered around it from 3.43 to 0.013 microns. On the other hand, for ATJ-S about 15 percent of the pores range from 4.66 to 3.42 microns in diameter, about 13 percent range from 0.023 to 0.018 micron in diameter and others are scattered around these intervals from 17.0 to 0.013 microns in diameter.

Except for a few exceptions, it can be said that the majority of the pores lie in the range of about 17 to 0.013 microns in diameter regardless of material class or state. A shift, however, towards smaller pore diameters with progression from virgin to backface/fired conditions was observed.

Material	Acurex Code	Bulk Density g/cc	Open Porosity Percent	Total Porosity Percent	Open Porosity as Percent Total Porosity	Specific Open Pore Volume cc/g
Carbitex 700	—	1.494	19.53	33.60	43.24	0.098
P901 – Backface	PA4	1.734	7.77	22.93	33.89	0.045
– Fired	PA4	1.728	8.76	23.20	37.76	0.051
– Virgin	J2 / J1	1.608 / 1.802	8.17 / 7.26	28.53 / 19.91	28.63 / 36.46	0.351 / 0.040
P903 – Virgin	S1	1.801	10.31	19.96	51.65	0.057
– Backface	PB5	1.858	10.05	17.42	57.68	0.052
– Fired	PB5	1.767	10.00	21.46	46.60	0.057
P903 HD – Virgin	S3	1.815	11.10	11.33	57.49	0.061
– Backface	PB13	1.787	11.18	20.58	54.33	0.063
– Fired	PB13	1.779	11.62	20.93	55.51	0.065
HRX 5125 – Virgin	S2	1.492	12.70	33.69	37.70	0.085
– Backface	PB7	1.510	11.70	32.89	35.57	0.078
– Fired	PB7	1.478	12.39	34.31	36.11	0.084
HRX 5875 – Backface	PB8	1.762	9.83	21.69	45.32	0.056
– Fired	PB8	1.681	11.48	25.29	45.40	0.068
– Virgin	L3	1.683	13.11	25.20	52.02	0.078
Nonprime HRX 5875 – Virgin	R1	1.622	14.32	27.91	51.31	0.088
MDAC 3-D – Virgin	L2	1.975	6.93	12.24	56.62	0.035
– Backface	PB6	1.943	7.70	13.64	56.45	0.040
– Fired	PB6	1.864	7.45	17.16	45.40	0.040
ATJ – Backface	PA2	1.702	17.11	24.33	70.29	0.100
– Fired	PA2	1.679	18.14	25.38	71.48	0.108
ATJ-S – Backface	PB1	1.826	14.31	18.84	75.96	0.078
– Fired	PB1	1.773	13.51	21.20	63.73	0.076
– Virgin	A4	1.814	13.74	19.38	70.91	0.076
G-90 – Virgin	L1	1.899	10.93	15.60	70.06	0.058
– Backface	PA3	1.864	12.51	17.15	72.92	0.067
– Fired	PA3	1.809	15.47	19.60	78.93	0.086
PG(c) – Virgin	H9	2.131	1.029	5.29	19.28	0.005
Planar 15% SiC/PG – Fired	PA1	2.124	0.079	—	—	0.004
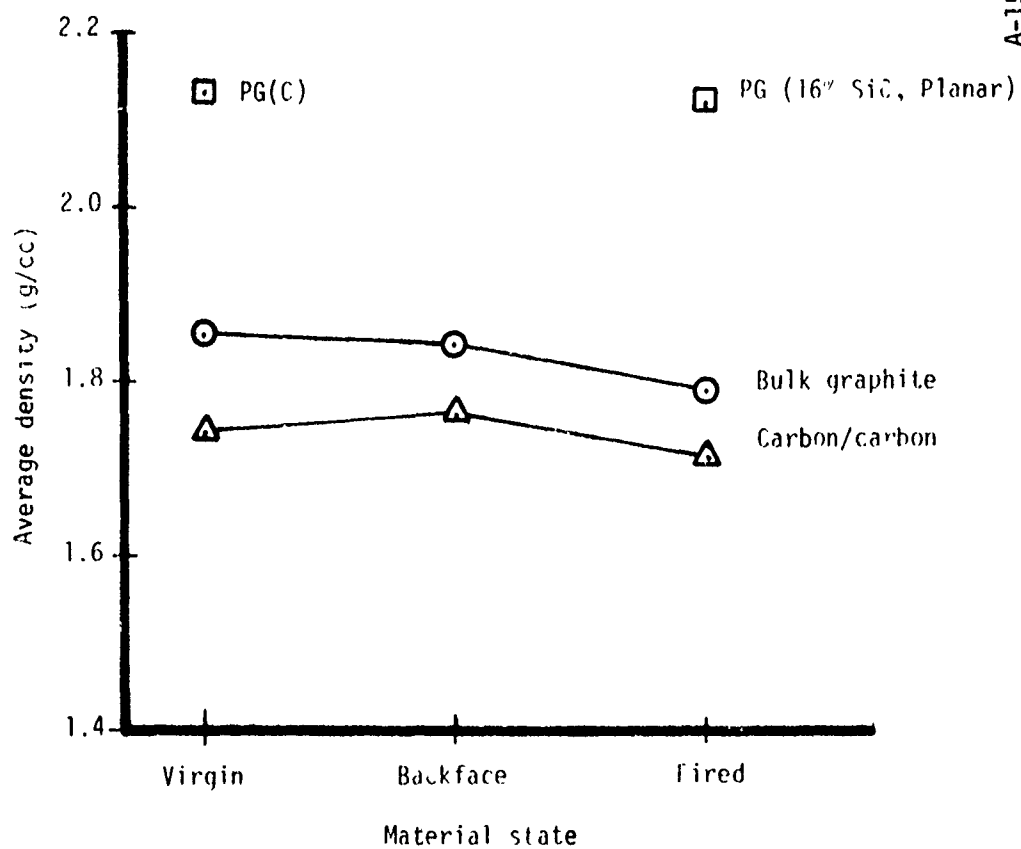
Figure A-35.   Average density of specimen materials at different material states.
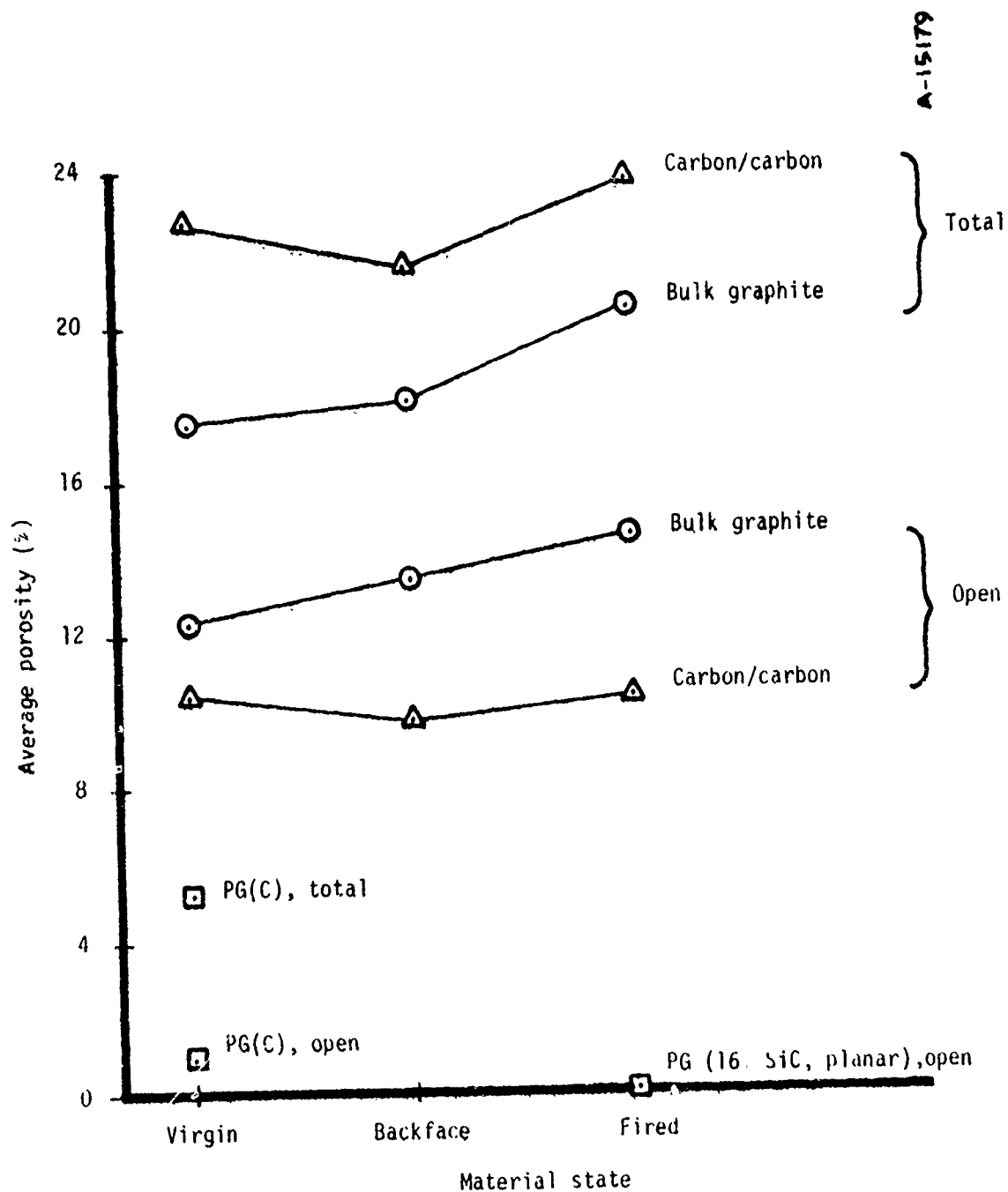
Figure A-36. Average open and total porosity by material class at different material states.
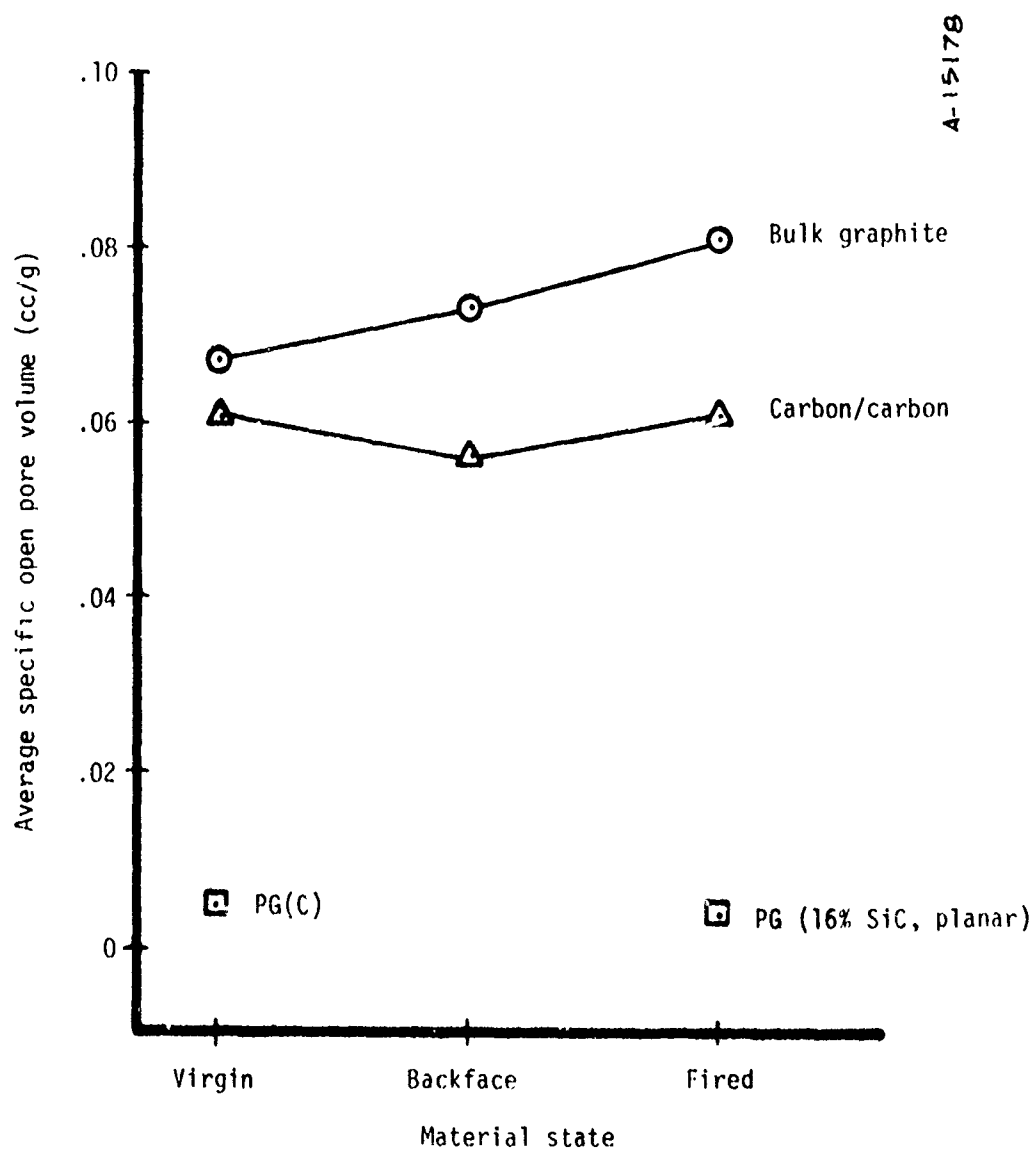
Figure A-37. Average specific open pore volume by material class at different material states.
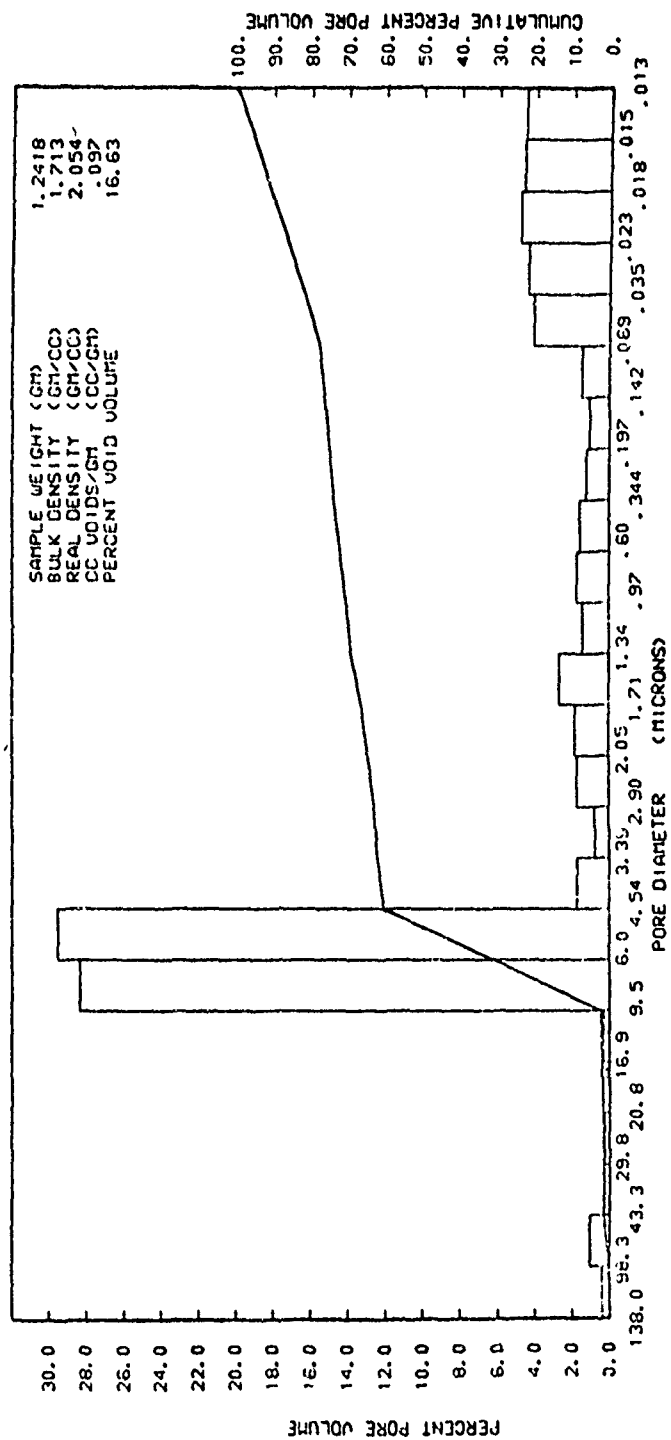
Figure A-38. Typical pore size distribution, ATJ bulk graphites.

SAMPLE WEIGHT (GM) 1.2418
BULK DENSITY (GM/CC) 1.713
REAL DENSITY (GM/CC) 2.054
CC VOIDS/GM (CC/GM) .097
PERCENT VOID VOLUME 16.63
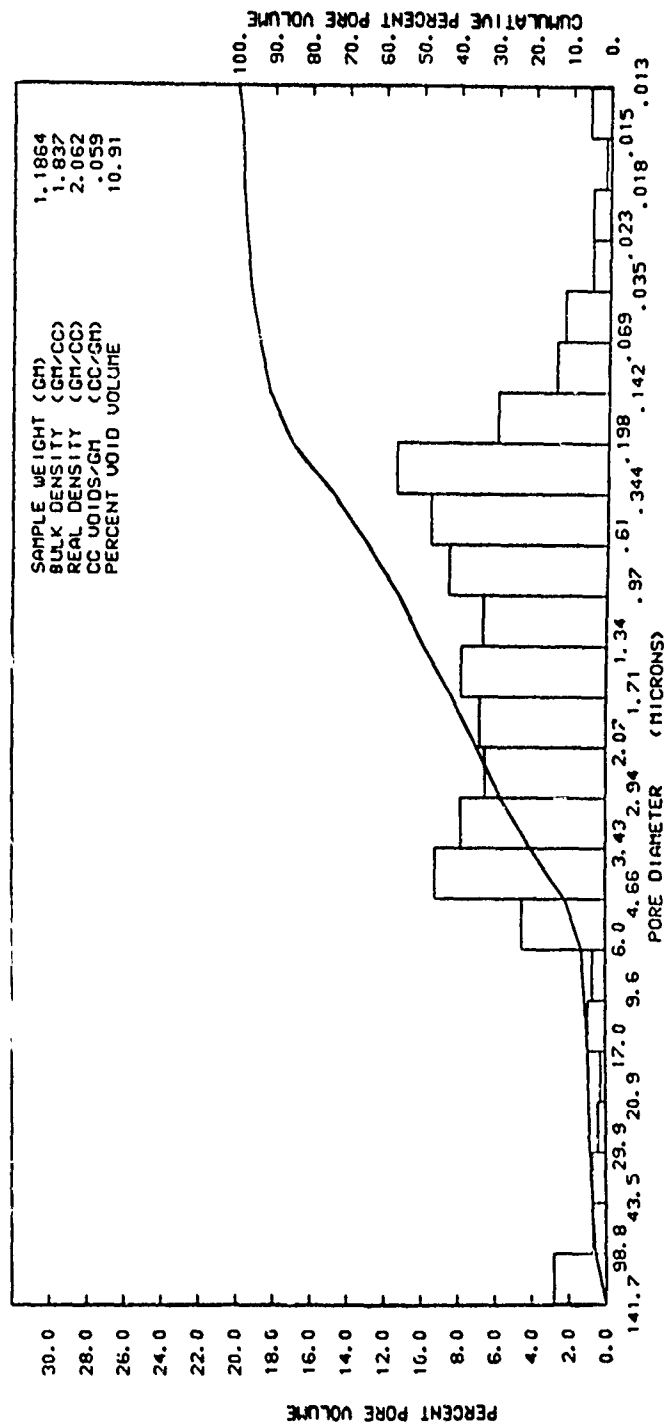
Figure A-39. Typical pore size distribution, high density pyrocarb 903.
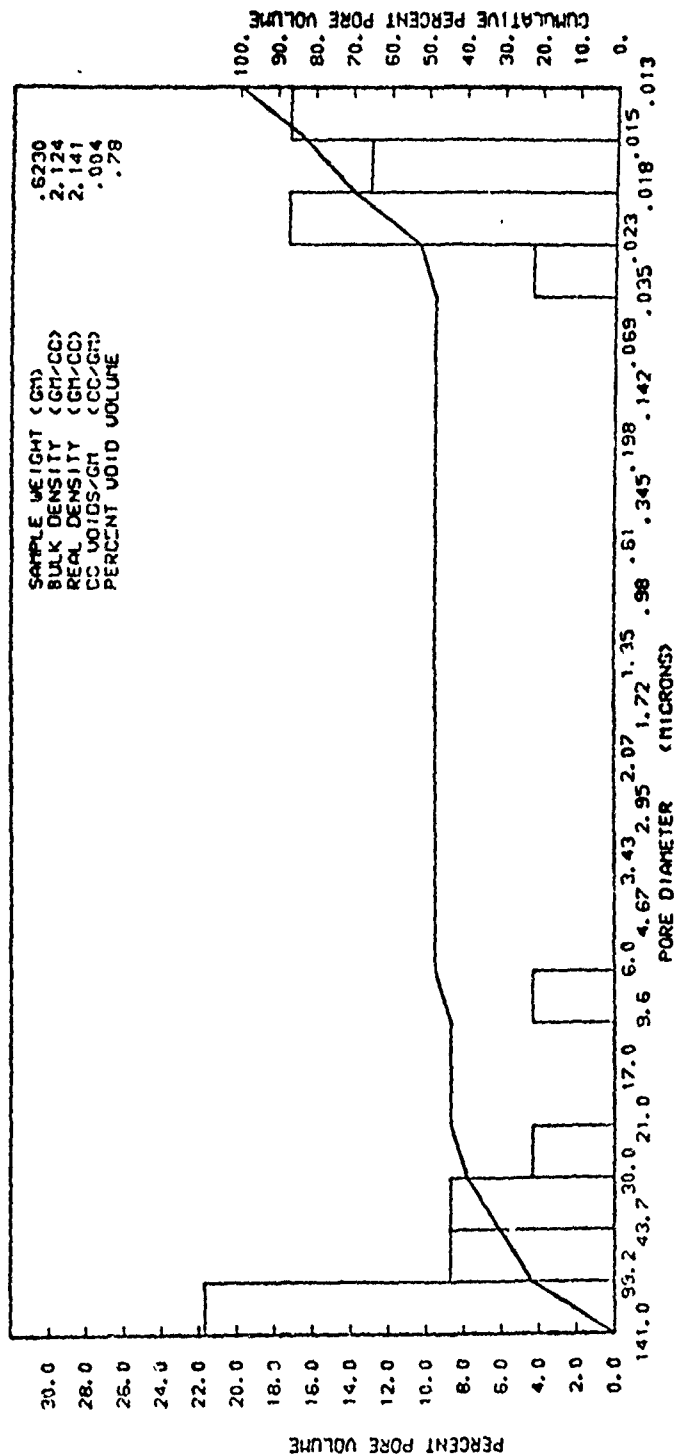
Figure A-40. Typical pore size distribution, 15% SiC/PG

Limited data was developed for vapor deposited carbons, but it was observed that the pore structure was radically different compared to bulk graphites or carbon/carbons.

REFERENCE FOR APPENDIX A

A-1. Hughes, M. C., et al., "Codeposited PG/SiC Nozzle Liners for Advanced ICBM Systems Vol. I Deposition Process Development," AFRPL-TR-74-15, April 1974.

APPENDIX B

GRAPHITIC MATERIALS THERMOPHYSICAL PROPERTIES

B.1 INTRODUCTION

There are many graphitic type materials typically used in the construction of solid propellant rocket motor nozzles. It is important that the thermal properties of these various materials be adequately established and generally accepted for meaningful and consistent predictions of thermal response of rocket motor nozzles. The purpose of this appendix is to provide a collection or recommended property values for selected types of graphitic materials. The properties collected are those that are relevant to the prediction of thermal response, i.e., specific heat, thermal conductivity, density, heat of formation and emissivity. For each type of material the following information is provided.

- List of manufacturers

- Manufacturers suggested property values

- Uncertainties in property values

- Sensitivity of thermal response to uncertainties in property values

- Recommended property values

This appendix is organized so that additional types of materials or new materials within an already included type may be easily added.

The recommended property values result from a consideration of the sensitivity of the thermal response to an assumed uncertainty in material properties. This sensitivity analysis was performed for the nozzle throat insert of an MX nozzle using ablation rate as the principal criteria. Since flow conditions in other regions of the nozzle are significantly different, the conclusions on throat response sensitivity do not necessarily apply elsewhere.

Material property uncertainties may arise from:

- Lack of property data

- Errors in property measurements

- Process variations (billet to billet)

- Within-billet variation

The thermal response is characterized by the time variation of:

- Surface temperature

- Surface recession

- Backwall temperature

For the purposes of the sensitivity analysis the environmental conditions were assumed to be:

- HTPB propellant (P_c = 1000 psia, T_c = 6642°R)

- M = 1

- $\rho_e u_e C_H$ = 0.7 - 14 lbm/ft²sec

- C_M/C_H = 0.6 - 0.8

The propellant gas properties and B' versus T maps were calculated by the GASKET code (Reference B-1) using the most appropriate surface kinetic model included in the GASKET code. The thermal response was calculated by the CMA code (Reference B-2) for the conditions given below.

- Material thickness equal to 2 inches (unless otherwise noted)

- Insulated backwall

- 40-second exposure

Only the principal results of the sensitivity study are presented in each Section to illustrate the sensitivity of the thermal response to the various properties. General conclusions regarding the thermal response are:

- The thermal response is insensitive to surface emissivity and heat of formation of the particular graphitic material

- The surface temperature is insensitive to values for the specific heat, thermal conductivity and density

- For surface temperatures less than approximately 6500°R*

---

*This requirement arises from limitation of the slope of the B' versus T curve. In the region of large slope, near the sublimation region, the conclusions may not be valid.

208

    — The mass loss rate and surface recession are insensitive to specific heat and thermal conductivity variations

    — The surface recession is directly proportional to density variation

- The backwall temperature is sensitive to variations in specific heat and thermal conductivity

These conclusions are valid for the types of graphitic materials examined and for typical MX nozzle throat conditions. They are not dependent upon the particular surface kinetic model or propellant (for XLDB, PEG/FEFO or HTPB).

Properties to be presented are categorized into four generic classes, namely:

- Bulk graphite

- Carbon/carbon

- Pyrolytic graphite

- Modified pyrolytic graphite

B.2 BULK GRAPHITES

Bulk graphites are in widespread use in nozzle thermal protection systems which operate at high temperatures and pressures. Presented herein are a brief description of the manufacturing process, a list of manufacturers of aerospace grades of bulk graphite, representative thermal properties, and the results of the analysis of the sensitivity of the thermal response to property variation.

B.2.1 Manufacturing Summary

Manufactured graphite, in aerospace grades, is produced in a similar fashion by all manufacturers. A filler, usually petroleum coke, and a binder, coal tar pitch, are mixed and then formed to a shape. This is baked to form amorphous carbon which is graphitized at temperatures ranging from 4000°F to 5500°F. Variations in each step have a significant effect on the properties of the finished product and contribute to the differences observed among the various commercial grades produced. In addition to these standard processes, certain grades of graphite are further densit.ed, either by hot-working finished billets or by multipitch impregnations and regraphitization of the finished billets. These processes produce a material that is quite anisotropic with respect to thermal and structural properties. The highest degree of anisotropy results from extrusion of a coarse grain material; wherease, an isostatically molded, fine grain material can be practically isotropic.

B.2.2 Materials Summary

Manufacturers and materials for which thermal property data are available are shown in Table B-1. Detailed values for thermal conductivity and specific heat are presented in Table B-2 through Table B-11. Figures B-1 through B-3 show these same thermal properties in graphical form. It should be noted that, in many cases, material properties are obtained from tests conducted by independent organizations, such as SoRI, ARC, LMSC, GE, and Aerotherm, rather than the material manufacturer.

The heat of formation for the various bulk graphites is assumed to be zero (the value for elemental carbon). The surface emissivity (total hemispherical) is initially a function of the surface finish; however, once the surface starts ablating all the graphites have essentially the same value, approximately 0.90.

For all the materials investigated it was necessary to estimate probable thermal property variations within one grade (billet to billet variations) and probable variations of properties within one billet of material. There is general agreement that these variations do exist and that they may have an impact on design considerations. No large body of data was found treating this area; however, References B-10 and B-11 offer some insight to the problem. Reference B-11 is a study of ATJ-S graphite and its property variations and is used as a source for the magnitude of variations. Variations in thermal conductivity of ±14 percent with respect to the nominal values are reported for billet to billet variations; variations of specific heat, density, and emissivity were found to be negligible. This reference also considered within-billet variations and found that they do exist, but, from a thermal property standpoint, these were negligible.

B.2.3 Sensitivity Analysis and Recommended Values

The results of the sensitivity analysis for bulk graphite are shown in Table B-12 and are consistent with the general conclusions given in Section B.1. Nominal property values for this sensitivity study were taken as those of ATJ-S. The variations in surface emissivity and specific heat were arbitrarily selected to determine their impact on the thermal response. The variation in density covered the range of values for all the bulk graphites about a nominal value of 1.83 g/cc. The thermal conductivity was allowed to vary by ±14 percent to reflect the reported billet to billet variations. (The error for measurement of thermal conductivity was reported as ±7 percent in Reference B-15.) The nominal values of T_{BW}, T_S, and recession for the with-grain case are shown in Table B-12. The results for the sensitivity, i.e., the percent fluctuation in T_{BW}, T_S, and recession,

TABLE B-1. BULK GRAPHITE MANUFACTURERS

Manufacturer	Product (s) (Density, G/CC)
Carborundum Co.	G-90 (1.90), Graphitite-G (1.88)
Great Lakes Carbon Corp.	H-205-85 (1.81)
Poco Graphite, Inc.	AXF-5Q (1.81)
Pure Carbon	P-03 (1.83)
Speer Carbon	8882-E (1.76)
Union Carbide	ATJ (1.73), ATJ-S (1.83), AGSR (1.55), CS (1.72)

TABLE B-2. THERMAL PROPERTIES ATJ (Reference B-12)

Temperature °R	Specific Heat Btu/lbm-°R	Thermal Conductivity Btu/ft-sec-°R x 10^{-3}	
		W/G	A/G
460	0.283	20.52	15.6
960	.340	16.08	11.76
1460	.390	12.36	9.37
1960	.430	9.67	7.96
2460	.462	7.86	6.29
3450	.505	6.46	5.09
4460	.521	5.78	4.74
5460	.525	5.39	4.56
6460	.525	5.32	4.44

Density = 107.6 lbm/ft^3 = 1.73 g/cc

TABLE B-3.   THERMAL PROPERTIES ATJ-S (Reference B-11)

Temperature °R	Specific Heat Btu/lbm-°R	Thermal Conductivity Btu/ft-sec-°R x 10^{-3}	
		W/G	A/G
460	0.283	25.80	19.56
960	.340	18.72	14.88
1460	.390	14.64	11.55
1960	.430	11.74	9.16
2460	.462	9.70	7.43
3460	.505	7.32	5.00
4460	.521	6.34	4.66
5460	.526	5.35	4.42
6460	.526	5.44	4.16

Density = 114.2 lbm/ft³ = 1.83 g/cc

TABLE B-4. THERMAL PROPERTIES AXF-5 ISOTROPIC (Reference B-12)

Temperature °R	Specific Heat Btu/lbm-°R	Thermal Conductivity Btu/ft-sec-°R x 10^{-3}
460	0.283	19.4
960	.340	15.0
1460	.390	12.48
1960	.430	10.19
2460	.462	8.57
3460	.505	6.59
4460	.521	5.95
5460	.525	5.56
6460	.525	5.56

Density = 113.2 lbm/ft^3 = 1.81 g/cc

TABLE B-5. THERMAL PROPERTIES AGSR (Reference B-12)

Temperature °R	Specific Heat Btu/lbm-°R	Thermal Conductivity Btu/ft-sec-°R x 10^{-3}	
		W/G	A/G
460	0.283	24.48	19.44
960	.340	18.72	15.00
1460	.390	14.28	11.34
1960	.430	11.27	8.90
2460	.462	9.26	7.36
3460	.505	6.95	5.51
4460	.521	6.25	4.86
5460	.525	6.20	4.86
6460	.525	6.20	4.86

Density = 96.77 lbm/ft^3 = 1.55 g/cc

TABLE B-6. THERMAL PROPERTIES CS (Reference B-12)

Temperature °R	Specific Heat Btu/lbm-°R	Thermal Conductivity Btu/ft-sec-°R x 10^{-3}	
		W/G	A/G
460	0.283	25.68	20.40
960	.340	20.88	16.32
1460	.390	16.68	12.96
1960	.430	13.56	10.66
2460	.462	11.17	8.80
3460	.505	8.80	6.94
4460	.521	7.82	6.13
5460	.525	7.40	5.78
6460	.525	7.30	5.78

Density = 107.5 lbm/ft^3 = 1.72 g/cc

TABLE B-7. THERMAL PROPERTIES G-90 (Reference B-12)

Temperature °R	Specific Heat Btu/lbm-°R	Thermal Conductivity Btu/ft-sec-°R x 10^{-3}	
		W/G	A/G
460	0.283	30.60	21.00
960	.340	22.68	16.92
1460	.390	16.68	13.44
1960	.430	12.96	10.76
2460	.462	10.88	9.14
3460	.505	8.10	7.16
4460	.521	7.16	6.36
5460	.525	6.95	6.13
6460	.525	6.95	6.13

Density = 118.5 lbm/ft³ = 1.9 g/cc

TABLE B-8. THERMAL PROPERTIES GRAPHITE "G" (Reference B-13)

Temperature °R	Specific Heat Btu/lbm-°R	Thermal Conductivity Btu/ft-sec-°R x 10^{-3}	
		W/G	A/G
460	0.283	27.72	20.04
960	.340	19.44	13.92
1460	.390	13.32	8.62
1960	.430	9.72	6.11
2460	.462	8.05	5.14
3460	.5^5	5.54	3.32
4460	.521	4.86	2.77
4960	.523	4.86	2.77

Density = 117.5 lbm/ft^3 = 1.88 g/cc

TABLE B-9. THERMAL PROPERTIES H-205-85 (Reference B-13)

Temperature °R	Specific Heat Btu/lbm-°R	Thermal Conductivity Btu/ft-sec-°R x 10^{-3}	
		W/G	A/G
460.	0.283	25.44	24.36
960.	.340	22.56	20.04
1460.	.390	18.24	15.00
1960.	.430	13.56	12.24
2460.	.462	11.33	11.05
2960.	----	9.84	10.68
3460.	.505	9.22	10.55
3960.	----	8.75	10.19
4460.	.521	8.56	9.72

Density = 113.2 lbm/ft^3 = 1.81 g/cc

B-10. THERMAL PROPERTIES P-03-ISOTROPIC (Reference B-13)

Temperature °R	Specific Heat Btu/lbm-°R	Thermal Conductivity Btu/ft-sec-°R x 10^{-3}
1110	0.350	27.768
1460	.390	21.672
1936	.428	14.580
2460	.462	10.692
3460	.505	7.908
4460	.521	7.224
5460	.525	6.948
Density = 114 lbm/ft³ = 1.83 g/cc		

B-11. THERMAL PROPERTIES SPEER 8882-E (Reference B-14)

Temperature °R	Specific Heat Btu/lbm-°R	Thermal Conductivity Btu/ft-sec-°R X 10^{-3}	
		W/G	A/G
460	0.340	53.16	44.04
1460	.390	36.96	25.44
1960	.430	21.00	14.04
2460	.462	12.96	9.80
3460	.505	10.50	9.06
4460	.521	10.50	9.06
6460	.525	10.50	9.06

Density = 109.9 lbm/ft^3 = 1.76 g/cc
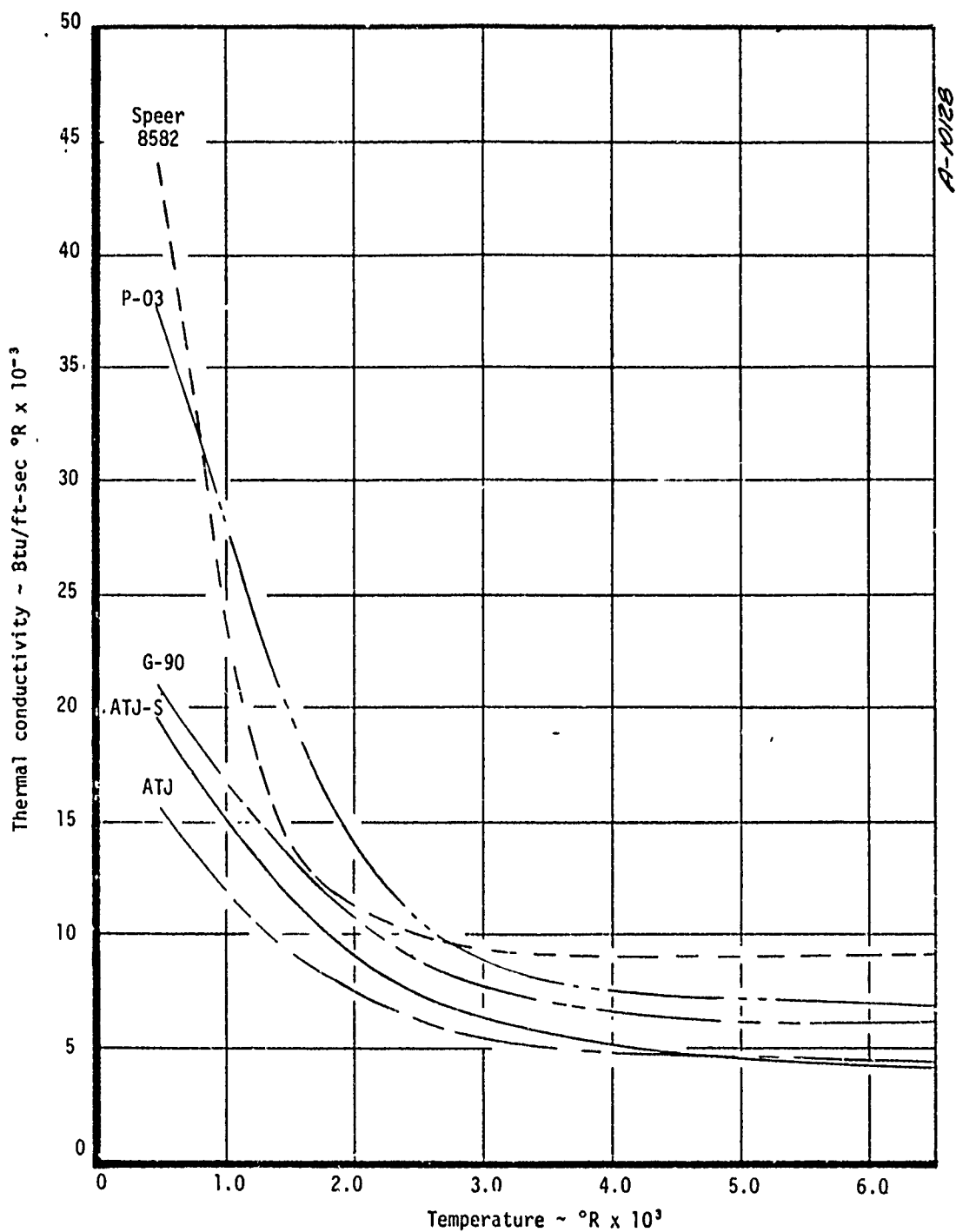
Figure B-1. Thermal conductivity of bulk graphites against grain direction (P-03 is isotropic).
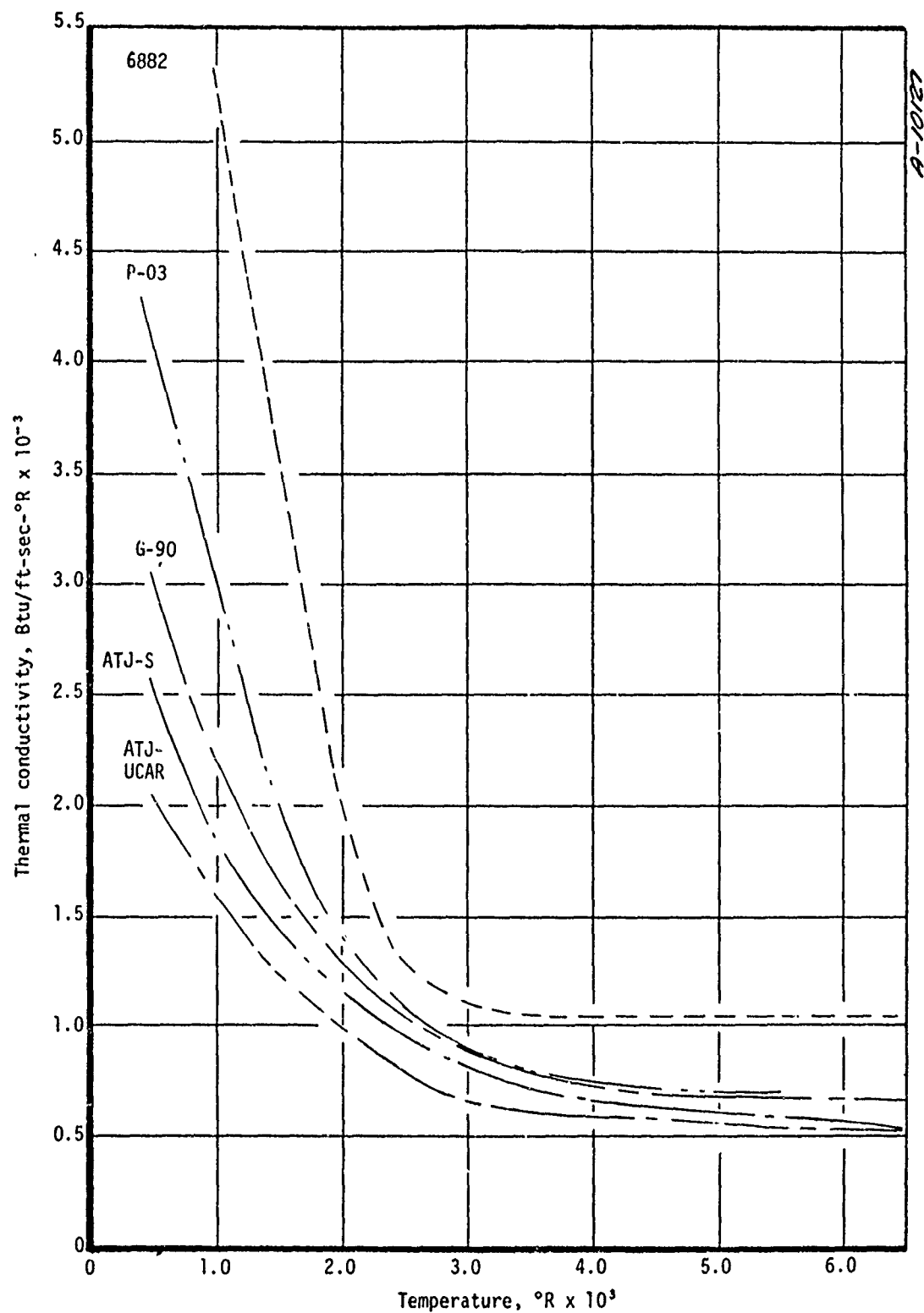
Figure B-2. Thermal conductivity of bulk graphites with grain direction.
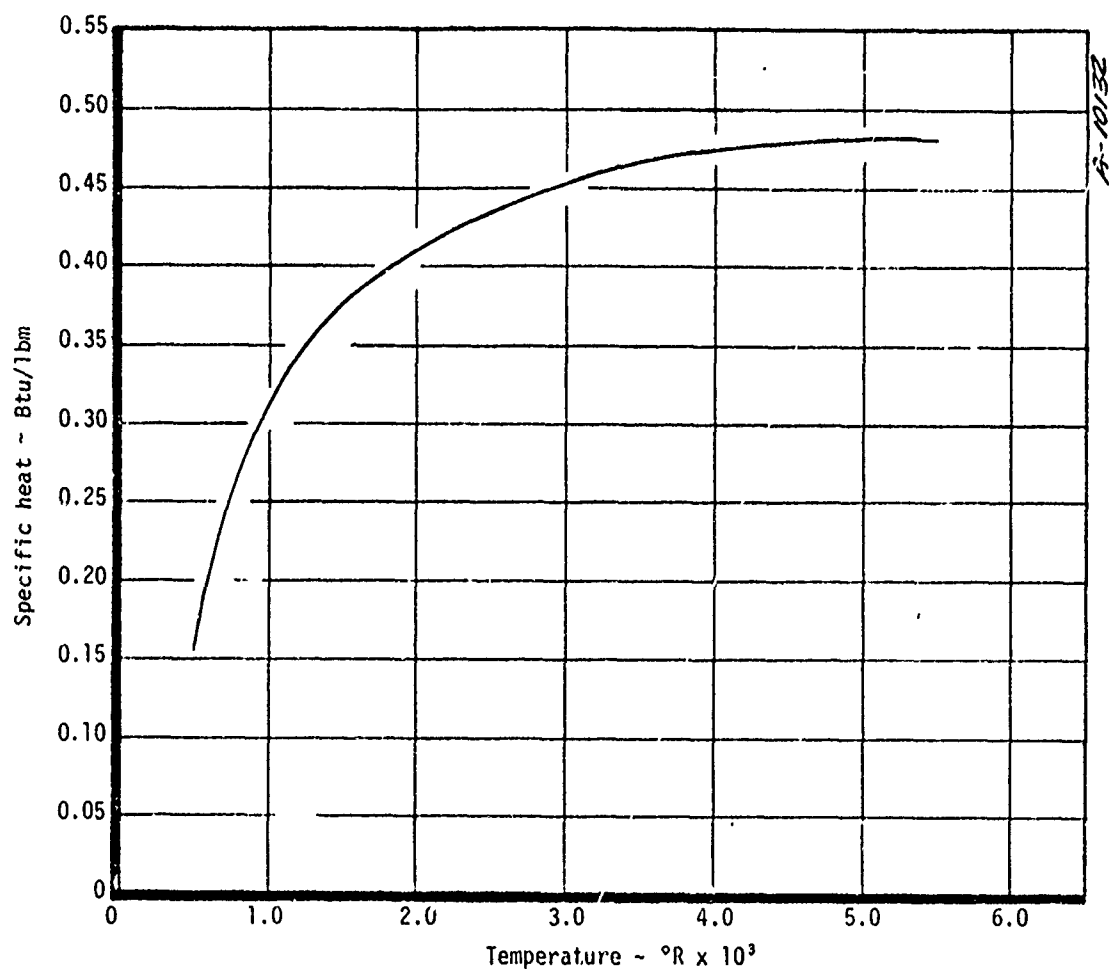
Figure B-3. Specific heat of bulk graphites.

TABLE B-12. EFFECT OF PROPERTY VARIATION ON THERMAL
RESPONSE FOR BULK GRAPHITES

Property	Variation*	T_{BW} (2320°R)	T_s (5490°R)	Recession[†] (.47 in)
ε	$\pm 30\%$	$\pm 4\%$	$\pm 0.5\%$	$\pm 2\%$
ρ	$\pm 10\%$	--	--	$\pm 10\%$
k	$\pm 14\%$	$\pm 7\%$	$\mp 0.1\%$	$\mp 2\%$
C_p	$\pm 10\%$	$\mp 6\%$	$\mp 2\%$	$\mp 1\%$
Worst combination of C_p and k		$\pm 16\%$	$\pm 2\%$	$\pm 3\%$

*ATJ-S selected for nominal values; with-grain results shown in
parenthesis above.

[†]Evaluated at end of 40 seconds.

were the same for both the with grain and against grain values of k. Also, a severe change in the surface kinetic model (from the bulk graphite model to the layer PG model) had very little effect on the sensitivity to property variations. (The sensitivity to the kinetic model itself was not considered in this investigation.)

From the results of the sensitivity analysis and the availability and scatter of materials properties, the following property values are recommended:

- ϵ = 0.9

- h_o = 0.0 Btu/lbm

- C_p - see Figure B-3

- k, ρ = a. Use manufacturers recommended values

              b. Use values for G-90 or ATJ-S as representative values

B.3 CARBON/CARBON COMPOSITES

This section contains a brief description of the manufacturing process, a list of carbon/carbon manufacturers and thermal properties of their products, and the results of a sensitivity study of the thermal response to possible property variations for carbon/carbon composite materials.

B.3.1 Manufacturing Summary

The class of materials known as carbon/carbon composites is a very broad category and there are many variations in material processing. Also, the precise details of these processes are proprietary; so, only a brief and very general description can be given for the processing of carbon composites. (See Reference B-30 for more details on the processing of carbon composites.)

A typical 2-D carbon/carbon composite starts out as a carbon or graphite phenolic, which is densified through a combination of liquid phase impregnation and/or gas phase (Carbon Vapor Deposition, CVD) densification. This material is then carbonized and graphitized or annealed at temperatures in excess of 5000°R. It is not unusual for the carbon composite materials to go through several impregnation or CVD cycles with graphitization or annealing at the appropriate time. The manufacture of 3-D composites is somewhat different, as data from AVCO shows. A preform is first constructed consisting of graphite fabrics pierced with graphite fibers. This preform is impregnated with a phenolic resin; carbonized at ~2460°R and then graphitized at ~5460°R. The great diversity among the carbon composites results from all the possible variations of process cycles and conditions that are possible.

B.3.2 Materials Survey

Table B-13 lists the companies and the products for which thermal properties were made available. Values for the density, specific heat, and thermal conductivity are given in Tables B-14 through B-19 for these materials. This same information is presented graphically in Figures B-4 through B-6 where the differences in thermal conductivity are apparent. The heat of formation can be assumed to be zero and the surface emissivity can be taken as 0.90. It should be noted that these composite materials are not as well characterized as the bulk graphites and that the properties are strongly dependent on the particular processing. The density may even vary significantly for the same material specification, for example, Pyrocarb 901 is given here with $\rho = 1.6$ g/cm^3 whereas a sample of Pyrocarb 901 tested by Aerotherm had $\rho = 1.8$ g/cm^3.

Billet to billet and within billet variations of properties are discussed in Reference B-31 and B-32. The density both within a billet and between billets was found to vary as much as ±5 percent. Thermal conductivity variations can be expected to be ±7 percent due to material variations and experimental error (Reference B-31). The specific heat is not always reported and in some cases must be approximated from values for other carbon/carbon materials.

B.3.3 Sensitivity Analysis and Recommended Values

The significant results of the sensitivity study for the carbon/carbon composites are given in Table B-20. The sensitivity to emissivity and heat of formation are not shown since thermal response was found to be insensitive to either. The property values for Haveg SP8040 were used as nominal values. Variations in C_p and k for this sensitivity study were larger than those used in the graphite studies. This was done for two reasons:

- Property values vary widely for the various materials classed as carbon/carbon composites

- Qualitative results for small variations were evaluated in the bulk graphite section (Section B.2)

The bulk graphite surface kinetic model in GASKET was used since at the time of these studies there were no models for carbon/carbon materials. This is acceptable since the results of the bulk graphite sensitivity study showed that the sensitivity to property variations was not dependent on the surface kinetic model. The results shown in Table B-20 support the general conclusion of Section B.1.

For detailed calculations the manufacturers recommended values should be used. The MOD 3 material is a three-dimensional weave and should not be used as representative of two-dimensional materials. If property values are not known, the SP8040 values can be used as representative. For

TABLE B-13.   CARBON/CARBON COMPOSITE MANUFACTURERS

Manufacturer	Products (Density, g/cc)
AVCO Corp.	MOD-3 (1.61)
Carborundum Co.	Carbitex 700 (1.5)
Haveg Industries, Inc.	FM-5228 (1.51), SP-8040 (1.4)
HITCO	PC-901 (1.6), PC-502-1 (1.2)

TABLE B-14. THERMAL PROPERTIES MOD 3 (Reference B-31)

| Temperature °R | Specific Heat* Btu/lbm-°R | Thermal Conductivity Btu/ft/sec-°R x 10⁻³ | | |
| | | W/P† | | A/P |
		x	y	z
960	.31	12.0	13.92	8.323
1460	.37	10.19	11.11	6.95
1960	.43	8.10	9.14	5.90
2460	.46	6.83	7.4	5.09
2960	.51	6.02	6.3	4.61
3460	.53	5.38	5.724	4.16
4460		4.56	4.74	3.82
5460	.53	4.28	4.28	3.72
Density = 100.51 lbm/ft³ = 1.61 g/cc				

*Estimated

†The thermal conductivity in the 45° x-y direction was also reported in Reference B-30 and is different from the above values.

TABLE B-15.   THERMAL PROPERTIES PYROCARB 901 (Reference B-32)

Temperature °R	Specific Heat* Btu/lbm-°R	Thermal Conductivity Btu/ft-sec-°R x 10^{-3}	
		W/P	A/P
460	0.18	7.22	1.92
640	0.21	8.75	2.56
960	0.31	7.75	2.21
1460	0.37	6.25	1.85
1960	0.43	5.48	1.64
2960	0.46	4.87	1.52
3960	0.51	4.76	1.55
4960	0.53	5.03	1.74
5460	0.53	5.33	1.94
Density = 100.51 lbm/ft^3 = 1.6 g/cc			

*Estimated

TABLE B-16. THERMAL PROPERTIES C/C 700 (Reference B-30)

Temperature °R	Specific Heat Btu/lbm	Thermal Conductivity Btu/ft-sec °R x 10^{-3}	
		W/P	A/P
530	0.18	15.0	5.62
960	0.31	9.5	3.70
1960	0.43	5.9	2.67
2460	0.46	5.66	2.08
2960	0.48	5.55	1.86
3460	0.49	5.75	1.97
3960	0.51	5.75	2.92
4460	0.51	6.50	2.77
5460	0.53	7.30	3.54
5960	0.53	7.85	3.85
Density = 93.5 lbm/ft^3 = 1.5 g/cc			

TABLE B-17. THERMAL PROPERTIES SP-8040 (Reference B-32)

Temperature °R	Specific Heat Btu/lbm-°R	Thermal Conductivity Btu/ft-sec-°R x 10^{-3}	
		W/P	A/P
530	0.245	5.30	2.50
800	0.260	5.75	2.95
1100	0.335	6.30	3.20
1500	0.450	7.60	3.40
2000	0.570	7.95	3.20
2500	0.580	7.85	2.80
3000	0.580	7.60	2.60
3500	0.580	7.40	2.70
4000	0.580	7.40	2.90
4500	0.580	7.70	3.3C
5500	0.580	9.30	4.90
Density = 87.0 lbm/ft³ = 1.4 g/cc			

TABLE B-18. THERMAL PROPERTIES PYROCARB 502-1 (Reference B-32)

Temperature °R	Specific Heat Btu/1bm-°R	Thermal Conductivity Btu/ft-sec-°R x 10^{-3}	
		W/P	A/P
530	0.240	3.10	1.50
800	0.275	3.70	1.52
1100	0.340	4.30	1.55
1500	0.415	6.10	1.90
2000	0.540	6.35	2.20
2500	0.540	5.75	2.00
3000	0.540	4.90	1.90
3500	0.540	5.40	2.40
4000	0.540	6.30	3.00
4500	0.540	7.35	4.15
5500	0.540	9.75	7.60
Density = 74.5 1bm/ft³ = 1.2 g/cc			

TABLE B-19. THERMAL PROPERTIES FM-5228 (Reference B-32)

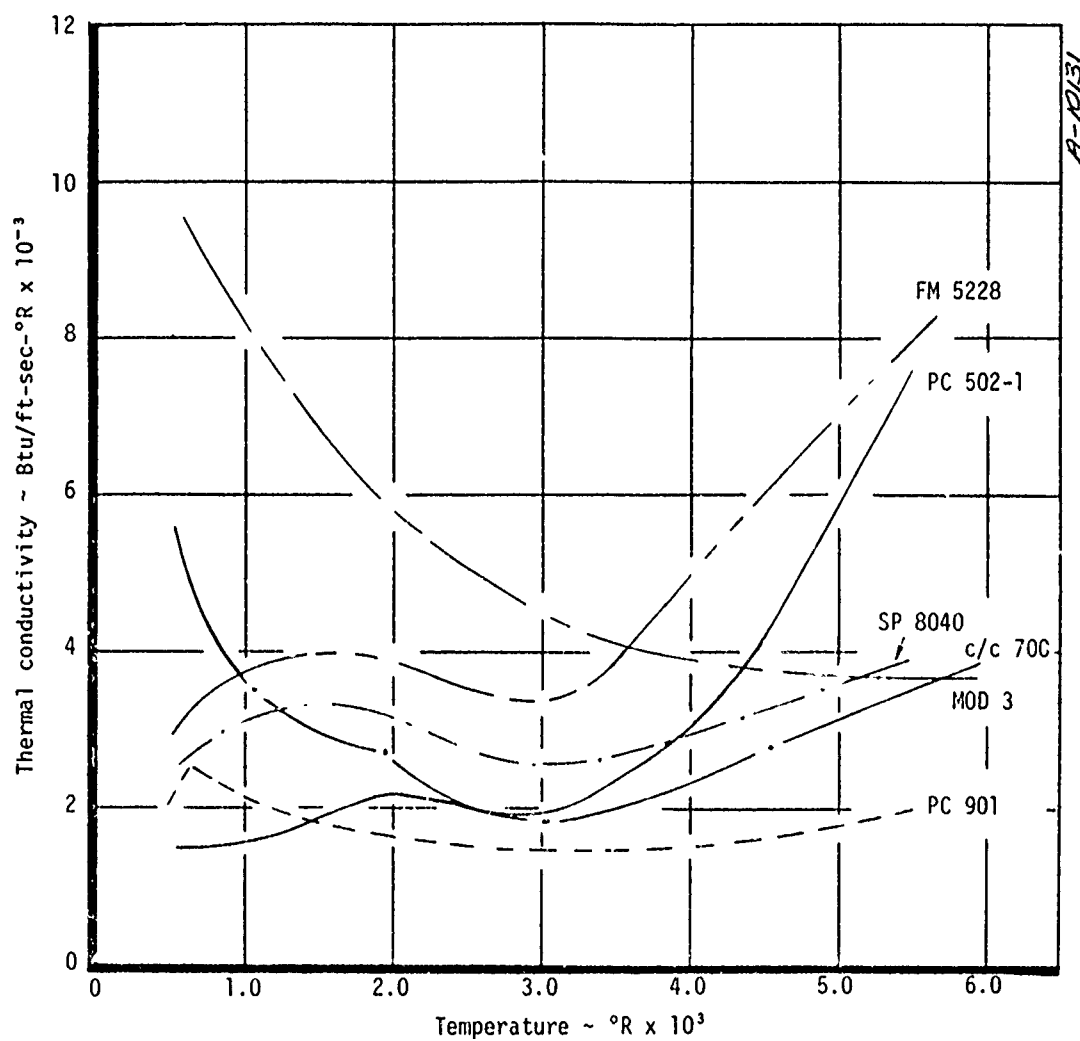| Temperature °R	Specific Heat Btu/lbm-°R	Thermal Conductivity Btu/ft-sec °R x 10^{-3}	
		W/P	A/P
530	0.215	4.15	3.0
800	0.240	4.70	3.5
1100	0.315	5.35	3.8
1500	0.455	8.30	4.0
2000	0.590	8.80	3.9
2500	0.600	8.70	3.6
3000	0.600	8.20	3.4
3500	0.600	8.10	3.9
4000	0.600	8.15	5.0
4500	0.600	8.50	6.0
5500	0.600	9.60	8.0

Density = 94 lbm/ft³ = 1.5 g/cc

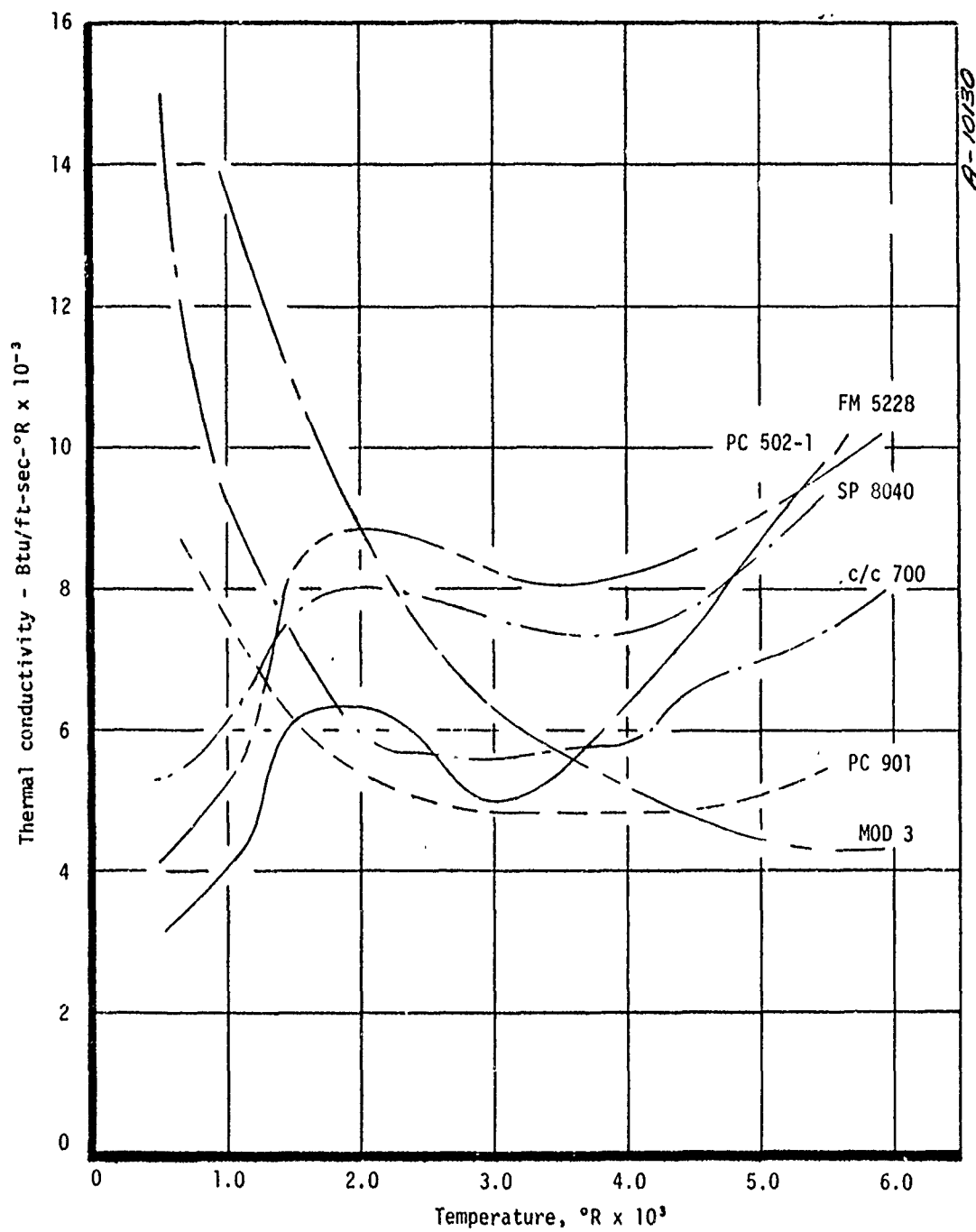Figure B-4. Thermal conductivities of carbon composites, against ply.

Figure B-5. Thermal conductivities of carbon composites, with ply.
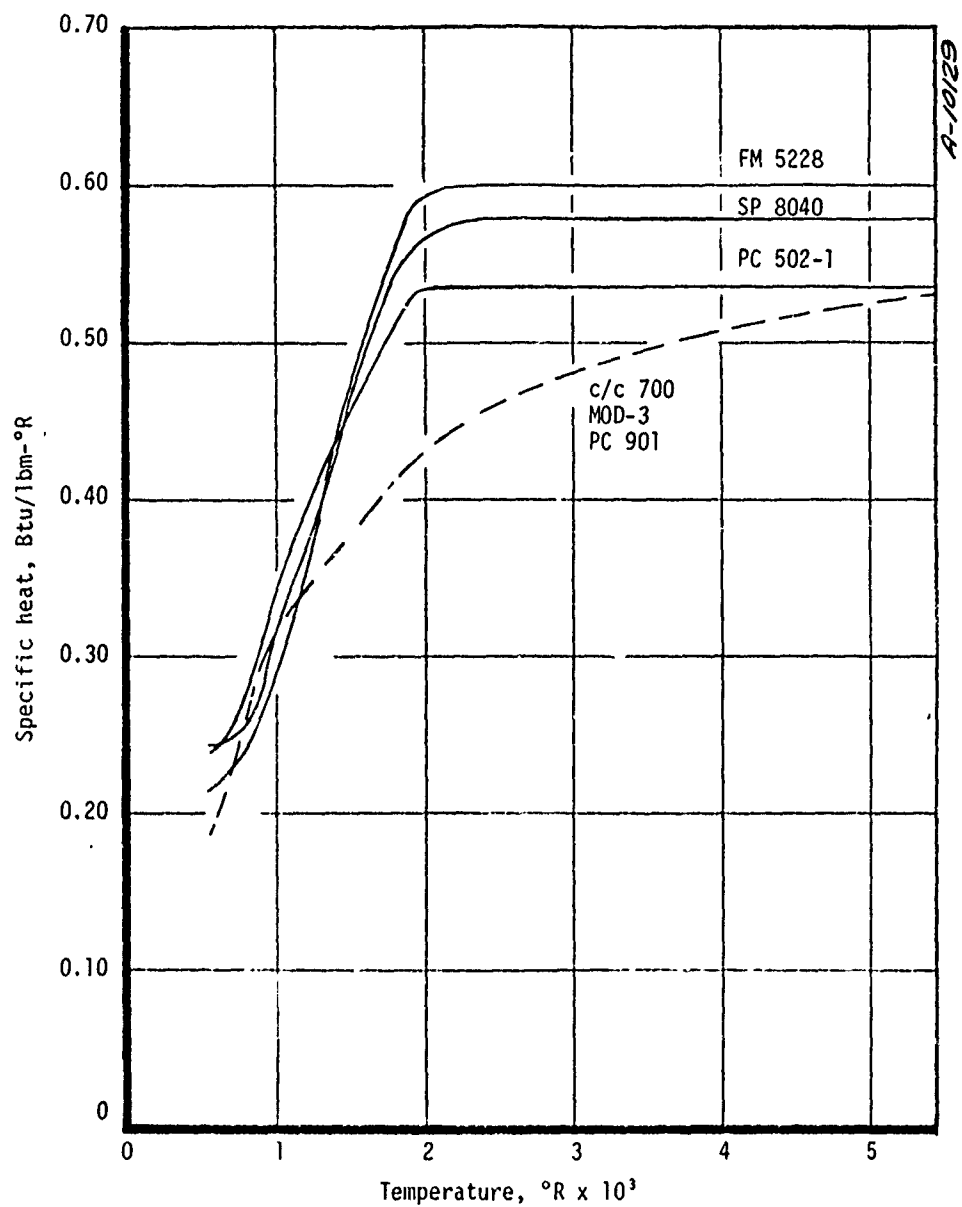
Figure B-6. Specific heat vs temperature for six carbon composites.

TABLE B-20. EFFECTS OF PROPERTY VARIATION ON THERMAL
RESPONSE FOR CARBON-CARBON COMPOSITES

Property	Variation*	T_{BW} (2370°R)	T_S† (5460°R)	Recession (0.625 in)
ρ	±10%	--	--	∓10%
k	+50%	+40%	∓1%	∓7%
C_p	+25%	∓25%	∓1%	∓2%

*Haveq, SP-8040 used for nominal values, with ply results
shown in parenthesis above.

†Bulk Graphite kinetic model used in GASKET.

Effect of property variations on results
are the same for with-ply and against-ply
values.

simplicity, constant values of k, both with and against ply, and C_p could be used. Although there are larger differences at low temperatures (T < 2500°R) these can usually be neglected since the carbon/carbon materials would probably be used in high temperature applications and the low temperature transient response would not greatly effect the results. However, when tailored properly property carbon/carbon materials are developed to the point where they are used as insulators as well as flame surfaces, then low temperature properties become significant.

B.4 PYROLYTIC GRAPHITE

Pyrolytic graphite is a polycrystalline, highly anisotropic form of graphite produced by the thermal decomposition of a hydrocarbon gas. PG plates (c plane) have been established as state-of-the-art, however, a-b plane coatings have yet to be successfully developed for ICBM size rocket nozzle throat inserts. A brief description of the manufacturing process, the reported thermal properties and the results of a sensitivity analysis are presented in this section.

B.4.1 Manufacturing Summary

Pyrolytic graphite is formed by the vapor deposition of a hydrocarbon gas, typically methane; however, other hydrocarbons such as acetylene or propane are often used either by themselves or mixed with methane. The deposition takes place on a preformed graphitic substate in an induction furnace operating at temperatures between 3500°R and 4500°R.

B.4.2 Material Survey

Table B-21 lists some pyrolytic graphite manufacturers. Thermal conductivity and specific heat values used by the rocket motor companies are shown in Figures B-7 through B-9.

The density of pyrolytic graphite is 2.2 gr/cc. The heat of formation is assumed to be zero (the value for elemental carbon). The surface emissivity (total hemispherical) is initially a function of the surface fininsh, however, once the surface starts ablating, all of the graphites have essentially the same value, approximately 0.90.

B.4.3 Sensitivity Analysis

Table B-22 shows only the results of the sensitivity analysis for variations in thermal conductivity. All other results are consistent with those reported in Section B.1. The large variations in thermal conductivity were arbitrarily selected to show the influence of very large property variations.

TABLE B-21. PYROLYTIC GRAPHITE MANUFACTURERS

| MANUFACTURER	PRODUCT(S)
Atlantic Research Corporation	PURE PG
General Atomic Company	ISOTROPIC CARBON
General Electric Company	PURE PG
Hitco Inc.	PURE PG
Materials Technology Corporation	PURE PG
Pfizer Corporation	PURE PG
Raytheon Corporation	PURE PG
Rocket Propulsion Establishment	PURE PG
Super Temp. Corporation	PURE PG
Union Carbide Corporation	PURE PG
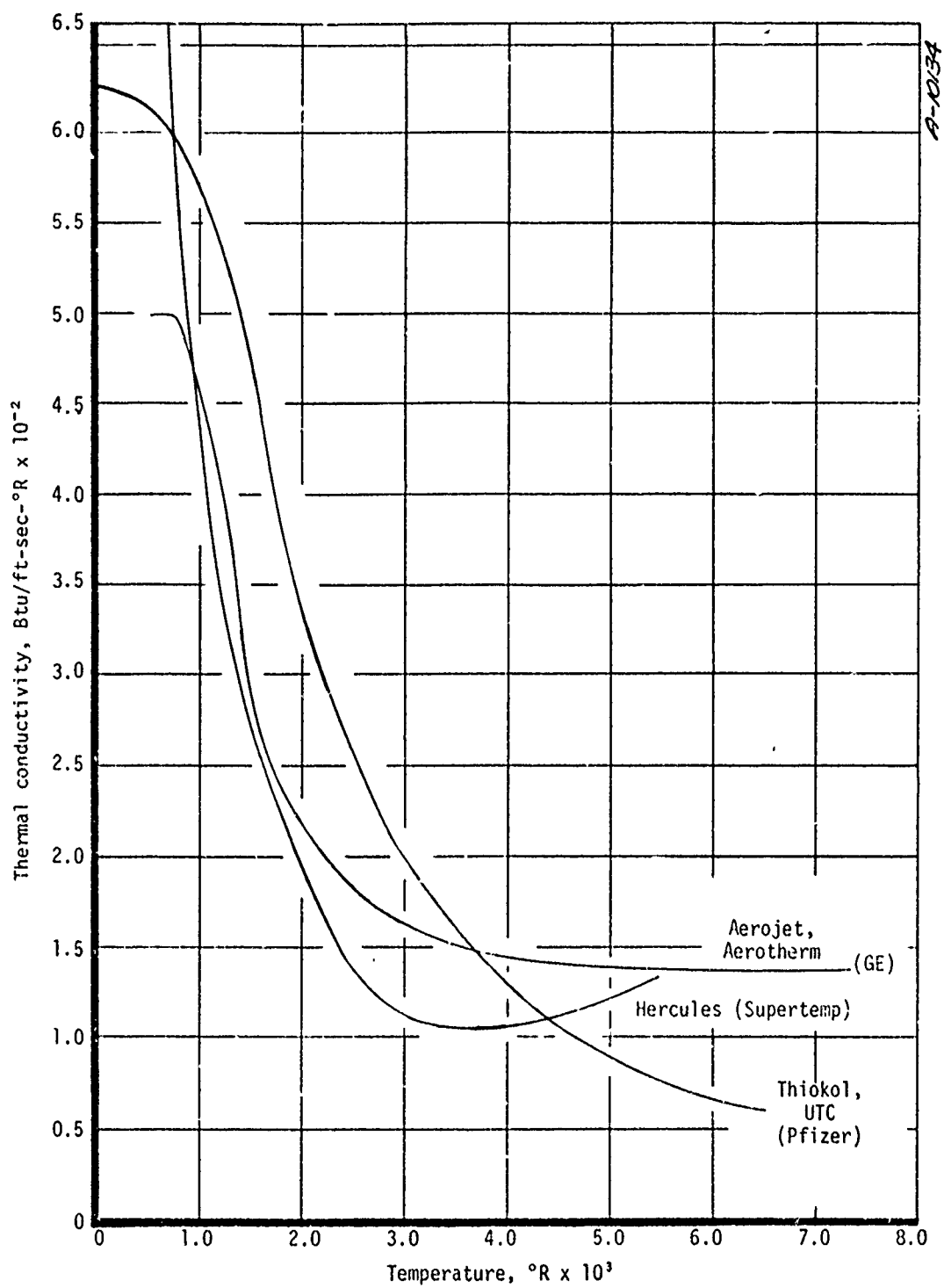
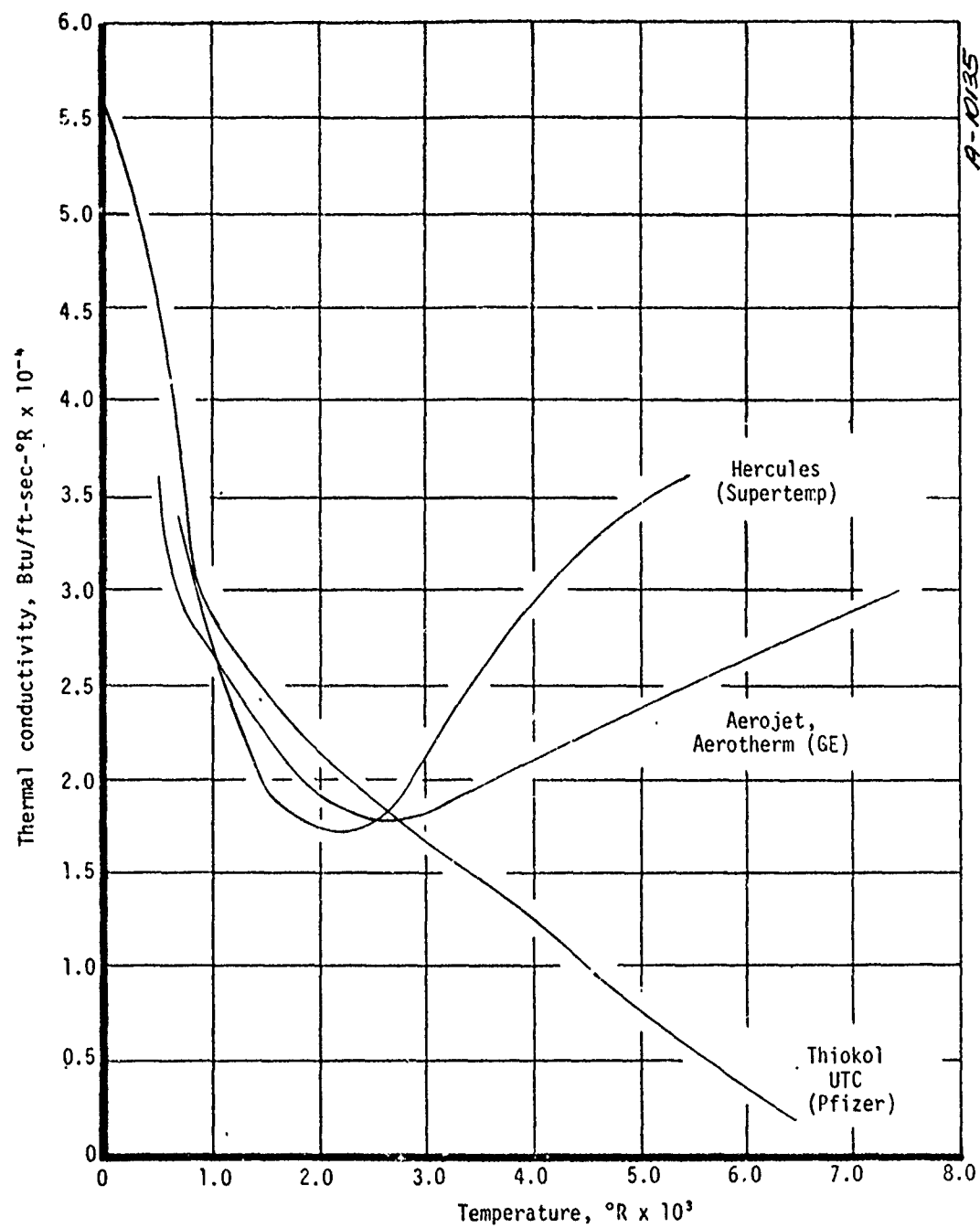Figure B-7. Thermal conductivity, a-b plane.

Figure B-8. Thermal conductivity, c direction.
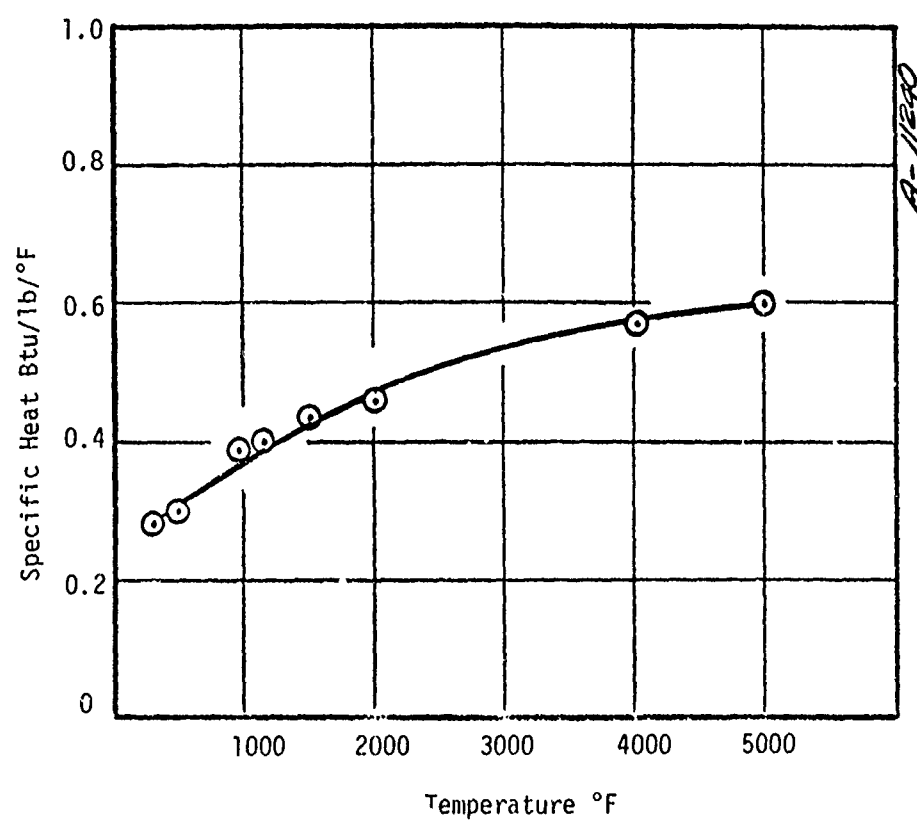
Figure B-9. Pyrolytic graphite specific heat.

TABLE B-22.   THERMAL RESPONSE FOR LAYER PG FOR
VARIATIONS IN THERMAL CONDUCTIVITY

Variation[†]	T_{BW} (860°R)	T_s* (6200°R)	Recession (0.0173 in)
-80%	-38%	+1%	+7%
-50%	-17%	+1%	+4%
+50%	+13%	-1%	-3%
+500%	+55%	=3%	-17%

*Layer PG kinetic model used in GASKET.

[†]Aerotherm PG property values taken as nominal. 100 mil PG on 2-inch ATJ substrate.

B.5 MODIFIED PYROLYTIC GRAPHITES

B.5.1 Codeposited Silicon Carbide/Pyrolytic Graphite

Codeposited SiC/PG is a relatively new material for rocket nozzle inserts. The primary manufacturer is Atlantic Research Corporation. A brief description of the manufacturing process, the reported thermal properties, and the results of the sensitivity analysis for SiC/PG are presented in this section.

B.5.1.1 Manufacturing Summary

Silicon carbide codeposited pyrolytic graphite (SiC/PG) is formed by the vapor deposition of a silicon and carbon carrying gas (e.g., 2 percent methane, 25 percent methyl trichlorosilane in nitrogen) on a preformed graphite substrate. The deposition process takes place in an induction furnace operating at temperatures between 3500°R and 4500°R. After being coated the material is annealed in a nitrogen environment at temperatures of 4200°R to 4700°R.

B.5.1.2 Material Survey

The only information collected on the thermal properties of SiC/PG is that provided by Atlantic Research Corporation and Southern Research Institute (References B-50 to B-52). The material tested was cut from one billet of SiC/PG which was nominally 20 percent SiC (by weight) with density of 2.29 g/cc. The actual SiC content varied from 16 to 24 percent. Reference B-52 indicates that the a-b plane thermal conductivity is only slightly affected by minor variations in SiC content; however, the c direction values may be altered by as much as 50 percent for a 5 percent change in SiC content. In addition to these variations the measured values of c direction thermal conductivity from two SoRI programs and the values calculated from TRW thermal stress tests are greatly different (Figure B-10). Figure B-11 shows the values of thermal conductivity and Figure B-12 shows the specific heat.* All of these are for a nominal 20 percent SiC content.

B.5.1.3 Sensitivity Analysis and Recommended Values

The recommended values for thermal conductivity (Reference B-50) and specific heat are given in Table B-23.

The heat of formation of SiC/PG can be calculated from:

$$H_o = -7.86 \ P_{SiC}$$
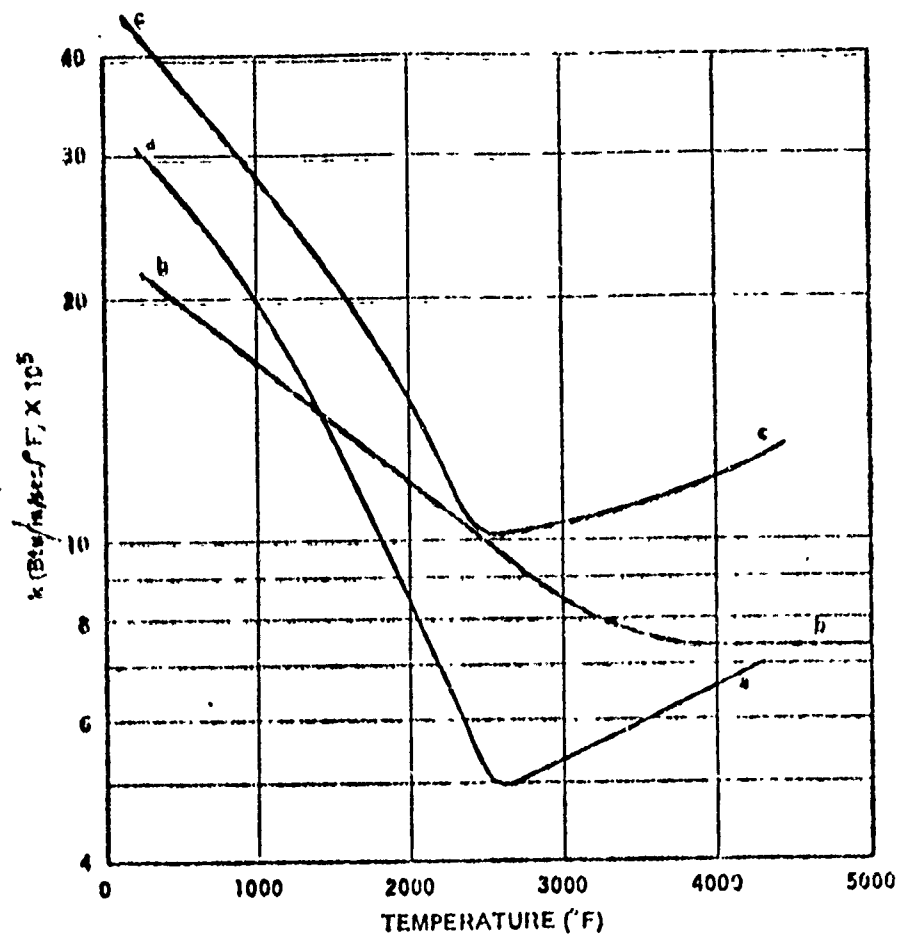
---

*Values supplied by Atlantic Research Corporation.

Figure B-10. Thermal conductivity of PG/20% SiC in the "c" direction (Reference B-50).

a. Old SoRI data generated under AIR LAUNCH
b. New SoRI data (Reference B-50)
c. Data backed out TRW thermal stress tests and recommended for nozzle design
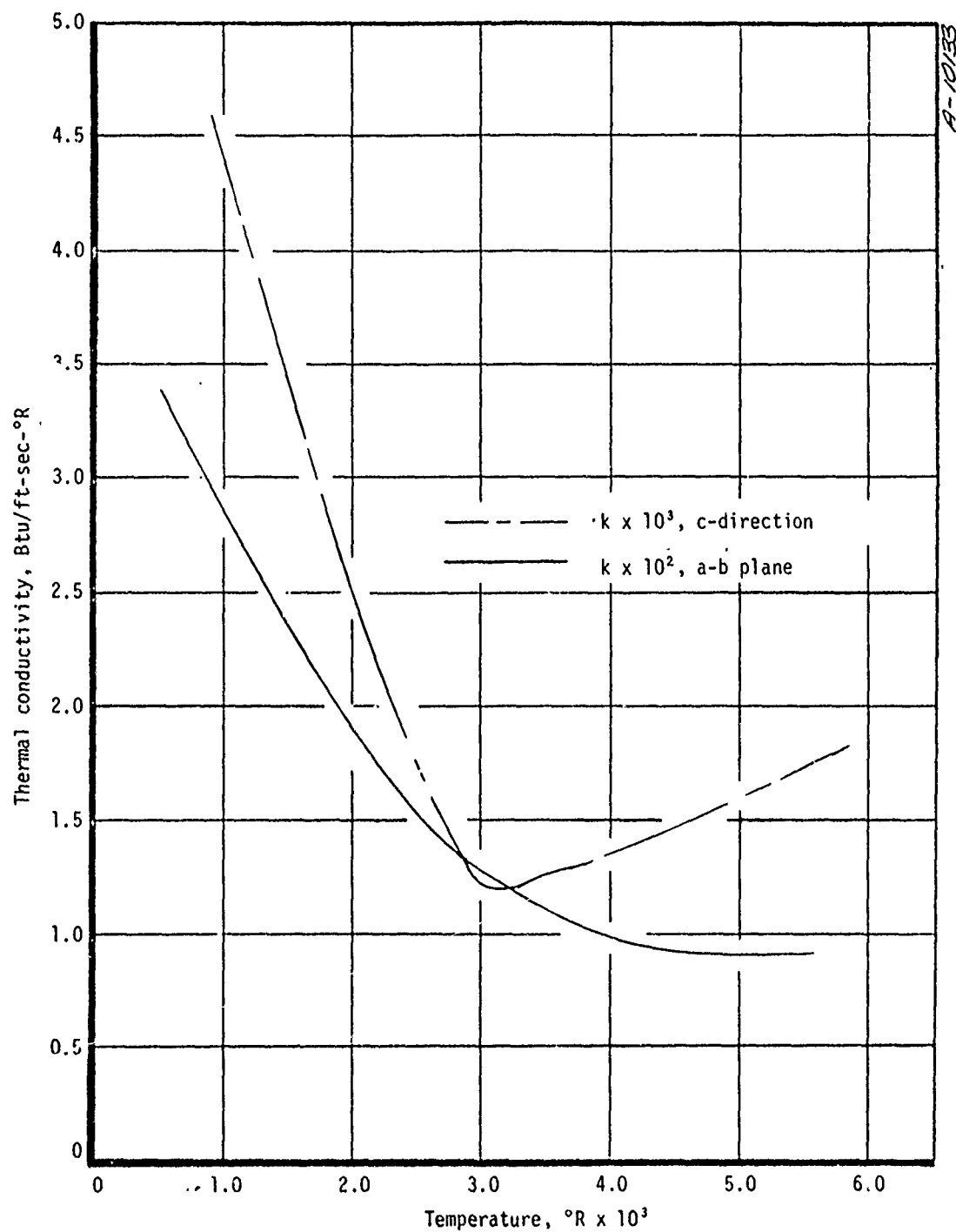
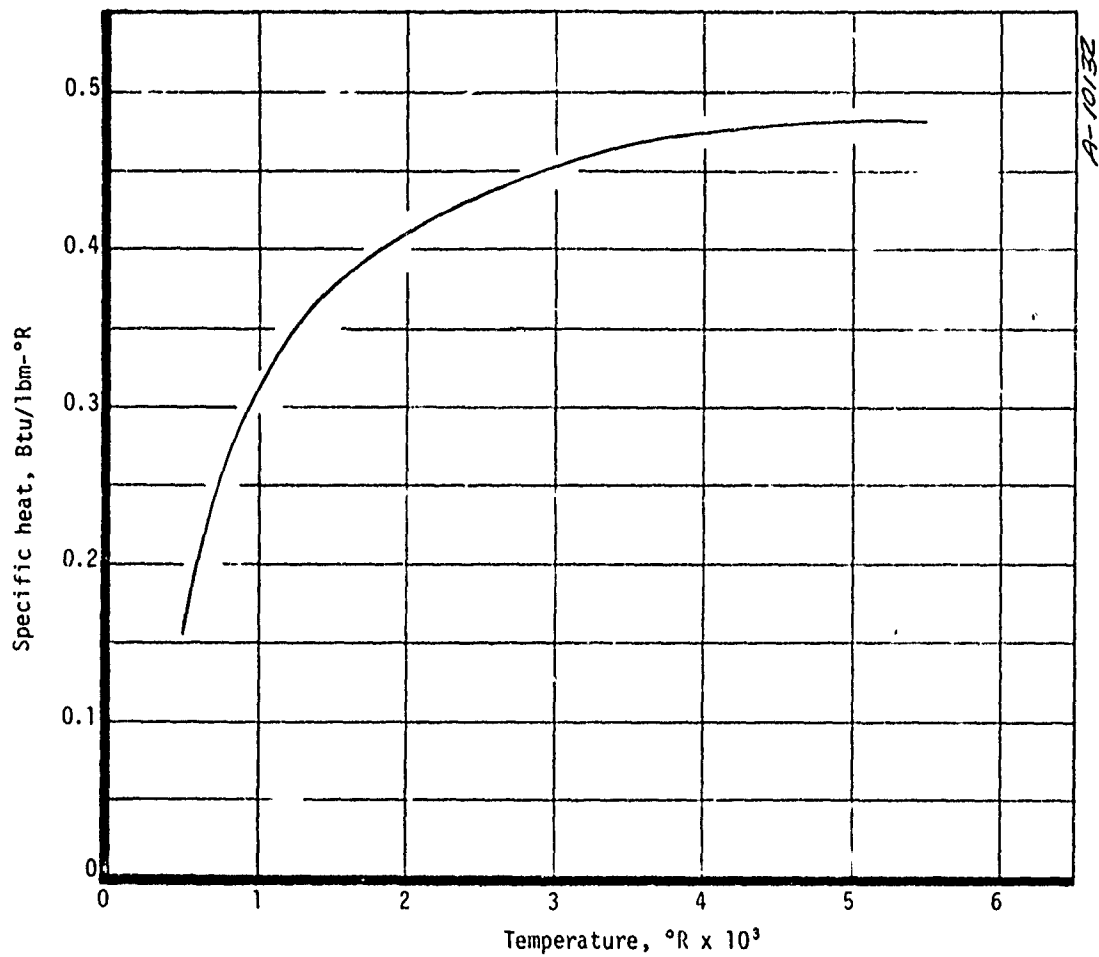Figure B-11. Thermal conductivity of 20% SiC/PG.

Figure B-12. Specific heat of SiC/PG.

TABLE B-23. THERMAL PROPERTIES SiC/PG ATLANTIC
RESEARCH — 20% SiC (References B-50
TO B-52

Temperature °R	Specific Heat Btu/lbm-°R	Thermal Conductivity Btu/ft-sec°R x 10^{-3}	
		a-b plane	c-direction
525	0.17	33.6	----
960	0.31	28.8	4.5
1460	0.37	24.0	3.46
2460	0.43	15.6	1.80
2960	0.45	13.2	1.23
3460	0.467	11.3	1.26
4460	0.475	9.0	1.45
4960	0.480	9.0	1.58
5460	0.480	9.0	----
density = 142.96 lbm/ft³ = 2.29 g/cc			

where P_{SiC} is the weight percent of SiC and H_o is given in Btu/1bm. It should be noted that the thermal response is very insensitive to the heat of formation.

The emissivity can be taken as 0.85.* Sample results of the sensitivity analysis are given in Table B-24.

TABLE B-24. EFFECTS OF PROPERTY VARIATION ON
THERMAL RESPONSE FOR SiC/PG (20
PERCENT BY WEIGHT SiC)

Property	Variation	T_{BW} $(2560^\circ R)$	T_a^* $(5400^\circ R)$	Recession $(0.33 \text{ in})^\dagger$
p	$\pm10\%$	----	----	$\pm10\%$
k	$\pm50\%$	$\pm50\%$	$\pm2\%$	$\pm2\%$
C_p	$\pm25\%$	$\pm10\%$	$\pm1\%$	$\pm1\%$

*Bulk graphite kinetic model used in GASKET.

†a-b plane results shown in parenthesis.

Effect of property variations on results same
for a-b plane and c direction values.

REFERENCES FOR APPENDIX B

B-1.   User's Manual, "Aerotherm Graphite Surface Kinetics Computer Program," Volumes 1 and 2, Acurex Corporation/Aerotherm Division, Mountain View, California, Aerotherm Report No. UM-72-25, AFRPL-TR-72-23, January 1972.

B-2.   User's Manual, "Aerotherm Charring Material Thermal Response and Ablation Program, Version 3", Acurex Corporation/Aerotherm Division, Mountain View, California, Aerotherm Report No. UM-70-14, AFRPL-TR-70-92, April 1970.

B-3 - Reserved for future use.
B-9.

B-10. Forney, Jr., D. M., ed., "Graphitic Materials for Advanced Reentry Systems — Part I," Air Force Materials Laboratory Report AFML-TR-70-133, Air Force Systems Command, Wright-Patterson Air Force Base, Ohio, August 1970.

B-11. Starrett, H. S., Pears, C. D., "Probable and Average Properties of ATJ-S(WS) Graphite," Southern Research Report, Southern Research Institute, Birmingham, Alabama, November 1972.

B-12. Pears, C. D., Starret, H. S., "Polygraphites Subjected to Temperature Stress Loadings," Southern Research Technical Report AFML-TR-73-59, Southern Research Institute, Birmingham, Alabama, March 1973.

B-13. The Aerospace Corporation, Reentry Materials Handbook, Aerospace Report TOR-1001(52855-20)-3, El Segundo, California, December 1968.

B-14. Baker, D. L., Bonnett, W. S., Davis, J. E., "Cooldown and Motor Firing Thermostructural Analysis of a 7.0 Inch Diameter Pyrolytic Graphite Insert," Aerotherm Report 73-74, Acurex Corporation/Aerotherm Division, Mountain View, California, July 1973.

B-15. Mann, W. H., Jr. and Pears, C. D., "A Radial Heat Flow Method for the Measurement of Thermal Conductivity to 5000°F," presented at the Conference on Thermal Conductivity Methods, Battelle Memorial Institute, October 26-28, 1961.

B-16 - Reserved for future use.
B-29.

B-30. "Properties of Carbon/Carbon Composites — Carbitex 700," Report TWR-7451, Thiokol Chemical Corporation.

B-31. Legg, J. K., Starrett, H. S., Sanders, H. G., and Pears, C. D., "Mechanical and Thermal Properties of MOD 3," Southern Research Institute, Technical Report No. AFML-TR-73-14, Volume IV, September 1973.

B-32. "The Thermal Properties of Pyrocarb 901," Final report to Hitco, Inc. by Southern Research Institute, SoRI-EAS-74-032, January 1974.

B-33. Baker, D. L., Schaefer, J. W., and Wool, M. R., "Thermal Property and Ablative Response Characterization of Pyrolized Materials," Aerotherm Corporation, Final Report 69-47, January 1969.

B-34 - Reserved for future use.
B-49.

B-50. Hughes, M. C. and Singleton, R. H., "Codeposited PG/SiC Nozzle Liners for Advanced ICBM Systems, Vol. II Coating Characteristics," AFRPL-TR-74-15, Atlantic Research Corporation, Alexandria, Virgina, August 1974.

B-51. Singleton, R. H. Bielawski, C., and Undercoffer, K. E., "Development and Evaluation of PG/SiC Codeposited Coatings for Rocket Nozzle Inserts, Volume I: Insert Test and Evaluation in High Performance Propellant Environments," AFRPL-TR-73-107, Atlantic Research Corporation, Alexandria, Virginia, February 1974.

B-52. Singleton, R. H., "Development and Evaluation of PG/SiC Codeposited Coatings for Rocket Nozzle Inserts, Volume 1: Thermal and Mechanical Properties of PG/SiC Codeposit," AFRPL-TR-73-70, Atlantic Research Corporation, Alexandria, Virginia, 1973.